Universitat Autònoma de Barcelona

Chronic overproduction of IL6 and IL10 modulates the microglial response after anterograde degeneration

Mireia Recasens Torné

Universitat Autònoma de Barcelona

Institut de Neurociències

Dept. Cell Biology, Physiology and Immunology

Chronic overproduction of IL6 and IL10 modulates the microglial response after anterograde degeneration

Mireia Recasens Torné

PhD. Directors: Dr. Berta González de Mingo

Dr. Beatriz Almolda Ardid

PhD. Academic Tutor: Dr. Bernardo Castellano López

Doctor of Philosophy Research Thesis

PhD in Neuroscience

Bellaterra, Barcelona

May 11th 2021

This dissertation has been developed in the Department of Cell Biology, Physiology and Immunology and the Institute of Neurosciences affiliated with the Universitat Autònoma de Barcelona, under the direction of Dr. Berta González de Mingo and Dr. Beatriz Almolda Ardid.

Mireia Recasens Torné	Dr. Berta González de Mingo	Dr. Beatriz Almolda Ardid

Dr. Bernardo Castellano López

Bellaterra, de 2021

INDEX

1. ABBREVIATIONS

ABC	Avidin-Biotin-Peroxidase Complex
AD	Alzheimer's disease
ADP	Adenosine diphosphate
ALRs	AIM2-like receptors
ALS	Amyotrophic lateral sclerosis
APCs	Antigen presenting cells
ATP	Adenosine triphosphate
BAMs	Barrier-associated macrophages
BB	Blocking buffer
BDNF	Brain-derived neurotrophic factor
CCL	Chemokine (c-c motif) ligand CCL
CNS	Central Nervous System
CNTF	Ciliary neurotrophic factor
CSIF	Cytokine synthesis inhibitory factor
CXCL	Chemokine (C-X-C motif) ligand
DAB	Diaminobenzidine
DAM	Disease associated microglia
DAMPs	Damage-associated molecular patters
DG	Dentate gyrus
EAE	Experimental autoimmune encephalomyelitis
ECM	Extracellular matrix
eEMPa	Early erythro-myeloid progenitors
FD	Fascia dentata
FNA	Facial nerve axotomy
GDNF	Glial-derived neurotrophic factor
GFAP	Glial fibrillary acidic protein

hGH	Human growth hormone gene
HSCs	Hematopoietic stem cells
IFN-γ	Interferon gamma
IHC	Immunohistochemistry
IIM	Innate Immune Memory
IL	Interleukin
IML	Inner molecular layer
i.p.	Intraperitoneally
LEA	Lateral entorhinal area
LPS	Lipopolysaccharide
M-CSFR	macrophage colony-stimulating factor receptor
MAC-1	Macrophage-1 antigen
MCAO	Middle cerebral artery occlusion
MEA	Medial entorhinal area
MgnD	Microglial neurodegenerative phenotype
MHCII	Major histocompatibility complex-II
ML	Molecular layer
MML	Medium molecular layer
MS	Multiple sclerosis
NGF	Nerve growth factor
NLRs	Nod-like receptors
NO	Nitric oxide
NPCs	Neuronal progenitor cells
OPCs	Oligodendrocyte progenitor cells
OML	Outer molecular layer
PAMPs	Pathogen associated molecular patterns
PBS	Phosphate buffer solution
PD	Parkinson’s disease

PP	Perforant pathway
PPT	Perforant pathway transection
PRRs	Patter recognition receptors
RLRs	RIG-like receptors
ROS	Reactive oxygen species
RT	Room temperature
SCI	Spinal cord injury
SRA	Scavenger receptor A
SV40	Simian virus
TBI	Traumatic brain injury
TBS	Tris-buffered saline
TGF-ß	Transforming growth factor beta
Th	T-helper
TLRs	Toll-like receptors
TMB	Tetramethylbenzidine
TNF-α	Tumour necrosis factor-α
Treg	T-regulatory
YS	Yolk sac
VEGF	Endothelial growth factor
WT	Wild-type

2. ABSTRACT

In CNS, neuroinflammation might be evoked by a variety of scenarios including acute or chronic brain diseases; producing activation of glial and immune peripheral cells. Among glial cells, microglia play a specific role being the representative of the immune system within the CNS. Their response against the damage is fast and characterized by adopt morphological changes, increased proliferate rate, migration, phagocytosis and secrete immunomodulatory molecules like cytokines. Cytokines are crucial molecules involved in the modulation of the molecular microenvironment and hence play a pivotal role in orchestrating microglial activation. In this sense, IL-6 and IL-10 has been proposed as a two immunoregulatory molecules of microglial cells, but their specific role remains unclear due to their controversial roles after brain diseases. In this context, the objective of the present thesis is to determine the modifications that local overproduction of IL-6 and IL-10 can exert on microglia cells and their implication in the evolution and resolution of the inflammatory process associated with an anterograde axonal injury. To address it, we performed the perforant pathway transection (PPT) in two transgenic mice, GFAP-IL6Tg and GFAP-IL10Tg, which produce the cytokines IL-6 and IL-10, respectively, under the GFAP promoter in astrocytes. Our results showed that, in steady state, both IL-6 and IL-10 chronic overproduction have the capacity to polarize microglial phenotype. After PPT, astrocyte-targeted production of both cytokines increases microglial/macrophage density. In the case of GFAP-IL6Tg mice this increase is due to both microglial proliferation and recruitment of monocytes, whereas in GFAP-IL10Tg is only produced by higher monocyte infiltration. Moreover, both IL-6 and IL-10 chronic overproduction changes microglial phenotype increasing the microglial phagocytic machinery. However, only IL-6 induces higher levels of TREM2, although reduces the clearance of neurodegenerating fibers in the dennervated area. About the peripheral immune cell recruitment, in addition to the increase in monocytes, in both transgenic animals we observe an upregulation of chemokines linked to the increase in T-cell infiltration. In this regard, one of the most

interesting results obtained in this study is that both IL-6 and IL-10 chronic overproduction modifies the antigen presenting capacity of microglial cells worsening their interaction with recruited lymphocytes. Specifically, GFAP-IL6Tg animals were depleted of $MHCII^+$ and $CD11c^+$ microglia cells in the parenchyma being this expression restricted to perivascular macrophages. The MHCII and CD11c expression was also impaired in GFAP-IL10Tg, showing less number of microglia cells expressing these markers after PPT. In addition to microglia and peripheral immune cell infiltration, our results also show modifications in the cytokine environment in both transgenic animals. Indeed, IL-6 chronic overproduction increases IL-6 and IL-1β pro-inflammatory cytokines, associated to innate immune response; and shows elevated levels of the anti-inflammatory cytokine IL-10. In the case of IL-10 astrocyte-targeted production, we observed an anti-inflammatory environment mainly with higher TGF-β and lower IL-2 and IFN-γ. Furthermore, both astrocyte-targeted production of IL-6 and IL-10 interferes in the communication between microglia and neurons trough the CD200R-CD200 axis. Finally, IL-6 chronic overexpression reduces the collateral sprouting associated to PPT, whereas IL-10 chronic overexpression does not modify this process. In conclusion, the results obtained in this thesis indicate that chronic and local exposure to IL6 and IL10 polarized the microglia towards a primed phenotype. Once they are exposed to a same second stimulus, the PPT paradigm, they present a different microglial activation profile conditioned by the first stimuli. Specifically, IL6-primed microglia present an activated profile unable to acquire an antigenic presentation function; whereas IL10-primed microglia shows a downregulated APC phenotype after PPT. These changes in microglial population only modify the outcome of lesion in GFAP-IL6Tg mice avoiding the generation of a pro-regenerative environment.

3. INTRODUCTION

Deciphering all the elements involved in the neuroinflammatory response has focused all the efforts of today's neuroscientists. Although great strides have been made in previous decades, there is still a long way to go. Multiple evidences suggested that an altered neuroinflammatory process leads the appearance or participates in the progression of a wide range of neurological diseases. For this reason, the study of the relation between the central nervous system (CNS) and the immune system is a priority. Hence, understand how microglia cells, as the representative of the immune system in the brain, orchestrate the neuroinflammatory response would be helpful for developing new therapies.

3.1. *Microglia cells*

3.1.1. Origin of microglia cells

Myeloid cells related to CNS derived from the haematopoiesis that occurs during embryonic development and throughout adulthood to produce and replenish the blood system; whereas astrocytes, oligodendrocytes and neurons shared the same origin. The haematopoiesis process consist in three waves: 1) primitive haematopoiesis, which take place in the extraembryonic yolk sac (YS) where early erythro-myeloid progenitors (eEMPs) are produced; 2) these EMPs migrate from the YS to fetal liver; 3) definitive haematopoiesis, where hematopoietic stem cells (HSCs) located in the bone marrow generates all the cell lineages (Bennett & Bennett, 2020; Dzierzak & Bigas, 2018; Prinz, Jung, & Priller, 2019; Y. Wu & Hirschi, 2020) (Figure 1). It is well established that microglia cells come from the first primitive haematopoiesis wave in the YS during the second embryonic week in rodents (Ginhoux et al., 2010; Smolders et al., 2019; Stremmel et al., 2018). In fact, microglia cells were originally thought to be the only adult macrophage population displaying eEMP origin (Hoeffel & Ginhoux, 2015; Perdiguero & Geissmann, 2016). However, a subpopulation of perivascular and meningeal macrophages, also called barrier-associated macrophages

(BAMs), shared eEMP microglia origin (Goldmann et al., 2016; Jordao et al., 2019; Schulz et al., 2012).

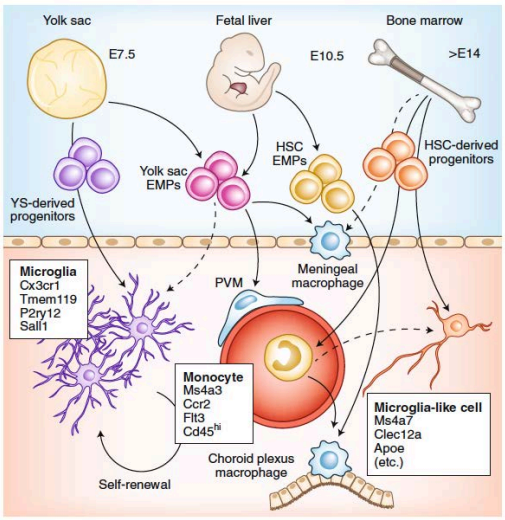

Figure 1. Origin of microglia*. Microglia come from primitive hematopoiesis. Yolk sac progenitors migrate to the developing brain before embryonic day 10.5. BAMs may initially derive from YS progenitors, although their progenitors (EMPs) may also journey through the fetal liver. Choroid plexus macrophages are HSC-derived and either derive from HSC-origin EMPs or from blood monocytes, as depicted. Solid arrows represent the well-established origins whereas dashed arrows show new hypothesis. From: (Bennett & Bennett, 2020).*

New theories are still on debate. For instance, a study using genetic fate mapping techniques, proposed that also a subset of microglia cells might come from the second wave around E12.5 (De et al., 2018). Although both microglia subpopulations shared gene profile, like Tmem119 and Sall1 expression and equal participation in synaptic pruning; they showed different brain distribution. Also, microglia cells from the second wave are more responsive to chronic brain injury than microglia that colonizes the brain at E9.5 (De et al., 2018). Another interesting finding in zebrafish models, showed the possible contribution of eEMPs, EMPs and HSC, the three potentially microglia precursors, in microglia replacement (Ferrero et al., 2018). Although in mice microglia replacement is HSC-derived cells independent, these studies emphasizes that the ontogeny of brain macrophages is more complex than

currently appreciated. Further studies are necessary to determine their origins and understand their functions and networks in the healthy brain.

3.2. Microglia contributions during development

During development, once into the brain, microglia propagate and disperse in a non-heterogeneous manner throughout the CNS (Lawson, Perry, & Gordon, 1992; Verdonk et al., 2016). Depending on the specific anatomical structure, microglia present different morphological features, lysosome content, membrane composition, electrophysiological activities and gene transcriptome profile that differs by other resident-tissue macrophages (Button et al., 2014; Chiu et al., 2013; De Biase et al., 2017; Gomez-Nicola, Fransen, Suzzi, & Perry, 2013; Hickman et al., 2013; Majumdar et al., 2007). These differences are consistent with the different origin of microglia and macrophages, because tissue-resident macrophages are generated from the second wave of the haematopoiesis process. Hence, microglia cells identity is associated with a unique signature gene. For example, in the healthy brain, only microglia cells but not macrophages express *Tmem119, P2ry12, Slc2a5, Olfml3* and *Sall1*, pointing to these molecules as putative candidates to distinguish between the two cell populations (Goldmann et al., 2016; Jordao et al., 2019; Zeisel et al., 2015). Results obtained from single-cell RNA sequencing, revealed also genetic differences and specific subtypes within the microglia population during development. Between P4 and P7, microglia associated with white matter express high levels of *Spp1, Igf1, Lgals1, Lgals3* and *Gpnmb* (Hammond et al., 2019; Q. Li et al., 2019). Moreover, Stowell and colleagues described a specific and unique microglia population in the cerebellum characterized by less ramified morphology, more sparsely distribution and with an elevated communication with dendrites and somas of Purkinje neurons, compared with cortical microglia cells (Stowell et al., 2018). In addition, Torres-Plata and colleagues described the simultaneous presence of ramified, primed, reactive and amoeboid phenotype in the human cerebral cortex of patients without any pathology (Torres-Platas, Cruceanu,

Chen, Turecki, & Mechawar, 2014). On the other hand, studies in aging models, has been established that microglia gene signature is also aging dependent (Orre et al., 2014). All this data suggests that although resident-microglia cells shared origin, the CNS environment defines their phenotype and it is not clear how these phenotype differences in the uninjured brain contribute to the development of various CNS pathologies.

One of the main functions of microglia cells during the early prenatal period is the establishment of the neuronal circuits of the CNS. Microglial cells regulate progenitor cells (NPCs) population by phagocytosis (Ashwell, 1990; Marin-Teva et al., 2004). However, at the same time, it has been described that microglia cells promotes neurogenesis of NPCs and neurons (Cunningham, Martinez-Cerdeno, & Noctor, 2013; Frost & Schafer, 2016; Sierra et al., 2010). Moreover, microglia play an important role performing synaptic pruning, remodelling synaptic circuits and inducing synapsis formation (Miyamoto et al., 2016; Sipe et al., 2016; Tremblay, Lowery, & Majewska, 2010; Wake, Moorhouse, Miyamoto, & Nabekura, 2013; Weinhard et al., 2018). It is important to take in account that any disturbance of these phenomena could produce evident disorders in the adulthood. For example, exacerbated microglia pruning evokes alterations in the synaptic development that correlates with worsening and high risk of suffers pathologies like Alzheimer's disease (AD), schizophrenia or autism (Q. Li & Barres, 2018; Vilalta & Brown, 2018). In addition to their interaction with neurons, they exert an important support to oligodendrocytes and their progenitors during myelinogenesis (Hagemeyer et al., 2017; Wlodarczyk et al., 2017).

3.3. Microglia in the adult healthy brain.

Adult microglia cells in homeostatic conditions are continuously scanning the milieu (Kettenmann, Hanisch, Noda, & Verkhratsky, 2011). The mechanisms regulating the motility and morphology are not clear. Some studies propose purinoreceptors, ion channels and neurotransmitters as possible controllers of these phenomena (Tremblay

et al., 2011). More recent studies have been showed that microglia ramification and surveillance are promoted by tonic activity of the potassium channel THIK-1 (Madry et al., 2018). In the adult brain, several studies either *in vivo* or *in vitro*, assumed that microglia participate in adult neurogenesis and maintain neuronal growth; phagocytising dead cells and leading synaptic pruning (Matsui & Mori, 2018; Sierra et al., 2010; Walton et al., 2006). In fact, depletion of microglia cells located in the DG inhibits hippocampal adult neurogenesis (Kreisel, Wolf, Keshet, & Licht, 2019). Moreover, the same study has been described a specific DG microglia profile that responds exclusively to the neurogenetic vascular endothelial growth factor (VEGF), suggesting a specific an unique cascade to support adult neurogenesis compared to other microglia populations.

Regulation of microglial activation during pathological conditions also involves the interaction with neurons (Cardona et al., 2006; Suzumura, 2013). Microglia cells release a wide range of molecules in order to regulate the synaptic activity and plasticity. In addition, this communication is bidirectional as neurons regulates microglia motility and activation. Specifically, microglia-neuron crosstalk can be modulated by neurotransmitters, purinergic and adenosine signalling, CX3CL1/CX3CR1 complex, complement systems, TREM2 signalling, CD200/CD200R and CD47/SIRPα, TLRs, cytokines and trough the endocannaboid signalling (Badimon et al., 2020; Manich et al., 2019; Marinelli, Basilico, Marrone, & Ragozzino, 2019). Specifically, microglia express CD200R1 and CX3CR1; whereas CD200 and CX3CL1 are highly expressed by neurons and with low levels by astrocytes and oligodendrocytes (Manich et al., 2019). In addition to microglia-neuron communication, it is well established that maintenance of oligodendrocyte progenitor cells (OPCs) and astrocyte activation and proliferation is drived by microglia (Hagemeyer et al., 2017).

3.4. Microglia cells in injured brain

Once microglia detects any disturbance in the microenvironment acquire an activation state that is characterized by morphological and phenotypical changes and motility. Microglia migration to the injured site depends on activation of its P2Y12 receptors that bind with adenosine triphosphate (ATP) or adenosine diphosphate (ADP) released from damaged neurons (Davalos et al., 2005; Haynes et al., 2006). In the following hours, activated microglia retract their processes, form new motile protrusions and change their morphology and phenotype depending of the severity of the lesion (Davalos et al., 2005; Nimmerjahn, Kirchhoff, & Helmchen, 2005; Stence, Waite, & Dailey, 2001).

For a long time, numerous attempts have been made to classify microglial cells. Thus, depending on their surface markers microglia was defined as M1 and M2 microglia, following the criteria used to describe peripheral macrophages (Orihuela, McPherson, & Harry, 2016; Tang & Le, 2016). The introduction of additional single-cell technologies, such as scRNA-seq and single-cell mass spectrometry, among others, has been provided the opportunity of a more accurate single-cell analysis. Hence, in relation to neurodegenerative diseases, a wide range of microglia phenotype signatures has been described, totally dependent on the specific disease (De Biase et al., 2017; Keren-Shaul et al., 2017). In AD, as an example, a unique microglia signature associated with β-amyloid plaque has been characterized by expressing high levels of genes involved in phagocytosis and immune response regulations such as *Lpl, Itgax*, *ApoE* and *Cst7* (Keren-Shaul et al., 2017). This niche of microglia cells has been linked with a protective role (Deczkowska, Amit, & Schwartz, 2018). In addition, these cells have been termed as disease associated microglia (DAM) or “microglial neurodegenerative phenotype” (MgnD) (Krasemann et al., 2017). In demyelination mouse models, activated microglia showed a dramatically lost of their homeostatic-associated signature and in parallel increased various genes linked to proliferation, inflammation and antigen presentation (Hammond et al., 2019; Jordao et al., 2019;

Masuda, Sankowski, Staszewski, & Prinz, 2020). In human spinal cord of amyotrophic lateral sclerosis (ALS) patients, microglial cells presented a loss of homeostatic microglia expression signature characterized by the increased expression of genes related to inflammation, downregulation of genes involved in microglia development and suppression of innate immune inflammation (Butovsky et al., 2015). A part of neurodegenerative disorders, analysis of single-cell levels has been performed in mouse models of LPS injection or facial nerve axotomy (FNA) (Masuda et al., 2020; Torres-Platas et al., 2014). Hence, it seems evident that the phenotype shift of microglia cells is highly dependent of the degree of the disease, aging and brain region and occurs at individual cell level (Hammond et al., 2019; Mathys et al., 2019; van der Poel et al., 2019).

Disruption of microglia communication with neurons also contributes to developing neurological diseases. In experimental autoimmune encephalomyelitis (EAE), FNA and LPS administration models, deficiency of CD200 or CX3CR1 evokes microglia activation and increased microglial toxicity (Cardona et al., 2006; Hoek et al., 2000). In addition, microglia cells also controls neuronal activity by the secretion of soluble factors such as brain-derived neurotrophic factor (BDNF), interleukin-10 (IL-10), IL-1β, or tumor necrosis factor-α (TNF-α) (Beattie, Hermann, Rogers, & Bresnahan, 2002; Coull et al., 2005; Cserep et al., 2020; Hewett, Jackman, & Claycomb, 2012; Lim et al., 2013). Badimon and colleagues recently described that neuronal ATP leads the expression of microglial adenosine production to regulate neuronal responses (Badimon et al., 2020).

Microglia and astrocyte communication is also very complicated but essential to understand the outcome of brain diseases. Their cross talk may be drive by the CXCL12-CXCR4 system. CXCL12 production by astrocytes interacts with the CXCR4 microglia receptor promoting the production of pro-inflammatory mediators such as TNF-α, IL-1β and IL-6 (Bezzi et al., 2001; Luo, Koyama, & Ikegaya, 2016). Moreover, the CX3CL1 chemokine produced by astrocytes and neurons binds with microglia's

fractalkine receptors suppressing their own production of pro-inflammatory mediators (Ali, Chugh, & Ekdahl, 2015). Moreover, a wide bibliography exist describing that microglia promotes the secretion of neurotrophic factors like the glial-derived neurotrophic factor (GDNF) or the BDNF by astrocytes which participate during repair and neuronal survival (Kwon & Koh, 2020; Norden, Fenn, Dugan, & Godbout, 2014). Moreover, microglia cells lead the phenotypic shift of astrocytes mediated by IL-1α, TNF-α and Complement component 1q production (Liddelow et al., 2017). In addition, it has been demonstrated that activated astrocytes are able to either promote microglia activation via IL-1β and IL-6 or inhibit the microglial inflammatory phenotype via galectin-1 (Burda & Sofroniew, 2017; Sofroniew, 2014; Zamanian et al., 2012). Finally, regarding oligodendrocytes, they can release a high concentration of ATP that microglia receives in order to initiate its rapid chemotactic responses.

Microglial cells considered as a unique representative of the immune system in the CNS, develops a high response against any perturbation of the brain environment. This microglial activation has been characterized by secretion of inflammatory mediators and phagocytic activity, among others. Moreover, microglia cells also modulate the bridge between innate immunity and adaptive immunity and also participate with their antigen presenting capacity.

3.4.1. Microglia in innate immunity

Microglial cells, as first line of defence, recognize the presence of tissue damage or signs of infections through their patter recognition receptors (PRRs) initiating the innate immune response (Ransohoff & Brown, 2012; Takeuchi & Akira, 2010). PRRs recognize two types of molecules: pathogen associated molecular patterns (PAMPs) expressed by microbes, and damage-associated molecular patters (DAMPs), molecules or proteins related to dying or damaged neurons. The main PRRs include Toll-like receptors (TLRs), Nod-like receptors (NLRs), RIG-like receptors (RLRs), AIM2-like receptors (ALRs), and C-type lectin receptors (Kigerl, de Rivero

Vaccari, Dietrich, Popovich, & Keane, 2014; Venegas & Heneka, 2017). In the CNS, astrocytes, oligodendrocytes, endothelial cells, and even neurons express functional levels of some of these receptors (Hanamsagar, Hanke, & Kielian, 2012), but their role have been mainly studied in microglia cells.

Microglial activation during the innate immune response has been extremely involved in neurological diseases. Recent research in the AD has been revealed that microglia cells could initiate and propagate the inflammation and point to CD33 as a microglial receptor that regulates the innate immune response (Ennerfelt & Lukens, 2020). In AD, increased levels of CD33 is linked with a low efficiency of phagocytic microglia cells and in consequence with a high presence of plaque depositions that contributes to worsen the disease (Griciuc et al., 2013). In the past years, the different subtypes of TLRs has been focused all the attention due to their importance to generate the innate immune response. Depending on the TLR involved and the activation intensity, detrimental or beneficial effects has been described (Kumar, 2019). It is known that microglia cells express TLR1-9. Specifically, TLR4 has been associated with a protective role against AD and also is stimulated by the plaques (Dansokho & Heneka, 2018; Michaud et al., 2013). In Parkinson's disease (PD), the lack of TLR4 reduces microglia activation and in consequence prevents the dopaminergic cell death (Noelker et al., 2013). Moreover, activation of TLR2 promotes a pro-inflammatory microglia phenotype and in the case of TLR9 participates in the clearance of plaques, reducing AD pathology in mice (Dansokho & Heneka, 2018; Scholtzova et al., 2017).

This microglia activation state differs depending on the type of injury, acquiring a specific memory that influences the following reaction against the next stimuli, in the so-called immunological memory. Innate immune memory (IIM) in microglia cells can be manifested in two ways: enhanced "immune training" or suppressed "immune tolerance" response. Neher and colleagues proposed the concept of "primed" microglia to refer a pre-activated microglia state as a result of a previous insult that can be acute

or chronic (Neher & Cunningham, 2019). After that, microglia exhibit IIM that is manifested as a “trained” (exacerbated) response to a second stimuli. On the other hand, microglia could acquire a “desensitized” state in response to the first stimuli and in consequence the response to the second will be “tolerant” developing “immune tolerance” (Neher & Cunningham, 2019). It is important to investigate how this IMM state and the dual nature of “trained” or “desensitized” microglial response reflects a protective or detrimental role during CNS disease. Recreating the both trained and tolerant models through the peripheral lipopolysaccharide (LPS) injections using AD mouse models, immune training increases cerebral β-amyloidosis and reduce the levels of IL-10; whereas immune tolerant microglial phenotype showed a reduction of pro-inflammatory cytokines like IL-6, IL-1β and IL-12 reducing the number of plaques (Wendeln et al., 2018). Moreover, in stroke mouse models, the tolerant response induces a reduction of infarct size and microglial activation (Wendeln et al., 2018).

Microglia cells also participate in the innate immune response through the secretion of a wide range of inflammatory modulators such as cytokines, chemokines and reactive oxygen species (ROS) (Konat, Kielian, & Marriott, 2006; Lehnardt, 2010). In fact, microglia can produce pro-inflammatory cytokines like IL-1β, IL-6, and TNF-α in response to DAMs and PAMs presence. Specifically, microglial production of IL-1-α and TNF-α evokes a neurotoxic astrocyte profile in AD, PD or multiple sclerosis (MS) patients (Liddelow et al., 2017). Neurotransmitters also regulate microglia immune phenotype. For example, depending on the type of glutamate receptor stimulation, microglial cells showed an activated phenotype or limits their neurotoxicity capacity (Taylor, Diemel, Cuzner, & Pocock, 2002). Moreover, stimulation of cholinergic and adrenergic receptors via GABA signalling inhibits microglial responses (Lee, 2013). Regarding chemokines, activated microglia are characterized for the release of CXCL10, CCL19 and CCL2 that are involved in the recruitment of peripheral immune

cells that participates in the adaptive immune response in the damaged CNS (Aloisi, 1999; Gyoneva & Ransohoff, 2015; Ransohoff & Brown, 2012; Streit, 2000).

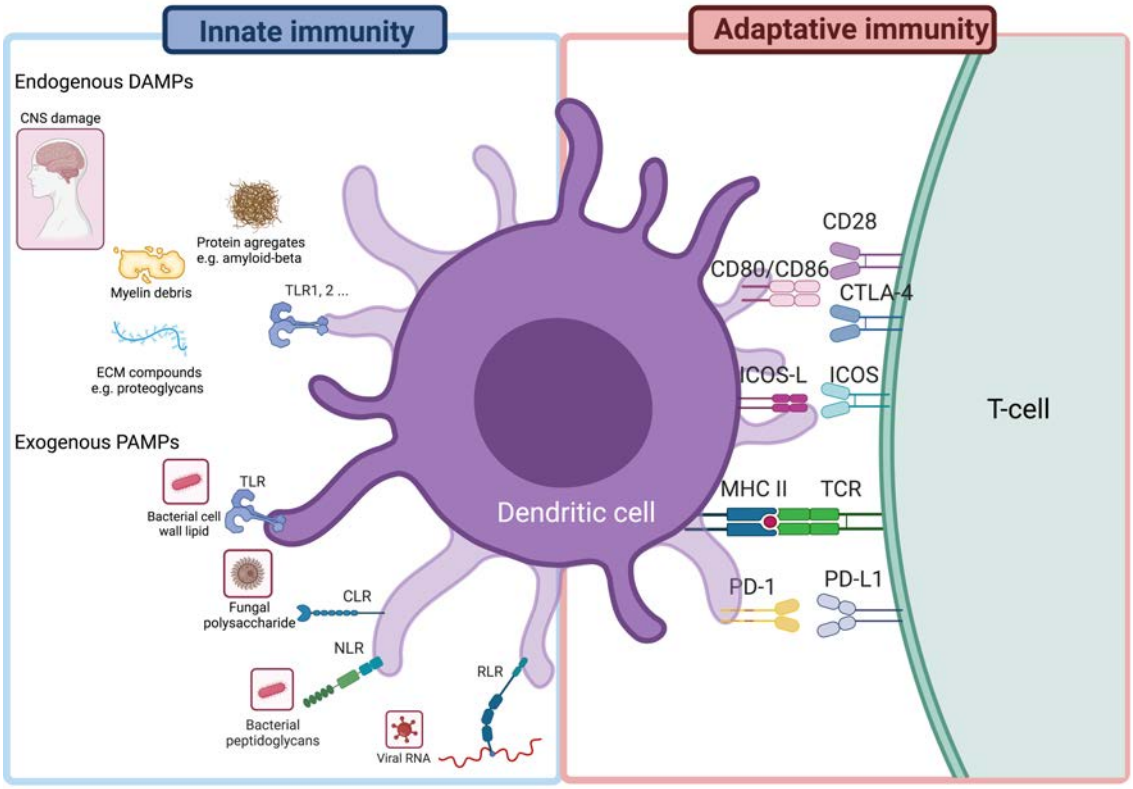

Figure 2. Innate vs adaptive immune response. *Microglial cells participate in innate immune response identifying endogenous damage-associated molecular patters (DAMPs) or exogenous associated molecular patterns (PAMPs) through the expression of a wide range of patter recognition receptors (PRRs). During adaptive immunity, microglial cells interact with T cells expressing costimulatory molecules such as MHCII, CD80, among others.*

3.4.2. Microglia in adaptive immunity

In many cases, innate immunity alone eradicates rapidly the damage; however, if a robust and more efficient response is desired the adaptive immunity must happen (Netea et al., 2016). Hence, one of the main objectives of innate immunity is to provide the essential information an input for adaptive immune response. The adaptive response is present in more complex vertebrates and requires the participation of specialized leukocytes, T and B cells, that generates specific surface molecules to control the damage. In the CNS, it is well known that in some chronic

neuroinflammatory diseases such as MS and narcolepsy, among others; adaptive immunity, instead of innate immunity, dominates the progression of the pathogenesis (Hemmer, Kerschensteiner, & Korn, 2015).

In addition to all the innate immune response's functions described above, microglia are the main endogenous CNS cells that are capable of presenting antigens to T cells participating in adaptive immune responses. Microglia has been described as the principal antigen-presenting cell (APC) within the CNS, under pathological conditions, due to their ability to express major histocompatibility complex-II (MHCII) and co-stimulatory molecules (Almolda, Gonzalez, & Castellano, 2011; Aloisi, 1999; Carson, 2002; Strachan-Whaley, Rivest, & Yong, 2014). Moreover, their phagocytic activity is crucial for the removal of apoptotic cells and clearance the debris in the injury site generating an appropriate microenvironment for regeneration and repair (Napoli & Neumann, 2009).

Infiltrated lymphocytes within the CNS parenchyma have been described under pathological conditions such as acute lesions like FNA, entorhinal cortex lesion or neurodegenerative diseases like MS (Babcock, Toft-Hansen, & Owens, 2008; Holmoy & Hestvik, 2008; Raivich et al., 1999). While in some circumstances lymphocyte infiltration has been associated with beneficial effects, as occurs in the FNA model, in other circumstances lymphocyte infiltration has been shown to contribute to the exacerbation of the pathology as occur in some autoimmune diseases (Dittel, 2008; Serpe, Sanders, & Jones, 2000). Infiltration of T-cells in the injured CNS requires their interaction with local APCs (Kawakami, 2004). Microglia cells play a crucial function modulating the lymphocyte response including their proliferation, differentiation and apoptosis trough the antigen presenting mechanism.

T-helper (Th) plays a key role in the regulation of immune responses and tissue inflammation. Depending on their pattern of cytokine production, Th cells can be divided into two major subtypes: T-helper 1 (Th1) lymphocytes, which produce pro-inflammatory cytokines like interferon gamma (IFN-γ) or TNF-α and T-helper 2 (Th2),

which secrete anti-inflammatory cytokines such as IL-4 and IL-10. However, the concept based on the presence/absence of Th1-Th2 has been increasingly questioned and overly simplistic, since other subpopulations of Th have been discovered such as effector T-cells including Th17, Th22, Th9, T-regulatory (Treg), among others (Gor, Rose, & Greenspan, 2003).

3.5. Role of peripheral macrophages in CNS diseases

Another important aspect to take into account is that additionally to microglia, peripheral macrophage infiltration is also crucial for the developing of some neurological diseases such as MS. Although, new transcriptomic techniques help us to differentiate between resident microglia and infiltrated macrophages, poor are known, especially when microglia become activated and controversial studies exist. The importance of infiltrating macrophages for neuroprotection, axonal regeneration and tissue repair has been reported in several studies. In an *in vitro* model of transected adult rat optic nerve; macrophages have the capacity to change the non-permissive environment to a permissive state for regeneration (David, Bouchard, Tsatas, & Giftochristos, 1990). Moreover, some studies have been described the role of infiltrated macrophages in axonal regeneration and healing following CNS injury, including enhancement of axonal growth and regeneration in sciatic nerve injury, promotion of functional recovery after spinal cord injury (SCI) supporting neuronal survival (Barrette et al., 2008; Cusimano et al., 2012; Shechter et al., 2009). The anti-inflammatory macrophages have been associated with their capacity to restrict accumulation of other inflammatory leukocytes such as neutrophils and to modify the inflammatory activity of microglia by the expression of anti-inflammatory cytokines (London, Cohen, & Schwartz, 2013). Despite the observations of beneficial roles of macrophages within the injured CNS, many studies have also reported detrimental roles. In patients with AD and MS patients, as well as in their animal models, macrophages infiltration has been associated with disease severity (Lucchinetti et al., 2000; Prineas & Wright,

1978). Popovich and co-workers found that the depletion of macrophages using clodronate liposomes improved neural and motor recovery after SCI (Popovich et al., 1999). Moreover, after EAE induction, animals genetically modified to avoid monocyte infiltration, showed less severe clinical disease suggesting that monocytes and not microglia evokes worsening of EAE (Ajami, Bennett, Krieger, McNagny, & Rossi, 2011). The mechanisms involved in these detrimental effects include the secretion of free radicals, proteases, and glutamate.

3.6. Inflammatory process modulation by cytokines: Role of IL-6 and IL-10 cytokines during inflammation in the CNS.

The balance between innate and adaptive immune responses within the CNS is orchestrated by cytokines. In fact, an uncontrolled production of cytokines could lead a chronic neuroinflammatory state. Furthermore, depending on the injury and the specific microenvironment, one cytokine might produce both pro- and anti-inflammatory effects.

In the CNS, cytokines are mainly secreted by neurons and glial cells (Mosmann & Coffman, 1989; Pineau & Lacroix, 2007; Vitkovic, Bockaert, & Jacque, 2000). Cytokines classically linked with pro-inflammatory properties, such as IL-1β, TNF-α, IFN-γ and IL-6, were found contributing to the disease progression in AD patients (Fakhoury, 2018; Sarlus & Heneka, 2017), and inducing microglia production of toxic factors such as reactive oxygen species (ROS) and nitric oxide (NO), which are harmful for the neurons (Hsieh & Yang, 2013; Smith, Das, Ray, & Banik, 2012). By contrast, the production of cytokines with anti-inflammatory properties, like IL-4, IL-10, IL-13 and transforming growth factor beta (TGF-ß), has been associated with neuroprotective effects and its production correlated with recovery phases in different CNS injuries (Al-Amin & Reza, 2014; McGeachy & Anderton, 2005; Vidal et al., 2013). Furthermore, anti-inflammatory molecules can suppress pro-inflammatory cytokine production and increase the presence of anti-inflammatory mediators in the environment (Laveti et al., 2013; Owens, 2002). In this regard, their immunomodulatory

effect has been studied in the CNS for many therapeutic approaches. Among the great variety of cytokines, our research group has been especially interested in the last years in two cytokines, the IL-6, as one of the main regulatory mediators of the neuroinflammation, and the IL-10, which is considered as a counter-regulatory cytokine involved in the termination of the inflammatory process.

3.6.1. Interleukin-6.

IL-6 was firstly studied in humans as a B-cell differentiation factor (Hirano, 1998) and presents a structure with a long-chain of four-helix bundle that binds to its specific receptor (IL-6R) (Kishimoto, Akira, Narazaki, & Taga, 1995). It is important to know that the binding of IL-6 to its receptor does not directly lead to an intracellular signalling as the association with the second transmembrane protein gp130, which acts as a signal transducer of IL-6, is necessary (Hibi et al., 1990). Signalling of IL-6 occurs via two different pathways: 1) the "classic signalling", via the membrane bound IL-6R (Kishimoto, 2010); or 2) the known as "trans-signalling", based on the presence of a soluble IL-6R molecule that allows that cells expressing gp130, but not IL-6R, on their membrane can be also stimulated by IL-6 (Campbell et al., 1993; Rose-John, 2012).

In the healthy CNS, low levels of both IL-6 and IL-6R expression was observed in neurons, glial cells and endothelial cells; whereas after a wide range of acute CNS injuries, such as traumatic brain injury (TBI), and neurodegenerative disorders, like AD, up-regulated levels of IL-6 has been detected (Erta, Quintana, & Hidalgo, 2012).

After CNS damage, both detrimental and beneficial roles of IL-6 have been described. Related with neuronal survival, IL-6 in combination with other cytokines such as IL-1β and TNF-α promotes neuronal death (Almolda et al., 2014; Conroy et al., 2004). However, expression of IL-6 could have neuroprotective effects after SCI, ischemia and sciatic nerve transection (Erta et al., 2012). Regarding microglia cells, *in vivo* and *in vitro* studies, demonstrated that IL-6 administration evokes microglial activation, increasing their proliferation capacity as well as its production of pro-

inflammatory molecules (Krady et al., 2008; Tilgner, Volk, & Kaltschmidt, 2001). Furthermore, increased levels of IL-6 promote microglial activation characterized by elevated levels of macrophage-1 antigen (MAC-1), Iba-1, CX3CR1, CD11b, class A Scavenger Receptor (SRA), CD68/ macrosialin and Ym-1 and increases their phagocytic activity (Campbell et al., 2014; Chiang, Stalder, Samimi, & Campbell, 1994). In addition, it has been demonstrated that administration of anti-IL-6R antibody decreases CD68-positive microglial cells following olfactory system's injury (Kobayashi, Tamari, Miyamura, & Takeuchi, 2013).

Related to T cell differentiation, it also accepted that IL-6 has the ability to drive lymphocyte differentiation as demonstrated by some studies where, in the presence of TGF-β, T-cell responses are polarized towards a T-regulatory phenotype, whereas the addition of IL-6 changes the phenotype of T-lymphocytes towards a Th17 pathogenic phenotype (Bettelli et al., 2006).

3.6.2. Interleukin-10.

Interleukin-10 (IL-10), first known as "cytokine synthesis inhibitory factor" (CSIF), was described as a novel immunoregulatory molecule secreted by type-2 T-helper cells that were able to inhibit the synthesis of IL-2 and IFN-γ in Th1 cells (Fiorentino, Bond, & Mosmann, 1989; Mosmann & Coffman, 1989; Strle et al., 2001). IL-10 is one of the most important immunoregulatory cytokines implicated in the immunological responses in the periphery and almost all immune cells can produce it (Lobo-Silva, Carriche, Castro, Roque, & Saraiva, 2016; Moore, de Waal Malefyt, Coffman, & O'Garra, 2001).

In the healthy CNS, both microglial and astrocytes produce IL-10 and the expression of the IL-10 receptor (IL-10R) has been described on microglia, astrocytes, oligodendrocytes, and neurons, depending on the type of injury (Ledeboer et al., 2002; Mizuno, Sawada, Marunouchi, & Suzumura, 1994; Molina-Holgado, Grencis, & Rothwell, 2001; Pousset, Cremona, Dantzer, Kelley, & Parnet, 2001; Strle et al., 2002; Xin et al., 2011; Zhou, Peng, Insolera, Fink, & Mata, 2009).

IL-10 is up-regulated after a wide range of CNS injuries including acute lesions, such as TBI, or in neurodegenerative diseases like EAE and AD (Apelt & Schliebs, 2001; Burmeister & Marriott, 2018; Garcia et al., 2017; Ledeboer et al., 2003). Although IL-10 has been classically defined with an anti-inflammatory profile, either beneficial and detrimental effects have been described in several *in vitro* and *in vivo* models of CNS injury, such as TBI, excitotoxicity and middle cerebral artery occlusion (MCAO), among others (Arimoto et al., 2007; Park, Lee, Jin, & Lee, 2007; Spera, Ellison, Feuerstein, & Barone, 1998; Xin et al., 2011). Moreover, different studies in the last years indicate that the route of IL-10 administration is essential for their protective or detrimental effects. Thus, we have previously demonstrated, that overproduction of IL-10 promotes neuronal survival after FNA (Villacampa et al., 2015). Furthermore, a complete prevention of EAE has been achieved by the intraparenchymal IL-10 administration, but when IL-10 was administered systemically there was no effect (Cua, Hutchins, LaFace, Stohlman, & Coffman, 2001) or, in some cases, worsened the disease (Cannella & Raine, 2004). Moreover, IL-10 also inhibits the expression of chemokines, such as C-C motif ligand (CCL)2 and C-X-C motif ligand (CXCL)2, which are implicated in the recruitment of monocytes, dendritic cells, neutrophils, and T cells (Kopydlowski et al., 1999).

3.7. Perforant pathway transection as a model to clarify mechanisms underlying inflammation response.

Perforant pathway transection (PPT) was established in the 1970s being one of the first models used to study neuronal plasticity in the adult brain (Lynch, Matthews, Mosko, Parks, & Cotman, 1972; Nadler & Cotman, 1978). This injury model consists in the disruption of the main excitatory input from the entorhinal cortex to the dentate gyrus (DG) of the hippocampus. Due to the highly laminated cytoarchitecture of the DG, this model is considered particularly useful because the lesion affects only one of

the many afferent fiber systems, making possible to easily recognize the denervated from the non-denervated layers.

3.7.1. Fascia dentata in normal mouse: entorhino-dentate projections, commissural projections, septo hippocampal projections.

The entorhinal cortex, through the perforant pathway (PP), is the main cortical source of input that the hippocampus receives (Amaral & Witter, 1989). Ramón y Cajal (1901) described the presence of fibers connecting the entorhinal cortex to the fascia dentata and hippocampus proper (cornu Ammonis). Electrophysiological studies had demonstrated that the axons of the PP constituted a powerful excitatory input to the hippocampus formed mainly by glutamatergic neurotransmitters (Adey, Merrillees, & Sunderland, 1956; Amaral & Witter, 1989). The entorhinal cortex is divided into two areas, the lateral entorhinal area (LEA) and the medial entorhinal area (MEA). Studies using anterograde and retrograde tracers in mouse, confirms that LEA is the origin of the lateral PP that terminates in the outer one-third of the molecular layer (ML) of the DG; whereas the MEA is the origin of the medial PP that ends in the middle one-third of the ML of the DG (van Groen, Miettinen, & Kadish, 2003). Moreover, it has been described that these two perforant pathways showed physiological and histochemical differences (Amaral & Witter, 1989). In contrast to other species, mouse projections to the ipsilateral DG originate exclusively from neurons located in layer II of the entorhinal cortex, and then the crossed entorhinodentate projection is lack in mice brain (van Groen, Kadish, & Wyss, 2002; van Groen et al., 2003).

The entorhinal cortex also projects to the CA3, CA1 and the subiculum of the hippocampus. In the case of both CA3 and CA1, the terminals are located in the stratum lacunosum moleculare (Stanfield, Caviness, & Cowan, 1979), whereas in the subiculum the terminals are in OML. These projections originate predominantly from neurons in layer III, but a small number of neurons in the deeper layers of the entorhinal cortex contribute to this projection. In mice, contralateral projection to the

CA3 and CA1 has been demonstrated and originate from the layer III of the entorhinal cortex. In the case of the subiculum, fibers are from both LEA and MEA, which is in contrast to most other species where its origin is restricted to the MEA area (Figure 3).

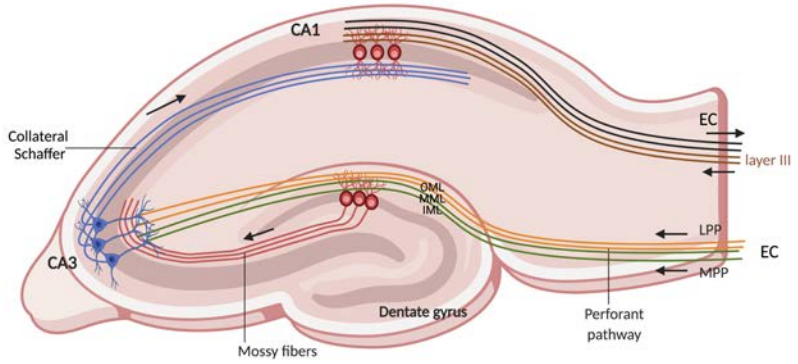

***Figure 3. Hippocampal connections**. The main inputs that hippocampus receives were from the entorhinal cortex (EC) that forms connections with the dentate gyrus (DG) and CA3 pyramidal neurons via the perforant path (PP). Specifically, the connections come from the lateral perforant pathway (LPP) and the medial perforant pathway (MPP) (orange and green). CA3 neurons also receive stimuli from the DG via the mossy fibres (red). CA3 neurons in turn send axons to CA1 pyramidal cells via the Schaffer's collateral (SC) (blue), as well as to CA1 cells in the contralateral hippocampus (blue). CA1 neurons also receive input directly from the EC layer III neurons (brown).*

3.7.2. Reorganization of the mouse fascia dentata after entorhinal cortex lesion

PPT causes the lost of about 80-90% of all synapses in the dennervated ML of the DG, followed by the reactive changes of nearby neurons that, by the mechanism of the collateral sprouting, replace up to 60-80% of all lost synapses by 4 weeks postlesion in rats (Deller, Del Turco, Rappert, & Bechmann, 2007). Several studies have been described structural and collateral sprouting differences between mice and rats. For example, in mice, the crossed PP seems to be almost absent (van Groen et al., 2002; van Groen et al., 2003). We will only explain the fiber's reorganization in the mouse because is the model that we used for the present study (Amaral & Witter,

1989; Deller et al., 2007). Collateral sprouting in mice is produced by: 1) glutamatergic commissural/associative (C/A) projections from mossy cells to the inner molecular layer (IML), 2) GABAergic fibers to the OML and 3) cholinergic septohippocampal fibers. In the following paragraphs we will describe it in detail. (Figure 4).

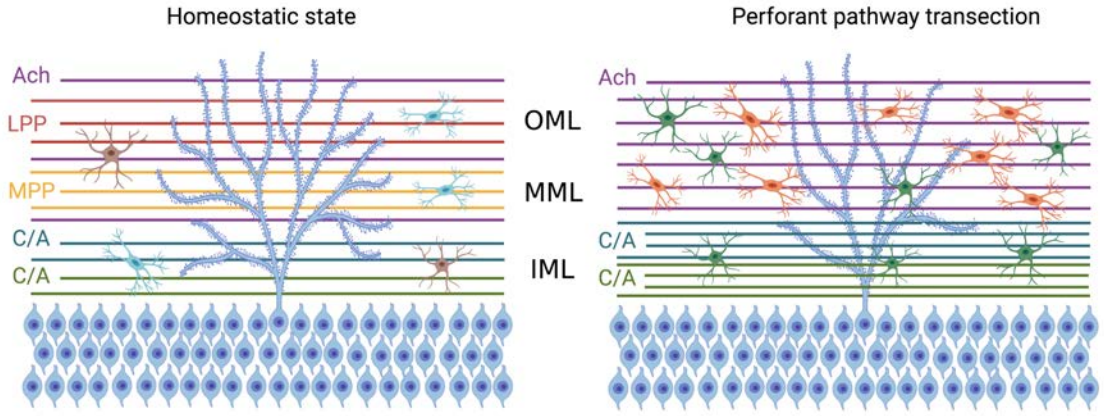

Figure 4. Hippocampal reorganitzation after PPT. *The molecular layer (ML) of the fascia dentate is a highly laminated structure with afferent inputs mainly originated from the entorhinal cortex. ML is divided in three specific regions: outer molecular layer (OML), medium molecular layer (MML) and inner molecular layer (IML). The apical dendrites of DG granule cells (blue) extend into the ML. Left figure: organization of ML in homestatic stage. The inner molecular layer (IML) is occupied by the glutamatergic commissural/associational fibers (C/A) that arise from mossy cells in the ipsi- or contralateral hilus. The middle and outer molecular layer (MML, OML) are occupied predominantly by the glutamatergic perforant path (MPP, LPP), which originates in the ipsilateral entorhinal cortex. Cholinergic axons (ACh) from the septal nuclei/diagonal band of Broca are interspersed throughout the molecular layer. Microglia (blue) and astrocytes (brown) is located through the ML. Right figure: PPT disrupts both medial and lateral perforant path evoking the elimination of the majority input into the dentate gyrus. Degeneration of these axons promotes sprouting in a laminar specific manner. Hence, the number of septohippocampal (Ach) and commissural/associational (C/A) increases in order to restore the synapsis loss. Microglia (orange) and astrocytes (green) become rapidly activated. Adapted from (Perederiy & Westbrook, 2013).*

Mossy cells are neurons located in the hilus of the dentate gyrus whose fibers, called associational/commissural fibers, project both ipsilaterally and contralaterally (Amaral & Witter, 1989). In mice, the mossy fibers are calretinin positive, which can

facilitate the identification of their unmyelinated axons in the IML by immunohistochemistry (Del Turco et al., 2003; Deller & Frotscher, 1997; Phinney, Calhoun, Woods, Deller, & Jucker, 2004). In addition, an expansion of the entire C/A termination zone was observed. However, this expansion of the IML should not be used as an indicator of C/A sprouting in C57BL/6 mice (Del Turco et al., 2003).

A second projection system that contributes to the reinnervation of the PPT-lesioned fascia dentata in rats is the GABAergic projections (Deller & Frotscher, 1997). Although the GABAergic projection to the OML has been described in healthy mice, no studies about the reorganization of these projections has been reported following PPT.

A third projection system contributing to the reorganitzation of the DG after PPT is the cholinergic septohippocampal fibers. This connection includes the cholinergic neurons located in the diagonal brand of Broca. In contrast to the C/A mossy fibers and the PP, these projections terminate in all the ML of the DG (Amaral & Witter, 1989). After PPT, an increase in the density of cholinergic (AChE-positive) fibers was observed in the dennervated area (Phinney et al., 2004; Stanfield et al., 1979; van Groen et al., 2002). Although these studies confirmed a significant increase in the density of AChE-positive fibers in single sections, Phinney and colleagues did not detect differences in the total length of AChE fibers concluding that the measurement of AChE fiber density in the dennervated OML should not be used as an indicator of cholinergic sprouting in mice.

Concomitant with this structural reorganization, morphological and functional changes in the post-synaptic mature granule cells has also been observed. The loss of the excitatory inputs in these granule neurons produces a retraction of dendrites, evoking a reduction of dendritic arbors complexity in the denervated area (Vuksic et al., 2011). In fact, around 90 days post-lesion a progressive lost of distal dendritic segments has been described, showing some recovery by 180 days post-lesion (Vuksic et al., 2011).

3.7.3. Signals that induce and promote collateral sprouting.

Over the past years, the study of the molecules involved in the regulation of the sprouting process has been a great interest. To identify the molecular and cellular crucial players during the sprouting process, the PPT model is once again a useful experimental paradigm. After PPT, these molecules has been identified as neurotrophic factors including the nerve growth factor (NGF), BDNF, ciliary neurotrophic factor (CNTF) as well as also compounds of the extracellular matrix (ECM), like tenascin-C, DSD-1 proteoglycan, reelin, brevican and neurocan; most of them produced by astrocytes (Deller, Haas, & Frotscher, 2001).

3.8. *Microglia activation after PPT.*

Microglia activation in the PPT paradigm has been extensively studied (citas). Few hours after PPT, microglia located within the OML and the medium molecular layer (MML) begin to display an activated morphology, which had developed slightly hypertrophic cell bodies with stout proximal processes and decreased distal ramifications. Around 24 hours after transection, microglial cells also begin to accumulate at the border between MML and IML zone, which was partially depleted for microglia (Dissing-Olesen et al., 2007). In the following hours, the morphological transformation of microglia is more marked until acquiring a hypertrophic microglia of a “bushy” appearance. During the first week, microglia activation persists and around the second week microglia starts recovery their homeostatic phenotype. Moreover, accumulation of groups of microglia cells was observed during the first days showing the so-called microglia “nests”, which have been related with microglial proliferation (Dissing-Olesen et al., 2007). This morphological change occurs in parallel to an up-regulation of certain activation markers such as Iba1, CD11b, CD45, CD34 and Mac 1 (Finsen et al., 1999; Ladeby, Wirenfeldt, Garcia-Ovejero, et al., 2005) and adhesion molecules like ICAM1, VLA-4 and LFA-1 (Hailer, Grampp, & Nitsch, 1999). Furthermore, MHCII and CD86 expression was observed only by subpopulations of the

PPT- induced activated microglia. The fact that microglial cells up-regulate molecules related with both innate and adaptive immunity such as TLR2, MHC-II and the co-stimulatory molecule CD86 points to their active role in the cross-talk with infiltrating leukocytes after PPT (Babcock et al., 2006; Bechmann, Peter, Beyer, Gimsa, & Nitsch, 2001).

PPT evokes a notable increase in the number of microglia/macrophages population during the first week (Dissing-Olesen et al., 2007; Finsen et al., 1999; Hailer et al., 1999; Ladeby, Wirenfeldt, Garcia-Ovejero, et al., 2005; Matthews, Cotman, & Lynch, 1976). Although microglia proliferation has been considered the main causes of microglia expansion after PPT; cell migration from adjacent non-affected areas, such as the IML, the CA1 and hilus and the recruitment of blood-derived cells also participate in this population expansion. (Hailer et al., 1999; Jensen, Gonzalez, Castellano, & Zimmer, 1994; Ladeby, Wirenfeldt, Dalmau, et al., 2005; Ladeby, Wirenfeldt, Garcia-Ovejero, et al., 2005; Wirenfeldt et al., 2007). In parallel of all this events, microglia cells produce a wide range of soluble factors, including several cytokines such as TGFβ1, IL-10, IL-6, IL-1β, TNF-α, IGF-1 and chemokines such as CCL2 that participates in the lesion outcome and can be involved in sprouting promotion (Babcock, Kuziel, Rivest, & Owens, 2003; Babcock et al., 2008; Finsen et al., 1999; Grebing et al., 2016; Ladeby, Wirenfeldt, Garcia-Ovejero, et al., 2005).

A part of microglia activation, it is well described that PPT evokes leukocytes infiltration, including macrophages and T cells (Babcock et al., 2003; Babcock et al., 2008; Bechmann et al., 2005; Fux, van Rooijen, & Owens, 2008). In this context, microglial cell “nests” have also been related with interaction with myelin specific T-cells after PPT (Grebing et al., 2016).

As we mentioned above, transection of the PP also results in anterograde axonal and a dense terminal degeneration, causing accumulation of myelin debris that persists for several weeks until it is eventually cleared by phagocytic microglia (Jensen

et al., 1994; Matthews et al., 1976). In this context, it has been reported the intracellular presence of myelin basic protein (MBP) particles in activated microglia cells after PPT.

Altogether, the important role of microglial cells during the immune response and their sensibility depending the milieu highlighted the importance to elucidate how both pro-inflammatory and anti-inflammatory cytokines may play in regulating the evolution and the outcome of PPT. In this context, the use of transgenic animals producing (either IL-6 or IL-10) within the CNS will be useful a tool to understand the role-played by these molecules in regulating glial and immune responses associated with anterograde degeneration.

4. HYPOTHESIS AND OBJECTIVES

Changes in the tissue microenvironment generated by modifications in specific cytokines polarize microglia conditioning their response to an inflammatory process in the central nervous system.

General objective:

To determine the modifications that local overproduction of IL6 and IL10 cytokines can exert on microglia cells and their implication in the evolution and resolution of the inflammatory process associated with an anterograde axonal injury.

Specific objectives:

1. To analyze the effects of astrocyte-targeted IL-6 and IL-10 production on microglial phenotype in the hippocampus under homeostasis.
2. To characterize the effects of astrocyte-targeted IL-6 and IL-10 production on the pattern of microglial activation in the ML of the DG after PPT.
3. To analyze the influence of astrocyte-targeted IL-6 and IL-10 expression on the monocyte/macrophage recruitment in the ML of the DG after PPT.
4. To determine the changes induced by astrocyte-targeted IL-6 and IL-10 production on lymphocyte infiltration and their differentiation in Th1, Th2, Th17 and T-reg in the ML of the DG after PPT.
5. To characterize the influence of astrocyte-targeted IL-6 and IL-10 expression on the molecular interactions between microglia/macrophages cells and infiltrated lymphocytes in the ML of the DG after PPT.
6. To analyze the changes induced by astrocyte-targeted IL-6 and IL-10 production on the profile of cytokines and chemokines expression after PPT.
7. To determine the changes induced by astrocyte-targeted IL-6 and IL-10 production on the communication microglia/neuron after PPT.

8. To asses the influence of astrocyte-targeted IL-6 and IL-10 production on collateral sprouting in the ML of the DG after PPT.

5. MATERIAL AND METHODS

5.1. Experimental animals

GFAP-IL6Tg, GFAP-IL10Tg and their corresponding wild-type (WT) littermates of both sexes were used in this study. Animals were bred at the Institute of Neurosciences of the Universitat Autònoma de Barcelona (UAB), maintained at constant temperature (24 ± 2 °C) and housed on a 12-hour light/dark cycle with food and water *ad libitum* during all the experiment. All experimental animal work was conducted in accordance to Spanish regulations (Ley 32/2007, Real Decreto 1201/2005, Ley 9/2003 and Real Decreto 178/2004) in agreement with European Union directives (86/609/CEE, 91/628/CEE and 92/65/CEE) and was approved by the Ethical Commission of the UAB. All efforts were made to minimize the number of animals used to produce reliable scientific data, as well as animal suffering.

5.2. Construction of GFAP-IL-10 fusion gene and production of transgenic mice.

The full-length cDNA encoding murine IL-10 was cloned into a construct containing the mouse glial fibrillary acidic protein (GFAP) promoter and the polyadenylation signal sequence from the human growth hormone gene (hGH), as previously described (Campbell, Stalder, Akwa, Pagenstecher, & Asensio, 1998). Briefly, the GFAP-IL-10 construct was microinjected into fertilized eggs from SJL/L mice. Transgenic offspring were identified by PCR using genomic DNA extracted from tail biopsies for the detection of hGH. The F1 offspring were backcrossed with the C57/BL6 strain for at least 10 generations to obtain the GFAP-IL-10Tg mice used in our study along with their corresponding wild-type (WT) littermates.

5.3. Construction of GFAP-IL6 fusion gene and production of transgenic mice.

Construction and characterization of the GFAP-IL6 transgenic mice was described previously (Campbell et al., 1993). Briefly, an expression vector derived from the GFAP gene was used to target expression of IL-6 astrocytes. A full-length cDNA for murine IL-6 was modified by replacing the 3' untranslated region with a 196-bp simian virus (SV40) late-region fragment providing a polyadenylyation signal. Then, the GFAP fusion genes were injected into fertilized eggs of (C57BL/6J x SJL) F1 hybrid mice, and transgenic offspring were identified by slot-blot analysis of tail DNA with 32P-labeled SV40 late-region fragment.

5.4. Lesion model and experimental groups

5.4.1. *Perforant pathway transection*

Adult (6-7 months-old) GFAP-IL6Tg, GFAP-IL10Tg and their corresponding WT mice were subjected to wire-knife unilateral PPT. Briefly, animals were intraperitoneally (i.p.) anaesthetized with a solution of ketamine (80mg/kg) and xylacine (20mg/kg) at dose of 0.1 mL/g body weight. Animals were fixed in a stereotaxic device (Kopf Instruments®) and a drilled trepanation was made on the left side of the skull (4.6 mm dorsal to Bregma and 2.5 mm laterally). A folded wire-knife (McHugh Milleux, m121) was inserted at an angle of 15º anterior and 10º lateral. The knife was unfolded at 3.6 mm ventrally and the perforant pathway was transected retracting the knife 3.3 mm. Finally, the knife was folded, take it out of the brain, and the skin was sutured with 2-0 silk and clean with iodine.

Non-lesioned and lesioned animals were distributed in different experimental groups for immunohistochemistry (IHC), flow cytometry and protein analysis, as detailed in Table 1.

5.5. Immunohistochemistry techniques

5.5.1. Tissue processing for IHC

Animals were i.p. deeply anaesthetized with a solution of ketamine/xylacine, as described above but injected at dose of 0.15 mL/g , and then intracardially perfused for 10 min with 4% paraformaldehyde in 0.1M phosphate buffer (pH 7.4). For Timm staining, animals were injected intraperitoneally with sodium selenite (10 mg/Kg) one hour before the sacrifice. Brains were immediately removed and post-fixed for 4h at 4ºC in the same fixative. Subsequently, after phosphate buffer rinses, samples were cryopreserved for 48h in a 30% sucrose solution and frozen with 2-methylbutane solution (320404, Sigma-Aldrich). Series of transversal parallel sections (30-μm-thick) were obtained using a Leica CM3050 cryostat and stored in free-floating Olmos anti-freeze solution at -20ºC until used.

5.5.2. Immunohistochemistry and immunofluorescence

For single immunohistochemistry, sections were washed several times with 0.05M Tris-buffered saline (TBS) pH 7.4 and with TBS containing 1% Triton-X100 (TBST, pH7.4). In the case of Pu.1 staining, sections were exposed to antigen retrieval protocol by treatment with sodium citrate buffer (pH 8.5) for 40 min at 80ºC. Subsequently, after 10 min of endogenous peroxidase blocking with 2% H_2O_2 in 70% methanol, sections were blocked for 1h in blocking buffer solution-1 (BB-1) containing 10% fetal bovine serum and 0.3% bovine serum albumin in TBST. After that, sections were incubated overnight at 4ºC followed by 1h at room temperature (RT) with primary antibodies diluted in BB, as specified in Table 1.

Sections from spleen and gut were used as positive control and sections incubated in BB-1 lacking the primary antibody were used as negative control. After washes with TBST, sections were incubated for 1h at RT with their respective secondary antibody (Table 1) diluted in BB. After 1h at RT in streptavidin-peroxidase, the reaction was visualized by incubating the sections in 3,3-diaminobenzidine (DAB) kit (SK-4100;

Vector Laboratories, USA) following the manufacturer's instructions. Finally, sections were mounted on slides, counterstained with 1% toluidine blue, dehydrated in graded alcohols and, after xylene treatment, coverslipped with DPX.

For double immunolabelling, sections were firstly processed as described above, but using a fluorochrome conjugated antibody as secondary antibody (Table 1). After several washes with TBST, sections were incubated for 1h at RT in BB. After washes, sections were incubated with secondary primary antibodies (Table 1), diluted in BB, overnight at 4ºC followed by one additional hour at RT. Subsequently, sections were washed with TBST and incubated with biotinylated secondary antibody (Table 1). Finally, sections were washed with TBST, followed by TBS and TB and the nuclei stained with 4,9,6-diamidino-2-phenylindole (DAPI) for 10 min (Table 1).

5.6. Terminal dUTP Nick End Labeling (TUNEL)

For Tunel staining, sections were mounted on slides and treated for 5 min with 100% methanol for endogenous peroxidase blocking. Then, sections were rinsed in 10 mM Tris buffer (pH 8) and 5 mM EDTA followed by incubation for 15 min at RT in the same buffer plus Proteinase K (20 μg/mL). After several washes with 5 mM EDTA, sections were incubated for 10 min at RT in TdT buffer containing 30 mM Tris, 140 mM sodium cacodilate and 1 mM cobalt chloride (pH 7.7). Sections were then incubated for 20 min at 37ºC in TdT buffer plus 0.161 U/μL TdT enzyme (Terminal Transferase, 3333566 Roche, Manheim, Germany) and 0.0161 nmol/μL of biotin-16-dUTP (1093070, Roche, Manheim, Germany). The reaction was stopped by submerging sections twice in citrate buffer (300 mM sodium chloride, 30 mM sodium citrate, 5 mM EDTA) for 5 min. After several washes with TBS, sections were incubated for 1 hour at RT with horseradish peroxidase-conjugated streptavidin (Table 1) and the peroxidase reaction visualized by incubation in a 3,3-DAB kit plus 1% of cobalt (SK-4100; Vector Laboratories, USA), following the manufacturer's instructions. After that, sections were incubated with Iba1

antibody (1:1000) (Table 1) using the same protocol described in the single IHC section. Sections from gut were used as positive control. Finally, sections were dehydrated in graded alcohols and, after xylene treatment, coverslipped in DPX.

5.7. FD Neurosilver kit™

Degenerative fibers in the OML and MML of the DG after PPT were analyzed on sections stained using the FD Neurosilver kit™ (PK301A, FD Neurotechnologies) according to manufacturer's instructions. Briefly, sections were incubated with 4% of PF for 7 days at 4ºC. After washes with destilated water, sections were incubated two times with solution A and B for 10 min each followed by incubation with solutions A, B and E for 10 min. Sections were then incubated two times with the mixture of solution C and F for 2 min. After that, sections were incubated with the solution D and F for 5 min followed by several washes with distilled water and solution G. Finally, sections were mountes in slides, dehydrated in xylene treatment coverslipped with DPX.

5.8. Timm Staining

Sprouting evaluation was done using the Timm staining technique, which reveals zinc and other heavy metals mainly located in the hippocampal mossy fibers. Sections were incubated to visualize metal precipitates, as described by Danscher (1982). Briefly, slides were rinsed for 15 min in 95% EtOH, then 2 minutes each in 70% alcohol, 50% alcohol and rinsed again for 30 min with dH_2O. Following rehydration, sections were incubated with the developer solution that contains arabic gum, sodium citrate, hydroquinone and silver lactate for 60 min in a water bath at 26ºC and protected from light (Danscher 1981). After that, sections were incubated for 12 min in 5% sodium thiosulfate and rinsed again with distillated water. Sections were postfixated for 30 in 70% of alchohol, dehydrated in xylene treatment and coverslipped with DPX.

5.9. Analysis and quantification

Densitometry quantification was performed with at least three WT and three Transgenic animals per group were analyzed. A total of 9 photographs from 3 different sections per animal containing the deafferented ML of DG in lesioned animals and the equivalent area in the NL were captured using the 20x objective with a DXM 1200F Nikon digital camera joined to a brightfield Nikon Eclipse 80i microscope, using the ACT-1 2.20 (Nikon corporation) software. By means of analySIS®, both the percentage of area occupied by the immunolabelling as well as the intensity of the immunoreaction (Mean Grey Value Mean) was recorded for each photograph. The AI index (Almolda et al., 2015) was calculated as function of the percentage of the immunolabelled area and the Mean Grey Value Mean.

Quantification of cell density was obtained using the "Automatic Cell Counter" (ITCN) plug-in from NIH Image J® software (Wayne Rasband, National Institutes of Health, USA). Data were expressed as cells/mm^2. In this case, a total of 6 photographs from 3 different sections per animal containing the deafferented ML of DG in lesioned animals as well as the equivalent area in the NL were captured with the 10x objective, using the same device and software referred above.

For manually quantification, cells in the ML of DG were manually counted on 20 different sections per animal using a 20x objective. Data were averaged and represented as cells/section.

5.10. Flow cytometry

5.10.1. *Tissue processing*

Animals were i.p. anaesthetized, as described above, and intracardially perfused for 1 min with cold 0.1M phosphate buffer solution (PBS). The brain was removed and the entire hippocampus was quickly dissected out.

5.10.2. Flow cytometry protocol

The phenotype of microglia/macrophage and lymphocyte populations in NL and PPT-lesioned animals were analyzed using flow cytometry as previously described (Almolda, Costa, Montoya, Gonzalez, & Castellano, 2009). In order to obtain a cell suspension, samples were dissociated through 140 µm and 70 µm meshes and digested for 30 min at 37ºC using type IV collagenase (17104-019, Life Technologies) and DNAsa I (D5025, Sigma). Subsequently, each cellular suspension was centrifuged at RT for 20 min at 2400 rpm in a discontinuous density Percoll gradient (17-0891-02, Amersham-Pharmacia) between 1.03 g/ml and 1.08 g/ml. Myelin in the upper layer was removed. Cells in the interphase and the clear upper-phase were collected, washed in PBS plus 2% serum and the Fc receptors were blocked by incubation for 10 min at 4ºC in a solution of purified CD16/32 diluted in PBS plus 2% serum. Afterwards, cells were labelled for 30 min at 4ºC with their respective antibodies (Table 2). In parallel, isotype-matched control antibodies for the different fluorochromes (BD Pharmingen) were used as negative control and a cell suspension of splenocytes as positive control. Data were extrapolated as number of cells using Cyto Count™ fluorescent beads, following the manufacturer's instructions (S2366, Dako Cytomation). Finally, cells were acquired using a FACS Canto flow cytometer (Becton Dickinson, San Jose, CA) and results analyzed using the FlowJo® software. The analysis was performed separately for each animal without any pooling.

5.11. Molecular biology techniques

5.11.1. *Tissue processing*

Anaesthetized animals, as described above, were intracardially perfused for 1 min with 0.1M phosphate buffer solution (PBS), the brain was removed and the entire hippocampus was dissected out, snap frozen individually in liquid nitrogen and stored at -80ºC until be used.

5.11.2. Enzyme-Linked ImmunoSorbent Assay (Elisa)

M-CSFR ELISA kit (MBS176501, MyBioSource) was performed according to manufacturer's instructions. Briefly, 100 µL of standards and hippocampus samples, with a final total protein concentration of 1 µg/µL, were added to the pre-coated plate and incubated for 90 min at 37ºC. Subsequently, the plate was incubated with 100 µL of biotinylated anti-mouse M-CSFR antibody for 60 min at 37ºC. After three washes with PBS, 100 µL of Avidin-Biotin-Peroxidase Complex (ABC) solution was added to the plate and incubated for 30 min at 37ºC followed by several washes with PBS. After that, samples were incubated with 90 µL of 3,3',5,5'-Tetramethylbenzidine (TMB) for 20 min at 37ºC, followed by 100 µL of TMB stop solution to each well. Finally, iMark Microplate Reader (Biorad) was used to read the plate at 450 nm. Data were expressed as pg/mL of protein.

5.11.3. Multiplex assays using Luminex®

The cytokines and the chemokines levels were analyzed using a Milliplex® MAP Mouse Cytokine/Chemokine kit (#MCYTOMAG-70K, Merck Millipore) according to manufacturer's instructions. Briefly, 25 µL of each hippocampus extracts with a final total protein concentration of 2.5 µg/µL were added to the plates, along with the standards in separate wells, containing 25 µL of custom fluorescent beads and 25 µL of matrix solution, and incubated overnight at 4ºC in a plate-shaker (750 rpm). After two washes with wash buffer (1x), the plate was incubated with 25 µL of detection antibodies for 30 min at RT followed by incubation with 25 µL of Streptavidin-Phycoerythrin for 30 min at RT in a plate-shaker (750 rpm). Finally, the plate was washed twice with wash buffer and 150 µL of Drive fluid was added. Luminex® MAGPIX® device with the xPONENT® 4.2 software was used to read the plate. Data were analyzed using the Milliplex® Analyst 5.1 software and expressed as pg/mL of protein.

5.12. Statistical analysis

Statistics were performed using the Graph Pad Prism 5.0 ® software. Unpaired Student's T-test to compare between WT and transgenic animals was used to determine significant differences. All experimental values were expressed as mean values ± SEM.

6. SUMMARY OF RESULTS AND DISCUSSION

This doctoral thesis is the compendium of the studies we have done to characterize the effects of chronic CNS-local overproduction of either IL-6 or IL-10 on microglial phenotype in homeostatic conditions and the pattern of microglial activation, leukocyte infiltration, cytokine/chemokine expression and sprouting process associated to anterograde degeneration. Specifically, along these studies, two lines of transgenic mice producing the pro-inflammatory IL6 or the anti-inflammatory IL10 using GFAP as promoter and expressed by astrocytes, were used: the GFAP-IL6Tg, characterized more than twenty years ago (Campbell et al., 1993), and the GFAP-IL10Tg generated in our laboratory and described by our research team (Almolda et al., 2014).

6.1. Chronic overexpression of IL6 or IL10 induces modifications in the NL hippocampus

6.1.1. *Both IL6 and IL10 overexpression induces an increase in the number of microglia/macrophages and modifies their phenotype.*

In NL conditions, both GFAP-IL6Tg and GFAP-IL10Tg mice show differences in the microglial population compared to WT, characterized by an increased number of microglia/macrophages and changes in their phenotype. Specifically, both animals presented higher number of CD11b+/CD45$^{low/int}$ and CD11b+/CD45^{high} cells (Article 1 and 2). Due to the lack of differences in proliferation, we suggested that chronic production of IL6 and IL10 could modulate the microglial population dynamics by either modifying the trafficking of monocytes, as we will explain below, or even changing the events of microglial colonization during development. In fact, preliminary results from our laboratory revealed higher numbers of microglial/macrophages in the hippocampus of NL GFAP-IL6Tg and NL GFAP-IL10Tg animals also during postnatal stages.

We also observed an altered microglial phenotype in both GFAP-IL6Tg and GFAP-IL10Tg mice, presenting 1) markers of general activation (higher Iba1, CD11b and CD45); 2) markers indicative of the activation of the phagocytic machinery (more

CD16/32 and CD68) and 3) higher expression of CD200R, pointing to modifications in the communication with neurons by CD200 (Article 1 and 2)(Figure 2-3). However, both transgenic animals presented particularities in this activated microglial phenotype. Additionally to all the mentioned markers, microglial cells in GFAP-IL10Tg animals also present the *novo* expression of CD150, a glycoprotein receptor, associated to T cell interactions (Howie et al., 2002). Several studies demonstrated that IL10 induces CD150 expression in microglial cells resulting in impaired T-cell responses (Almolda et al., 2015; Mantovani et al., 2004; McBride, Jung, de Vries, & Aversa, 2002; Zhang, Zhang, & You, 2018). In GFAP-IL6Tg mice, on the other hand, we highlight the apparition of a unique $CD11b^{+}/CD45^{high}/MHCII^{-}/CD86^{+}$ microglia population in the parenchyma, suggesting that CD86 probably develops an alternative role independent of MHCII (Article 2). Nolan et al found a similar phenotype in peripheral macrophages associated with innate immune responses (Nolan et al., 2009).

In parallel to changes in the microglial phenotype, we also reported modifications in the population of perivascular macrophages (PVM). Indeed, while in NL WT and NL GFAP-IL10Tg mice PVM express MHCII and CD86, confirming their role as APCs, in NL GFAP-IL6Tg animals PVM additionally express CD80 (Article 1 and 2). The apparition of this costimulatory molecule, usually induced only later after activation (Sharpe & Freeman, 2002), exclusively in this transgenic animal indicates that chronic production of IL6 generates an inflammatory environment that is able to transform PVM in the APC observed in chronic neuroinflammatory situations like EAE.

6.2. Both IL6 and IL10 induces infiltration of peripheral immune cells

Concomitant to microglial modifications, transgenic animals also presented a higher infiltration of peripheral immune cells in homeostatic conditions. Both GFAP-IL6Tg and GFAP-IL10Tg mice presented major number of intraparenchymal monocytes ($CD11b/CD45^{high}/Ly6C^{+}$ cells), phenomenon that could participate in increasing the number of microglia/macrophages cells in these animals. Regarding

lymphocytes, only GFAP-IL6Tg mice presented a higher number of T cells in the NL parenchyma (Article 1 and 2). Among all the T cells subtypes studied, it is interesting to mention that GFAP-IL6Tg animals show increased presence of $CD4^+$ T-helper, $CD8^+$ T-cytotoxic and $CD3^+/CD4^-/CD8^-$ γδ T cells (Article 2). In *in vitro* studies, it was demonstrated the ability of IL6 to induce a unique non-classical effector $CD8^+$ T cell subpopulation, called Tc17, whose primary function is to contribute to inflammation and the infiltration of lymphocytes and myeloid cells and characterized by a higher production of IL-17 (Gartlan et al., 2015; Mittrucker, Visekruna, & Huber, 2014). In our study we demonstrate higher IL17 production together with higher presence of CD8+ T-cells opening the possibility that these T-cells could correspond to the Tc17 subpopulation (Article 2). In the case of GFAP-IL6Tg, modifications in the peripheral immune cell's trafficking could be attributed to the disruption of the BBB, as widely reported (Brett, Mizisin, Powell, & Campbell, 1995; Campbell et al., 1993). However the explanation underlying this result in GFAP-IL10Tg remains unknown, as no apparent alterations in the BBB or in the principal chemoattractant molecules, CXCL10 and CCL2, were reported in these mice in homeostasis (Article 1).

Due to the changes observed in the infiltration of T-cells as well as in the costimulatory molecules in both parenchymal microglial/macrophages and PVM populations, we want to explore whether these populations are really communicating to each other. Then, we analyse the expression of CD28 and CTLA-4, the principal co-receptors of CD86 and CD80, in T-cells. Our results show that although NL GFAP-IL6Tg mice presented PVM with enhanced costimulatory machinery, with CD80 and CD86, the higher number of infiltrated T cells do not express either CD28 or CTLA-4, indicating that PVM do not activate T-cells, at least in a CD28 and CTLA-4-dependent manner (Article 2). In this sense, some studies suggested that CD80/CD86 costimulation by APCs could be produced through an alternative receptor like CD276 (Janakiram et al., 2017; Mandelbrot et al., 2001).

Finally, we also observed differences in the cytokine milieu in the hippocampus of both transgenic animals. These differences are higher in GFAP-IL6Tg mice, showing increased in the pro-inflammatory IL-6 and IL-17 and the anti-inflammatory IL-10 and IL-13 cytokines, but mild in GFAP-IL10Tg mice with only IL10 up-regulation (Article 1 and 2). It is important to mention that although GFAP-IL6Tg mice show a BBB disruption, the IL6 serum levels in this transgenic animal shows no differences with WT discarding and effect of astrocyte-targeted production of IL6 on the peripheral immune system (Article 2).

Taking all the results of both transgenic NL animals, we hypothesize that microglial cells in both GFAP-IL6Tg and GFAP-IL10Tg are in a “primed” state as a consequence of the chronic and local production of IL6 and IL10. The different environments generated in transgenic animals would act as a polarization stimuli, conditioning the response of microglia cells to a second stimulus. The concept of primed microglia was first described as an altered microglial activation state produced by the presence of an initial inflammatory stimuli, such as LPS-administration, but actually was also observed in physiological processes like aging (Garner, Amin, Johnson, Scarlett, & Burton, 2018; Neher & Cunningham, 2019; Niraula, Sheridan, & Godbout, 2017). Apart from their activation state, the response of primed microglial to a second inflammatory stimuli, is different, either enhancing or supressing their activation depending on the type, duration and intensity of the initial stimuli (Neher & Cunningham, 2019). Hence, if our hypothesis is true, we expect that the primed microglia observed in GFAP-IL6Tg and GFAP-IL10Tg will respond different to a second stimulus, which in our case was the transection of the perforant pathway.

6.3. Chronic overproduction IL-6 and IL-10 modulates the immune response after PPT

After the second stimuli, the PPT lesion, microglial cells observed in GFAP-IL6Tg and GFAP-IL10Tg animals respond differently compared to its respective WT. As we will explain in the following paragraphs, the number and the phenotype of microglial cells, the infiltration of peripheral immune cells, specially T cells, as well as the cytokine environment are modified in both transgenic animals. These alterations induce changes in one of the aspects of the resolution of the injury, the axonal sprouting process. Thus, while in GFAP-IL10Tg animals no difference compared to WT is observed in the ability to generate axonal sprouting, GFAP-IL6Tg animals showed a reduction in this property.

6.4. Chronic overproduction of IL-6 and IL-10 modifies microglia cell density and phenotype.

In the PPT paradigm, microglial cells located in the dennervated areas (the OML and MML) of the DG, rapidly respond changing their morphology and upregulating a wide range of molecules related with general activation like Iba1, CD45 and with the antigen presentation functions like MHCII and CD86 (Bechmann et al., 2001; Jensen, Finsen, & Zimmer, 1997; Wirenfeldt et al., 2005; Wirenfeldt et al., 2007). Microglial cells also reacts increasing their proliferation rate at early time points and phagocytise the debris, derived from PP degenerating fibers, which have accumulated in the dennervated area. Although microglia proliferation has been considered the main causes of microglia expansion after PPT; it is well established that microglia from non-affected area, such as the IML, the CA1 and the hilus, migrates to the OML and MML also participating in the immune response (Hailer et al., 1999; Jensen et al., 1994; Ladeby, Wirenfeldt, Dalmau, et al., 2005; Ladeby, Wirenfeldt, Garcia-Ovejero, et al., 2005; Wirenfeldt et al., 2007). Finally, microglia cells return to homeostatic phenotype while the sprouting process is taking place.

In the present study we observe that microglial activation in both GFAP-IL6Tg and GFAP-IL10Tg presented a different pattern characterized by an increased number of cells and changes in their phenotype related mainly to their phagocytic capacity and their antigen presenting skill (Article 1 and 2). The increased microglial/macrophage cell density observed in GFAP-IL6Tg mice is associated to higher proliferation, correlating with the well described role of IL-6 promoting microglial proliferation (Kloss, Kreutzberg, & Raivich, 1997; Streit, 2000), and with the increased recruitment of bone marrow derived monocytes ($Ly6C^{+}$) as a result of the BBB breakdown and the increased levels of chemokines (CXCL10 and CCL2) (Article 2). However, in GFAP-IL10Tg the augmented density of microglia/macrophages is only induced by monocyte recruitment, due to the higher levels of chemokines, as no modifications in the BBB integrity and lower proliferation rate were observed after PPT (Article 1).

However, despite both transgenic animals presented increased number of microglia/macrophage population, when the dynamics of microglial activation along the lesion is compared to their respective NL animals, the net change in microglial/macrophage cell activation after PPT is less pronounced in both GFAP-IL6Tg and GFAP-IL10Tg mice than in WT. Moreover, comparing the activation profile of both $CD11b+CD45^{low/int}$ and $CD11b+CD45^{high}$ populations, we suggested that they probably develop similar functions as they shared major part of activation markers (Article 1 and 2).

Concomitant with these differences in the microglia/macrophage cell density, microglial cells also display an altered microglial activation pattern in both transgenic animals after PPT compared to their WT. Microglial/macrophage population in both GFAP-IL6Tg and GFAP-IL10Tg mice shows increased levels of general activation markers (Iba1, CD11b and CD45), higher levels of molecules related with phagocytosis (CD68, CD16/32) as well as elevated levels of CD200R, a molecule involved in the microglia-neuron crosstalk (Article 1-2 and Figures 2-3).

Phagocytic activity is considered an important feature of microglial activation phenotype after CNS damage. In the present study, although both transgenic animals expressed elevated levels of CD68 and CD16/32, exclusively GFAP-IL6Tg also presented higher expression of TREM2, a myeloid receptor associated to phagocytosis (Manich et al., 2020)(Figure 2). Several studies in demyelinating models, like EAE or cuprizone, associate TREM2 induction with a more efficient phagocytosis of myelin (Takahashi, Rochford, & Neumann, 2005). In fact, in TREM2KO mice, microglia cells presented less activation and were inefficient phagocyting myelin debris (Nugent et al., 2020; Piccio et al., 2007; Poliani et al., 2015). The singular higher expression of TREM2 in IL6 transgenic animal leads us to think that the phagocytosis in these animals will be more efficient. However, surprisingly, GFAP-IL6Tg showed higher presence of Neurosilver^{+} degenerating fibers in the dennervated area (Article 2 and Figure 4), indicating an inefficient elimination of debris, as already demonstrated in these transgenic mice line on the cuprizone model (Petkovic, Campbell, Gonzalez, & Castellano, 2016). Then, the elevated TREM2 levels observed should be related to another microglial functions. In fact, a part from their phagocytic particularities, emerging evidence indicates that TREM2 modulates neuroinflammation polarizing overactivated microglial inflammatory features to a protective microglial phenotype in neurodegenerative diseases like AD or PD (Xue & Du, 2021; Y. Zhang et al., 2018). Their suppressive neuroinflammatory properties has been linked to a reduction of pro-inflammatory mediators, such as IL-1β and TNF-α, and increased release of anti-inflammatory cytokines like IL-10 and TGF-β, when TREM2 is upregulated (C. Li, Zhao, Lin, Gong, & An, 2019; Ulland et al., 2017; Zhong et al., 2017). Therefore, the upregulation of TREM2 in GFAP-IL6Tg mice would be one of the responsibles of the higher levels of IL-10 observed in these animals through the NF-kB microglial signalling (C. Li et al., 2019).

In parallel, as part of their microglial activation phenotype, we described for the first time the expression of CD200R in the PPT paradigm. Although the CD200R

pattern of expression correlates with the microglial activation phenotype window in all the genotypes studied, both GFAP-IL6Tg and GFAP-IL10Tg mice show higher levels of CD200R at earlier time points (Figure 3). Several studies associate modifications in the CD200-CD200R axis with tissue protection during CNS inflammation (Manich et al., 2019). For example, ablation of CD200 or blockage of CD200R after SCI produced a pro-inflammatory and an activated microglia/macrophage profile impairing recovery (Cohen et al., 2017; Lago, Pannunzio, Amo-Aparicio, Lopez-Vales, & Peluffo, 2018). This protective role and neurorepair features were linked to the CD200 capacity to promote the expression of neurotrophic factors, such as GDNF, by either a direct interaction with microglial CD200R o indirectly by binding to other putative receptors (Bespalov & Saarma, 2007; Manich et al., 2019; Turner, Eren-Kocak, Inui, Watson, & Akil, 2016; Varnum, Kiyota, Ingraham, Ikezu, & Ikezu, 2015). Interestingly in this regard, in parallel to higher CD200R, we observe an earlier downregulation of CD200 only in GFAP-IL6Tg mice correlating with lower collateral sprouting (Article 2 and Figure 3). These results pointed towards CD200-CD200R interaction as a candidate to participate in axonal sprouting along the PPT paradigm.

Finally, concerning microglial APCs functions, both transgenic animals present modifications in MHCII and CD11c expression compared to their respective WT. While GFAP-IL10Tg mice showed a reduction of microglia cells expressing either MHCII or CD11c (Article 1); GFAP-IL6Tg animals do not show parenchymatic $MHCII^{+}$ or $CD11c^{+}$ microglia at any time of the lesion, being this phenotype restricted to PVM population (Article 2). These results imply that IL6-induced activated microglia are inadequate to act as APCs and thus to drive an adaptive immune response; whereas IL-10 induces a downregulatory phenotype during the adaptive immune response of PPT. It is important to mention here, that both GFAP-IL6Tg and GFAP-IL10Tg animals showed higher levels of IL10, a potent inhibitor of MHCII expression on macrophages and microglia (Article 1 and 2) (Kremlev & Palmer, 2005; Lodge & Sriram, 1996; Mittal, Cho, Ishido, & Roche, 2015; Sawada, Suzumura, Hosoya, Marunouchi, & Nagatsu,

1999), pointing towards IL10 as the responsible of the variations in MHCII expression observed in both transgenic animals. Similarly, glioma cancer stem cells (gCSCs) supress adaptive immunity producing high amounts of IL-10 and other anti-inflammatory cytokines, like TGFβ, with the aim to inhibit the expression of costimulatory molecules driving microglia/macrophages to an immunosuppressive state (Rolle, Sengupta, & Lesniak, 2012; Sevenich, 2018; A. Wu et al., 2010).

6.5. IL-6 and IL-10 astrocyte targeted production increases peripheral immune cells infiltration

Apart from microglial activation, it is well described that PPT evokes leukocytes infiltration, including monocytes, macrophages and T cells (Babcock et al., 2003; Babcock et al., 2008; Bechmann et al., 2005; Fux et al., 2008). It is well established that peripheral monocytes reached the brain parenchyma early after PPT and transformed to ramified microglia (Kaminski et al., 2012). Regarding the lymphocyte infiltration, T cells entrance to the dennervated area is produced in two waves, the first around 48 hours and the second at 7 dpl. Although microglial cell "nests" have been related to interaction with myelin specific T-cells after PPT (Grebing et al., 2016), the main function of both leukocyte populations remains unknown in the PPT paradigm.

In the present study, both GFAP-IL6Tg and GFAP-IL10Tg mice show a higher number of $CD11b^{+}/CD45^{high}Ly6C+$ monocytes as well as increased number of T cells compared to WT. The altered pattern of T cell infiltration consists in a continuous entrance of cells being impossible to distinguish the two waves of entrance observed in WT (Article 1 and 2). However, when we analyse the presence of costimulatory molecules in these T-cells, again, we do not observed neither CD28 nor CTLA4 in GFAP-IL6Tg mice, supporting our hypothesis commented in the NL animals that the T-cells are not activated in this paradigm, at least using the classical B7-CD28/CTLA4 signalling (Article 2). This greater presence of peripheral immune cells and their persistence along the progression of the lesion, correlated with increased levels of

CCL2 and CXCL10 in both transgenics (Article 1 and 2). Moreover, as we commented above, we have to take in consideration that GFAP-IL6Tg also presented BBB breakdown contributing together with these chemokines to the peripheral cell recruitment.

6.6. IL-6 and IL-10 astrocyte targeted production modifies cytokine/chemokine environment

In the PPT paradigm and in parallel to all the events previously mentioned, some studies described that microglia cells produce a wide range of soluble factors, including cytokines such as IL-1β, TGFβ1, TNF-α, IGF-1 and chemokines such as CCL2 that participates in the lesion outcome (Babcock et al., 2003; Babcock et al., 2008; Finsen et al., 1999; Grebing et al., 2016; Ladeby, Wirenfeldt, Garcia-Ovejero, et al., 2005).

In addition to the already discussed modifications in chemokines involved in the recruitment of macrophages and T cells, GFAP-IL6Tg and GFAP-IL10Tg animals showed an altered cytokine milieu that may drive the type of the immune response generated in the dennervated areas of these mice. In this sense, chronic overproduction of IL6 results in increased levels of both IL6 and IL-1β, two classical pro-inflammatory cytokines strongly related with the innate immune response (Dinarello, 2018; Hewett et al., 2012; Lobo-Silva et al., 2016; Mori, Maher, & Conti, 2016; Swardfager, Winer, Herrmann, Winer, & Lanctot, 2013). On the other hand, chronic overproduction of IL-10 causes an anti-inflammatory environment characterized by increased levels of TGFβ and downregulated levels of IL2 and IFNγ, giving raise a deactivated microglia phenotype (Article 1 and 2). Furthermore, the lack of differences in the shift of T lymphocyte subtypes observed in GFAP-IL6Tg mice would be explained by the unaltered levels of two cytokines closely related to T-cell differentiation, the IL17 and the IL13, observed in this mice after PPT (Article 2) (Waisman, Hauptmann, & Regen, 2015).

6.7. Chronic overexpression of IL-6 reduces collateral sprouting whereas no effects are observed in GFAP-IL10Tg mice

An appropriately regulated inflammatory response after nerve injury is essential for axon regeneration and recovery. Cytokines participated in the axonal growth after a CNS damage being IL-6 and IL-10 two of the most studied in this phenomenon. In the case of IL-6, they direct contribution to axonal repair is controversial because both detrimental and beneficial role have been attributed; whereas IL-10 is mainly associated with promoting nerve regeneration (Atkins et al., 2007; Hakkoum, Stoppini, & Muller, 2007; Jancalek, Dubovy, Svizenska, & Klusakova, 2010; Koulaxouzidis et al., 2015; Sakalidou, Leibig, Boyle, Koulaxouzidis, & Penna, 2011; Shuto et al., 2001; Siqueira Mietto et al., 2015; Yang, Wen, Ou, Cui, & Fan, 2012) PPT paradigm is a well-established model used to study axonal sprouting. This axonal sprouting is produced when fibers from non-deafferentated areas growth in an attempt to supply the loss of afferences produced in the granular neurons as a result of the transection of the perforant pathway. Collateral sprouts could derive from different near areas such as 1) glutamatergic C/A projections from mossy cells to the IML, 2) GABAergic fibers to the OML and 3) cholinergic septohippocampal fibers. Although various techniques are described to study the collateral sprouting such as the detection of AChE cholinergic fibers, the visualizing of mossy fibres through Timm staining were one of the main characterized (Del Turco et al., 2003; Deller et al., 2007; Drojdahl, Hegelund, Poulsen, Wree, & Finsen, 2002).

One of the most interesting results in this thesis is that IL-6 chronic overproduction impairs collateral sprouting after PPT (Article 2); whereas no differences were observed in GFAP-IL10Tg mice (Figure 5). In the case of GFAP-IL6Tg mice, in parallel to the deficient microglial phagocytosis of degenerating fibers, the inefficacy of this microglia to express an APC phenotype, and the modified CD200-CD200R axis, the persistence of a pro-inflammatory cytokine environment in these transgenic animals could also worsen collateral sprouting. In this line, several studies described that the

expression of pro-inflammatory cytokines, like TNF-α and IL-1β, promotes the astrocyte secretion of proteoglicans, a compounds of the extracellular matrix with widely-demonstrated inhibitory role of axonal sprouting (Deller et al., 2001; Gu et al., 2007; Haas, Rauch, Thon, Merten, & Deller, 1999; Siebert, Conta Steencken, & Osterhout, 2014; Thon et al., 2000).

7. CONCLUSIONS

The results obtained in this thesis indicate that chronic and local exposure to IL6 and IL10 polarized the microglia towards a primed phenotype. Once they are exposed to a same second stimulus, the PPT paradigm, they present a different microglial activation profile conditioned by the first stimuli. Specifically, IL6-primed microglia present an activated profile unable to acquire an antigenic presentation function; whereas IL10-primed microglia shows a downregulated APC phenotype after PPT. These changes in microglial population only modify the outcome of lesion in GFAP-IL6Tg mice avoiding the generation of a pro-regenerative environment.

Specific conclusions:

- Both IL-6 and IL-10 chronic overproduction have the capacity to polarize microglial phenotype in steady state.
- Astrocyte-targeted production of IL-6 and IL-10 increases microglial/macrophage density after PPT.
- Both IL-6 and IL-10 chronic overproduction increases microglial phagocytic machinery, although only IL-6 induces higher levels of TREM2 after PPT.
- IL-6 chronic overexpression reduces the clearance of neurodegenerating fibers in the dennervated area after PPT.
- Both IL-6 and IL-10 chronic overproduction increases the expression of chemokines promoting monocyte/macrophage recruitment after PPT.
- Astrocyte-targeted production of IL-6 and IL-10 increases the recruitment of lymphocytes to the dennervated area after PPT.
- IL-6 and IL-10 chronic overproduction modifies the antigen presenting capacity of microglial cells worsening their interaction with recruited lymphocytes after PPT.

- IL-6 chronic overproduction increases IL-6 and IL-1β pro-inflammatory cytokines, associated to innate immune response; and shows elevated levels of the anti-inflammatory cytokine IL-10 after PPT.
- IL-10 astrocyte targeted production generates an anti-inflammatory environment mainly with higher TGFβ and lower IL-2 and IFN-γ after PPT.
- Both astrocyte-targeted production of IL-6 and IL-10 interferes in the communication between microglia and neurons trough the CD200R-CD200 axis after PPT.
- IL-6 chronic overexpression reduces collateral sprouting, whereas IL-10 chronic overexpression does not modify this process after PPT.

BIBLIOGRAPHY

Adey, W. R., Merrillees, N. C., & Sunderland, S. (1956). The entorhinal area; behavioural, evoked potential, and histological studies of its interrelationships with brain-stem regions. *Brain, 79*(3), 414-439. doi:10.1093/brain/79.3.414

Ajami, B., Bennett, J. L., Krieger, C., McNagny, K. M., & Rossi, F. M. (2011). Infiltrating monocytes trigger EAE progression, but do not contribute to the resident microglia pool. *Nat Neurosci, 14*(9), 1142-1149. doi:10.1038/nn.2887

Al-Amin, M. M., & Reza, H. M. (2014). Neuroinflammation: Contemporary anti-inflammatory treatment approaches. *Neurosciences (Riyadh), 19*(2), 87-92.

Ali, I., Chugh, D., & Ekdahl, C. T. (2015). Role of fractalkine-CX3CR1 pathway in seizure-induced microglial activation, neurodegeneration, and neuroblast production in the adult rat brain. *Neurobiol Dis, 74*, 194-203. doi:10.1016/j.nbd.2014.11.009

Almolda, B., Costa, M., Montoya, M., Gonzalez, B., & Castellano, B. (2009). CD4 microglial expression correlates with spontaneous clinical improvement in the acute Lewis rat EAE model. *J Neuroimmunol, 209*(1-2), 65-80. doi:10.1016/j.jneuroim.2009.01.026

Almolda, B., de Labra, C., Barrera, I., Gruart, A., Delgado-Garcia, J. M., Villacampa, N., . . . Castellano, B. (2015). Alterations in microglial phenotype and hippocampal neuronal function in transgenic mice with astrocyte-targeted production of interleukin-10. *Brain Behav Immun, 45*, 80-97. doi:10.1016/j.bbi.2014.10.015

Almolda, B., Gonzalez, B., & Castellano, B. (2011). Antigen presentation in EAE: role of microglia, macrophages and dendritic cells. *Front Biosci (Landmark Ed), 16*, 1157-1171.

Almolda, B., Villacampa, N., Manders, P., Hidalgo, J., Campbell, I. L., Gonzalez, B., & Castellano, B. (2014). Effects of astrocyte-targeted production of interleukin-6 in the mouse on the host response to nerve injury. *Glia, 62*(7), 1142-1161. doi:10.1002/glia.22668

Aloisi, F. (1999). The role of microglia and astrocytes in CNS immune surveillance and immunopathology. *Adv Exp Med Biol, 468*, 123-133. doi:10.1007/978-1-4615-4685-6_10

Amaral, D. G., & Witter, M. P. (1989). The three-dimensional organization of the hippocampal formation: a review of anatomical data. *Neuroscience, 31*(3), 571-591. doi:10.1016/0306-4522(89)90424-7

Apelt, J., & Schliebs, R. (2001). Beta-amyloid-induced glial expression of both pro- and anti-inflammatory cytokines in cerebral cortex of aged transgenic Tg2576 mice with Alzheimer plaque pathology. *Brain Res, 894*(1), 21-30.

Arimoto, T., Choi, D. Y., Lu, X., Liu, M., Nguyen, X. V., Zheng, N., . . . Bing, G. (2007). Interleukin-10 protects against inflammation-mediated degeneration of dopaminergic neurons in substantia nigra. *Neurobiol Aging, 28*(6), 894-906. doi:10.1016/j.neurobiolaging.2006.04.011

Ashwell, K. (1990). Microglia and cell death in the developing mouse cerebellum. *Brain Res Dev Brain Res, 55*(2), 219-230. doi:10.1016/0165-3806(90)90203-b

Atkins, S., Loescher, A. R., Boissonade, F. M., Smith, K. G., Occleston, N., O'Kane, S., . . . Robinson, P. P. (2007). Interleukin-10 reduces scarring and enhances regeneration at a site of sciatic nerve repair. *J Peripher Nerv Syst, 12*(4), 269-276. doi:10.1111/j.1529-8027.2007.00148.x

Babcock, A. A., Kuziel, W. A., Rivest, S., & Owens, T. (2003). Chemokine expression by glial cells directs leukocytes to sites of axonal injury in the CNS. *J Neurosci, 23*(21), 7922-7930.

Babcock, A. A., Toft-Hansen, H., & Owens, T. (2008). Signaling through MyD88 regulates leukocyte recruitment after brain injury. *J Immunol, 181*(9), 6481-6490.

Babcock, A. A., Wirenfeldt, M., Holm, T., Nielsen, H. H., Dissing-Olesen, L., Toft-Hansen, H., . . . Owens, T. (2006). Toll-like receptor 2 signaling in response to brain injury: an innate bridge to neuroinflammation. *J Neurosci, 26*(49), 12826-12837. doi:10.1523/JNEUROSCI.4937-05.2006

Badimon, A., Strasburger, H. J., Ayata, P., Chen, X., Nair, A., Ikegami, A., . . . Schaefer, A. (2020). Negative feedback control of neuronal activity by microglia. *Nature, 586*(7829), 417-423. doi:10.1038/s41586-020-2777-8

Barrette, B., Hebert, M. A., Filali, M., Lafortune, K., Vallieres, N., Gowing, G., . . . Lacroix, S. (2008). Requirement of myeloid cells for axon regeneration. *J Neurosci, 28*(38), 9363-9376. doi:10.1523/JNEUROSCI.1447-08.2008

Beattie, M. S., Hermann, G. E., Rogers, R. C., & Bresnahan, J. C. (2002). Cell death in models of spinal cord injury. *Prog Brain Res, 137*, 37-47. doi:10.1016/s0079-6123(02)37006-7

Bechmann, I., Goldmann, J., Kovac, A. D., Kwidzinski, E., Simburger, E., Naftolin, F., . . . Priller, J. (2005). Circulating monocytic cells infiltrate layers of anterograde axonal degeneration where they transform into microglia. *FASEB J, 19*(6), 647-649. doi:10.1096/fj.04-2599fje

Bechmann, I., Peter, S., Beyer, M., Gimsa, U., & Nitsch, R. (2001). Presence of B7--2 (CD86) and lack of B7--1 (CD(80) on myelin phagocytosing MHC-II-positive rat microglia is associated with nondestructive immunity in vivo. *FASEB J, 15*(6), 1086-1088. doi:10.1096/fj.00-0563fje

Bennett, M. L., & Bennett, F. C. (2020). The influence of environment and origin on brain resident macrophages and implications for therapy. *Nat Neurosci, 23*(2), 157-166. doi:10.1038/s41593-019-0545-6

Bespalov, M. M., & Saarma, M. (2007). GDNF family receptor complexes are emerging drug targets. *Trends Pharmacol Sci, 28*(2), 68-74. doi:10.1016/j.tips.2006.12.005

Bettelli, E., Carrier, Y., Gao, W., Korn, T., Strom, T. B., Oukka, M., . . . Kuchroo, V. K. (2006). Reciprocal developmental pathways for the generation of pathogenic effector TH17 and regulatory T cells. *Nature, 441*(7090), 235-238. doi:10.1038/nature04753

Bezzi, P., Domercq, M., Brambilla, L., Galli, R., Schols, D., De Clercq, E., . . . Volterra, A. (2001). CXCR4-activated astrocyte glutamate release via TNFalpha: amplification by microglia triggers neurotoxicity. *Nat Neurosci, 4*(7), 702-710. doi:10.1038/89490

Brett, F. M., Mizisin, A. P., Powell, H. C., & Campbell, I. L. (1995). Evolution of neuropathologic abnormalities associated with blood-brain barrier breakdown in transgenic mice expressing interleukin-6 in astrocytes. *J*

Neuropathol Exp Neurol, 54(6), 766-775. doi:10.1097/00005072-199511000-00003

Burda, J. E., & Sofroniew, M. V. (2017). Seducing astrocytes to the dark side. *Cell Res, 27*(6), 726-727. doi:10.1038/cr.2017.37

Burmeister, A. R., & Marriott, I. (2018). The Interleukin-10 Family of Cytokines and Their Role in the CNS. *Front Cell Neurosci, 12*, 458. doi:10.3389/fncel.2018.00458

Butovsky, O., Jedrychowski, M. P., Cialic, R., Krasemann, S., Murugaiyan, G., Fanek, Z., . . . Weiner, H. L. (2015). Targeting miR-155 restores abnormal microglia and attenuates disease in SOD1 mice. *Ann Neurol, 77*(1), 75-99. doi:10.1002/ana.24304

Button, E. B., Mitchell, A. S., Domingos, M. M., Chung, J. H., Bradley, R. M., Hashemi, A., . . . Duncan, R. E. (2014). Microglial cell activation increases saturated and decreases monounsaturated fatty acid content, but both lipid species are proinflammatory. *Lipids, 49*(4), 305-316. doi:10.1007/s11745-014-3882-y

Campbell, I. L., Abraham, C. R., Masliah, E., Kemper, P., Inglis, J. D., Oldstone, M. B., & Mucke, L. (1993). Neurologic disease induced in transgenic mice by cerebral overexpression of interleukin 6. *Proc Natl Acad Sci U S A, 90*(21), 10061-10065. doi:10.1073/pnas.90.21.10061

Campbell, I. L., Erta, M., Lim, S. L., Frausto, R., May, U., Rose-John, S., . . . Hidalgo, J. (2014). Trans-signaling is a dominant mechanism for the pathogenic actions of interleukin-6 in the brain. *J Neurosci, 34*(7), 2503-2513. doi:10.1523/JNEUROSCI.2830-13.2014

Campbell, I. L., Stalder, A. K., Akwa, Y., Pagenstecher, A., & Asensio, V. C. (1998). Transgenic models to study the actions of cytokines in the central nervous system. *Neuroimmunomodulation, 5*(3-4), 126-135. doi:10.1159/000026329

Cannella, B., & Raine, C. S. (2004). Multiple sclerosis: cytokine receptors on oligodendrocytes predict innate regulation. *Ann Neurol, 55*(1), 46-57. doi:10.1002/ana.10764

Cardona, A. E., Pioro, E. P., Sasse, M. E., Kostenko, V., Cardona, S. M., Dijkstra, I. M., . . . Ransohoff, R. M. (2006). Control of microglial neurotoxicity by the fractalkine receptor. *Nat Neurosci, 9*(7), 917-924. doi:10.1038/nn1715

Carson, M. J. (2002). Microglia as liaisons between the immune and central nervous systems: functional implications for multiple sclerosis. *Glia, 40*(2), 218-231. doi:10.1002/glia.10145

Chiang, C. S., Stalder, A., Samimi, A., & Campbell, I. L. (1994). Reactive gliosis as a consequence of interleukin-6 expression in the brain: studies in transgenic mice. *Dev Neurosci, 16*(3-4), 212-221. doi:10.1159/000112109

Chiu, I. M., Morimoto, E. T., Goodarzi, H., Liao, J. T., O'Keeffe, S., Phatnani, H. P., . . . Maniatis, T. (2013). A neurodegeneration-specific gene-expression signature of acutely isolated microglia from an amyotrophic lateral sclerosis mouse model. *Cell Rep, 4*(2), 385-401. doi:10.1016/j.celrep.2013.06.018

Cohen, M., Ben-Yehuda, H., Porat, Z., Raposo, C., Gordon, S., & Schwartz, M. (2017). Newly Formed Endothelial Cells Regulate Myeloid Cell Activity Following Spinal Cord Injury via Expression of CD200 Ligand. *J Neurosci, 37*(4), 972-985. doi:10.1523/JNEUROSCI.2199-16.2016

Conroy, S. M., Nguyen, V., Quina, L. A., Blakely-Gonzales, P., Ur, C., Netzeband, J. G., . . . Gruol, D. L. (2004). Interleukin-6 produces neuronal loss in developing cerebellar granule neuron cultures. *J Neuroimmunol, 155*(1-2), 43-54. doi:10.1016/j.jneuroim.2004.06.014

Coull, J. A., Beggs, S., Boudreau, D., Boivin, D., Tsuda, M., Inoue, K., . . . De Koninck, Y. (2005). BDNF from microglia causes the shift in neuronal anion gradient underlying neuropathic pain. *Nature, 438*(7070), 1017-1021. doi:10.1038/nature04223

Cserep, C., Posfai, B., Lenart, N., Fekete, R., Laszlo, Z. I., Lele, Z., . . . Denes, A. (2020). Microglia monitor and protect neuronal function through specialized somatic purinergic junctions. *Science, 367*(6477), 528-537. doi:10.1126/science.aax6752

Cua, D. J., Hutchins, B., LaFace, D. M., Stohlman, S. A., & Coffman, R. L. (2001). Central nervous system expression of IL-10 inhibits autoimmune encephalomyelitis. *J Immunol, 166*(1), 602-608.

Cunningham, C. L., Martinez-Cerdeno, V., & Noctor, S. C. (2013). Microglia regulate the number of neural precursor cells in the developing cerebral cortex. *J Neurosci, 33*(10), 4216-4233. doi:10.1523/JNEUROSCI.3441-12.2013

Cusimano, M., Biziato, D., Brambilla, E., Donega, M., Alfaro-Cervello, C., Snider, S., . . . Pluchino, S. (2012). Transplanted neural stem/precursor cells instruct phagocytes and reduce secondary tissue damage in the injured spinal cord. *Brain, 135*(Pt 2), 447-460. doi:10.1093/brain/awr339

Dansokho, C., & Heneka, M. T. (2018). Neuroinflammatory responses in Alzheimer's disease. *J Neural Transm (Vienna), 125*(5), 771-779. doi:10.1007/s00702-017-1831-7

Davalos, D., Grutzendler, J., Yang, G., Kim, J. V., Zuo, Y., Jung, S., . . . Gan, W. B. (2005). ATP mediates rapid microglial response to local brain injury in vivo. *Nat Neurosci, 8*(6), 752-758. doi:10.1038/nn1472

David, S., Bouchard, C., Tsatas, O., & Giftochristos, N. (1990). Macrophages can modify the nonpermissive nature of the adult mammalian central nervous system. *Neuron, 5*(4), 463-469. doi:10.1016/0896-6273(90)90085-t

De Biase, L. M., Schuebel, K. E., Fusfeld, Z. H., Jair, K., Hawes, I. A., Cimbro, R., . . . Bonci, A. (2017). Local Cues Establish and Maintain Region-Specific Phenotypes of Basal Ganglia Microglia. *Neuron, 95*(2), 341-356 e346. doi:10.1016/j.neuron.2017.06.020

De, S., Van Deren, D., Peden, E., Hockin, M., Boulet, A., Titen, S., & Capecchi, M. R. (2018). Two distinct ontogenies confer heterogeneity to mouse brain microglia. *Development, 145*(13). doi:10.1242/dev.152306

Deczkowska, A., Amit, I., & Schwartz, M. (2018). Microglial immune checkpoint mechanisms. *Nat Neurosci, 21*(6), 779-786. doi:10.1038/s41593-018-0145-x

Del Turco, D., Woods, A. G., Gebhardt, C., Phinney, A. L., Jucker, M., Frotscher, M., & Deller, T. (2003). Comparison of commissural sprouting in the mouse and rat fascia dentata after entorhinal cortex lesion. *Hippocampus, 13*(6), 685-699. doi:10.1002/hipo.10118

Deller, T., Del Turco, D., Rappert, A., & Bechmann, I. (2007). Structural reorganization of the dentate gyrus following entorhinal denervation: species differences between rat and mouse. *Prog Brain Res, 163*, 501-528. doi:10.1016/S0079-6123(07)63027-1

Deller, T., & Frotscher, M. (1997). Lesion-induced plasticity of central neurons: sprouting of single fibres in the rat hippocampus after unilateral entorhinal cortex lesion. *Prog Neurobiol, 53*(6), 687-727.

Deller, T., Haas, C. A., & Frotscher, M. (2001). Sprouting in the hippocampus after entorhinal cortex lesion is layer- specific but not translaminar: which molecules may be involved? *Restor Neurol Neurosci, 19*(3-4), 159-167.

Dinarello, C. A. (2018). Overview of the IL-1 family in innate inflammation and acquired immunity. *Immunol Rev, 281*(1), 8-27. doi:10.1111/imr.12621

Dissing-Olesen, L., Ladeby, R., Nielsen, H. H., Toft-Hansen, H., Dalmau, I., & Finsen, B. (2007). Axonal lesion-induced microglial proliferation and microglial cluster formation in the mouse. *Neuroscience, 149*(1), 112-122. doi:10.1016/j.neuroscience.2007.06.037

Dittel, B. N. (2008). Direct suppression of autoreactive lymphocytes in the central nervous system via the CB2 receptor. *Br J Pharmacol, 153*(2), 271-276. doi:10.1038/sj.bjp.0707493

Drojdahl, N., Hegelund, I. V., Poulsen, F. R., Wree, A., & Finsen, B. (2002). Perforant path lesioning induces sprouting of CA3-associated fibre systems in mouse hippocampal formation. *Exp Brain Res, 144*(1), 79-87. doi:10.1007/s00221-002-1025-9

Dzierzak, E., & Bigas, A. (2018). Blood Development: Hematopoietic Stem Cell Dependence and Independence. *Cell Stem Cell, 22*(5), 639-651. doi:10.1016/j.stem.2018.04.015

Ennerfelt, H. E., & Lukens, J. R. (2020). The role of innate immunity in Alzheimer's disease. *Immunol Rev, 297*(1), 225-246. doi:10.1111/imr.12896

Erta, M., Quintana, A., & Hidalgo, J. (2012). Interleukin-6, a major cytokine in the central nervous system. *Int J Biol Sci, 8*(9), 1254-1266. doi:10.7150/ijbs.4679

Fakhoury, M. (2018). Microglia and Astrocytes in Alzheimer's Disease: Implications for Therapy. *Curr Neuropharmacol, 16*(5), 508-518. doi:10.2174/1570159X15666170720095240

Ferrero, G., Mahony, C. B., Dupuis, E., Yvernogeau, L., Di Ruggiero, E., Miserocchi, M., . . . Wittamer, V. (2018). Embryonic Microglia Derive from Primitive Macrophages and Are Replaced by cmyb-Dependent Definitive Microglia in Zebrafish. *Cell Rep, 24*(1), 130-141. doi:10.1016/j.celrep.2018.05.066

Finsen, B., Jensen, M. B., Lomholt, N. D., Hegelund, I. V., Poulsen, F. R., & Owens, T. (1999). Axotomy-induced glial reactions in normal and cytokine transgenic mice. *Adv Exp Med Biol, 468*, 157-171.

Fiorentino, D. F., Bond, M. W., & Mosmann, T. R. (1989). Two types of mouse T helper cell. IV. Th2 clones secrete a factor that inhibits cytokine production by Th1 clones. *J Exp Med, 170*(6), 2081-2095. doi:10.1084/jem.170.6.2081

Frost, J. L., & Schafer, D. P. (2016). Microglia: Architects of the Developing Nervous System. *Trends Cell Biol, 26*(8), 587-597. doi:10.1016/j.tcb.2016.02.006

Fux, M., van Rooijen, N., & Owens, T. (2008). Macrophage-independent T cell infiltration to the site of injury-induced brain inflammation. *J Neuroimmunol, 203*(1), 64-72. doi:10.1016/j.jneuroim.2008.06.025

Garcia, J. M., Stillings, S. A., Leclerc, J. L., Phillips, H., Edwards, N. J., Robicsek, S. A., . . . Dore, S. (2017). Role of Interleukin-10 in Acute Brain Injuries. *Front Neurol, 8*, 244. doi:10.3389/fneur.2017.00244

Garner, K. M., Amin, R., Johnson, R. W., Scarlett, E. J., & Burton, M. D. (2018). Microglia priming by interleukin-6 signaling is enhanced in aged mice. *J Neuroimmunol, 324*, 90-99. doi:10.1016/j.jneuroim.2018.09.002

Gartlan, K. H., Markey, K. A., Varelias, A., Bunting, M. D., Koyama, M., Kuns, R. D., . . . Hill, G. R. (2015). Tc17 cells are a proinflammatory, plastic lineage of pathogenic CD8+ T cells that induce GVHD without antileukemic effects. *Blood, 126*(13), 1609-1620. doi:10.1182/blood-2015-01-622662

Ginhoux, F., Greter, M., Leboeuf, M., Nandi, S., See, P., Gokhan, S., . . . Merad, M. (2010). Fate mapping analysis reveals that adult microglia derive from primitive macrophages. *Science, 330*(6005), 841-845. doi:10.1126/science.1194637

Goldmann, T., Wieghofer, P., Jordao, M. J., Prutek, F., Hagemeyer, N., Frenzel, K., . . . Prinz, M. (2016). Origin, fate and dynamics of macrophages at central nervous system interfaces. *Nat Immunol, 17*(7), 797-805. doi:10.1038/ni.3423

Gomez-Nicola, D., Fransen, N. L., Suzzi, S., & Perry, V. H. (2013). Regulation of microglial proliferation during chronic neurodegeneration. *J Neurosci, 33*(6), 2481-2493. doi:10.1523/JNEUROSCI.4440-12.2013

Gor, D. O., Rose, N. R., & Greenspan, N. S. (2003). TH1-TH2: a procrustean paradigm. *Nat Immunol, 4*(6), 503-505. doi:10.1038/ni0603-503

Grebing, M., Nielsen, H. H., Fenger, C. D., K, T. J., von Linstow, C. U., Clausen, B. H., . . . Finsen, B. (2016). Myelin-specific T cells induce interleukin-1beta expression in lesion-reactive microglial-like cells in zones of axonal degeneration. *Glia, 64*(3), 407-424. doi:10.1002/glia.22937

Griciuc, A., Serrano-Pozo, A., Parrado, A. R., Lesinski, A. N., Asselin, C. N., Mullin, K., . . . Tanzi, R. E. (2013). Alzheimer's disease risk gene CD33 inhibits microglial uptake of amyloid beta. *Neuron, 78*(4), 631-643. doi:10.1016/j.neuron.2013.04.014

Gu, W. L., Fu, S. L., Wang, Y. X., Li, Y., Wang, X. F., Xu, X. M., & Lu, P. H. (2007). Expression and regulation of versican in neural precursor cells and their lineages. *Acta Pharmacol Sin, 28*(10), 1519-1530. doi:10.1111/j.1745-7254.2007.00659.x

Gyoneva, S., & Ransohoff, R. M. (2015). Inflammatory reaction after traumatic brain injury: therapeutic potential of targeting cell-cell communication by chemokines. *Trends Pharmacol Sci, 36*(7), 471-480. doi:10.1016/j.tips.2015.04.003

Haas, C. A., Rauch, U., Thon, N., Merten, T., & Deller, T. (1999). Entorhinal cortex lesion in adult rats induces the expression of the neuronal chondroitin sulfate proteoglycan neurocan in reactive astrocytes. *J Neurosci, 19*(22), 9953-9963.

Hagemeyer, N., Hanft, K. M., Akriditou, M. A., Unger, N., Park, E. S., Stanley, E. R., . . . Prinz, M. (2017). Microglia contribute to normal myelinogenesis and to oligodendrocyte progenitor maintenance during adulthood. *Acta Neuropathol, 134*(3), 441-458. doi:10.1007/s00401-017-1747-1

Hailer, N. P., Grampp, A., & Nitsch, R. (1999). Proliferation of microglia and astrocytes in the dentate gyrus following entorhinal cortex lesion: a quantitative bromodeoxyuridine-labelling study. *Eur J Neurosci, 11*(9), 3359-3364.

Hakkoum, D., Stoppini, L., & Muller, D. (2007). Interleukin-6 promotes sprouting and functional recovery in lesioned organotypic hippocampal slice cultures. *J Neurochem, 100*(3), 747-757. doi:10.1111/j.1471-4159.2006.04257.x

Hammond, T. R., Dufort, C., Dissing-Olesen, L., Giera, S., Young, A., Wysoker, A., . . . Stevens, B. (2019). Single-Cell RNA Sequencing of Microglia throughout the Mouse Lifespan and in the Injured Brain Reveals Complex Cell-State Changes. *Immunity, 50*(1), 253-271 e256. doi:10.1016/j.immuni.2018.11.004

Hanamsagar, R., Hanke, M. L., & Kielian, T. (2012). Toll-like receptor (TLR) and inflammasome actions in the central nervous system. *Trends Immunol, 33*(7), 333-342. doi:10.1016/j.it.2012.03.001

Haynes, S. E., Hollopeter, G., Yang, G., Kurpius, D., Dailey, M. E., Gan, W. B., & Julius, D. (2006). The P2Y12 receptor regulates microglial activation by extracellular nucleotides. *Nat Neurosci, 9*(12), 1512-1519. doi:10.1038/nn1805

Hemmer, B., Kerschensteiner, M., & Korn, T. (2015). Role of the innate and adaptive immune responses in the course of multiple sclerosis. *Lancet Neurol, 14*(4), 406-419. doi:10.1016/S1474-4422(14)70305-9

Hewett, S. J., Jackman, N. A., & Claycomb, R. J. (2012). Interleukin-1beta in Central Nervous System Injury and Repair. *Eur J Neurodegener Dis, 1*(2), 195-211.

Hibi, M., Murakami, M., Saito, M., Hirano, T., Taga, T., & Kishimoto, T. (1990). Molecular cloning and expression of an IL-6 signal transducer, gp130. *Cell, 63*(6), 1149-1157. doi:10.1016/0092-8674(90)90411-7

Hickman, S. E., Kingery, N. D., Ohsumi, T. K., Borowsky, M. L., Wang, L. C., Means, T. K., & El Khoury, J. (2013). The microglial sensome revealed by direct RNA sequencing. *Nat Neurosci, 16*(12), 1896-1905. doi:10.1038/nn.3554

Hirano, T. (1998). Interleukin 6 and its receptor: ten years later. *Int Rev Immunol, 16*(3-4), 249-284. doi:10.3109/08830189809042997

Hoeffel, G., & Ginhoux, F. (2015). Ontogeny of Tissue-Resident Macrophages. *Front Immunol, 6*, 486. doi:10.3389/fimmu.2015.00486

Hoek, R. M., Ruuls, S. R., Murphy, C. A., Wright, G. J., Goddard, R., Zurawski, S. M., . . . Sedgwick, J. D. (2000). Down-regulation of the macrophage lineage through interaction with OX2 (CD200). *Science, 290*(5497), 1768-1771. doi:10.1126/science.290.5497.1768

Holmoy, T., & Hestvik, A. L. (2008). Multiple sclerosis: immunopathogenesis and controversies in defining the cause. *Curr Opin Infect Dis, 21*(3), 271-278. doi:10.1097/QCO.0b013e3282f88b48

Howie, D., Okamoto, S., Rietdijk, S., Clarke, K., Wang, N., Gullo, C., . . . Terhorst, C. (2002). The role of SAP in murine CD150 (SLAM)-mediated T-cell proliferation and interferon gamma production. *Blood, 100*(8), 2899-2907. doi:10.1182/blood-2002-02-0445

Hsieh, H. L., & Yang, C. M. (2013). Role of redox signaling in neuroinflammation and neurodegenerative diseases. *Biomed Res Int, 2013*, 484613. doi:10.1155/2013/484613

Janakiram, M., Shah, U. A., Liu, W., Zhao, A., Schoenberg, M. P., & Zang, X. (2017). The third group of the B7-CD28 immune checkpoint family: HHLA2, TMIGD2, B7x, and B7-H3. *Immunol Rev, 276*(1), 26-39. doi:10.1111/imr.12521

Jancalek, R., Dubovy, P., Svizenska, I., & Klusakova, I. (2010). Bilateral changes of TNF-alpha and IL-10 protein in the lumbar and cervical dorsal root ganglia following a unilateral chronic constriction injury of the sciatic nerve. *J Neuroinflammation, 7*, 11. doi:10.1186/1742-2094-7-11

Jensen, M. B., Finsen, B., & Zimmer, J. (1997). Morphological and immunophenotypic microglial changes in the denervated fascia dentata of adult rats: correlation with blood-brain barrier damage and astroglial reactions. *Exp Neurol, 143*(1), 103-116. doi:10.1006/exnr.1996.6337

Jensen, M. B., Gonzalez, B., Castellano, B., & Zimmer, J. (1994). Microglial and astroglial reactions to anterograde axonal degeneration: a histochemical and immunocytochemical study of the adult rat fascia dentata after entorhinal perforant path lesions. *Exp Brain Res, 98*(2), 245-260.

Jordao, M. J. C., Sankowski, R., Brendecke, S. M., Sagar, Locatelli, G., Tai, Y. H., . . . Prinz, M. (2019). Single-cell profiling identifies myeloid cell subsets with distinct fates during neuroinflammation. *Science, 363*(6425). doi:10.1126/science.aat7554

Kaminski, M., Bechmann, I., Pohland, M., Kiwit, J., Nitsch, R., & Glumm, J. (2012). Migration of monocytes after intracerebral injection at entorhinal cortex lesion site. *J Leukoc Biol, 92*(1), 31-39. doi:10.1189/jlb.0511241

Kawakami, K. (2004). Regulation by innate immune T lymphocytes in the host defense against pulmonary infection with Cryptococcus neoformans. *Jpn J Infect Dis, 57*(4), 137-145.

Keren-Shaul, H., Spinrad, A., Weiner, A., Matcovitch-Natan, O., Dvir-Szternfeld, R., Ulland, T. K., . . . Amit, I. (2017). A Unique Microglia Type Associated with Restricting Development of Alzheimer's Disease. *Cell, 169*(7), 1276-1290 e1217. doi:10.1016/j.cell.2017.05.018

Kettenmann, H., Hanisch, U. K., Noda, M., & Verkhratsky, A. (2011). Physiology of microglia. *Physiol Rev, 91*(2), 461-553. doi:10.1152/physrev.00011.2010

Kigerl, K. A., de Rivero Vaccari, J. P., Dietrich, W. D., Popovich, P. G., & Keane, R. W. (2014). Pattern recognition receptors and central nervous system repair. *Exp Neurol, 258*, 5-16. doi:10.1016/j.expneurol.2014.01.001

Kishimoto, T. (2010). IL-6: from its discovery to clinical applications. *Int Immunol, 22*(5), 347-352. doi:10.1093/intimm/dxq030

Kishimoto, T., Akira, S., Narazaki, M., & Taga, T. (1995). Interleukin-6 family of cytokines and gp130. *Blood, 86*(4), 1243-1254.

Kloss, C. U., Kreutzberg, G. W., & Raivich, G. (1997). Proliferation of ramified microglia on an astrocyte monolayer: characterization of stimulatory and inhibitory cytokines. *J Neurosci Res, 49*(2), 248-254.

Kobayashi, M., Tamari, K., Miyamura, T., & Takeuchi, K. (2013). Blockade of interleukin-6 receptor suppresses inflammatory reaction and facilitates functional recovery following olfactory system injury. *Neurosci Res, 76*(3), 125-132. doi:10.1016/j.neures.2013.03.015

Konat, G. W., Kielian, T., & Marriott, I. (2006). The role of Toll-like receptors in CNS response to microbial challenge. *J Neurochem, 99*(1), 1-12. doi:10.1111/j.1471-4159.2006.04076.x

Kopydlowski, K. M., Salkowski, C. A., Cody, M. J., van Rooijen, N., Major, J., Hamilton, T. A., & Vogel, S. N. (1999). Regulation of macrophage chemokine expression by lipopolysaccharide in vitro and in vivo. *J Immunol, 163*(3), 1537-1544.

Koulaxouzidis, G., Reim, G., Fluhr, J. W., Simunovic, F., Stark, G. B., & Witzel, C. (2015). In Situ Deactivation of Interleukin-6 Enhances Early Peripheral Nerve Regeneration in a Murine Injury Model. *J Reconstr Microsurg, 31*(7), 508-515. doi:10.1055/s-0035-1555114

Krady, J. K., Lin, H. W., Liberto, C. M., Basu, A., Kremlev, S. G., & Levison, S. W. (2008). Ciliary neurotrophic factor and interleukin-6 differentially activate microglia. *J Neurosci Res, 86*(7), 1538-1547. doi:10.1002/jnr.21620

Krasemann, S., Madore, C., Cialic, R., Baufeld, C., Calcagno, N., El Fatimy, R., . . . Butovsky, O. (2017). The TREM2-APOE Pathway Drives the Transcriptional Phenotype of Dysfunctional Microglia in Neurodegenerative Diseases. *Immunity, 47*(3), 566-581 e569. doi:10.1016/j.immuni.2017.08.008

Kreisel, T., Wolf, B., Keshet, E., & Licht, T. (2019). Unique role for dentate gyrus microglia in neuroblast survival and in VEGF-induced activation. *Glia, 67*(4), 594-618. doi:10.1002/glia.23505

Kremlev, S. G., & Palmer, C. (2005). Interleukin-10 inhibits endotoxin-induced pro-inflammatory cytokines in microglial cell cultures. *J Neuroimmunol, 162*(1-2), 71-80. doi:10.1016/j.jneuroim.2005.01.010

Kumar, V. (2019). Toll-like receptors in the pathogenesis of neuroinflammation. *J Neuroimmunol, 332*, 16-30. doi:10.1016/j.jneuroim.2019.03.012

Kwon, H. S., & Koh, S. H. (2020). Neuroinflammation in neurodegenerative disorders: the roles of microglia and astrocytes. *Transl Neurodegener, 9*(1), 42. doi:10.1186/s40035-020-00221-2

Ladeby, R., Wirenfeldt, M., Dalmau, I., Gregersen, R., Garcia-Ovejero, D., Babcock, A., . . . Finsen, B. (2005). Proliferating resident microglia express the stem cell antigen CD34 in response to acute neural injury. *Glia, 50*(2), 121-131. doi:10.1002/glia.20159

Ladeby, R., Wirenfeldt, M., Garcia-Ovejero, D., Fenger, C., Dissing-Olesen, L., Dalmau, I., & Finsen, B. (2005). Microglial cell population dynamics in the injured adult central nervous system. *Brain Res Brain Res Rev, 48*(2), 196-206. doi:10.1016/j.brainresrev.2004.12.009

Lago, N., Pannunzio, B., Amo-Aparicio, J., Lopez-Vales, R., & Peluffo, H. (2018). CD200 modulates spinal cord injury neuroinflammation and outcome through CD200R1. *Brain Behav Immun, 73*, 416-426. doi:10.1016/j.bbi.2018.06.002

Laveti, D., Kumar, M., Hemalatha, R., Sistla, R., Naidu, V. G., Talla, V., . . . Nagpal, R. (2013). Anti-inflammatory treatments for chronic diseases: a review. *Inflamm Allergy Drug Targets, 12*(5), 349-361. doi:10.2174/18715281113129990053

Lawson, L. J., Perry, V. H., & Gordon, S. (1992). Turnover of resident microglia in the normal adult mouse brain. *Neuroscience, 48*(2), 405-415. doi:10.1016/0306-4522(92)90500-2

Ledeboer, A., Breve, J. J., Wierinckx, A., van der Jagt, S., Bristow, A. F., Leysen, J. E., . . . Van Dam, A. M. (2002). Expression and regulation of interleukin-10 and interleukin-10 receptor in rat astroglial and microglial cells. *Eur J Neurosci, 16*(7), 1175-1185.

Ledeboer, A., Wierinckx, A., Bol, J. G., Floris, S., Renardel de Lavalette, C., De Vries, H. E., . . . van dam, A. M. (2003). Regional and temporal expression patterns of interleukin-10, interleukin-10 receptor and adhesion molecules in the rat

spinal cord during chronic relapsing EAE. *J Neuroimmunol, 136*(1-2), 94-103.
Lee, M. (2013). Neurotransmitters and microglial-mediated neuroinflammation. *Curr Protein Pept Sci, 14*(1), 21-32. doi:10.2174/1389203711314010005
Lehnardt, S. (2010). Innate immunity and neuroinflammation in the CNS: the role of microglia in Toll-like receptor-mediated neuronal injury. *Glia, 58*(3), 253-263. doi:10.1002/glia.20928
Li, C., Zhao, B., Lin, C., Gong, Z., & An, X. (2019). TREM2 inhibits inflammatory responses in mouse microglia by suppressing the PI3K/NF-kappaB signaling. *Cell Biol Int, 43*(4), 360-372. doi:10.1002/cbin.10975
Li, Q., & Barres, B. A. (2018). Microglia and macrophages in brain homeostasis and disease. *Nat Rev Immunol, 18*(4), 225-242. doi:10.1038/nri.2017.125
Li, Q., Cheng, Z., Zhou, L., Darmanis, S., Neff, N. F., Okamoto, J., . . . Barres, B. A. (2019). Developmental Heterogeneity of Microglia and Brain Myeloid Cells Revealed by Deep Single-Cell RNA Sequencing. *Neuron, 101*(2), 207-223 e210. doi:10.1016/j.neuron.2018.12.006
Liddelow, S. A., Guttenplan, K. A., Clarke, L. E., Bennett, F. C., Bohlen, C. J., Schirmer, L., . . . Barres, B. A. (2017). Neurotoxic reactive astrocytes are induced by activated microglia. *Nature, 541*(7638), 481-487. doi:10.1038/nature21029
Lim, S. H., Park, E., You, B., Jung, Y., Park, A. R., Park, S. G., & Lee, J. R. (2013). Neuronal synapse formation induced by microglia and interleukin 10. *PLoS One, 8*(11), e81218. doi:10.1371/journal.pone.0081218
Lobo-Silva, D., Carriche, G. M., Castro, A. G., Roque, S., & Saraiva, M. (2016). Balancing the immune response in the brain: IL-10 and its regulation. *J Neuroinflammation, 13*(1), 297. doi:10.1186/s12974-016-0763-8
Lodge, P. A., & Sriram, S. (1996). Regulation of microglial activation by TGF-beta, IL-10, and CSF-1. *J Leukoc Biol, 60*(4), 502-508.
London, A., Cohen, M., & Schwartz, M. (2013). Microglia and monocyte-derived macrophages: functionally distinct populations that act in concert in CNS plasticity and repair. *Front Cell Neurosci, 7*, 34. doi:10.3389/fncel.2013.00034
Lucchinetti, C., Bruck, W., Parisi, J., Scheithauer, B., Rodriguez, M., & Lassmann, H. (2000). Heterogeneity of multiple sclerosis lesions: implications for the pathogenesis of demyelination. *Ann Neurol, 47*(6), 707-717. doi:10.1002/1531-8249(200006)47:6<707::aid-ana3>3.0.co;2-q
Luo, C., Koyama, R., & Ikegaya, Y. (2016). Microglia engulf viable newborn cells in the epileptic dentate gyrus. *Glia, 64*(9), 1508-1517. doi:10.1002/glia.23018
Lynch, G., Matthews, D. A., Mosko, S., Parks, T., & Cotman, C. (1972). Induced acetylcholinesterase-rich layer in rat dentate gyrus following entorhinal lesions. *Brain Res, 42*(2), 311-318. doi:10.1016/0006-8993(72)90533-1
Madry, C., Kyrargyri, V., Arancibia-Carcamo, I. L., Jolivet, R., Kohsaka, S., Bryan, R. M., & Attwell, D. (2018). Microglial Ramification, Surveillance, and Interleukin-1beta Release Are Regulated by the Two-Pore Domain K(+) Channel THIK-1. *Neuron, 97*(2), 299-312 e296. doi:10.1016/j.neuron.2017.12.002
Majumdar, A., Cruz, D., Asamoah, N., Buxbaum, A., Sohar, I., Lobel, P., & Maxfield, F. R. (2007). Activation of microglia acidifies lysosomes and leads to degradation of Alzheimer amyloid fibrils. *Mol Biol Cell, 18*(4), 1490-1496. doi:10.1091/mbc.e06-10-0975

Mandelbrot, D. A., Oosterwegel, M. A., Shimizu, K., Yamada, A., Freeman, G. J., Mitchell, R. N., . . . Sharpe, A. H. (2001). B7-dependent T-cell costimulation in mice lacking CD28 and CTLA4. *J Clin Invest, 107*(7), 881-887. doi:10.1172/JCI11710

Manich, G., Gomez-Lopez, A. R., Almolda, B., Villacampa, N., Recasens, M., Shrivastava, K., . . . Castellano, B. (2020). Differential Roles of TREM2+ Microglia in Anterograde and Retrograde Axonal Injury Models. *Front Cell Neurosci, 14*, 567404. doi:10.3389/fncel.2020.567404

Manich, G., Recasens, M., Valente, T., Almolda, B., Gonzalez, B., & Castellano, B. (2019). Role of the CD200-CD200R Axis During Homeostasis and Neuroinflammation. *Neuroscience, 405*, 118-136. doi:10.1016/j.neuroscience.2018.10.030

Mantovani, A., Sica, A., Sozzani, S., Allavena, P., Vecchi, A., & Locati, M. (2004). The chemokine system in diverse forms of macrophage activation and polarization. *Trends Immunol, 25*(12), 677-686. doi:10.1016/j.it.2004.09.015

Marin-Teva, J. L., Dusart, I., Colin, C., Gervais, A., van Rooijen, N., & Mallat, M. (2004). Microglia promote the death of developing Purkinje cells. *Neuron, 41*(4), 535-547. doi:10.1016/s0896-6273(04)00069-8

Marinelli, S., Basilico, B., Marrone, M. C., & Ragozzino, D. (2019). Microglia-neuron crosstalk: Signaling mechanism and control of synaptic transmission. *Semin Cell Dev Biol, 94*, 138-151. doi:10.1016/j.semcdb.2019.05.017

Masuda, T., Sankowski, R., Staszewski, O., & Prinz, M. (2020). Microglia Heterogeneity in the Single-Cell Era. *Cell Rep, 30*(5), 1271-1281. doi:10.1016/j.celrep.2020.01.010

Mathys, H., Davila-Velderrain, J., Peng, Z., Gao, F., Mohammadi, S., Young, J. Z., . . . Tsai, L. H. (2019). Single-cell transcriptomic analysis of Alzheimer's disease. *Nature, 570*(7761), 332-337. doi:10.1038/s41586-019-1195-2

Matsui, T. K., & Mori, E. (2018). Microglia support neural stem cell maintenance and growth. *Biochem Biophys Res Commun, 503*(3), 1880-1884. doi:10.1016/j.bbrc.2018.07.130

Matthews, D. A., Cotman, C., & Lynch, G. (1976). An electron microscopic study of lesion-induced synaptogenesis in the dentate gyrus of the adult rat. II. Reappearance of morphologically normal synaptic contacts. *Brain Res, 115*(1), 23-41.

McBride, J. M., Jung, T., de Vries, J. E., & Aversa, G. (2002). IL-10 alters DC function via modulation of cell surface molecules resulting in impaired T-cell responses. *Cell Immunol, 215*(2), 162-172. doi:10.1016/s0008-8749(02)00007-2

McGeachy, M. J., & Anderton, S. M. (2005). Cytokines in the induction and resolution of experimental autoimmune encephalomyelitis. *Cytokine, 32*(2), 81-84. doi:10.1016/j.cyto.2005.07.012

Michaud, J. P., Halle, M., Lampron, A., Theriault, P., Prefontaine, P., Filali, M., . . . Rivest, S. (2013). Toll-like receptor 4 stimulation with the detoxified ligand monophosphoryl lipid A improves Alzheimer's disease-related pathology. *Proc Natl Acad Sci U S A, 110*(5), 1941-1946. doi:10.1073/pnas.1215165110

Mittal, S. K., Cho, K. J., Ishido, S., & Roche, P. A. (2015). Interleukin 10 (IL-10)-mediated Immunosuppression: MARCH-I INDUCTION REGULATES

ANTIGEN PRESENTATION BY MACROPHAGES BUT NOT DENDRITIC CELLS. *J Biol Chem, 290*(45), 27158-27167. doi:10.1074/jbc.M115.682708

Mittrucker, H. W., Visekruna, A., & Huber, M. (2014). Heterogeneity in the differentiation and function of CD8(+) T cells. *Arch Immunol Ther Exp (Warsz), 62*(6), 449-458. doi:10.1007/s00005-014-0293-y

Miyamoto, A., Wake, H., Ishikawa, A. W., Eto, K., Shibata, K., Murakoshi, H., . . . Nabekura, J. (2016). Microglia contact induces synapse formation in developing somatosensory cortex. *Nat Commun, 7*, 12540. doi:10.1038/ncomms12540

Mizuno, T., Sawada, M., Marunouchi, T., & Suzumura, A. (1994). Production of interleukin-10 by mouse glial cells in culture. *Biochem Biophys Res Commun, 205*(3), 1907-1915. doi:10.1006/bbrc.1994.2893

Molina-Holgado, F., Grencis, R., & Rothwell, N. J. (2001). Actions of exogenous and endogenous IL-10 on glial responses to bacterial LPS/cytokines. *Glia, 33*(2), 97-106.

Moore, K. W., de Waal Malefyt, R., Coffman, R. L., & O'Garra, A. (2001). Interleukin-10 and the interleukin-10 receptor. *Annu Rev Immunol, 19*, 683-765. doi:10.1146/annurev.immunol.19.1.683

Mori, S., Maher, P., & Conti, B. (2016). Neuroimmunology of the Interleukins 13 and 4. *Brain Sci, 6*(2). doi:10.3390/brainsci6020018

Mosmann, T. R., & Coffman, R. L. (1989). Heterogeneity of cytokine secretion patterns and functions of helper T cells. *Adv Immunol, 46*, 111-147. doi:10.1016/s0065-2776(08)60652-5

Nadler, J. V., & Cotman, C. W. (1978). Interactions between afferents to the dentate gyrus after entorhinal lesion during development: long-term regulation of choline acetyl-transferase activity. *Brain Res, 142*(1), 174-181. doi:10.1016/0006-8993(78)90188-9

Napoli, I., & Neumann, H. (2009). Microglial clearance function in health and disease. *Neuroscience, 158*(3), 1030-1038. doi:10.1016/j.neuroscience.2008.06.046

Neher, J. J., & Cunningham, C. (2019). Priming Microglia for Innate Immune Memory in the Brain. *Trends Immunol, 40*(4), 358-374. doi:10.1016/j.it.2019.02.001

Netea, M. G., Joosten, L. A., Latz, E., Mills, K. H., Natoli, G., Stunnenberg, H. G., . . . Xavier, R. J. (2016). Trained immunity: A program of innate immune memory in health and disease. *Science, 352*(6284), aaf1098. doi:10.1126/science.aaf1098

Nimmerjahn, A., Kirchhoff, F., & Helmchen, F. (2005). Resting microglial cells are highly dynamic surveillants of brain parenchyma in vivo. *Science, 308*(5726), 1314-1318. doi:10.1126/science.1110647

Niraula, A., Sheridan, J. F., & Godbout, J. P. (2017). Microglia Priming with Aging and Stress. *Neuropsychopharmacology, 42*(1), 318-333. doi:10.1038/npp.2016.185

Noelker, C., Morel, L., Lescot, T., Osterloh, A., Alvarez-Fischer, D., Breloer, M., . . . Hartmann, A. (2013). Toll like receptor 4 mediates cell death in a mouse MPTP model of Parkinson disease. *Sci Rep, 3*, 1393. doi:10.1038/srep01393

Nolan, A., Kobayashi, H., Naveed, B., Kelly, A., Hoshino, Y., Hoshino, S., . . . Gold, J. A. (2009). Differential role for CD80 and CD86 in the regulation of the innate

immune response in murine polymicrobial sepsis. *PLoS One, 4*(8), e6600. doi:10.1371/journal.pone.0006600

Norden, D. M., Fenn, A. M., Dugan, A., & Godbout, J. P. (2014). TGFbeta produced by IL-10 redirected astrocytes attenuates microglial activation. *Glia, 62*(6), 881-895. doi:10.1002/glia.22647

Nugent, A. A., Lin, K., van Lengerich, B., Lianoglou, S., Przybyla, L., Davis, S. S., . . . Di Paolo, G. (2020). TREM2 Regulates Microglial Cholesterol Metabolism upon Chronic Phagocytic Challenge. *Neuron, 105*(5), 837-854 e839. doi:10.1016/j.neuron.2019.12.007

Orihuela, R., McPherson, C. A., & Harry, G. J. (2016). Microglial M1/M2 polarization and metabolic states. *Br J Pharmacol, 173*(4), 649-665. doi:10.1111/bph.13139

Orre, M., Kamphuis, W., Osborn, L. M., Melief, J., Kooijman, L., Huitinga, I., . . . Hol, E. M. (2014). Acute isolation and transcriptome characterization of cortical astrocytes and microglia from young and aged mice. *Neurobiol Aging, 35*(1), 1-14. doi:10.1016/j.neurobiolaging.2013.07.008

Owens, T. (2002). Identification of new therapeutic targets for prevention of CNS inflammation. *Expert Opin Ther Targets, 6*(2), 203-215. doi:10.1517/14728222.6.2.203

Park, K. W., Lee, H. G., Jin, B. K., & Lee, Y. B. (2007). Interleukin-10 endogenously expressed in microglia prevents lipopolysaccharide-induced neurodegeneration in the rat cerebral cortex in vivo. *Exp Mol Med, 39*(6), 812-819. doi:10.1038/emm.2007.88

Perdiguero, E. G., & Geissmann, F. (2016). The development and maintenance of resident macrophages. *Nat Immunol, 17*(1), 2-8. doi:10.1038/ni.3341

Perederiy, J. V., & Westbrook, G. L. (2013). Structural plasticity in the dentate gyrus- revisiting a classic injury model. *Front Neural Circuits, 7*, 17. doi:10.3389/fncir.2013.00017

Petkovic, F., Campbell, I. L., Gonzalez, B., & Castellano, B. (2016). Astrocyte-targeted production of interleukin-6 reduces astroglial and microglial activation in the cuprizone demyelination model: Implications for myelin clearance and oligodendrocyte maturation. *Glia, 64*(12), 2104-2119. doi:10.1002/glia.23043

Phinney, A. L., Calhoun, M. E., Woods, A. G., Deller, T., & Jucker, M. (2004). Stereological analysis of the reorganization of the dentate gyrus following entorhinal cortex lesion in mice. *Eur J Neurosci, 19*(7), 1731-1740. doi:10.1111/j.1460-9568.2004.03280.x

Piccio, L., Buonsanti, C., Mariani, M., Cella, M., Gilfillan, S., Cross, A. H., . . . Panina-Bordignon, P. (2007). Blockade of TREM-2 exacerbates experimental autoimmune encephalomyelitis. *Eur J Immunol, 37*(5), 1290-1301. doi:10.1002/eji.200636837

Pineau, I., & Lacroix, S. (2007). Proinflammatory cytokine synthesis in the injured mouse spinal cord: multiphasic expression pattern and identification of the cell types involved. *J Comp Neurol, 500*(2), 267-285. doi:10.1002/cne.21149

Poliani, P. L., Wang, Y., Fontana, E., Robinette, M. L., Yamanishi, Y., Gilfillan, S., & Colonna, M. (2015). TREM2 sustains microglial expansion during aging and response to demyelination. *J Clin Invest, 125*(5), 2161-2170. doi:10.1172/JCI77983

Popovich, P. G., Guan, Z., Wei, P., Huitinga, I., van Rooijen, N., & Stokes, B. T. (1999). Depletion of hematogenous macrophages promotes partial hindlimb recovery and neuroanatomical repair after experimental spinal cord injury. *Exp Neurol, 158*(2), 351-365. doi:10.1006/exnr.1999.7118

Pousset, F., Cremona, S., Dantzer, R., Kelley, K. W., & Parnet, P. (2001). IL-10 and IL-4 regulate type-I and type-II IL-1 receptors expression on IL-1 beta-activated mouse primary astrocytes. *J Neurochem, 79*(4), 726-736.

Prineas, J. W., & Wright, R. G. (1978). Macrophages, lymphocytes, and plasma cells in the perivascular compartment in chronic multiple sclerosis. *Lab Invest, 38*(4), 409-421.

Prinz, M., Jung, S., & Priller, J. (2019). Microglia Biology: One Century of Evolving Concepts. *Cell, 179*(2), 292-311. doi:10.1016/j.cell.2019.08.053

Raivich, G., Jones, L. L., Werner, A., Bluthmann, H., Doetschmann, T., & Kreutzberg, G. W. (1999). Molecular signals for glial activation: pro- and anti-inflammatory cytokines in the injured brain. *Acta Neurochir Suppl, 73*, 21-30.

Ransohoff, R. M., & Brown, M. A. (2012). Innate immunity in the central nervous system. *J Clin Invest, 122*(4), 1164-1171. doi:10.1172/JCI58644

Rolle, C. E., Sengupta, S., & Lesniak, M. S. (2012). Mechanisms of immune evasion by gliomas. *Adv Exp Med Biol, 746*, 53-76. doi:10.1007/978-1-4614-3146-6_5

Rose-John, S. (2012). IL-6 trans-signaling via the soluble IL-6 receptor: importance for the pro-inflammatory activities of IL-6. *Int J Biol Sci, 8*(9), 1237-1247. doi:10.7150/ijbs.4989

Sakalidou, M., Leibig, N., Boyle, V., Koulaxouzidis, G., & Penna, V. (2011). Interleukin-10 and regeneration in an end-to-side nerve repair model of the rat. *J Peripher Nerv Syst, 16*(4), 334-340. doi:10.1111/j.1529-8027.2011.00368.x

Sarlus, H., & Heneka, M. T. (2017). Microglia in Alzheimer's disease. *J Clin Invest, 127*(9), 3240-3249. doi:10.1172/JCI90606

Sawada, M., Suzumura, A., Hosoya, H., Marunouchi, T., & Nagatsu, T. (1999). Interleukin-10 inhibits both production of cytokines and expression of cytokine receptors in microglia. *J Neurochem, 72*(4), 1466-1471.

Scholtzova, H., Do, E., Dhakal, S., Sun, Y., Liu, S., Mehta, P. D., & Wisniewski, T. (2017). Innate Immunity Stimulation via Toll-Like Receptor 9 Ameliorates Vascular Amyloid Pathology in Tg-SwDI Mice with Associated Cognitive Benefits. *J Neurosci, 37*(4), 936-959. doi:10.1523/JNEUROSCI.1967-16.2016

Schulz, C., Gomez Perdiguero, E., Chorro, L., Szabo-Rogers, H., Cagnard, N., Kierdorf, K., . . . Geissmann, F. (2012). A lineage of myeloid cells independent of Myb and hematopoietic stem cells. *Science, 336*(6077), 86-90. doi:10.1126/science.1219179

Serpe, C. J., Sanders, V. M., & Jones, K. J. (2000). Kinetics of facial motoneuron loss following facial nerve transection in severe combined immunodeficient mice. *J Neurosci Res, 62*(2), 273-278. doi:10.1002/1097-4547(20001015)62:2<273::AID-JNR11>3.0.CO;2-C

Sevenich, L. (2018). Brain-Resident Microglia and Blood-Borne Macrophages Orchestrate Central Nervous System Inflammation in Neurodegenerative Disorders and Brain Cancer. *Front Immunol, 9*, 697. doi:10.3389/fimmu.2018.00697

Sharpe, A. H., & Freeman, G. J. (2002). The B7-CD28 superfamily. *Nat Rev Immunol, 2*(2), 116-126. doi:10.1038/nri727

Shechter, R., London, A., Varol, C., Raposo, C., Cusimano, M., Yovel, G., . . . Schwartz, M. (2009). Infiltrating blood-derived macrophages are vital cells playing an anti-inflammatory role in recovery from spinal cord injury in mice. *PLoS Med, 6*(7), e1000113. doi:10.1371/journal.pmed.1000113

Shuto, T., Horie, H., Hikawa, N., Sango, K., Tokashiki, A., Murata, H., . . . Ishikawa, Y. (2001). IL-6 up-regulates CNTF mRNA expression and enhances neurite regeneration. *Neuroreport, 12*(5), 1081-1085. doi:10.1097/00001756-200104170-00043

Siebert, J. R., Conta Steencken, A., & Osterhout, D. J. (2014). Chondroitin sulfate proteoglycans in the nervous system: inhibitors to repair. *Biomed Res Int, 2014*, 845323. doi:10.1155/2014/845323

Sierra, A., Encinas, J. M., Deudero, J. J., Chancey, J. H., Enikolopov, G., Overstreet-Wadiche, L. S., . . . Maletic-Savatic, M. (2010). Microglia shape adult hippocampal neurogenesis through apoptosis-coupled phagocytosis. *Cell Stem Cell, 7*(4), 483-495. doi:10.1016/j.stem.2010.08.014

Sipe, G. O., Lowery, R. L., Tremblay, M. E., Kelly, E. A., Lamantia, C. E., & Majewska, A. K. (2016). Microglial P2Y12 is necessary for synaptic plasticity in mouse visual cortex. *Nat Commun, 7*, 10905. doi:10.1038/ncomms10905

Siqueira Mietto, B., Kroner, A., Girolami, E. I., Santos-Nogueira, E., Zhang, J., & David, S. (2015). Role of IL-10 in Resolution of Inflammation and Functional Recovery after Peripheral Nerve Injury. *J Neurosci, 35*(50), 16431-16442. doi:10.1523/JNEUROSCI.2119-15.2015

Smith, J. A., Das, A., Ray, S. K., & Banik, N. L. (2012). Role of pro-inflammatory cytokines released from microglia in neurodegenerative diseases. *Brain Res Bull, 87*(1), 10-20. doi:10.1016/j.brainresbull.2011.10.004

Smolders, S. M., Kessels, S., Vangansewinkel, T., Rigo, J. M., Legendre, P., & Brone, B. (2019). Microglia: Brain cells on the move. *Prog Neurobiol, 178*, 101612. doi:10.1016/j.pneurobio.2019.04.001

Sofroniew, M. V. (2014). Astrogliosis. *Cold Spring Harb Perspect Biol, 7*(2), a020420. doi:10.1101/cshperspect.a020420

Spera, P. A., Ellison, J. A., Feuerstein, G. Z., & Barone, F. C. (1998). IL-10 reduces rat brain injury following focal stroke. *Neurosci Lett, 251*(3), 189-192.

Stanfield, B. B., Caviness, V. S., Jr., & Cowan, W. M. (1979). The organization of certain afferents to the hippocampus and dentate gyrus in normal and reeler mice. *J Comp Neurol, 185*(3), 461-483. doi:10.1002/cne.901850304

Stence, N., Waite, M., & Dailey, M. E. (2001). Dynamics of microglial activation: a confocal time-lapse analysis in hippocampal slices. *Glia, 33*(3), 256-266.

Stowell, R. D., Wong, E. L., Batchelor, H. N., Mendes, M. S., Lamantia, C. E., Whitelaw, B. S., & Majewska, A. K. (2018). Cerebellar microglia are dynamically unique and survey Purkinje neurons in vivo. *Dev Neurobiol, 78*(6), 627-644. doi:10.1002/dneu.22572

Strachan-Whaley, M., Rivest, S., & Yong, V. W. (2014). Interactions between microglia and T cells in multiple sclerosis pathobiology. *J Interferon Cytokine Res, 34*(8), 615-622. doi:10.1089/jir.2014.0019

Streit, W. J. (2000). Microglial response to brain injury: a brief synopsis. *Toxicol Pathol, 28*(1), 28-30. doi:10.1177/019262330002800104

Stremmel, C., Schuchert, R., Wagner, F., Thaler, R., Weinberger, T., Pick, R., . . . Schulz, C. (2018). Yolk sac macrophage progenitors traffic to the embryo during defined stages of development. *Nat Commun, 9*(1), 75. doi:10.1038/s41467-017-02492-2

Strle, K., Zhou, J. H., Broussard, S. R., Venters, H. D., Johnson, R. W., Freund, G. G., . . . Kelley, K. W. (2002). IL-10 promotes survival of microglia without activating Akt. *J Neuroimmunol, 122*(1-2), 9-19.

Strle, K., Zhou, J. H., Shen, W. H., Broussard, S. R., Johnson, R. W., Freund, G. G., . . . Kelley, K. W. (2001). Interleukin-10 in the brain. *Crit Rev Immunol, 21*(5), 427-449.

Suzumura, A. (2013). Neuron-microglia interaction in neuroinflammation. *Curr Protein Pept Sci, 14*(1), 16-20. doi:10.2174/1389203711314010004

Swardfager, W., Winer, D. A., Herrmann, N., Winer, S., & Lanctot, K. L. (2013). Interleukin-17 in post-stroke neurodegeneration. *Neurosci Biobehav Rev, 37*(3), 436-447. doi:10.1016/j.neubiorev.2013.01.021

Takahashi, K., Rochford, C. D., & Neumann, H. (2005). Clearance of apoptotic neurons without inflammation by microglial triggering receptor expressed on myeloid cells-2. *J Exp Med, 201*(4), 647-657. doi:10.1084/jem.20041611

Takeuchi, O., & Akira, S. (2010). Pattern recognition receptors and inflammation. *Cell, 140*(6), 805-820. doi:10.1016/j.cell.2010.01.022

Tang, Y., & Le, W. (2016). Differential Roles of M1 and M2 Microglia in Neurodegenerative Diseases. *Mol Neurobiol, 53*(2), 1181-1194. doi:10.1007/s12035-014-9070-5

Taylor, D. L., Diemel, L. T., Cuzner, M. L., & Pocock, J. M. (2002). Activation of group II metabotropic glutamate receptors underlies microglial reactivity and neurotoxicity following stimulation with chromogranin A, a peptide up-regulated in Alzheimer's disease. *J Neurochem, 82*(5), 1179-1191. doi:10.1046/j.1471-4159.2002.01062.x

Thon, N., Haas, C. A., Rauch, U., Merten, T., Fassler, R., Frotscher, M., & Deller, T. (2000). The chondroitin sulphate proteoglycan brevican is upregulated by astrocytes after entorhinal cortex lesions in adult rats. *Eur J Neurosci, 12*(7), 2547-2558.

Tilgner, J., Volk, B., & Kaltschmidt, C. (2001). Continuous interleukin-6 application in vivo via macroencapsulation of interleukin-6-expressing COS-7 cells induces massive gliosis. *Glia, 35*(3), 234-245.

Torres-Platas, S. G., Cruceanu, C., Chen, G. G., Turecki, G., & Mechawar, N. (2014). Evidence for increased microglial priming and macrophage recruitment in the dorsal anterior cingulate white matter of depressed suicides. *Brain Behav Immun, 42*, 50-59. doi:10.1016/j.bbi.2014.05.007

Tremblay, M. E., Lowery, R. L., & Majewska, A. K. (2010). Microglial interactions with synapses are modulated by visual experience. *PLoS Biol, 8*(11), e1000527. doi:10.1371/journal.pbio.1000527

Tremblay, M. E., Stevens, B., Sierra, A., Wake, H., Bessis, A., & Nimmerjahn, A. (2011). The role of microglia in the healthy brain. *J Neurosci, 31*(45), 16064-16069. doi:10.1523/JNEUROSCI.4158-11.2011

Turner, C. A., Eren-Kocak, E., Inui, E. G., Watson, S. J., & Akil, H. (2016). Dysregulated fibroblast growth factor (FGF) signaling in neurological and psychiatric disorders. *Semin Cell Dev Biol, 53*, 136-143. doi:10.1016/j.semcdb.2015.10.003

Ulland, T. K., Song, W. M., Huang, S. C., Ulrich, J. D., Sergushichev, A., Beatty, W. L., . . . Colonna, M. (2017). TREM2 Maintains Microglial Metabolic Fitness in Alzheimer's Disease. *Cell, 170*(4), 649-663 e613. doi:10.1016/j.cell.2017.07.023

van der Poel, M., Ulas, T., Mizee, M. R., Hsiao, C. C., Miedema, S. S. M., Adelia, . . . Huitinga, I. (2019). Transcriptional profiling of human microglia reveals grey-white matter heterogeneity and multiple sclerosis-associated changes. *Nat Commun, 10*(1), 1139. doi:10.1038/s41467-019-08976-7

van Groen, T., Kadish, I., & Wyss, J. M. (2002). Species differences in the projections from the entorhinal cortex to the hippocampus. *Brain Res Bull, 57*(3-4), 553-556. doi:10.1016/s0361-9230(01)00683-9

van Groen, T., Miettinen, P., & Kadish, I. (2003). The entorhinal cortex of the mouse: organization of the projection to the hippocampal formation. *Hippocampus, 13*(1), 133-149. doi:10.1002/hipo.10037

Varnum, M. M., Kiyota, T., Ingraham, K. L., Ikezu, S., & Ikezu, T. (2015). The anti-inflammatory glycoprotein, CD200, restores neurogenesis and enhances amyloid phagocytosis in a mouse model of Alzheimer's disease. *Neurobiol Aging, 36*(11), 2995-3007. doi:10.1016/j.neurobiolaging.2015.07.027

Venegas, C., & Heneka, M. T. (2017). Danger-associated molecular patterns in Alzheimer's disease. *J Leukoc Biol, 101*(1), 87-98. doi:10.1189/jlb.3MR0416-204R

Verdonk, F., Roux, P., Flamant, P., Fiette, L., Bozza, F. A., Simard, S., . . . Danckaert, A. (2016). Phenotypic clustering: a novel method for microglial morphology analysis. *J Neuroinflammation, 13*(1), 153. doi:10.1186/s12974-016-0614-7

Vidal, P. M., Lemmens, E., Avila, A., Vangansewinkel, T., Chalaris, A., Rose-John, S., & Hendrix, S. (2013). ADAM17 is a survival factor for microglial cells in vitro and in vivo after spinal cord injury in mice. *Cell Death Dis, 4*, e954. doi:10.1038/cddis.2013.466

Vilalta, A., & Brown, G. C. (2018). Neurophagy, the phagocytosis of live neurons and synapses by glia, contributes to brain development and disease. *FEBS J, 285*(19), 3566-3575. doi:10.1111/febs.14323

Villacampa, N., Almolda, B., Vilella, A., Campbell, I. L., Gonzalez, B., & Castellano, B. (2015). Astrocyte-targeted production of IL-10 induces changes in microglial reactivity and reduces motor neuron death after facial nerve axotomy. *Glia, 63*(7), 1166-1184. doi:10.1002/glia.22807

Vitkovic, L., Bockaert, J., & Jacque, C. (2000). "Inflammatory" cytokines: neuromodulators in normal brain? *J Neurochem, 74*(2), 457-471. doi:10.1046/j.1471-4159.2000.740457.x

Vuksic, M., Del Turco, D., Vlachos, A., Schuldt, G., Muller, C. M., Schneider, G., & Deller, T. (2011). Unilateral entorhinal denervation leads to long-lasting dendritic alterations of mouse hippocampal granule cells. *Exp Neurol, 230*(2), 176-185. doi:10.1016/j.expneurol.2011.04.011

Waisman, A., Hauptmann, J., & Regen, T. (2015). The role of IL-17 in CNS diseases. *Acta Neuropathol, 129*(5), 625-637. doi:10.1007/s00401-015-1402-7

Wake, H., Moorhouse, A. J., Miyamoto, A., & Nabekura, J. (2013). Microglia: actively surveying and shaping neuronal circuit structure and function. *Trends Neurosci, 36*(4), 209-217. doi:10.1016/j.tins.2012.11.007

Walton, N. M., Sutter, B. M., Laywell, E. D., Levkoff, L. H., Kearns, S. M., Marshall, G. P., 2nd, . . . Steindler, D. A. (2006). Microglia instruct subventricular zone neurogenesis. *Glia, 54*(8), 815-825. doi:10.1002/glia.20419

Weinhard, L., di Bartolomei, G., Bolasco, G., Machado, P., Schieber, N. L., Neniskyte, U., . . . Gross, C. T. (2018). Microglia remodel synapses by presynaptic trogocytosis and spine head filopodia induction. *Nat Commun, 9*(1), 1228. doi:10.1038/s41467-018-03566-5

Wendeln, A. C., Degenhardt, K., Kaurani, L., Gertig, M., Ulas, T., Jain, G., . . . Neher, J. J. (2018). Innate immune memory in the brain shapes neurological disease hallmarks. *Nature, 556*(7701), 332-338. doi:10.1038/s41586-018-0023-4

Wirenfeldt, M., Babcock, A. A., Ladeby, R., Lambertsen, K. L., Dagnaes-Hansen, F., Leslie, R. G., . . . Finsen, B. (2005). Reactive microgliosis engages distinct responses by microglial subpopulations after minor central nervous system injury. *J Neurosci Res, 82*(4), 507-514. doi:10.1002/jnr.20659

Wirenfeldt, M., Dissing-Olesen, L., Anne Babcock, A., Nielsen, M., Meldgaard, M., Zimmer, J., . . . Finsen, B. (2007). Population control of resident and immigrant microglia by mitosis and apoptosis. *Am J Pathol, 171*(2), 617-631. doi:10.2353/ajpath.2007.061044

Wlodarczyk, A., Holtman, I. R., Krueger, M., Yogev, N., Bruttger, J., Khorooshi, R., . . . Owens, T. (2017). A novel microglial subset plays a key role in myelinogenesis in developing brain. *EMBO J, 36*(22), 3292-3308. doi:10.15252/embj.201696056

Wu, A., Wei, J., Kong, L. Y., Wang, Y., Priebe, W., Qiao, W., . . . Heimberger, A. B. (2010). Glioma cancer stem cells induce immunosuppressive macrophages/microglia. *Neuro Oncol, 12*(11), 1113-1125. doi:10.1093/neuonc/noq082

Wu, Y., & Hirschi, K. K. (2020). Tissue-Resident Macrophage Development and Function. *Front Cell Dev Biol, 8*, 617879. doi:10.3389/fcell.2020.617879

Xin, J., Wainwright, D. A., Mesnard, N. A., Serpe, C. J., Sanders, V. M., & Jones, K. J. (2011). IL-10 within the CNS is necessary for CD4+ T cells to mediate neuroprotection. *Brain Behav Immun, 25*(5), 820-829. doi:10.1016/j.bbi.2010.08.004

Xue, F., & Du, H. (2021). TREM2 Mediates Microglial Anti-Inflammatory Activations in Alzheimer's Disease: Lessons Learned from Transcriptomics. *Cells, 10*(2). doi:10.3390/cells10020321

Yang, P., Wen, H., Ou, S., Cui, J., & Fan, D. (2012). IL-6 promotes regeneration and functional recovery after cortical spinal tract injury by reactivating intrinsic growth program of neurons and enhancing synapse formation. *Exp Neurol, 236*(1), 19-27. doi:10.1016/j.expneurol.2012.03.019

Zamanian, J. L., Xu, L., Foo, L. C., Nouri, N., Zhou, L., Giffard, R. G., & Barres, B. A. (2012). Genomic analysis of reactive astrogliosis. *J Neurosci, 32*(18), 6391-6410. doi:10.1523/JNEUROSCI.6221-11.2012

Zeisel, A., Munoz-Manchado, A. B., Codeluppi, S., Lonnerberg, P., La Manno, G., Jureus, A., . . . Linnarsson, S. (2015). Brain structure. Cell types in the mouse cortex and hippocampus revealed by single-cell RNA-seq. *Science, 347*(6226), 1138-1142. doi:10.1126/science.aaa1934

Zhang, L., Zhang, J., & You, Z. (2018). Switching of the Microglial Activation Phenotype Is a Possible Treatment for Depression Disorder. *Front Cell Neurosci, 12*, 306. doi:10.3389/fncel.2018.00306

Zhang, Y., Feng, S., Nie, K., Li, Y., Gao, Y., Gan, R., . . . Zhang, Y. (2018). TREM2 modulates microglia phenotypes in the neuroinflammation of Parkinson's disease. *Biochem Biophys Res Commun, 499*(4), 797-802. doi:10.1016/j.bbrc.2018.03.226

Zhong, L., Zhang, Z. L., Li, X., Liao, C., Mou, P., Wang, T., . . . Chen, X. F. (2017). TREM2/DAP12 Complex Regulates Inflammatory Responses in Microglia via the JNK Signaling Pathway. *Front Aging Neurosci, 9*, 204. doi:10.3389/fnagi.2017.00204

Zhou, Z., Peng, X., Insolera, R., Fink, D. J., & Mata, M. (2009). IL-10 promotes neuronal survival following spinal cord injury. *Exp Neurol, 220*(1), 183-190. doi:10.1016/j.expneurol.2009.08.018

ANNEX I

Table 1. Antibodies used in IHC

	Target antigen	Host	Dilution	Cat Number	Manufacturer
Primary antibodies					
	Caspase 3	Rabbit	1:1000	AF835	R&D Systems
	CD11b	Rat	1:1000	MCA74GA	AbD Serotec
	CD39	Sheep	1:500	AF4398	R&D Systems
	GFAP	Mouse	1:6000	63893	Sigma Aldrich
	GFAP	Rabbit	1:1800	Z0334	Dakopatts
	Iba1	Rabbit	1:3000	019-19741	Wako
	IL-10	Rat	1:200	Ab33471	Abcam
	IL-10R	Rabbit	1:100	Sc-985	Santa cruz
	MCSF-R	Rabbit	1:125	Ab32633	Abcam
	PH3	Rabbit	1:3000	06-570	Millipore
	Pu.1	Rabbit	1:400	2258S	Cell Signaling
	CD45	Rat	1:1000	MCA1031G	AbD Serotec
	BrdU	Rat	1:120	Ab6326	Abcam
	CD28	Rabbit	1:50	ab203084	Abcam
	CD3	Hamster	1:500	MCA2690	AbD Serotec
	MHCII (IA)	Rat hybridoma	1:25	TIB-120	ATCC
	CD206	Rat	1:500	MCA2235GA	AbD Serotec
	CTLA-4	Rabbit	1:25	ab237712	Abcam
	Laminin	Rabbit	1:500	AMP420	Biorad
	TMEM119	Rabbit	1:1000	ab209064	Abcam
Secondary antibodies					
	Alexa 488	Mouse	1:500	A11029	Invitrogen
	Alexa 488	Rabbit	1:500	A21206	Invitrogen
	Alexa 488	Rat	1:500	A11006	Invitrogen
	Alexa 555	Rabbit	1:500	A21428	Invitrogen
	Alexa 555	Rat	1:1000	A11006	Invitrogen
	Alexa 568	Rat	1:500	A11077	Invitrogen
	Alexa 647	Rat	1:500	A21247	Invitrogen
	Biotinylated	Rabbit	1:500	BA-1000	Vector Laboratories
	Biotinylated	Rat	1:500	BA-4001	Vector Laboratories
	Biotinylated	Sheep	1:500	Ab6899	Abcam
	Biotinylated	Hamster	1:500	BA-9100	Vector Laboratories
	Biotinylated	Goat	1:500		Vector Laboratories
	Cy2	Mouse	1:500	PA42003	GE Healthcare

					Lifescience
	Streptavidin-HRP		1:500	SA-5004	Vector Laboratories
	Streptavidin Alexa Fluor-488		1:500	S11223	Molecular Probes
	Streptavidin Alexa Fluor-555		1:500	S32355	Molecular Probes
Fluorescent stain	DAPI		1:10000	D9542	Sigma Aldrich

Table 2. Antibodies used in Flow Cytometry

Fc blocker	Target antigen	Format	Dilution	Cat Number	Manufacturer
	CD16/32	Purified	1:250	553142	BD Pharmingen
Primary antibodies					
	CD3e	FITC	1:400	553062	BD Pharmingen
	CD4	APC-Cy7	1:400	552051	BD Pharmingen
	CD8	PerCP	1:400	553036	BD Pharmingen
	CD11b	APC-Cy7	1:400	557657	BD Pharmingen
	CD11c	PE	1:400	557401	BD Pharmingen
	CD45	PerCPCy5	1:400	557235	BD Pharmingen
	CD80	APC	1:400	560016	BD Pharmingen
	CD86	PE-Cy7	1:400	560582	BD Pharmingen
	F4/80	APC	1:400	17-4801-82	eBioscience
	FoxP3	PE-Cy7	1:400	25-5773-80	eBioscience
	Gata3	PE	1:400	560074	BD Pharmingen
	ICOSL	PE	1:400	12-5985-82	eBioscience
	Ly6C	FITC	1:400	553104	BD Pharmingen
	MHCII	FITC	1:400	553623	BD Pharmingen
	RORγt	APC	1:400	17-6988-82	eBioscience
	T-bet	PerCP-Cy5.5	1:400	45-5825-80	eBioscience

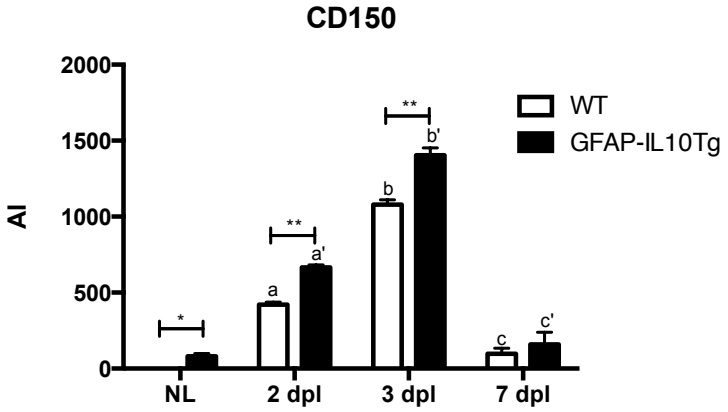

Figure 1. CD150 expression. In NL conditions, GFAP-IL10Tg animals presented significantly higher levels of CD150 than WT. After PPT, although both animals showed the same activation patter, GFAP-IL10Tg mice expressed higher levels at 2 and 3 dpl compared to WT. Data are mean ± SEM. The significances are represented as: * WT vs GFAP-IL10Tg; in WT animals, a: indicates significance vs NL, b: significance vs 2dpl, and c: significance vs 3dpl; in transgenic animals a', b' and c' indicates significance vs NL, 2dpl and 3dpl, respectively.

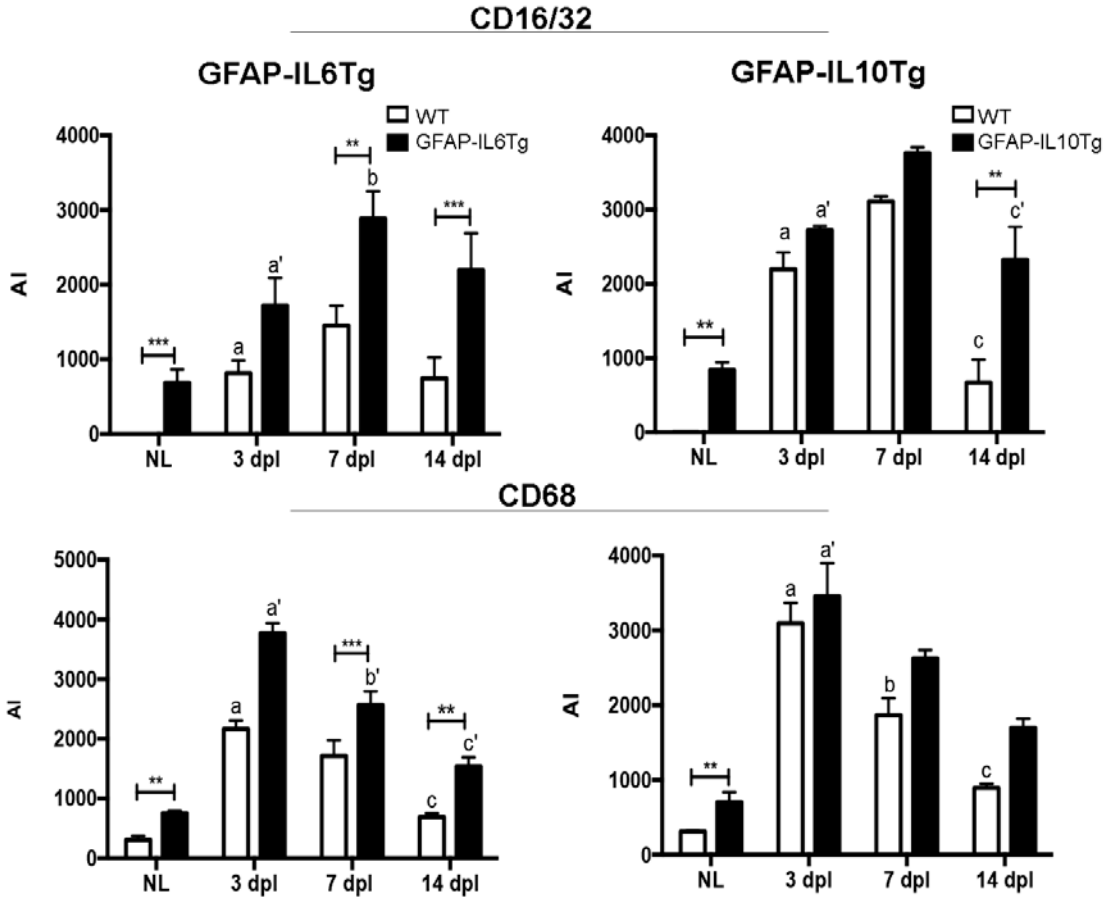

Figure 2. Microglial phagocytosis. Both NL GFAP-IL6Tg and NL GFAP-IL10Tg animals showed significantly higher levels of CD68 and CD16/32 than WT. After PPT, GFAP-IL6Tg mice presented increased expression of CD68 and CD16/32 at 7 and 14 dpl compared to their respective WT. In the case of GFAP-IL10Tg mice, we only observed higher expression of CD16/32 at 14 dpl. Data are mean ± SEM. The significances are represented as: * WT vs GFAP-IL10Tg; in WT animals, a: indicates significance vs NL, b: significance vs 3dpl, and c: significance vs 7dpl; in transgenic animals a', b' and c' indicates significance vs NL, 3dpl and 7dpl, respectively.

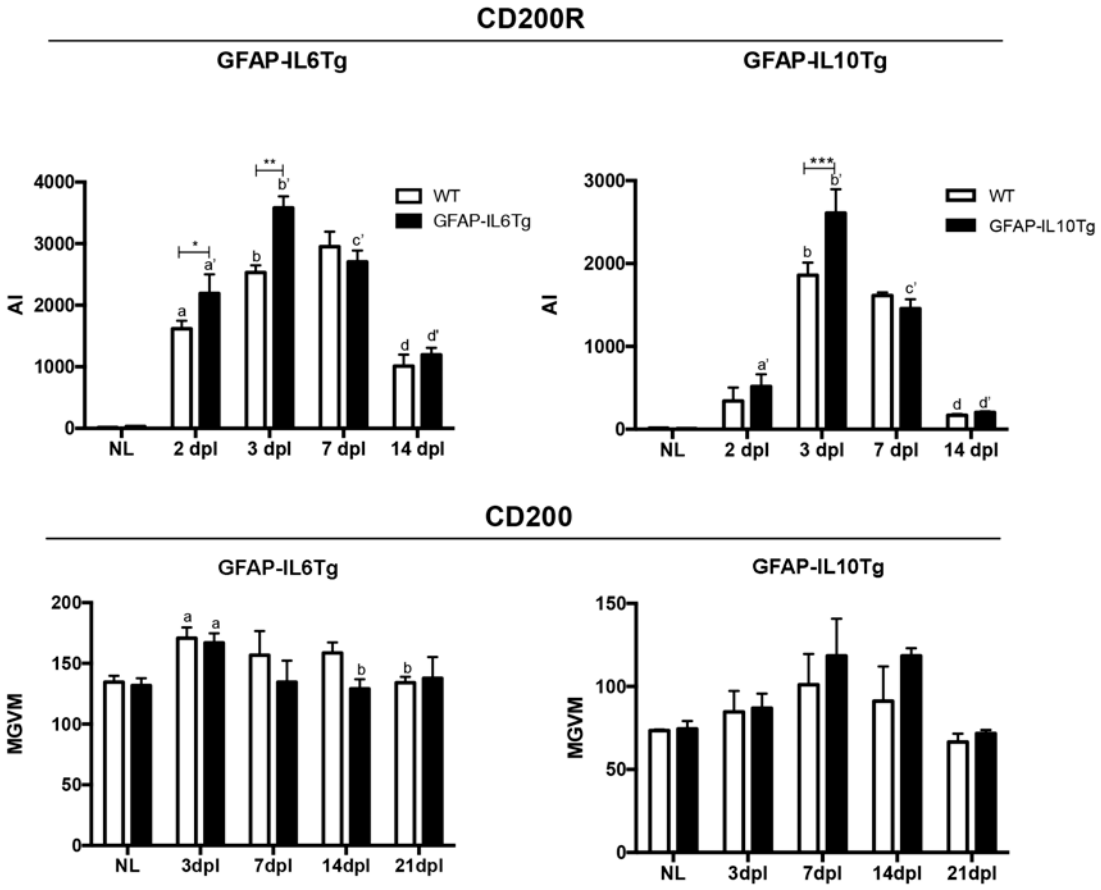

Figure 3. CD200-CD200R expression. Regarding CD200R, both GFAP-IL6Tg and GFAP-IL10Tg mice showed increased levels at 3 dpl than WT. Regarding CD200 expression, both animals presented induction of CD200 but with earlier downregulation only observerd in GFAP-IL6Tg animals. Data are mean ± SEM. The significances in CD200R graphs are represented as: * WT vs GFAP-IL10Tg; in WT animals, a: indicates significance vs NL, b: significance vs 3dpl, and c: significance vs 7dpl; in transgenic animals a', b' and c' indicates significance vs NL, 3dpl and 7dpl, respectively. Significance in CD200 graphs are represented as: a: indicates significance vs NL and b: indicates significance vs 3dpl.

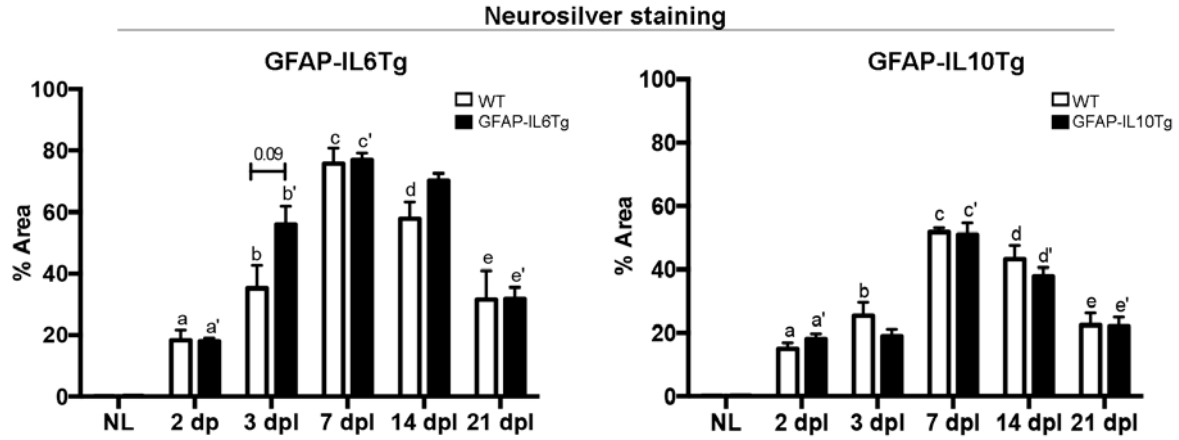

Figure 4. Neurosilver. At 3 dpl, GFAP-IL6Tg animals showed increased presence of degenerating fibers in the dennervated area than WT. No differences were observed between GFAP-IL10Tg mice compared to WT. Data are mean ± SEM. The significances are represented as: a: indicates significance vs NL, b: significance vs 2dpl, c: significance vs 3dpl; d: significance vs 7dpl; e: significance vs 14 dpl; in transgenic animals a', b', c', d' and e' indicates significance vs NL, 2dpl, 3dpl, 7dpl and 14 dpl respectively.

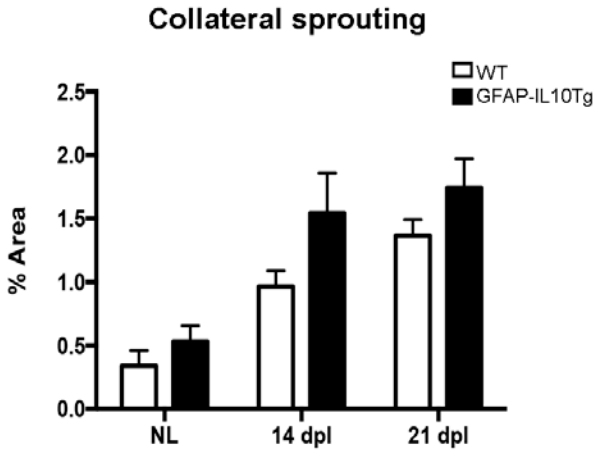

Figure 5. Collateral sprouting. Both GFAP-IL10Tg and WT animals presented equal percentage of $Timm^{+}$ fibers along the progression of the lesion. Data are mean ± SEM.

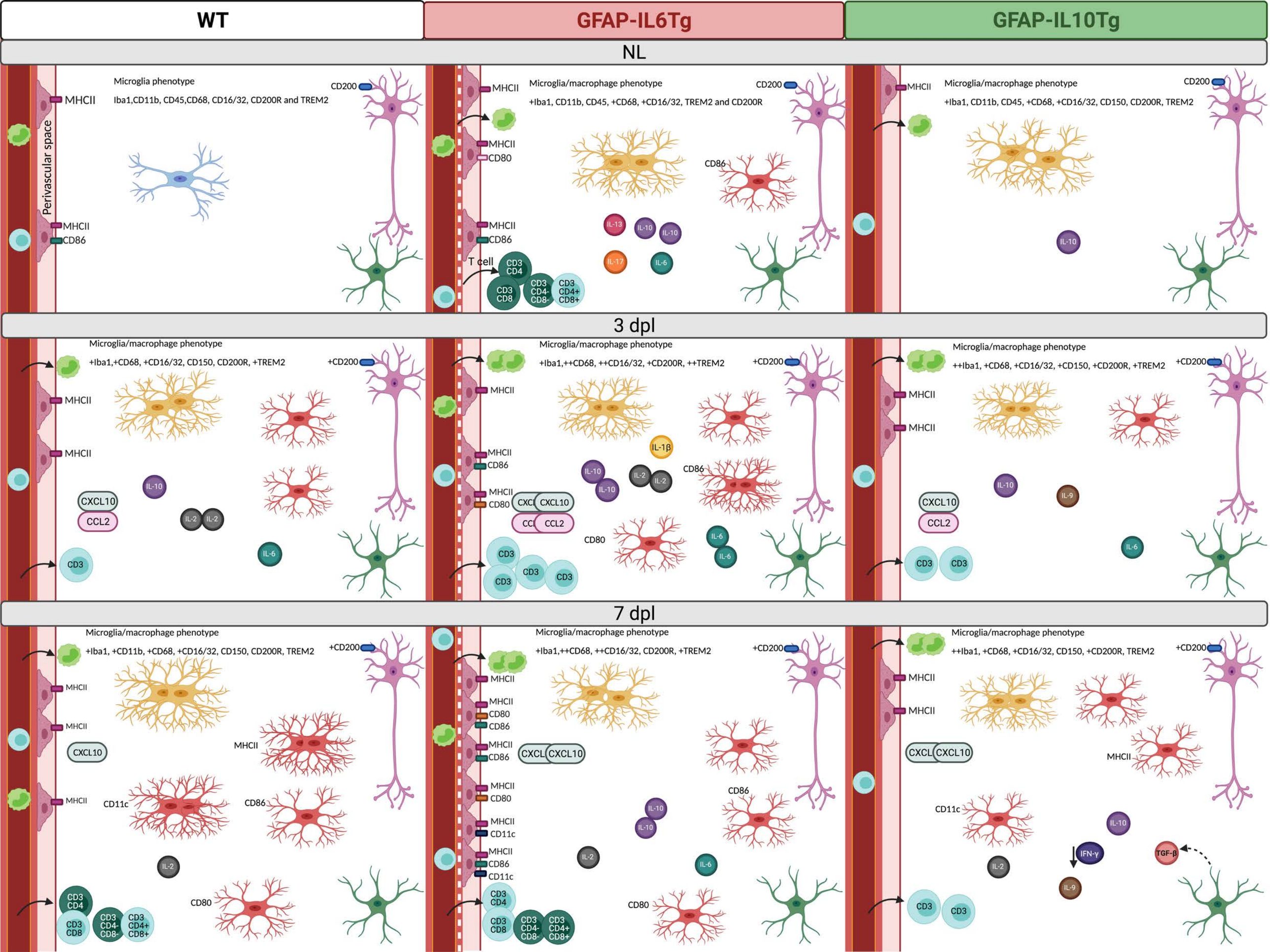
WT
GFAP-IL6Tg
GFAP-IL10Tg
NL
Perivascular space
MHCII
CD86
Microglia phenotype
Iba1,CD11b, CD45,CD68, CD16/32, CD200R and TREM2
CD200
Microglia/macrophage phenotype
+Iba1, CD11b, CD45, +CD68, +CD16/32, TREM2 and CD200R
CD80
T cell
CD3
CD4
CD8
CD4-
CD8-
CD4+
CD8+
IL-13
IL-10
IL-17
IL-6
+Iba1, CD11b, CD45, +CD68, +CD16/32, CD150, CD200R, TREM2
3 dpl
Microglia/macrophage phenotype
+Iba1,+CD68, +CD16/32, CD150, CD200R, +TREM2
+CD200
CXCL10
CCL2
IL-2
IL-1β
IL-9
+Iba1,++CD68, ++CD16/32, +CD200R, ++TREM2
++Iba1, +CD68, +CD16/32, +CD150, +CD200R, +TREM2
7 dpl
+Iba1, +CD11b, +CD68, +CD16/32, CD150, CD200R, TREM2
CD11c
+Iba1,++CD68, ++CD16/32, CD200R, +TREM2
++Iba1, +CD68, +CD16/32, CD150, +CD200R, TREM2
IFN-γ
TGF-β

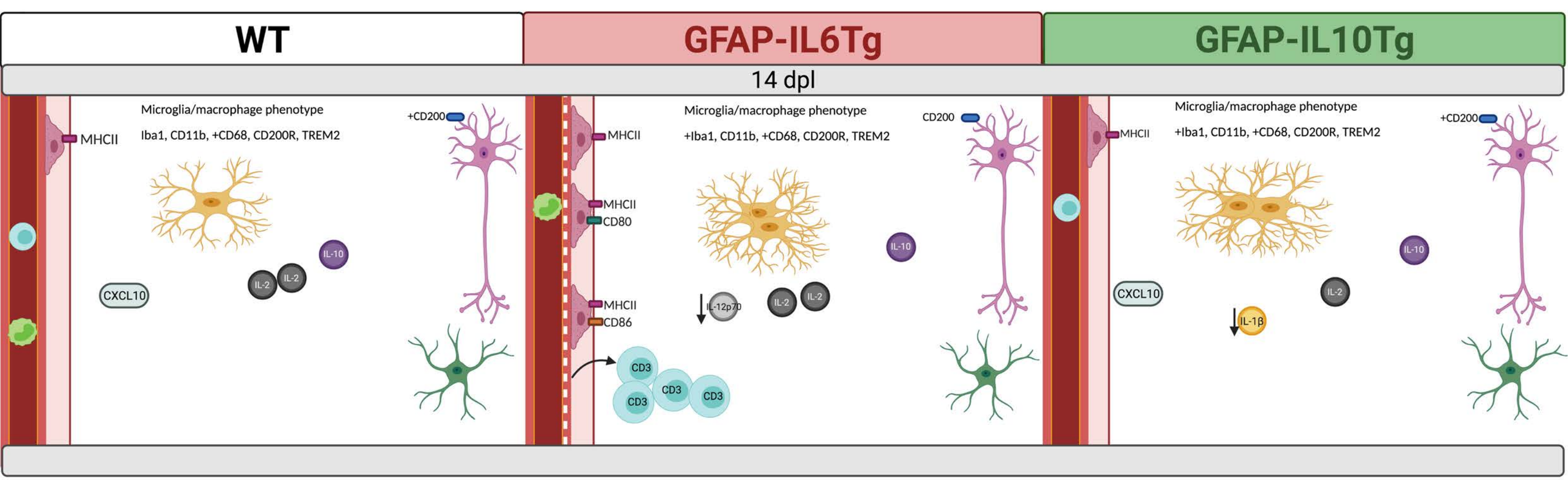
WT
GFAP-IL6Tg
GFAP-IL10Tg
14 dpl
Microglia/macrophage phenotype
Iba1, CD11b, +CD68, CD200R, TREM2
MHCII
+CD200
IL-10
IL-2
IL-2
CXCL10
MHCII
CD80
MHCII
CD86
Microglia/macrophage phenotype
+Iba1, CD11b, +CD68, CD200R, TREM2
IL-12p70
IL-2
IL-2
CD3
CD3
CD3
CD3
CD200
IL-10
MHCII
Microglia/macrophage phenotype
+Iba1, CD11b, +CD68, CD200R, TREM2
+CD200
IL-10
CXCL10
IL-2
IL-1β
CD11b/CD45low
CD11b/CD45int
CD11b/CD45high
Perivascular macrophages
(CD11b/CD45high)
Monocyte
Lymphocyte
Astrocyte
Neuron

ANNEX II

Received: 7 February 2018 | Revised: 6 November 2018 | Accepted: 12 November 2018
DOI: 10.1002/glia.23573

GLIA
WILEY

RESEARCH ARTICLE

Astrocyte-targeted IL-10 production decreases proliferation and induces a downregulation of activated microglia/macrophages after PPT

Mireia Recasens | Kalpana Shrivastava | Beatriz Almolda | Berta González | Bernardo Castellano

Department of Cell Biology, Physiology and Immunology, Institute of Neuroscience, Universitat Autònoma de Barcelona, Barcelona, Spain

Correspondence
Beatriz Almolda, Unitat d'Histologia, Torre M5, Facultat de Medicina Universitat Autònoma de Barcelona, 08193 Bellaterra, Barcelona, Spain.
Email: beatriz.almolda@uab.cat

Funding information
Ministerio de Ciencia e Innovación, Grant/Award Number: BFU2014-55459BFU2017-87843-R; Spanish Ministry of Science and Innovation, Grant/Award Numbers: BFU2017-87843-R, BFU2014-55459

Abstract

When central nervous system (CNS) homeostasis is altered, microglial cells become rapidly activated, proliferate and release a broad range of molecules. Among the plethora of molecules involved in the regulation of microglial activation, cytokines are considered crucial. Although production of interleukin-10 (IL-10) has been demonstrated after different types of CNS injuries and associated with protective functions, the specific role played by IL-10 modulating microglial cells remains unclear. Hence, the objective of this study was to evaluate the effects of transgenic astrocyte IL-10 production on microglial activation associated with axonal anterograde degeneration. To address it, the hippocampal area subjected to perforant pathway transection (PPT) was analyzed by immunohistochemistry (IHC), flow cytometry and protein microarray in transgenic (GFAP-IL10Tg) mice and their corresponding wild types (WT) littermates. Our results demonstrated increased microglial/macrophages density in nonlesioned and PPT-lesioned GFAP-IL10Tg animals when compared with nonlesioned and lesioned WT, respectively. This increase was not due to proliferation, as GFAP-IL10Tg mice showed a reduced proliferation of microglial cells, but was related to an increased population of CD11b+/CD45^{high} monocyte/macrophages. Despite this higher number, the microglia/macrophage population in transgenic animals displayed a downregulated phenotype characterized by lower MHCII, ICOSL, and CD11c. Moreover, a sustained T-cell infiltration was found in transgenic animals. We strongly suggest these modifications must be associated with indirect effects derived from the influence of IL-10 on astrocytes and/or neurons, which express IL-10R. We finally suggested that TGF-β produced by astrocytes, along with IL-2 and CXCL10 might be crucial molecules mediating the effects of transgenic IL-10.

KEYWORDS
cytokines, flow cytometry, IL-10R, macrophage infiltration, T-cell

1 | INTRODUCTION

Interleukin 10 (IL-10) is one of the most important immunoregulatory cytokines implicated in the immunological responses (Cooper et al., 2008; Moore, de Waal Malefyt, Coffman, & O'Garra, 2001). In the central nervous system (CNS), IL-10 is upregulated after a wide range of injuries including acute lesions, such as traumatic brain injury (TBI) (Kamm, Vanderkolk, Lawrence, Jonker, & Davis, 2006), as well as chronic neurodegenerative diseases like Alzheimer's disease (Apelt & Schliebs, 2001) and multiple sclerosis (Ledeboer et al., 2003). Both microglial cells and astrocytes (Hulshof, Montagne, De Groot, & Van Der Valk, 2002; Ledeboer et al., 2002) have been described as one of the principal sources of IL-10 in basal conditions as well as after CNS injury. This cytokine is able to exert its action through the IL-10 receptor (IL-10R), which, depending on the circumstance, could be expressed on microglia (Mizuno, Sawada, Marunouchi, & Suzumura,

1994; Strle et al., 2002), astrocytes (Pousset, Cremona, Dantzer, Kelley, & Parnet, 2001; Xin et al., 2011), oligodendrocytes (Cannella & Raine, 2004) and neurons (Xin et al., 2011; Zhou, Peng, Insolera, Fink, & Mata, 2009). Beneficial effects derived from IL-10 administration have been reported after several in vitro and in vivo models of CNS injury, such as TBI, excitotoxicity and middle cerebral artery occlusion (MCAO), among others (Arimoto et al., 2007; Park, Lee, Jin, & Lee, 2007; Spera, Ellison, Feuerstein, & Barone, 1998; Xin et al., 2011). Notably, the route of administration of IL-10 has been reported to be essential to achieve its beneficial effects (Croxford, Feldmann, Chernajovsky, & Baker, 2001; Cua, Hutchins, LaFace, Stohlman, & Coffman, 2001).

In order to increase our knowledge on the role that IL-10 plays on microglial cell modulation, we constructed a new transgenic mice line, the GFAP-IL10Tg, in which the production of IL-10 is under the control of the GFAP promoter and therefore its production is mainly restricted to GFAP+ astrocytes. In these animals, the production of IL-10 is closely linked to the synthesis of GFAP and consequently, after a lesion, when the production of GFAP in reactive astrocytes increases, the production of this cytokine will also increase. Our previous studies have demonstrated that GFAP-IL10Tg animals show important microglial alterations in different cerebral areas including cerebral cortex, cerebellum and hippocampus, even in basal conditions (Almolda et al., 2015). In particular, transgenic expression of IL-10 induced an important increase in microglial cell density, and a specific activated microglial phenotype characterized by changes in morphology; increased expression of molecules like Iba1, CD11b, CD16/32 and F4/80; and "de novo" expression of CD150 (Almolda et al., 2015). After an experimental injury and specifically in the paradigm of facial nerve axotomy, a model of retrograde neuronal degeneration, we have reported crucial modifications in the activation pattern of microglial cells in GFAP-IL10Tg animals that correlate with a significant increase in neuronal survival (Villacampa et al., 2015), indicating the impact of this cytokine in the regulation of microglial activation and lesion outcome.

In this context, to expand our understanding on the role of IL-10 in other pathological scenarios, the objective of our study was to analyze the effects that transgenic astrocyte-targeted production of IL-10 has on the microglial response after anterograde axonal degeneration. We had used the perforant pathway transection (PPT) paradigm for this study, as it is a well-characterized model based on the specific anatomical organization of the hippocampal formation and its connections with the entorhinal cortex. In mice, a total PPT, involving the transection of all axons in the path produces anterograde axonal and terminal degeneration affecting 85% of the presynaptic elements in the outer two thirds of the molecular layer (ML) of the hippocampal dentate gyrus (DG) (Kovac et al., 2004). It is well established that this degeneration induces a local and quick activation of microglial cells characterized by changes in their morphology and expression of certain activation markers (Finsen et al., 1999; Ladeby, Wirenfeldt, Garcia-Ovejero, et al., 2005). Moreover, activated microglia proliferate and migrate leading to a significant increase in microglial cell density in the denervated area (Ladeby, Wirenfeldt, Dalmau, et al., 2005; Ladeby, Wirenfeldt, Garcia-Ovejero, et al., 2005). In parallel to microglial activation, PPT evokes leukocyte infiltration that includes macrophages and T lymphocytes (Babcock, Kuziel, Rivest, & Owens, 2003; Babcock, Toft-Hansen, & Owens, 2008; Bechmann et al., 2005; Fux, van Rooijen, & Owens, 2008). These events take place in conjunction with production of cytokines and chemokines such as IL-10, IL-6, IL-1β, TNF-α, and CCL2 (Babcock et al., 2003; Babcock et al., 2008; Finsen et al., 1999; Grebing et al., 2016; Ladeby, Wirenfeldt, Garcia-Ovejero, et al., 2005; Matthews, Cotman, & Lynch, 1976).

The main observations of the present work revealed that, in the PPT paradigm, transgenic production of IL-10 induces a plentiful increase in the number of activated microglial cells that paradoxically correlates negatively with cell proliferation but positively with a major presence of the monocyte/macrophage population. Remarkably, both activated microglia and monocyte/macrophage populations in transgenic animals displayed a downregulated phenotype with lower expression of MHCII, ICOSL, and CD11c. Moreover, transgenic IL-10 induces modifications in T-cell infiltration producing a constant presence of these cells along all time-points studied after PPT. All these modifications take place in parallel with changes in the levels of cytokines and chemokines.

2 | MATERIALS AND METHODS

2.1 | Animals

GFAP-IL10Tg and their corresponding wild-type (WT) littermates of both sexes were used in this study. GFAP-IL10Tg have been constructed and recently characterized by our group (Almolda et al., 2015). During all the experiment, animals were bred at the Institute of Neurosciences of the Universitat Autònoma de Barcelona (UAB), maintained at constant temperature (24 ± 2°C) and housed on a 12-hr light/dark cycle with food and water ad libitum. All experimental animal work was conducted in accordance to Spanish regulations (Ley 32/2007, Real Decreto 1201/2005, Ley 9/2003 and Real Decreto 178/2004) in agreement with European Union directives (86/609/CEE, 91/628/CEE and 92/65/CEE) and was approved by the Ethical Commission of the UAB. All efforts were made to minimize the number of animals used to produce reliable scientific data, as well as animal suffering.

2.2 | Perforant pathway transection

Adult (6–7 months-old) GFAP-IL10Tg (n = 83) and WT mice (n = 79) were subjected to wire-knife unilateral PPT. Briefly, animals were intraperitoneally (i.p.) anaesthetized with a solution of ketamine (80 mg/kg) and xylazine (20 mg/kg) at dose of 0.1 mL/g body weight. Animals were fixed in a stereotaxic device (Kopf Instruments) and a drilled trepanation was made on the left side of the skull (4.6 mm dorsal to Bregma and 2.5 mm laterally). A folded wire-knife (m121; McHugh Milleux, Downers Grove IL, USA) was inserted at an angle of 15° anterior and 10° lateral. The knife was unfolded at 3.6 mm ventrally and the perforant pathway was transected retracting the knife 3.3 mm. Finally, the knife was folded, take it out of the brain, and the skin was sutured with 2–0 silk and clean with iodine.

2.3 | Experimental groups

Nonlesioned (NL) and lesioned animals were distributed in different experimental groups and analyzed at 2, 3, 7, 14 and 21 days postlesion (dpl) for immunohistochemistry (IHC), flow cytometry, and protein analysis. A total of 45 WT and 46 GFAP-IL10Tg animals were used for IHC, 23 WT and 15 GFAP-IL10Tg for flow cytometry, and 15 WT and 18 GFAP-IL10Tg for protein analysis.

2.4 | 5′ Bromodeoxyuridine injections

In order to determine microglia/macrophage proliferation, the labeling of proliferative cells with 5′ bromodeoxyuridine (BrdU) was used. BrdU is a synthetic thymidine analog which incorporates into the DNA of dividing cells during S-phase and can be transferred to daughter cells upon replication. Lesioned WT (n = 5) and GFAP-IL10Tg animals (n = 6) were intraperitoneally (i.p.) injected with BrdU (50 mg/kg) diluted in TB (0.05 Trizma base, pH 7.4) every 24 hr from the day of lesion to 7 dpl, and subsequently sacrificed.

2.5 | Tissue processing for IHC

Animals were deeply anaesthetized with a solution of ketamine/xylazine (80:20) injected i.p. at a dose of 0.15 mL/g and then intracardially perfused for 10 min with 4% paraformaldehyde in 0.1 M phosphate buffer (pH 7.4). Brains used for free-floating sectioning were immediately removed and postfixed for 4 hr at 4°C in the same fixative. Subsequently, after phosphate buffer rinses, samples were cryopreserved in a 30% sucrose solution in 0.1 M phosphate buffer for 48 hr at 4°C and frozen in ice-cold 2-methylbutane solution (320404, Sigma-Aldrich, St. Louis). Series of horizontal parallel sections (30-μm-thick) were obtained using a Leica CM3050 cryostat and stored in free-floating Olmos anti-freeze solution at −20°C until used. Brains used for paraffin sections were removed and postfixed in the same fixative overnight at 4°C, and subsequently embedded in paraffin. Horizontal parallel sections (10-μm-thick) were obtained using a Leitz 1512 microtome, placed on gelatin-coated slides and dried overnight at 37°C.

Only animals displaying microglial activation (monitored by Iba1 IHC) in the outer two thirds of the deafferented ML of the DG were included in this study.

2.6 | Single IHC

Microglial morphology, distribution and density were analyzed using antibodies against Iba1 and Pu.1. Microglial proliferation was determined using anti-phospho-Histone H3 (pH3) and BrdU whereas microglial death was studied with anti-caspase 3. Lymphocyte recruitment was analyzed using the antibody against CD3, a pan marker for T-lymphocytes. In all cases, free-floating sections were washed several times with 0.05 M Tris-buffered saline (TBS) pH 7.4 and with TBS containing 1% Triton-X100 (TBST, pH 7.4). Specifically, for Pu.1 staining, sections were then exposed to antigen retrieval protocol by treatment with sodium citrate buffer (pH 8.5), at 80°C, for 40 min. Subsequently, endogenous peroxidase was blocked by incubating the sections for 10 min with 2% H_2O_2 in 70% methanol. For BrdU detection, DNA was denatured by first incubating in 0.082 N HCl for 10 min at 4°C and then for 30 min in 0.82 N HCl at 37°C. Sections were then rinsed with borate buffer (pH 8.5) and 0.5% Triton X-100 in TBS. Afterwards, all sections were incubated for 1 hr at room temperature (RT) in blocking buffer (BB) solution containing 10% fetal bovine serum and 0.3% bovine serum albumin in TBST. Thereafter, sections were incubated overnight at 4°C plus one additional hour at RT with the corresponding primary antibodies (specified in Table 1) diluted in BB. Sections incubated in BB lacking the primary antibody were used as negative control and sections from spleen and gut were used as positive control for the different immunostains. After washes with TBST, sections were incubated for 1 hr at RT with the corresponding biotinylated secondary antibody, followed by 1 hr at RT with horseradish peroxidase (HRP)-conjugated streptavidin diluted in BB (Table 1). The reaction was visualized with the 3,3-diaminobenzidine (DAB) kit (SK-4100; Vector Laboratories, Burlingame, California) following the manufacturer's instructions. For the study of the blood brain barrier (BBB) integrity, after endogenous peroxidase blocking and nonspecific-binding blocking solution, sections were incubated for 1 hr in biotinylated anti-mouse IgG diluted in the same blocking solution. After 1 hr at RT in horseradish streptavidin-peroxidase, the final reaction was visualized by incubating the sections with a DAB kit following the manufacturer's instructions.

Finally, all sections were mounted on slides, counterstained with 1% toluidine blue, dehydrated in graded alcohols and, after xylene treatment, coverslipped with DPX. Sections were analyzed with a Nikon Eclipse 80i brightfield microscope.

2.7 | Double IHC

Double immunolabeling combining pH3 with CD39 was carried out to determine the proliferative capacity of microglial cells. Sections were firstly processed for pH3 as described above, but using an anti-rabbit Alexa-Fluor 555 conjugated antibody as secondary antibody (Table 1). Then, after several washes with TBST, sections were incubated for 1 hr at RT in the blocking buffer solution-2 (BB-2) containing 10% donkey serum and 0.3% bovine serum albumin in TBST. After washes, sections were incubated with sheep anti-CD39 (Table 1), diluted in BB-2, overnight at 4°C followed by one additional hour at RT. Subsequently, sections were washed with TBST and incubated with biotinylated anti-sheep secondary antibody (Table 1). After washes with TBST, sections were incubated for 1 hr at RT with Alexa-Fluor 488-conjugated streptavidin diluted in the BB-2. Finally, sections were washed with TBST, followed by TBS and TB and the nuclei stained with 4,9,6-diamidino-2-phenylindole (DAPI) for 10 min (Table 1).

To study IL-10R expression in astrocytes, double immunolabeling combining IL-10R and GFAP was carried out. Sections were washed with TBST and incubated for 1 hr at RT in the blocking buffer solution-3 (BB-3) containing 0.2% gelatin (powder food grade, 104078, Merck, Burlington, Massachusetts, USA) in TBS with 0.5% Triton. Afterwards, sections were incubated with rabbit anti-IL-10R (Table 1) for 48 hr at 4°C followed by one additional hour at RT. After washes, sections were incubated for 1 hr at RT with biotinylated anti-rabbit secondary antibody followed by the incubation with Alexa-Fluor 555-conjugated streptavidin (Table 1). Sections were then washed with TBST and incubated in BB-3 for 1 hr at RT followed by incubation with both mouse anti-GFAP (Table 1) overnight at 4°C followed by 1 additional hour at RT. After washes with TBST, sections

TABLE 1 Reagents used in immunohistochemistry (IHC)

	Target antigen	Host	Dilution	Cat number	Manufacturer
Primary antibodies	GFAP	Rabbit	1:1,800	Z0334	Dakopatts
	IL-10	Rat	1:200	Ab33471	Abcam
	IL-10R	Rabbit	1:100	Sc-985	Santa Cruz
	Iba1	Rabbit	1:3,000	019–19,741	Wako
	GFAP	Mouse	1:6,000	63,893	Sigma-Aldrich
	Pu.1	Rabbit	1:400	2258S	Cell Signaling
	pH3	Rabbit	1:3,000	06–570	Millipore
	BrdU	Rat	1:120	Ab6326	Abcam
	CD39	Sheep	1:500	AF4398	R&D Systems
	Caspase 3	Rabbit	1:1,000	AF835	R&D Systems
	TGF- β1	Rabbit	1:100	Sc-146	Santa Cruz
	CD3	Hamster	1:500	MCA2690	AbD Serotec
Secondary antibodies	Biotinylated	Rabbit	1:500	BA-1000	Vector Laboratories
	Biotinylated	Sheep	1:500	Ab6899	Abcam
	Biotinylated	Rat	1:500	BA-4001	Vector Laboratories
	Biotinylated	Hamster	1:500	BA-9100	Vector Laboratories
	Alexa 555	Rabbit	1:500	A21428	Invitrogen
	Alexa 488	Mouse	1:500	A11029	Invitrogen
	Alexa 568	Rat	1:500	A11077	Invitrogen
	Alexa 647	Rat	1:500	A21247	Invitrogen
	Alexa 488	Rabbit	1:500	A21206	Invitrogen
Alexa Fluor-555 conjugated Streptavidin			1:500	S32355	Molecular Probes
Alexa Fluor-488 conjugated Streptavidin			1:500	S11223	Molecular Probes
HRP-conjugated Streptavidin			1:500	SA-5004	Vector Laboratories
DAPI			1:10,000	D9542	Sigma-Aldrich

were incubated for 1 hr at RT with anti-mouse Alexa-Fluor 488 diluted in BB-3. After washes with TBST, TBS and TB, nuclei were stained with DAPI (Table 1).

To examine the production of TGF-β1 by astrocytes, double immunolabeling combining TGF-β1 and GFAP was performed. Deparaffinized sections were exposed to antigen retrieval protocol by treatment with sodium citrate buffer (pH 6), at 90°C, for 20 min. After washes with TBST, sections were incubated for 1 hr in BB and incubated with rabbit anti-TGF-β1 (Table 1) diluted in BB, overnight at 4°C, followed by one additional hour at RT. Subsequently, sections were washed with TBST and incubated with anti-rabbit Alexa-Fluor 555 diluted in BB for 1 hr at RT. After washes, sections were incubated again for 1 hr in BB and incubated with mouse anti-GFAP (Table 1), overnight at 4°C, followed by one additional hour at RT. After washes with TBST, sections were incubated with anti-mouse Alexa-Fluor 488 diluted in the BB for 1 hr at RT. Finally, after several washes of TBST, TBS, and TB, nuclei were stained with DAPI (Table 1).

Finally, all double-immunostained sections were mounted on slides, coverslipped with Fluoromount GTM (0100-01; SouthernBiotech, Birmingham, AL) and analyzed using a Nikon Eclipse E600 fluorescence microscope and a Zeiss LSM700 confocal microscope.

2.8 | Terminal dUTP nick end labeling

In addition to caspase-3 immunohistochemistry, the study of microglial cell death was performed on sections double stained for terminal dUTP nick end labeling (TUNEL) and Iba1. To accomplish that, sections were mounted on slides and treated for 5 min with 100% methanol for endogenous peroxidase blocking. Then, sections were rinsed in 10 mM Tris buffer (pH 8) and 5 mM EDTA followed by incubation for 15 min at RT in the same buffer plus Proteinase K (20 μg/mL). After several washes with 5 mM EDTA, sections were incubated for 10 min at RT in TdT buffer containing 30 mM Tris, 140 mM sodium cacodylate, and 1 mM cobalt chloride (pH 7.7). Sections were then incubated for 20 min at 37°C in TdT buffer plus 0.161 U/μL TdT enzyme (Terminal Transferase, 3333566; Roche, Manheim, Germany) and 0.0161 nmol/μL of biotin-16-dUTP (1093070; Roche). The reaction was stopped by submerging sections twice in citrate buffer (300 mM sodium chloride, 30 mM sodium citrate, 5 mM EDTA) for 5 min. After several washes with TBS, sections were incubated for 1 hr at RT with HRP-conjugated streptavidin (Table 1) and the peroxidase reaction visualized by incubation in a 3,3-DAB kit plus 1% of cobalt (SK-4100; Vector Laboratories), following the manufacturer's instructions. Subsequently, sections were incubated with Iba1 antibody (1:1,000) (Table 1) using the same protocol described in the single IHC section. Sections from gut were used as positive control. Finally, sections were dehydrated in graded alcohols and, after xylene treatment, coverslipped in DPX.

2.9 | Densitometric analysis

In order to analyze microglial reactivity in NL and lesioned animals, a densitometric analysis was performed on sections stained for Iba1. At

TABLE 2 Antibodies used in flow cytometry

Target antigen		Format	Dilution	Cat number	Manufacturer
Fc blocker	CD16/32	Purified	1:250	553142	BD Pharmingen
Primary antibodies	CD11b	APC-Cy7	1:400	557657	BD Pharmingen
	CD45	PerCPCy5	1:400	557235	BD Biosciences
	MHCII	FITC	1:400	553623	BD Pharmingen
	CD11c	PE	1:400	557401	BD Pharmingen
	Ly6C	FITC	1:400	553104	BD Bioscience
	ICOSL	PE	1:400	12-5985-82	BD Bioscience

least three WT and three GFAP-IL10Tg animals per group were analyzed. A total of nine photographs from three different sections per animal containing the deafferented ML of DG in lesioned animals and the equivalent area in the NL were captured using the 20× objective with a DXM 1200F Nikon digital camera joined to a brightfield Nikon Eclipse 80i microscope, using the ACT-1 2.20 (Nikon Corporation, Minato, Tokio) software. By means of analySIS, the percentage of area occupied by the immunolabeling as well as the intensity of the immunoreaction (Mean Grey Value Mean) was recorded for each photograph. The AI index (Almolda et al., 2015) was calculated as function of the percentage of the immunolabeled area and the Mean Grey Value Mean.

Quantification of microglial cell density was performed on sections immunostained for the transcription factor Pu.1. In this case, a total of six photographs from three different sections per animal containing the deafferented ML of DG in lesioned animals as well as the equivalent area in the NL were captured with the 10× objective, using the same device and software referred above. The number of Pu1+ cells in the ML of DG was obtained using the "Automatic Cell Counter" (ITCN) plug-in from NIH Image J software (Wayne Rasband, National Institutes of Health, USA). Data were expressed as cells/mm^2.

Quantification of microglial cell proliferation was carried out on sections immunostained for the mitotic marker pH3 as well as BrdU in both NL and PPT-lesioned animals at 2, 3, and 7 dpl in the case of pH3 and at 7 dpl in the case of BrdU. For pH3, a minimum of three WT and three GFAP-IL10Tg animals per group were analyzed, whereas in the case of BrdU five WT and six GFAP-IL10Tg animals were used. The number of both pH3+ and BrdU+ microglial cells in the ML of DG were manually counted on 20 (for pH3) and 10 different sections (for BrdU) per animal using a 20× objective. Data were averaged and represented as pH3+ cells or BrdU+ cells/section.

To evaluate T lymphocyte infiltration, sections stained for CD3 were used. At least three WT and three GFAP-IL-10Tg in both NL and PPT-lesioned animals at 2, 3, 7, and 14 dpl were used. All CD3+ cells in the ML of DG were manually counted on 20 sections per animal using a 20× objective. Data were averaged and represented as CD3+ cells/section.

2.10 | Flow cytometry analysis

The phenotype of microglia and monocyte/macrophage populations in NL and PPT-lesioned animals (at 3 and 7 dpl) were analyzed using flow cytometry as previously described (Almolda, Costa, Montoya, Gonzalez, & Castellano, 2009). Briefly, anaesthetized animals were intracardially perfused for 1 min with 0.1 M phosphate buffer solution (PBS), the brain removed and the entire hippocampus was quickly dissected out. In order to obtain a cell suspension, samples were dissociated through 140 μm and 70 μm meshes and digested for 30 min at 37°C using type IV collagenase (17104-019; Life Technologies, Carlsbad, California) and DNAsa I (D5025; Sigma, St. Louis). Subsequently, each cellular suspension was centrifuged at RT for 20 min at 2400 rpm in a discontinuous density Percoll gradient (17-0891-02; Amersham-Pharmacia, United Kingdom) between 1.03 g/mL and 1.08 g/mL. Myelin in the upper layer was removed. Cells in the interphase and the clear upper-phase were collected, washed in PBS plus 2% serum and the Fc receptors were blocked by incubation for 10 min at 4°C in a solution of purified CD16/32 diluted in PBS plus 2% serum. Afterwards, cells were labeled for 30 min at 4°C with the two following combinations of surface antibodies: (a) anti-CD11b-APC-Cy7, anti-CD45-PerCPCy5, anti-MHCII- FITC, and anti-CD11c-PE; and (b) anti-CD11b-APC-Cy7, anti-CD45-PerCPCy5, anti-Ly6C-FITC, and anti-ICOSL-PE (Table 2). In parallel, isotype-matched control antibodies for the different fluorochromes (BD Pharmingen, Switzerland) were used as negative control and a cell suspension of splenocytes as positive control. Data were extrapolated as number of cells using Cyto Count fluorescent beads, following the manufacturer's instructions (S2366; Dako Cytomation, Denmark). Finally, cells were acquired using a FACS Canto flow cytometer (Becton Dickinson, San Jose, CA) and results analyzed using the FlowJo software. The analysis was performed separately for each animal without any pooling.

2.11 | Tissue processing for protein analysis

Animals used for protein analysis were i.p anaesthetized and perfused for 1 min with cold 0.1 M PBS (pH 7.4). Subsequently, the entire hippocampus was dissected out, snap frozen individually in liquid nitrogen and stored at −80°C. Total protein was extracted by solubilization of samples on lysis buffer containing 25 mM HEPES, 2% Igepal, 5 mM $MgCl_2$, 1.3 mM EDTA, 1 mM EGTA, 0.1 M PMSF and protease (1:100, P8340; Sigma-Aldrich), and phosphatase inhibitor cocktails (1:100, P0044; Sigma-Aldrich) for 2 hr at 4°C. After solubilization, samples were centrifuged at 13,000 rpm for 5 min at 4°C and the supernatants collected. Total protein concentration was determined with a commercial Pierce BCA Protein Assay kit (#23225; Thermo Scientific, Massachusetts, USA) according to manufacturer's protocol. Protein

lysates were aliquot and stored at −80°C until used for ELISA and protein microarray analysis. The hippocampus from each animal was analyzed separately.

2.12 | Cytokine analysis

The cytokines IL-10, IL-6, IL-2, IL-9, IFN-γ, IL-1β, IL-5, IL-12p70 and the chemokines CXCL10 and CCL2 were analyzed using a Milliplex MAP Mouse Cytokine/Chemokine kit (#MCYTOMAG-70K; Merck Millipore, Burlington, Massachusetts, USA) according to manufacturer's instructions. Briefly, 25 μL of each hippocampus extracts with a final total protein concentration of 2.5 μg/μL were added to the plates, along with the standards in separate wells, containing 25 μL of custom fluorescent beads and 25 μL of matrix solution, and incubated overnight at 4°C in a plate-shaker (750 rpm). After two washes with wash buffer (1x), the plate was incubated with 25 μL of detection antibodies for 30 min at RT followed by incubation with 25 μL of Streptavidin-Phycoerythrin for 30 min at RT in a plate-shaker (750 rpm). Finally, the plate was washed twice with wash buffer and 150 μL of Drive fluid was added. Luminex MAGPIX device with the xPONENT 4.2 software was used to read the plate. Data were analyzed using the Milliplex Analyst 5.1 software and expressed as pg/mL of protein.

2.13 | Statistical analysis

Statistics were performed using the Graph Pad Prism 5.0 software. Standard two-tailed, unpaired Student's *t* test was used to compare between WT and GFAP-IL10Tg animals to determine significant differences. All experimental values were expressed as mean values ± *SEM*.

3 | RESULTS

3.1 | Dynamics of IL-10/IL-10R expression in DG after PPT

In order to determine the putative change in both IL-10 production and IL-10R expression in the deafferented DG, IHC and Luminex assay was used.

In agreement with our previous observations (Almolda et al., 2015), the current results show that although IL-10 was detected in the NL hippocampus of both WT and GFAP-IL10Tg animals, its expression was almost three times higher in GFAP-IL10Tg than in WT (Figure 1a). After PPT in WT animals, IL-10 significantly increased at 3 dpl and abruptly decreased at 7 dpl and 14 dpl to levels similar to those observed in NL animals. In contrast, in GFAP-IL10Tg animals, levels of IL-10 at 3 dpl increased insignificantly and then decreased at 7 dpl and returned to basal levels at 14 dpl. Nevertheless, when compared with WT animals, GFAP-IL10Tg mice presented a significant higher expression of IL-10 at 14 dpl (Figure 1a).

Colocalization studies combining IL-10R with GFAP allowed us to identify IL-10R+ cells located in the ML of the DG mainly as GFAP+ astrocytes in NL GFAP-IL10Tg mice (Figure 1d,e) as well as in both PPT-lesioned WT and transgenic animals (Figure 1f–i), but not in NL WT (Figure 1b,c). It is important to mention that, in the granular layer (GL), in addition to IL-10R+ astrocytes, we found immunostaining associated with the cytoplasm of DG neurons of both WT and GFAP-IL10Tg mice in all the experimental conditions (Figure 1b–i).

3.2 | Transgenic production of IL-10 induces changes in the number, morphology and distribution of microglia/macrophage population after PPT

3.2.1 | Analysis of microglial/macrophage cell morphology and distribution

Changes in morphology and distribution of the microglia/macrophage cell population induced by transgenic production of IL-10 were assessed by Iba1 IHC.

In correspondence with our previous study (Almolda et al., 2015), microglial cells in NL GFAP-IL10Tg mice showed a significant increase in Iba1 immunoreactivity (Figure 2b,k) when compared with NL WT animals (Figure 2a). This increased immunoreactivity in NL GFAP-IL10Tg mice was accompanied by important morphological alterations including increased ramification, thicker processes, and presence of microglial cells with elongated shapes (Figure 2n,o).

After PPT, remarkable alterations in both microglial activation and morphology were detected in the ML of the DG in both WT and GFAP-IL10Tg mice, although with notable differences between the two genotypes.

In WT mice, Iba1 levels progressively increased from 2 dpl, reaching a maximum at 7 dpl, to thereafter decrease from 14 to 21 dpl. In contrast, in GFAP-IL10Tg mice, Iba1 upregulation was delayed until 3 dpl and the expression levels were always significantly higher than in WT at all time-points analyzed, except at 2 dpl. In both experimental groups, at 21 dpl, Iba1 levels were similar to their corresponding NL animals (Figure 2k). To graphically represent the dynamics of microglial activation along PPT lesion timeline, we calculated the fold-changes with respect to the corresponding NL animals in both WT and GFAP-IL10Tg animals. This representation revealed that, although the levels of Iba1 in transgenic animals were higher than in WT, the upregulation of this marker with respect to its basal levels was less pronounced in transgenic animals than in WT, along the progression of the PPT lesion (Figure 2l,m).

As far as the cell morphology is concerned, at 3 and 7 dpl, microglial cells displayed the typical "bushy" shapes, characterized by short and stubby ramifications in the lesioned outer and medial molecular layers (OML and MML) of DG in both genotypes (Figure 2c,f). In both groups, microglia returned to ramified morphologies at 14 dpl but it was not until 21 dpl when these cells were similar in morphology to their corresponding NL animals (Figure 2g–j). Although more evident at 3 dpl, morphological differences between WT and GFAP-IL10Tg animals were observed at all time-points analyzed. The microglial cells in transgenic animals always presented more as well as thicker processes (Figure 2p,q). Moreover, in both WT and GFAP-IL10Tg mice, at 3 and 7 dpl, we observed some microglial cells assembled in clusters consisting of 2 to 4 cells along the OML and the MML (Figure 2c,d). No differences in terms of number and distribution of

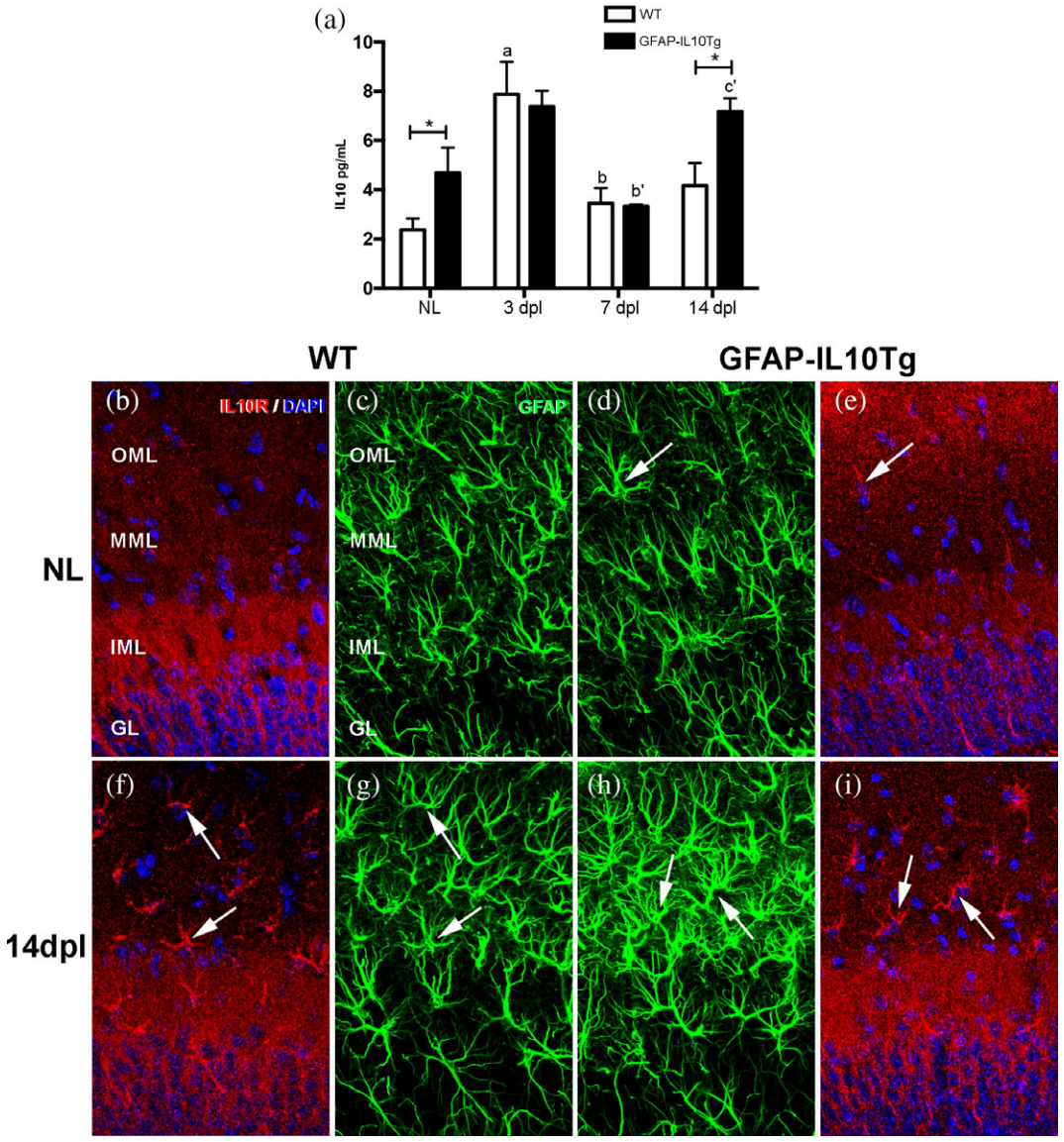

FIGURE 1 IL-10 and IL-10R expression. (a) Graph showing the expression pattern of IL-10 in nonlesioned (NL) and PPT-lesioned animals, from 3 to 14 dpl, in WT and GFAP-IL10Tg mice. Note that in basal conditions, IL-10 expression was around two times higher in GFAP-IL10Tg than in WT. After PPT, IL-10 expression in transgenic animals was significantly higher at 14 dpl than WT mice (*$p \leq .05$). Data are represented as mean ± *SEM*. The significances are represented as: * WT vs. GFAP-IL10Tg; in WT animals, a: Indicates significance vs. NL, b: Significance vs. 3 dpl, and c: Significance vs. 7 dpl; in transgenic animals a', b', and c' indicates significance vs. NL, 3 dpl and 7 dpl, respectively. (b–i) Representative images of double IHC combining IL-10R (red) and GFAP (green). Nuclei were stained with DAPI (blue). Note that, major part of IL-10R+ cells corresponds to GFAP+ astrocytes (arrows). In all experimental conditions, in the granular layer (GL), besides IL-10R+ astrocyte processes, we found immunostaining associated with the cytoplasm of DG neurons. GL: Granular layer, IML: Inner molecular layer, MML: Medial molecular layer, OML: Outer molecular layer [Color figure can be viewed at wileyonlinelibrary.com]

these microglial clusters were found between both lesioned experimental groups.

In parallel to changes found in the OML and the MML, both WT and GFAP-IL10Tg animals, showed a progressive reduction of the area occupied by Iba1 staining in the inner molecular layer (IML) along the early time-points (3 dpl and 7 dpl) (Figure 2c–f).

3.2.2 | Analysis of microglia/macrophage cell density after PPT

To evaluate putative modifications in the number of microglia/macrophages cells, we used the IHC for the transcription factor Pu.1, a specific marker for myeloid cells and commonly used for this purpose (Gomez-Nicola, Fransen, Suzzi, & Perry, 2013).

Concomitant with changes in Iba1 expression and morphology, the IHC for Pu.1 revealed that in comparison to NL WT animals, there was nearly a two-fold increase in the number of Pu.1+ cells in the ML of the DG in NL GFAP-IL10Tg (Figure 3a). After PPT, although both WT and transgenic experienced a progressive increase in the number of Pu.1+ cells, the dynamics of this increase was quite different. In WT animals, the number of Pu.1+ cells progressively increased from 2 dpl, peaked at 3 dpl, remained stable at 7 dpl and then gradually decreased from 14 to 21 dpl (Figure 3a),

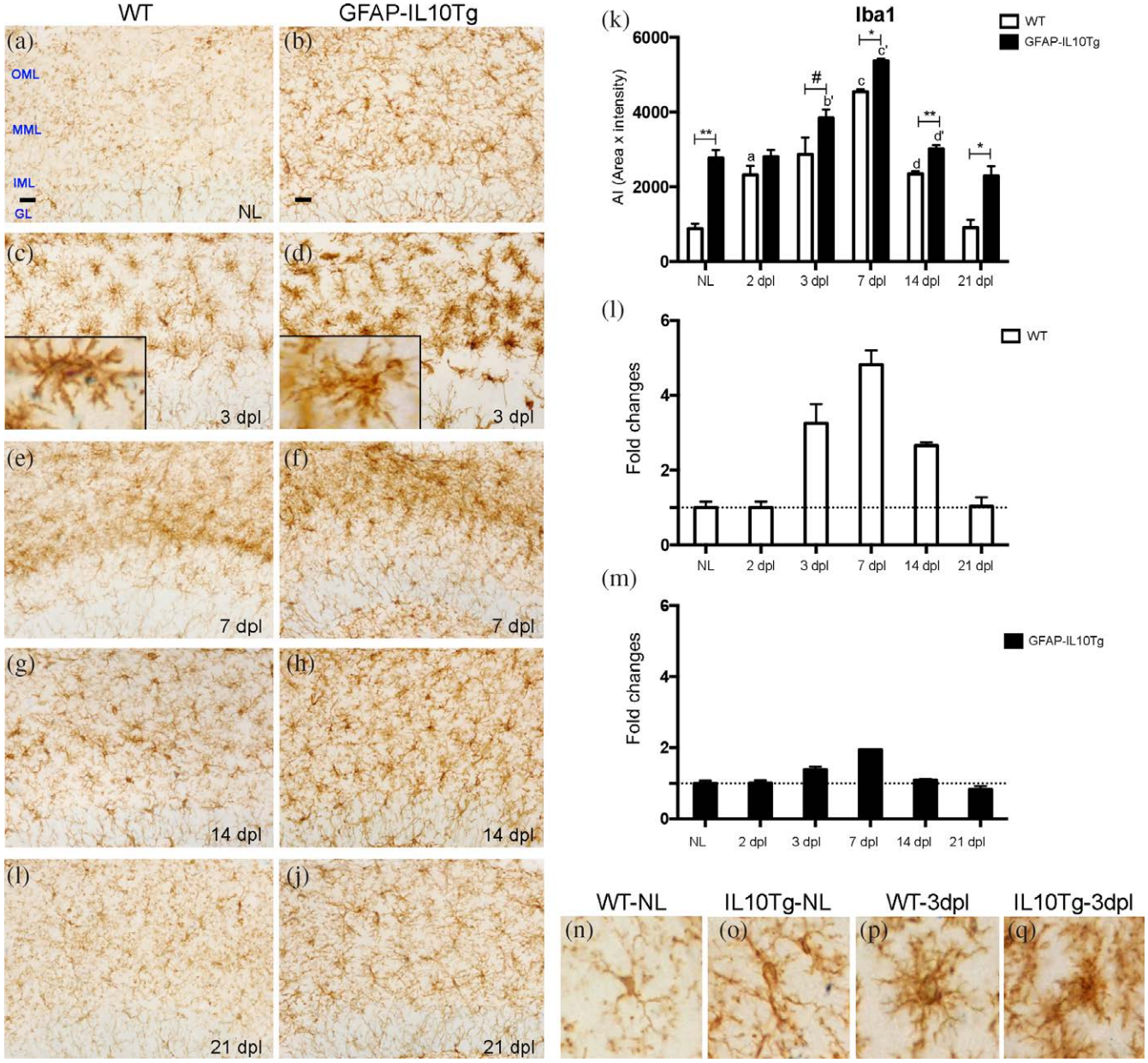

FIGURE 2 Iba1 immunohistochemistry. Representative images from WT and GFAP-IL10Tg mice showing single Iba1 staining in the granular (GL) as well as in the inner, medial, and outer molecular layers (IML, MML and OML, respectively) of the DG in nonlesioned (NL) (a–b) and PPT-lesioned mice from 3 to 21 dpl (c–j). Note that at 3 dpl in comparison to WT (c and p), microglial cells in GFAP-IL10Tg animals (d and q) presented higher Iba1 expression and thicker processes. In both WT and GFAP-IL10Tg animals, it is possible to distinguish the presence of microglial clusters (insets in c and d). Scale bar = 10 μm. (k) Graph showing the time course of Iba1 staining, expressed as AI (area × intensity). Note that, GFAP-IL10Tg animals showed increased levels of Iba1 in both NL and at 3, 7, 14, and 21 dpl after PPT. (l and m) Graphs showing the fold changes increase of Iba1 expression in comparison to the corresponding NL animals in both WT (l) and GFAP-IL10Tg mice (m). Remarkably, transgenic animals showed lower fold increase than WT. Data are represented as mean ± *SEM*. The significances are represented as: * WT vs. GFAP-IL10Tg; in WT animals, a: Indicates significance vs. NL, b: Significance vs. 3 dpl, and c: Significance vs. 7 dpl; in transgenic animals a', b', and c' indicates significance vs. NL, 3 dpl and 7 dpl, respectively (**$p \leq .01$, *$p \leq .05$, #$p \leq .1$) [Color figure can be viewed at wileyonlinelibrary.com]

being at these later time-points still higher than NL WT animals. In GFAP-IL10Tg animals, the progressive increase in the number of Pu.1+ cells was delayed to 3 dpl, but continued to increase at 7 dpl. Similar to WT, at 14 and 21 dpl, the number of Pu.1+ cells in transgenic animals gradually declined to achieve the nearby same number than NL GFAP-IL10Tg animals (Figure 3a). Furthermore, the number of Pu.1+ cells at 3 and 7 dpl was higher in GFAP-IL10Tg mice than in WT. However, when we represented the dynamics of Pu.1 upregulation, again we detected that while WT animals showed a nearly six-fold increase over their basal levels (Figure 3b), in GFAP-IL10Tg animals did not reach the four-fold increase at any time-point analyzed (Figure 3c).

In both lesioned experimental groups, a very similar decrease in the number of Pu.1+ cells was found in their respective IML (data not shown).

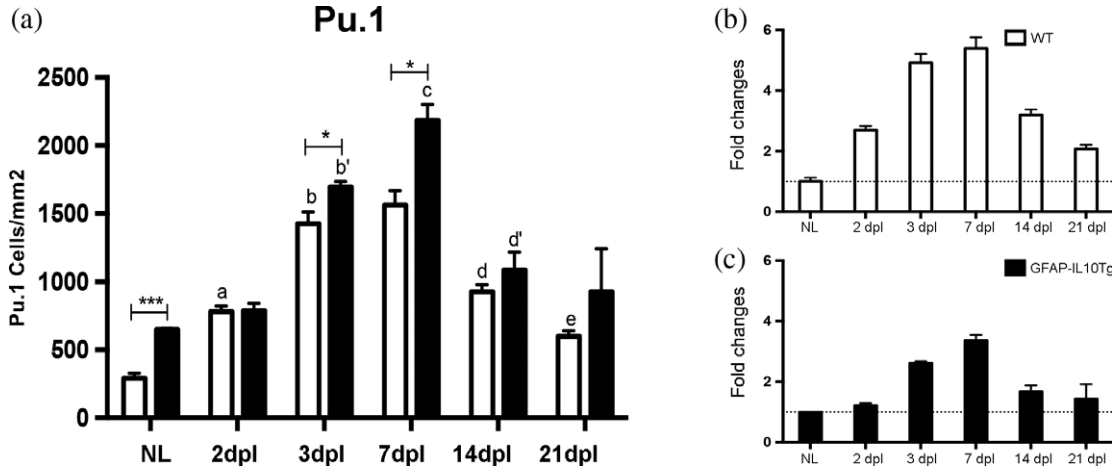

FIGURE 3 Pu.1 immunohistochemistry. (a) Graph showing the quantification of Pu.1^{+} cells in nonlesioned (NL) and lesioned animals from 2 to 21 dpl after PPT, in WT and GFAP-IL10Tg mice. Note that, transgenic animals showed higher number of Pu.1+ cells in NL and at 3 and 7 dpl. (b and c) Graphs showing the fold changes increase of Pu.1+ cells in WT (b) and GFAP-IL10Tg (c) in comparison to their corresponding NL animals. Data are represented as mean ± *SEM*. The significances are represented as: * WT vs. GFAP-IL10Tg; in WT animals, a: Indicates significance vs. NL, b: Significance vs. 3 dpl, and c: Significance vs. 7 dpl; in transgenic animals a', b', and c' indicates significance vs. NL, 3 dpl and 7 dpl, respectively (***$p \leq .0001$; *$p \leq .05$)

3.3 | Transgenic IL-10 production alters microglial cell proliferation after PPT but has no effects on microglial cell death

The analysis of microglial proliferation was performed on sections stained for pH3 and BrdU (Figure 4), whereas apoptosis was analyzed on sections developed for TUNEL and caspase-3 IHC (data not shown).

Few pH3+ cells were seen in the ML of DG in both NL WT and NL GFAP-IL10Tg animals with no differences between them (Figure 4a). After PPT, in WT animals, there was a pronounced increase in the number of pH3+ cells at 2 dpl. The number of pH3+ cells progressively decreased from 3 to 7 dpl, although the amount of pH3+ cells was still higher than in NL WT animals (Figure 4a). In contrast, in GFAP-IL10Tg mice, the initial increase in the number of pH3+ cells was delayed until 3 dpl, and at 7 dpl this number abruptly decreased to levels comparable to NL transgenic animals (Figure 4a). Moreover, in the same area, the total number of accumulated BrdU+ cells until 7 dpl was significantly lower in GFAP-IL10Tg animals than in WT (Figure 4b). Double IHC combining pH3+ and the microglial marker CD39 revealed that the majority of pH3+ cells in both WT and GFAP-IL10Tg animals corresponded to CD39+ microglia/macrophages (Figure 4c,d).

No microglial apoptosis was seen in our study as no TUNEL or caspase-3 positive staining was found in the lesioned ML of DG in neither WT nor GFAP-IL10Tg animals at any analyzed time-point (data not shown).

3.4 | IL-10 increases the number and changes the phenotype of microglia and macrophages after PPT

Using flow cytometry, we determined possible modifications induced by the transgenic production of IL-10 in both the number and the phenotype of the microglia/macrophage population after PPT. This study was focused on NL and 3–7 dpl time-points where the major differences in terms of cell morphology, distribution, and microglial density were observed.

We identified the microglia/macrophages population based on the positive expression of CD11b in combination with levels of CD45 (Figure 5a,b). This helped in differentiating homeostatic microglia from activated microglia, as well as from macrophages. Ramified or homeostatic microglia was identified as CD11b+/CD45^{low} phenotype, and activated microglia as CD11b+/CD45^{int}. Importantly, activated CD45^{int} microglia express a lower level of CD45 than macrophages (CD11b+/CD45^{high}) in the CNS, which allows distinguishing each of these populations. We will use the term CD11b+/CD45$^{low/int}$ to refer to the population of homeostatic and activated microglia jointly in this study.

In NL WT animals, we identified a population of CD11b+/CD45^{low} cells and a small population of CD11b+/CD45^{high} cells. In comparison to WT, in NL GFAP-IL10Tg animals, there was around a three-fold increase in the number of both cell populations (Figure 5d,e). After PPT, both WT and GFAP-IL10Tg mice presented a gradual increase, from 3 to 7 dpl, in the population of CD11b+/CD45^{high} positive cells, whereas the population of CD11b+/CD45$^{low/int}$ positive cells only experimented a slight increase at 7 dpl. Noticeably, the numbers of both CD11b+/CD45$^{low/int}$ and CD11b+/CD45^{high} cell populations were always higher in GFAP-IL10Tg animals than in WT at all time-points analyzed (Figure 5d,e).

To assess the effects of transgenic production of IL-10 on the phenotype of microglia and macrophage populations, the expression of different cell activation markers such as MHCII, ICOSL, and CD11c in the population of CD11b+/CD45$^{low/int}$ and CD11b+/CD45^{high} was analyzed (Figure 5c).

In NL GFAP-IL10Tg animals, the CD11b+/CD45$^{low/int}$ population presented a higher number of cells expressing ICOSL and Ly6C than NL WT animals, whereas the number of MHCII+ and CD11c+ cells was similar to WT. Observing the CD11b+/CD45^{high} population in NL transgenic animals, we only found an increase in the number of Ly6C+ cells when compared with NL WT (Figure 5m).

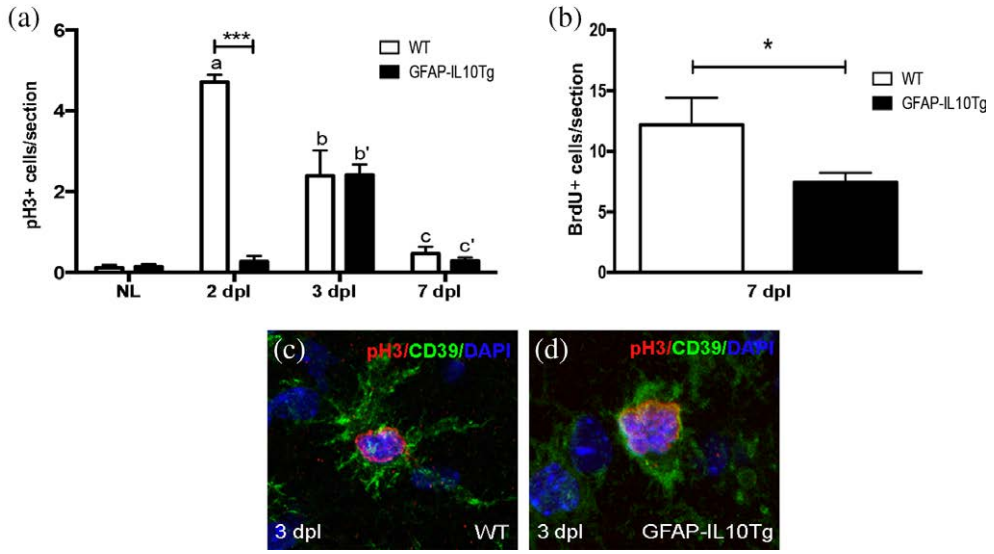

FIGURE 4 Microglial proliferation. (a) Graph showing the quantification of pH3+ cells in nonlesioned (NL) and PPT-lesioned animals from 2 to 7 dpl, in WT and GFAP-IL10Tg animals. Note that, transgenic animals showed a delayed and reduced microglial cell proliferation compared with WT (***$p \leq .0001$). (b) Graph showing the quantification of BrdU+ cells in PPT-lesioned animals at 7 dpl in WT and GFAP-IL10Tg animals. Note that total number of BrdU+ proliferating cells is significantly lower in transgenic animals. (c and d) Representative images of double IHC combining pH3 (red) and CD39 (green). Nuclei were stained with DAPI (blue). Data are represented as mean ± *SEM*. The significances are represented as: * WT vs. GFAP-IL10Tg; in WT animals, a: Indicates significance vs. NL, b: Significance vs. 2 dpl, c: Significance vs. 3 dpl and d: Significance vs. 7 dpl; in transgenic animals a', b', c', and d' indicates significance vs. NL, 2 dpl, 3 dpl, and 7 dpl, respectively [Color figure can be viewed at wileyonlinelibrary.com]

After PPT, CD11b+/CD45$^{low/int}$ cell population in WT mice presented a progressive upregulation, from 3 to 7 dpl, in the number of cells expressing CD11c (Figure 5j), whereas the number of ICOSL+ and Ly6C+ cells increased at 3 dpl and remained stable at 7 dpl, and the number of MHCII+ cells was unaltered (Figure 5f,h,l). No significant changes in any of these markers were detected in the CD11b+/CD45$^{low/int}$ cell population of GFAP-IL10Tg mice along the different time-points after PPT in comparison to NL transgenic mice. Remarkably, when compared with WT animals, the numbers of ICOSL+ and Ly6C+ cells were higher in GFAP-IL10Tg mice at 3 dpl, whereas the number of CD11c+ cells found in transgenic at 7 dpl was low.

In WT animals after PPT, from 3 to 7 dpl, a progressive upregulation in the number of cells expressing all the activation markers analyzed (MHCII, ICOSL, CD11c, and Ly6C) was found in the population of CD11b+/CD45^{high} cells (Figure 5g,i,k,m). In contrast, in GFAP-IL10Tg animals, the number of CD11b+/CD45^{high} cells expressing all these markers increased at 3 dpl and remained similar at 7 dpl (Figure 5g,i,k,m). When compared with WT, a higher number of Ly6C+ cells at 3 dpl as well as a reduction in the number of MHCII+, ICOSL+ and CD11c+ cells, at 7 dpl, were found in transgenic animals.

Finally, in order to evaluate putative modifications that could explain the differences in the number of macrophages detected in transgenic animals, we analyzed the integrity of the BBB by detection of mouse IgG. Our analysis showed that after PPT there were alterations of the BBB leading to leakage in the denervated area of the DG in both WT and GFAP-IL10Tg animals without any detectable differences between genotypes (data not shown).

3.5 | Transgene-encoded IL-10 changes the T-cell infiltration pattern after PPT

To explore if transgenic production of IL-10 was able to modify the pattern of T-cell infiltration after PPT, we analyzed sections immunostained for CD3 in NL and lesioned WT and transgenic at 2, 3, 7 and 14 dpl (Figure 6). In both NL WT and NL GFAP-IL10Tg animals, CD3+ cells were practically undetectable in the ML of the DG (Figure 6). After PPT, WT animals showed two waves of T-cell infiltration, the first wave at 2 dpl and the second at 7 dpl. Between these two time points, that is to say at 3 dpi, the number of CD3+ cells decreased considerably. In contrast, in GFAP-IL10Tg animals, it was not possible to distinguish these two waves of T-cell infiltration, as the number of CD3+ T-cells increased at 3 dpl and remained elevated along all the time-points after PPT. Hence, the number of CD3+ cells was significantly higher in GFAP-IL10Tg mice than in WT, at 3 dpl (Figure 6).

3.6 | Transgenic IL-10 production modifies the cytokine/chemokine microenvironment associated to PPT

We finally addressed whether all the modifications observed after PPT in transgenic animals were in correlation with alterations in the levels of cytokines and chemokines. Thus, we specifically analyzed the expression of different cytokines and chemokines involved in: (a) microglial cell activation, such as IL-6, IL-1β, IFN-γ, IL-2, IL-9 and IL-12p70; (b) microglial cell proliferation like IL-5; and (c) monocyte/macrophage as well as T-cell recruitment such as CXCL10 and CCL2.

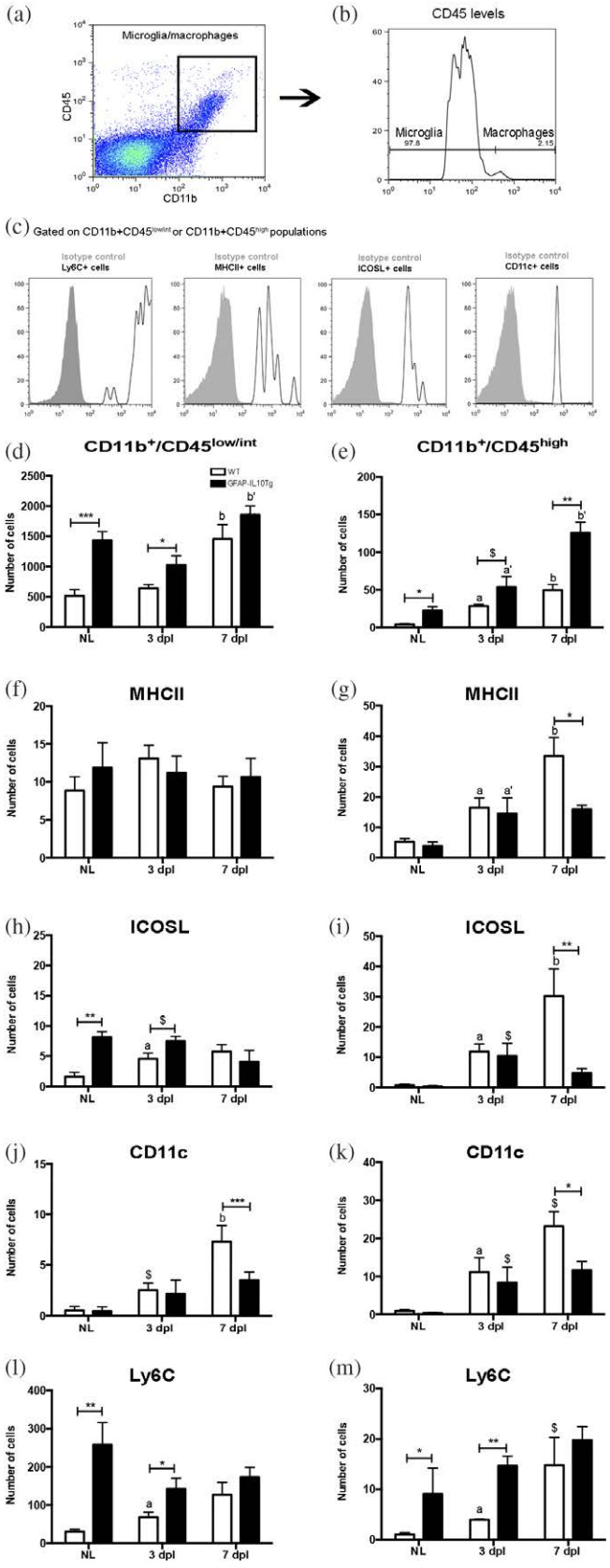

FIGURE 5 Flow cytometry analysis of microglia and macrophage populations. (a) Representative dot-plot of CD11b/CD45 expression in cells obtained from hippocampus of nonlesioned (NL) WT animals. The square delimits the CD11b+/CD45+ population of cells used in this study. (b) Representative histogram where the populations of CD11b+/CD45$^{low/int}$ cells (microglia) and CD11b+/CD45^{high} cells (macrophages) were defined. (c) Representative histogram-plot showing the expression of Ly6C, MHCII, ICOSL and CD11c in the population of microglia/macrophages in comparison to the corresponding isotype control, in which the positive staining was defined. (d and e) Graphs showing the number of cells in the CD11b+/CD45$^{low/int}$ (d) and CD11b+/CD45^{high} (e) populations in NL and PPT-lesioned animals. (f–m) Graphs showing the expression levels of the different activation markers MHCII, ICOSL, CD11c and Ly6C in CD11b+/CD45$^{low/int}$ (f, h, j, and l) and CD11b+/CD45^{high} populations (g, i, k, m) ($\$p \leq .1$, $*p \leq .05$, $**p \leq .01$ and $***p \leq .0001$). Data are represented as mean ± *SEM*. The significances are represented as: * WT vs. GFAP-IL10Tg; in WT animals, a: Indicates significance vs. NL and b: Significance vs. 3 dpl; in transgenic animals a' and b' indicates significance vs. NL and 3 dpl, respectively [Color figure can be viewed at wileyonlinelibrary.com]

No differences in any cytokine or chemokine analyzed were detected when NL WT and NL GFAP-IL10Tg animals were compared (Figure 7a–i). After PPT, in both WT and GFAP-IL10Tg animals, we found an important increase in IL-6 (four-fold) and CCL2 (two-fold) expression, at 3 dpl, which returned to basal levels at 7 dpl, without significant differences between the two genotypes (Figure 7a,i). In addition, at both 3 and 7 dpl a high increase in CXCL10 expression (more than 20-fold) was observed in WT, as well as in GFAP-IL10Tg mice where the expression was even higher at 7 dpl (Figure 7h). Expression of IL-2 in WT animals followed a particular time-course, increasing at 3 dpl, decreasing at 7 dpl and increasing again at 14 dpl (Figure 7b). Upregulation of IL-2 expression in GFAP-IL10Tg animals was only detected at 14 dpl, and was always lower than the observed in WT animals at the different time-points analyzed after PPT (Figure 7b). Similarly, expression of IL1β only decreased at 14 dpl in transgenic animals (Figure 7e). In the case of IFN-γ, in WT animals, levels of expression decreased at 7 dpl whereas no changes were observed in GFAP-IL10Tg animals (Figure 7d). Regarding IL-5, our results demonstrated a distinct pattern of expression in GFAP-IL10Tg animals increasing at 14 dpl instead of the decrease that occurs at 7 dpl in WT animals (Figure 7f). Finally, no significant changes were found in the expression of IL-12p70 after PPT in either WT or GFAP-IL10Tg animals in comparison to their corresponding NL animals (Figure 7g).

Above results are summarized in Figure 8. Briefly, the cytokines/chemokines that presented the most important modifications between WT and GFAP-IL10Tg mice were IL-2, that was lower in transgenic animals along all the time-points analyzed, IL-5 that showed less expression at 3 dpl (Figure 7f) and IL-9 and CXCL10 that presented higher expression at 7 dpl (Figure 7c).

Finally, analysis of TGF-β1 immunostaining demonstrated a higher expression of this cytokine in astrocytes of GFAP-IL10Tg animals, especially at early time-points (Figure 9).

4 | DISCUSSION

In the present study, we demonstrated that astrocyte-targeted IL-10 production induces significant changes in the activation pattern of microglia/macrophage cell population after PPT. These changes include: (a) increase in cell density and (b) a downregulated activation phenotype. Our observations also revealed that, after PPT, IL-10 reduces and delays microglial proliferation while increase the number

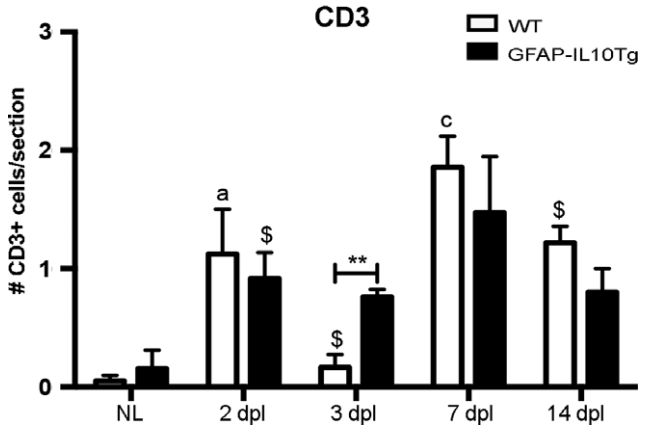

FIGURE 6 T-cell infiltration. Graph showing the quantification of CD3+ cells in nonlesioned (NL) and lesioned animals from 2 to 14 dpl, in WT and GFAP-IL10Tg mice. Note that, at 3 dpl, in comparison to WT, GFAP-IL10Tg mice showed a higher number of CD3+ cells ($\$p \leq .1$, $^{**}p \leq .01$). Data are represented as mean ± *SEM*. The significances are represented as: * WT vs. GFAP-IL10Tg; a: Indicates significance vs. NL and c: Significance vs. 3 dpl

of monocyte/macrophages as well as T-cell infiltration. All these changes are linked to slight modifications in the expression profile of some cytokines/chemokines, especially IL-2, and, as discussed later, must be associated with indirect effects derived from the influence of IL-10 over astrocytes and/or neurons, the main cells expressing IL-10R.

4.1 | Increased microglia/macrophage cell density in GFAP-IL10Tg mice after PPT is not due to microglial proliferation but due to the recruitment of bone-marrow-derived monocytes

The total transection of the PP projections connecting the entorhinal cortex with the DG of the hippocampus leads to a rapid activation of microglial cells in the outer two thirds of the ML (i.e., the MML and OML), characterized not only by changes in their phenotype but also by a notable increase in the number of cells (Dissing-Olesen et al., 2007; Finsen et al., 1999; Hailer, Grampp, & Nitsch, 1999; Ladeby, Wirenfeldt, Garcia-Ovejero, et al., 2005; Matthews et al., 1976). In concordance, our results showed that after PPT the number of microglia/macrophages augmented progressively in both WT and GFAP-IL10Tg animals although with some dissimilarities. Our observations demonstrated that in most of the analyzed time-points, the number of microglia/macrophages was significantly higher in GFAP-IL10Tg animals than in WT, indicating that IL-10 production must have an essential impact on the underlying mechanisms regulating microglial/macrophage increase in this paradigm.

Microglial proliferation has been considered one of the causes of microglial/macrophages expansion in the PPT paradigm. As already reported (Dissing-Olesen et al., 2007; Ladeby, Wirenfeldt, Garcia-Ovejero, et al., 2005; Wirenfeldt et al., 2007), the number of microglia/macrophages showed a significant increase in the deafferented outer two thirds of the ML, within the first 3 days postlesion. In agreement, our study show that majority of proliferating pH3+ microglial cells were observed at early time-points in WT mice, especially at 2 dpl but also at 3 dpl. In contrast, GFAP-IL10Tg animals exhibited a delay in microglial cell proliferation as well as a reduction in the total number of mitotic cells, which correlates with the lower fold-increase reported in these transgenic animals in terms of Iba1 and Pu.1. Although it seems paradoxical, having in mind the high increase in the number of microglia/macrophages observed in GFAP-IL10Tg animals, it is important to take into an account that the amount of these cells in transgenic animals is already higher under NL basal conditions. These results presumably designate IL-10 as a microglial proliferation inhibitory molecule. However, in vitro studies reported that IL-10 administration does not have a direct effect on microglial proliferation (Kloss, Kreutzberg, & Raivich, 1997; Lam & Schlichter, 2015; Sawada, Suzumura, Hosoya, Marunouchi, & Nagatsu, 1999; Strle et al., 2002), suggesting that microglial proliferative alterations reported in our study might actually be an indirect effect mediated by IL-10. We believe most of the microglial cell modifications observed in this study might be indirect consequences derived from the effects of IL-10 on astrocytes or neurons, as they are the principal cell types expressing IL10R after PPT. As discussed in the following sections, one of the probable actions of IL-10 is to greatly diminish the levels of IL-2, a cytokine directly implied on the potentiation of microglial proliferation (Sawada, Suzumura, & Marunouchi, 1995).

In addition to proliferation, it is reported that, microglial/macrophage cell expansion after PPT is due to the cell migration of microglia from adjacent non-affected areas, such as the IML, the CA1, and the hilus (Gehrmann, Schoen, & Kreutzberg, 1991; Jensen, Gonzalez, Castellano, & Zimmer, 1994) along with the recruitment of bone-marrow-derived monocytes/macrophages (Babcock et al., 2003; Bechmann et al., 2005; Ladeby, Wirenfeldt, Garcia-Ovejero, et al., 2005). In this context, we found that although the migration of microglial cells from the IML was contributing to the increase in the number of microglia/macrophages in the OML and MML in both WT and GFAP-IL10Tg animals, the number of microglial cells decreased similarly in the IML, suggesting that this migrating phenomenon is not responsible for the changes produced by transgenic IL-10. We believe, if the increased number of microglial cells observed in transgenic animals could not be explained by proliferation or migration, it is more plausible that IL-10 would influence the recruitment of bone-marrow-derived monocytes/macrophages. In this regard, our results showed that in comparison to WT, in GFAP-IL10Tg mice there was an increase in the population of CD11b+/CD45^{high} cells, at all time-points analyzed, presumably comprising macrophages, monocytes, and dendritic cells. Among these CD11b+/CD45^{high} cells population, transgenic animals presented a high number of Ly6C+ cells, which are considered as "inflammatory monocytes" (Yang, Zhang, Yu, Yang, & Wang, 2014). This supports our hypothesis that IL-10 may be able to increase monocyte infiltration in this paradigm or at least may modify the phenotype of microglia toward a more macrophage/monocyte-like phenotype. To clarify the contribution of blood-derived monocyte/macrophages in transgenic animals, further experiments using chimera animals will be very necessary.

Another possibility that we have explored to explain the increase in the number of microglia/macrophages in transgenic animals is that IL-10 could prevent the restoration of microglial cell number. After different types of injuries, the restoration of microglial cell numbers is

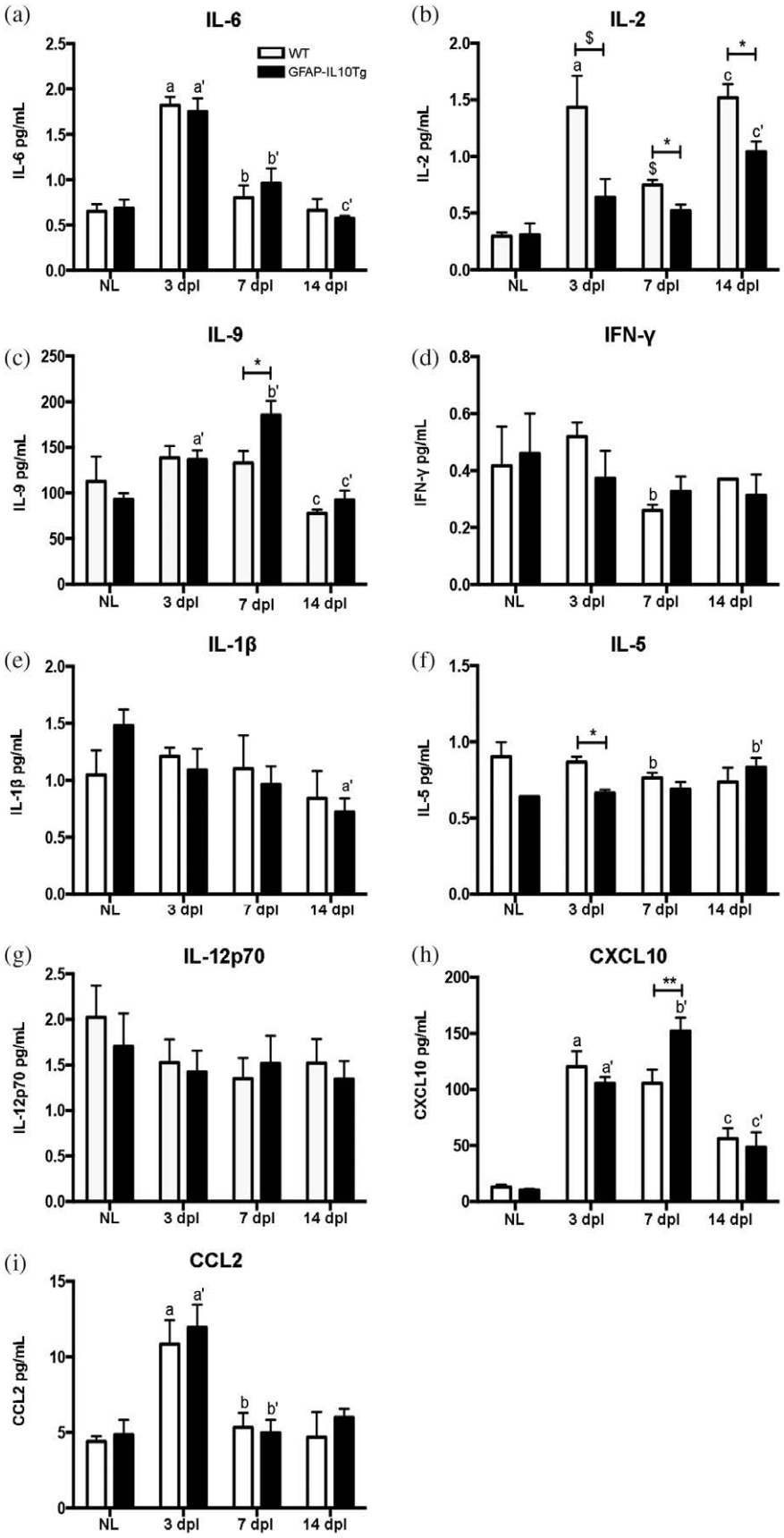

FIGURE 7 Cytokines and chemokines expression. (a–i) Graphs showing the time course expression of IL-6, IL-2, IL-9, IFN-γ, IL-1β, IL-5 and IL-12p70 cytokines, and the chemokines CXCL10 and CCL2 in nonlesioned (NL) and PPT-lesioned animals from 3 to 14 dpl in both WT and GFAP-IL10Tg animals ($$p \leq .10$; $^{**}p \leq .01$, $^{*}p \leq .05$). Data are represented as mean ± *SEM*. The significance is represented as: * WT vs. GFAP-IL10Tg; in WT animals, a indicates significance vs. NL and b: Significance vs. 3 dpl; in transgenic animals a' and b' indicate significance vs. NL and 3 dpl, respectively

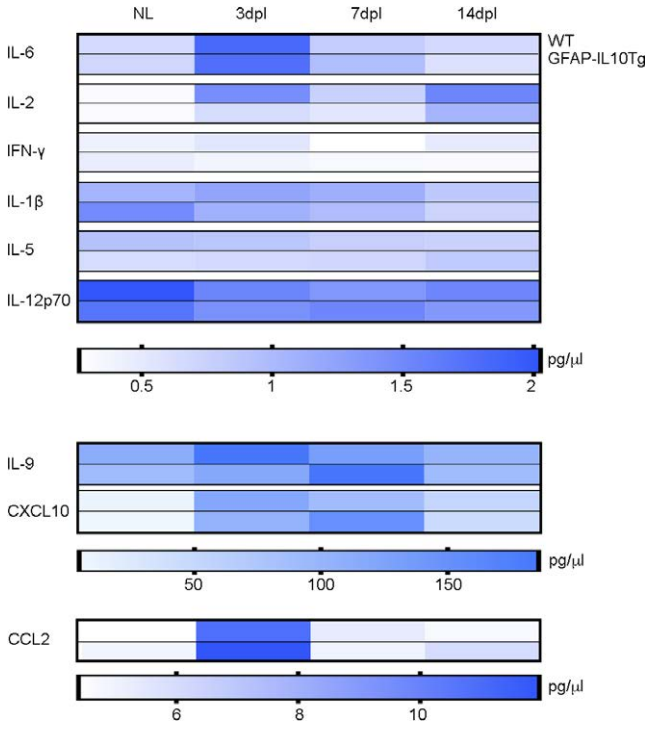

FIGURE 8 Heatmap showing the changes in cytokines and chemokines in nonlesioned (NL) and lesioned animals in WT and GFAP-IL10Tg animals [Color figure can be viewed at wileyonlinelibrary.com]

commonly regulated by programmed cell death, or apoptosis (Jones, Kreutzberg, & Raivich, 1997; Streit, Walter, & Pennell, 1999), and IL-10 has been associated to protection of microglia from apoptosis (Strle et al., 2002). We could not detect any evidence of apoptosis, monitored by caspase-3 and TUNEL, at any time-point analyzed in either WT or GFAP-IL10Tg animals. Our observations are in concordance with previous studies showing that after entorhinal cortex lesion in rats, the DG was devoid of TUNEL+ cells at all stages after lesion (Bechmann et al., 1999), but differ from one study (Wirenfeldt et al., 2007) showing CD11b+/CD45^{int}/Annexin V+ cells in the entire hippocampus of deafferented mice at 3–14 dpl. This controversy highlights the need of more specific studies to clarify whether there are apoptosis of microglia/macrophages in this paradigm and the exact mechanism of this death.

4.2 | Astrocyte-targeted production of IL-10 modulates the activation phenotype of microglia/macrophages toward a downregulated phenotype

In addition to alterations in the number of both microglia and macrophage cell populations, our results indicate that IL-10 has an effect on the activation phenotype of both cell populations directing them toward a downregulated phenotype. While PPT-activated microglia and macrophages in WT animals experimented an increase in ICOSL and CD11c; in GFAP-IL10Tg mice, despite the higher number of microglia/macrophages, these populations do not display any change in the expression of activation markers after PPT, that is, values remained similar to those found in their corresponding NL animals. These observations suggest that transgenic IL-10 may have a role deactivating the induction of microglial reactivity after PPT. In fact, several studies have demonstrated a downregulatory effect of IL-10 over microglia and macrophage activation in vitro (Kremlev & Palmer, 2005; Ledeboer, Breve, Poole, Tilders, & Van Dam, 2000; Lodge & Sriram, 1996; Sawada et al., 1999), and in vivo (Jackson, Messinger, Palmer, Peduzzi, & Morrow, 2003; Pang, Rodts-Palenik,

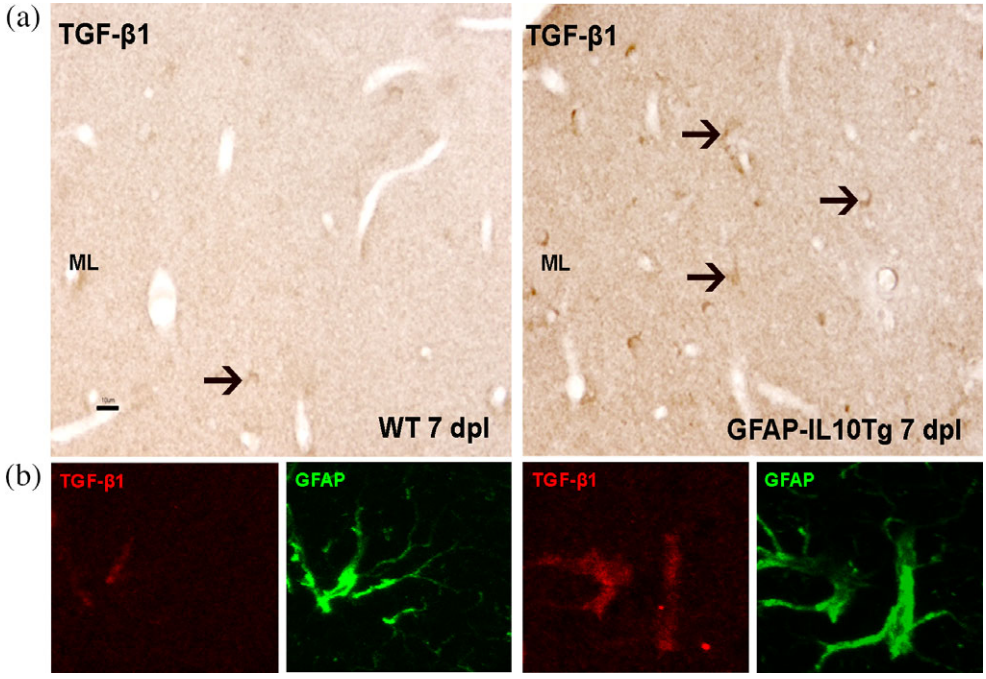

FIGURE 9 TGF-β1 expression in astrocytes after PPT. (a) Representative images from WT and GFAP-IL10Tg mice showing single TGF-β1 staining in PPT-lesioned animals at 7 dpl. Black arrows indicate TGF-β1^{+} cells. Scale bar = 10 μm. (b) Representative images of TGF-β1 (red) and GFAP (green) double-labeling at 7 dpl in both WT and GFAP-IL10Tg animals showing colocalization of both markers [Color figure can be viewed at wileyonlinelibrary.com]

Cai, Bennett, & Rhodes, 2005; Ren et al., 2011; Shechter et al., 2009; van Strien et al., 2010; Yang et al., 2009).

The activation markers analyzed in this study, MHCII, ICOSL, and CD11c, are molecules commonly related to the antigen presenting capacity. The fact that the population of microglia and macrophages in GFAP-IL10Tg animals presented lower number of positive cells for these markers, indicates that they have lower molecular resources to interact with T-cells. These results, together with the sustained presence of T-cells observed in transgenic animals, suggest alterations in the microglia/macrophage capacity to cross-talk with lymphocytes.

The unique marker that we observed upregulated in both microglia and macrophage populations in GFAP-IL10Tg mice is Ly6C. Interestingly, Ly6C expression was not exclusively detected on the CD11b+/CD45^{high} population but also on the CD11b+/CD45$^{low/int}$ microglia population, indicating their phenotype of "inflammatory monocytes." These results are in concordance with other studies using chimeras that showed a small number of cells with microglia-like phenotype characterized by the expression of CD45^{int}/CD11b+/GFP+/Ly6C+. Furthermore, using a model of West Nile virus infection, some authors showed that, in non-irradiated mice, Ly6C^{high} inflammatory monocytes migrate to the infected CNS and develop a microglial phenotype maintaining their Ly6C expression (Getts et al., 2008). Moreover, it has been reported that Ly6C^{high}/CCR2+ monocytes specifically accumulated in CNS lesions and can be differentiated into microglial cells (Mildner et al., 2007). The fact that expression of Ly6C in the population of microglia was only detected in GFAP-IL10Tg animals opens the possibility that may be, infiltrated monocytes in transgenic animals are able to differentiate into microglia maintaining the expression of Ly6C. Determinations of the mechanism underlying this conversion or the molecules regulating it are interesting targets for future investigations.

4.3 | Astrocyte-targeted production of IL-10 produces alterations in the cytokine/chemokine profile after PPT

In concomitance with glial response and leucocyte infiltration, several studies have reported changes in the expression levels of cytokines and chemokines after PPT (Babcock et al., 2003; Babcock et al., 2008; Finsen et al., 1999; Grebing et al., 2016; Ladeby, Wirenfeldt, Garcia-Ovejero, et al., 2005; Matthews et al., 1976). Interestingly, our findings show no variation in most of the cytokines analyzed, after PPT including IL-1β, IFN-γ, IL-9, IL-5, and IL-12p70. Only the cytokines IL-6 and IL-2 were upregulated in the lesioned hippocampus of WT animals. Moreover in line with previous studies (Babcock et al., 2003), on the PPT-lesioned hippocampus of WT animals, we found an upregulation of the chemokines monocyte chemoattractant protein (MCP1/CCL2) and interferon inducible protein-10 (IP-10/CXCL10). Both these molecules are implicated in the recruitment of macrophages and T-cells to the injured hippocampus (Babcock et al., 2003), in concordance with the infiltration of both CD11b+/CD45^{high} and T-cell populations we have found.

Astrocyte-targeted production of IL-10 produced only mild effects on the cytokine/chemokine profile. The most affected cytokine was IL-2, a cytokine closely related with the activation of T-cells, driving the differentiation of naïve T-cells to effector or memory T-cells (Liao, Lin, & Leonard, 2011). IL-2 expression was significantly lower in GFAP-IL10Tg animals than in WT at all time-points after PPT, suggesting that, not only microglia/macrophage but also lymphocyte function are affected by transgenic IL-10 production. IL-2 deficiency has been linked to increase T-cell trafficking to the brain after facial nerve axotomy (Huang, Meola, & Petitto, 2012). In our study, we observed that, the infiltration of T-cells remained high in transgenic animals throughout the different time-points after PPT possibly due to low IL-2 expression. Noticeably, higher levels of CXCL10 detected in GFAP-IL10Tg mice at 7 dpl also correlated with a stable infiltration of T-cells as well as with an increased number of CD11b+/CD45^{high} population. This observation reinforces our hypothesis that transgenic production of IL-10 is able to induce an increased recruitment of bone-marrow-derived monocytes by modifying the expression of key chemokines.

Finally, we want to point out that IL-5, a cytokine produced by microglia and astrocytes in the CNS (Sawada et al., 1999), and whose function has been related to induction of microglial proliferation in vitro (Liva & de Vellis, 2001; Ringheim, 1995), decreased in transgenic animals at 3 dpl. At this time-point, the number of proliferating microglia was also seen to be lower than in WT possibly due to low IL-5 levels.

4.4 | Astrocytes and neurons are the principal cells expressing IL-10R after PPT

IL-10R expression was described in microglial cells under both healthy (Gonzalez et al., 2009) and inflammatory conditions in the CNS (Hulshof et al., 2002; Strle et al., 2002). Assuming these evidences, we hypothesized that the altered microglial/macrophage phenotype found in GFAP-IL10Tg after PPT may be due to a direct effect of IL-10 on microglia bearing the IL-10R. However, when we analyzed the cell types expressing IL-10R we found that its expression was detected mainly in astrocytes and neurons at all time-points after PPT. These results are in agreement with previous in vitro and in vivo studies reporting the expression of IL-10R in astrocytes under basal conditions and after LPS administration (Ledeboer et al., 2002; Norden, Fenn, Dugan, & Godbout, 2014) and in specific populations of neurons, such as the facial (Xin et al., 2011) and spinal cord motorneurons (Zhou et al., 2009). In no case, we were able to detect this receptor in microglia cells. Therefore, changes found in the microglia/macrophage populations in this study may be more likely due to an indirect effect through neurons and/or astrocytes. Furthermore, our previous studies demonstrated that in basal conditions, GFAP-IL10Tg animals has modifications, not only in microglial cells, but remarkably also in neuronal electrophysiology showing lower excitability of the hippocampal CA3-CA1 synapsis and absence of long-term potentiation (Almolda'15). Moreover, we have reported that transgenic IL-10 production plays a neuroprotective role after facial nerve axotomy (Villacampa'16). Therefore, we cannot exclude the possibility that these basal modifications in neurons could impact the development of the PPT lesion. Although there is abundant information about the communication between microglia and neurons and how these cell types regulated each other by both

contact-dependent or contact-independent mechanisms (Chavarria & Cardenas, 2013; Eyo & Wu, 2013); but there is a lack of data on microglia-astrocyte communication. Only a scarce number of studies have been focused on whether astrocytes can influence the phenotype of microglial cells under basal conditions or after activation (Abutbul et al., 2012; Schilling, Nitsch, Heinemann, Haas, & Eder, 2001; Tanaka et al., 1999). In particular, a study conducted by Norden et al. (2014), demonstrated that astrocytes stimulated by IL-10 are able to produce TGF-β and that this TGF-β attenuates LPS-induced microglial activation. In agreement with this, we also found an increase in the TGF-β1 expression in astrocytes of GFAP-IL10Tg, especially at early time-points, coinciding with the major differences observed in microglia/macrophage populations (Figure 9). Furthermore, TGF-β has been demonstrated as a strong inhibitor of microglial proliferation (Jones, Kreutzberg, & Raivich, 1998) and, in the context of PPT, as a beneficial treatment to preserve the neuronal projections in the deafferented area (Eyupoglu, Bechmann, & Nitsch, 2003). Interestingly, this beneficial effect of TGF-β in the hippocampus is linked to a reduction in microglial activation (Eyupoglu et al., 2003), coinciding with the downregulated phenotype of microglia/macrophages observed in GFAP-IL10Tg animals. Thus, these observations suggest that, in the PPT paradigm, TGF-β is one of the candidate molecules to mediate the effects observed in GFAP-IL10Tg by modifying microglia-astrocyte communication.

5 | CONCLUSION

Altogether these results revealed that astrocyte-targeted production of IL-10 increases the numbers of microglia/macrophages along the PPT, by increasing the infiltration of monocyte/macrophages. Transgenic IL-10 production also reduces the proliferation and changes the phenotype of microglia/macrophage cells promoting a lower activation state in both populations. Apart from microglia/macrophages, astrocyte-targeted production of IL-10 affected T-cell infiltration inducing a sustained presence of these cells along all time-points after PPT.

Finally, our observations indicate that the effects of IL-10 on the population of microglia/macrophages and lymphocytes occurs indirectly acting through astrocytes and neurons since these are the cells that express IL-10R after PPT. TGF-β produced by astrocytes, IL-2, and CXCL10 are the molecules that can be mainly involved in the actions of IL-10 in the PPT paradigm.

ACKNOWLEDGMENTS

The authors would like to thank Miguel A. Martil and Isabella Appiah for their outstanding technical help and Núria Barba for her help on confocal microscopy. This work was supported by the Spanish Ministry of Science and Innovation (BFU2014-55459) and (BFU2017-87843-R) to BCL.

ORCID

Beatriz Almolda https://orcid.org/0000-0001-6631-4385

REFERENCES

Abutbul, S., Shapiro, J., Szaingurten-Solodkin, I., Levy, N., Carmy, Y., Baron, R., … Monsonego, A. (2012). TGF-beta signaling through SMAD2/3 induces the quiescent microglial phenotype within the CNS environment. *Glia*, *60*(7), 1160–1171. https://doi.org/10.1002/glia.22343

Almolda, B., Costa, M., Montoya, M., Gonzalez, B., & Castellano, B. (2009). CD4 microglial expression correlates with spontaneous clinical improvement in the acute Lewis rat EAE model. *Journal of Neuroimmunology*, *209*(1–2), 65–80. https://doi.org/10.1016/j.jneuroim.2009.01.026

Almolda, B., de Labra, C., Barrera, I., Gruart, A., Delgado-Garcia, J. M., Villacampa, N., … Castellano, B. (2015). Alterations in microglial phenotype and hippocampal neuronal function in transgenic mice with astrocyte-targeted production of interleukin-10. *Brain, Behavior, and Immunity*, *45*, 80–97. https://doi.org/10.1016/j.bbi.2014.10.015

Apelt, J., & Schliebs, R. (2001). Beta-amyloid-induced glial expression of both pro- and anti-inflammatory cytokines in cerebral cortex of aged transgenic Tg2576 mice with Alzheimer plaque pathology. *Brain Research*, *894*(1), 21–30.

Arimoto, T., Choi, D. Y., Lu, X., Liu, M., Nguyen, X. V., Zheng, N., … Bing, G. (2007). Interleukin-10 protects against inflammation-mediated degeneration of dopaminergic neurons in substantia nigra. *Neurobiology of Aging*, *28*(6), 894–906. https://doi.org/10.1016/j.neurobiolaging.2006.04.011

Babcock, A. A., Kuziel, W. A., Rivest, S., & Owens, T. (2003). Chemokine expression by glial cells directs leukocytes to sites of axonal injury in the CNS. *The Journal of Neuroscience*, *23*(21), 7922–7930.

Babcock, A. A., Toft-Hansen, H., & Owens, T. (2008). Signaling through MyD88 regulates leukocyte recruitment after brain injury. *Journal of Immunology*, *181*(9), 6481–6490.

Bechmann, I., Goldmann, J., Kovac, A. D., Kwidzinski, E., Simburger, E., Naftolin, F., … Priller, J. (2005). Circulating monocytic cells infiltrate layers of anterograde axonal degeneration where they transform into microglia. *The FASEB Journal*, *19*(6), 647–649. https://doi.org/10.1096/fj.04-2599fje

Bechmann, I., Mor, G., Nilsen, J., Eliza, M., Nitsch, R., & Naftolin, F. (1999). FasL (CD95L, Apo1L) is expressed in the normal rat and human brain: Evidence for the existence of an immunological brain barrier. *Glia*, *27*(1), 62–74.

Cannella, B., & Raine, C. S. (2004). Multiple sclerosis: Cytokine receptors on oligodendrocytes predict innate regulation. *Annals of Neurology*, *55*(1), 46–57. https://doi.org/10.1002/ana.10764

Chavarria, A., & Cardenas, G. (2013). Neuronal influence behind the central nervous system regulation of the immune cells. *Frontiers in Integrative Neuroscience*, *7*, 64. https://doi.org/10.3389/fnint.2013.00064

Cooper, P. J., Mitre, E., Moncayo, A. L., Chico, M. E., Vaca, M. G., & Nutman, T. B. (2008). Ascaris lumbricoides-induced interleukin-10 is not associated with atopy in schoolchildren in a rural area of the tropics. *The Journal of Infectious Diseases*, *197*(9), 1333–1340. https://doi.org/10.1086/586904

Croxford, J. L., Feldmann, M., Chernajovsky, Y., & Baker, D. (2001). Different therapeutic outcomes in experimental allergic encephalomyelitis dependent upon the mode of delivery of IL-10: A comparison of the effects of protein, adenoviral or retroviral IL-10 delivery into the central nervous system. *Journal of Immunology*, *166*(6), 4124–4130.

Cua, D. J., Hutchins, B., LaFace, D. M., Stohlman, S. A., & Coffman, R. L. (2001). Central nervous system expression of IL-10 inhibits autoimmune encephalomyelitis. *Journal of Immunology*, *166*(1), 602–608.

Dissing-Olesen, L., Ladeby, R., Nielsen, H. H., Toft-Hansen, H., Dalmau, I., & Finsen, B. (2007). Axonal lesion-induced microglial proliferation and microglial cluster formation in the mouse. *Neuroscience*, *149*(1), 112–122. https://doi.org/10.1016/j.neuroscience.2007.06.037

Eyo, U. B., & Wu, L. J. (2013). Bidirectional microglia-neuron communication in the healthy brain. *Neural Plasticity*, *2013*, 456857. https://doi.org/10.1155/2013/456857

Eyupoglu, I. Y., Bechmann, I., & Nitsch, R. (2003). Modification of microglia function protects from lesion-induced neuronal alterations and promotes sprouting in the hippocampus. *The FASEB Journal*, *17*(9), 1110–1111. https://doi.org/10.1096/fj.02-0825fje

Finsen, B., Jensen, M. B., Lomholt, N. D., Hegelund, I. V., Poulsen, F. R., & Owens, T. (1999). Axotomy-induced glial reactions in normal and cytokine transgenic mice. *Advances in Experimental Medicine and Biology*, *468*, 157–171.

Fux, M., van Rooijen, N., & Owens, T. (2008). Macrophage-independent T cell infiltration to the site of injury-induced brain inflammation. *Journal of Neuroimmunology*, *203*(1), 64–72. https://doi.org/10.1016/j.jneuroim.2008.06.025

Gehrmann, J., Schoen, S. W., & Kreutzberg, G. W. (1991). Lesion of the rat entorhinal cortex leads to a rapid microglial reaction in the dentate gyrus. A light and electron microscopical study. *Acta Neuropathologica*, *82*(6), 442–455.

Getts, D. R., Terry, R. L., Getts, M. T., Muller, M., Rana, S., Shrestha, B., … King, N. J. (2008). Ly6c+ "inflammatory monocytes" are microglial precursors recruited in a pathogenic manner in West Nile virus encephalitis. *The Journal of Experimental Medicine*, *205*(10), 2319–2337. https://doi.org/10.1084/jem.20080421

Gomez-Nicola, D., Fransen, N. L., Suzzi, S., & Perry, V. H. (2013). Regulation of microglial proliferation during chronic neurodegeneration. *The Journal of Neuroscience*, *33*(6), 2481–2493. https://doi.org/10.1523/JNEUROSCI.4440-12.2013

Gonzalez, P., Burgaya, F., Acarin, L., Peluffo, H., Castellano, B., & Gonzalez, B. (2009). Interleukin-10 and interleukin-10 receptor-I are upregulated in glial cells after an excitotoxic injury to the postnatal rat brain. *Journal of Neuropathology and Experimental Neurology*, *68*(4), 391–403. https://doi.org/10.1097/NEN.0b013e31819dca30

Grebing, M., Nielsen, H. H., Fenger, C. D., K, T. J., von Linstow, C. U., Clausen, B. H., … Finsen, B. (2016). Myelin-specific T cells induce interleukin-1beta expression in lesion-reactive microglial-like cells in zones of axonal degeneration. *Glia*, *64*(3), 407–424. https://doi.org/10.1002/glia.22937

Hailer, N. P., Grampp, A., & Nitsch, R. (1999). Proliferation of microglia and astrocytes in the dentate gyrus following entorhinal cortex lesion: A quantitative bromodeoxyuridine-labelling study. *The European Journal of Neuroscience*, *11*(9), 3359–3364.

Huang, Z., Meola, D., & Petitto, J. M. (2012). Dissecting the effects of endogenous brain IL-2 and normal versus autoreactive T lymphocytes on microglial responsiveness and T cell trafficking in response to axonal injury. *Neuroscience Letters*, *526*(2), 138–143. https://doi.org/10.1016/j.neulet.2012.08.018

Hulshof, S., Montagne, L., De Groot, C. J., & Van Der Valk, P. (2002). Cellular localization and expression patterns of interleukin-10, interleukin-4, and their receptors in multiple sclerosis lesions. *Glia*, *38*(1), 24–35.

Jackson, C. A., Messinger, J., Palmer, M. T., Peduzzi, J. D., & Morrow, C. D. (2003). Gene expression in the muscle and central nervous system following intramuscular inoculation of encapsidated or naked poliovirus replicons. *Virology*, *314*(1), 45–61.

Jensen, M. B., Gonzalez, B., Castellano, B., & Zimmer, J. (1994). Microglial and astroglial reactions to anterograde axonal degeneration: A histochemical and immunocytochemical study of the adult rat fascia dentata after entorhinal perforant path lesions. *Experimental Brain Research*, *98*(2), 245–260.

Jones, L. L., Kreutzberg, G. W., & Raivich, G. (1997). Regulation of CD44 in the regenerating mouse facial motor nucleus. *The European Journal of Neuroscience*, *9*(9), 1854–1863.

Jones, L. L., Kreutzberg, G. W., & Raivich, G. (1998). Transforming growth factor beta's 1, 2 and 3 inhibit proliferation of ramified microglia on an astrocyte monolayer. *Brain Research*, *795*(1–2), 301–306.

Kamm, K., Vanderkolk, W., Lawrence, C., Jonker, M., & Davis, A. T. (2006). The effect of traumatic brain injury upon the concentration and expression of interleukin-1beta and interleukin-10 in the rat. *The Journal of Trauma*, *60*(1), 152–157. https://doi.org/10.1097/01.ta.0000196345.81169.a1

Kloss, C. U., Kreutzberg, G. W., & Raivich, G. (1997). Proliferation of ramified microglia on an astrocyte monolayer: Characterization of stimulatory and inhibitory cytokines. *Journal of Neuroscience Research*, *49*(2), 248–254.

Kovac, A. D., Kwidzinski, E., Heimrich, B., Bittigau, P., Deller, T., Nitsch, R., & Bechmann, I. (2004). Entorhinal cortex lesion in the mouse induces transsynaptic death of perforant path target neurons. *Brain Pathology*, *14*(3), 249–257.

Kremlev, S. G., & Palmer, C. (2005). Interleukin-10 inhibits endotoxin-induced pro-inflammatory cytokines in microglial cell cultures. *Journal of Neuroimmunology*, *162*(1–2), 71–80. https://doi.org/10.1016/j.jneuroim.2005.01.010

Ladeby, R., Wirenfeldt, M., Dalmau, I., Gregersen, R., Garcia-Ovejero, D., Babcock, A., … Finsen, B. (2005). Proliferating resident microglia express the stem cell antigen CD34 in response to acute neural injury. *Glia*, *50*(2), 121–131. https://doi.org/10.1002/glia.20159

Ladeby, R., Wirenfeldt, M., Garcia-Ovejero, D., Fenger, C., Dissing-Olesen, L., Dalmau, I., & Finsen, B. (2005). Microglial cell population dynamics in the injured adult central nervous system. *Brain Research. Brain Research Reviews*, *48*(2), 196–206. https://doi.org/10.1016/j.brainresrev.2004.12.009

Lam, D., & Schlichter, L. C. (2015). Expression and contributions of the Kir2.1 inward-rectifier K(+) channel to proliferation, migration and chemotaxis of microglia in unstimulated and anti-inflammatory states. *Frontiers in Cellular Neuroscience*, *9*, 185. https://doi.org/10.3389/fncel.2015.00185

Ledeboer, A., Breve, J. J., Poole, S., Tilders, F. J., & Van Dam, A. M. (2000). Interleukin-10, interleukin-4, and transforming growth factor-beta differentially regulate lipopolysaccharide-induced production of pro-inflammatory cytokines and nitric oxide in co-cultures of rat astroglial and microglial cells. *Glia*, *30*(2), 134–142.

Ledeboer, A., Breve, J. J., Wierinckx, A., van der Jagt, S., Bristow, A. F., Leysen, J. E., … Van Dam, A. M. (2002). Expression and regulation of interleukin-10 and interleukin-10 receptor in rat astroglial and microglial cells. *The European Journal of Neuroscience*, *16*(7), 1175–1185.

Ledeboer, A., Wierinckx, A., Bol, J. G., Floris, S., Renardel de Lavalette, C., De Vries, H. E., … van dam, A. M. (2003). Regional and temporal expression patterns of interleukin-10, interleukin-10 receptor and adhesion molecules in the rat spinal cord during chronic relapsing EAE. *Journal of Neuroimmunology*, *136*(1–2), 94–103.

Liao, W., Lin, J. X., & Leonard, W. J. (2011). IL-2 family cytokines: New insights into the complex roles of IL-2 as a broad regulator of T helper cell differentiation. *Current Opinion in Immunology*, *23*(5), 598–604. https://doi.org/10.1016/j.coi.2011.08.003

Liva, S. M., & de Vellis, J. (2001). IL-5 induces proliferation and activation of microglia via an unknown receptor. *Neurochemical Research*, *26*(6), 629–637.

Lodge, P. A., & Sriram, S. (1996). Regulation of microglial activation by TGF-beta, IL-10, and CSF-1. *Journal of Leukocyte Biology*, *60*(4), 502–508.

Matthews, D. A., Cotman, C., & Lynch, G. (1976). An electron microscopic study of lesion-induced synaptogenesis in the dentate gyrus of the adult rat. II. Reappearance of morphologically normal synaptic contacts. *Brain Research*, *115*(1), 23–41.

Mildner, A., Schmidt, H., Nitsche, M., Merkler, D., Hanisch, U. K., Mack, M., … Prinz, M. (2007). Microglia in the adult brain arise from Ly-6ChiCCR2+ monocytes only under defined host conditions. *Nature Neuroscience*, *10*(12), 1544–1553. https://doi.org/10.1038/nn2015

Mizuno, T., Sawada, M., Marunouchi, T., & Suzumura, A. (1994). Production of interleukin-10 by mouse glial cells in culture. *Biochemical and Biophysical Research Communications*, *205*(3), 1907–1915. https://doi.org/10.1006/bbrc.1994.2893

Moore, K. W., de Waal Malefyt, R., Coffman, R. L., & O'Garra, A. (2001). Interleukin-10 and the interleukin-10 receptor. *Annual Review of Immunology*, *19*, 683–765. https://doi.org/10.1146/annurev.immunol.19.1.683

Norden, D. M., Fenn, A. M., Dugan, A., & Godbout, J. P. (2014). TGFbeta produced by IL-10 redirected astrocytes attenuates microglial activation. *Glia*, *62*(6), 881–895. https://doi.org/10.1002/glia.22647

Pang, Y., Rodts-Palenik, S., Cai, Z., Bennett, W. A., & Rhodes, P. G. (2005). Suppression of glial activation is involved in the protection of IL-10 on maternal *E. coli* induced neonatal white matter injury. *Brain Research. Developmental Brain Research*, *157*(2), 141–149. https://doi.org/10.1016/j.devbrainres.2005.03.015

Park, K. W., Lee, H. G., Jin, B. K., & Lee, Y. B. (2007). Interleukin-10 endogenously expressed in microglia prevents lipopolysaccharide-induced neurodegeneration in the rat cerebral cortex in vivo. *Experimental & Molecular Medicine*, *39*(6), 812–819. https://doi.org/10.1038/emm.2007.88

Pousset, F., Cremona, S., Dantzer, R., Kelley, K. W., & Parnet, P. (2001). IL-10 and IL-4 regulate type-I and type-II IL-1 receptors expression on IL-1 beta-activated mouse primary astrocytes. *Journal of Neurochemistry*, *79*(4), 726–736.

Ren, X., Akiyoshi, K., Dziennis, S., Vandenbark, A. A., Herson, P. S., Hurn, P. D., & Offner, H. (2011). Regulatory B cells limit CNS inflammation and neurologic deficits in murine experimental stroke. *The Journal of Neuroscience*, *31*(23), 8556–8563. https://doi.org/10.1523/JNEUROSCI.1623-11.2011

Ringheim, G. E. (1995). Mitogenic effects of interleukin-5 on microglia. *Neuroscience Letters*, *201*(2), 131–134.

Sawada, M., Suzumura, A., Hosoya, H., Marunouchi, T., & Nagatsu, T. (1999). Interleukin-10 inhibits both production of cytokines and expression of cytokine receptors in microglia. *Journal of Neurochemistry*, *72*(4), 1466–1471.

Sawada, M., Suzumura, A., & Marunouchi, T. (1995). Induction of functional interleukin-2 receptor in mouse microglia. *Journal of Neurochemistry*, *64*(5), 1973–1979.

Schilling, T., Nitsch, R., Heinemann, U., Haas, D., & Eder, C. (2001). Astrocyte-released cytokines induce ramification and outward K+ channel expression in microglia via distinct signalling pathways. *The European Journal of Neuroscience*, *14*(3), 463–473.

Shechter, R., London, A., Varol, C., Raposo, C., Cusimano, M., Yovel, G., … Schwartz, M. (2009). Infiltrating blood-derived macrophages are vital cells playing an anti-inflammatory role in recovery from spinal cord injury in mice. *PLoS Medicine*, *6*(7), e1000113. https://doi.org/10.1371/journal.pmed.1000113

Spera, P. A., Ellison, J. A., Feuerstein, G. Z., & Barone, F. C. (1998). IL-10 reduces rat brain injury following focal stroke. *Neuroscience Letters*, *251*(3), 189–192.

Streit, W. J., Walter, S. A., & Pennell, N. A. (1999). Reactive microgliosis. *Progress in Neurobiology*, *57*(6), 563–581.

Strle, K., Zhou, J. H., Broussard, S. R., Venters, H. D., Johnson, R. W., Freund, G. G., … Kelley, K. W. (2002). IL-10 promotes survival of microglia without activating Akt. *Journal of Neuroimmunology*, *122*(1–2), 9–19.

Tanaka, J., Toku, K., Zhang, B., Ishihara, K., Sakanaka, M., & Maeda, N. (1999). Astrocytes prevent neuronal death induced by reactive oxygen and nitrogen species. *Glia*, *28*(2), 85–96.

van Strien, M. E., Mercier, D., Drukarch, B., Breve, J. J., Poole, S., Binnekade, R., … van Dam, A. M. (2010). Anti-inflammatory effect by lentiviral-mediated overexpression of IL-10 or IL-1 receptor antagonist in rat glial cells and macrophages. *Gene Therapy*, *17*(5), 662–671. https://doi.org/10.1038/gt.2010.8

Villacampa, N., Almolda, B., Vilella, A., Campbell, I. L., Gonzalez, B., & Castellano, B. (2015). Astrocyte-targeted production of IL-10 induces changes in microglial reactivity and reduces motor neuron death after facial nerve axotomy. *Glia*, *63*(7), 1166–1184. https://doi.org/10.1002/glia.22807

Wirenfeldt, M., Dissing-Olesen, L., Anne Babcock, A., Nielsen, M., Meldgaard, M., Zimmer, J., … Finsen, B. (2007). Population control of resident and immigrant microglia by mitosis and apoptosis. *The American Journal of Pathology*, *171*(2), 617–631. https://doi.org/10.2353/ajpath.2007.061044

Xin, J., Wainwright, D. A., Mesnard, N. A., Serpe, C. J., Sanders, V. M., & Jones, K. J. (2011). IL-10 within the CNS is necessary for CD4+ T cells to mediate neuroprotection. *Brain, Behavior, and Immunity*, *25*(5), 820–829. https://doi.org/10.1016/j.bbi.2010.08.004

Yang, J., Jiang, Z., Fitzgerald, D. C., Ma, C., Yu, S., Li, H., … Zhang, G. X. (2009). Adult neural stem cells expressing IL-10 confer potent immunomodulation and remyelination in experimental autoimmune encephalitis. *The Journal of Clinical Investigation*, *119*(12), 3678–3691. https://doi.org/10.1172/JCI37914

Yang, J., Zhang, L., Yu, C., Yang, X. F., & Wang, H. (2014). Monocyte and macrophage differentiation: Circulation inflammatory monocyte as biomarker for inflammatory diseases. *Biomarker Research*, *2*(1), 1. https://doi.org/10.1186/2050-7771-2-1

Zhou, Z., Peng, X., Insolera, R., Fink, D. J., & Mata, M. (2009). IL-10 promotes neuronal survival following spinal cord injury. *Experimental Neurology*, *220*(1), 183–190. https://doi.org/10.1016/j.expneurol.2009.08.018

How to cite this article: Recasens M, Shrivastava K, Almolda B, González B, Castellano B. Astrocyte-targeted IL-10 production decreases proliferation and induces a downregulation of activated microglia/macrophages after PPT. *Glia*. 2019; 67:741–758. https://doi.org/10.1002/glia.23573

Journal of Neuroinflammation

RESEARCH Open Access

Chronic exposure to IL-6 induces a desensitized phenotype of the microglia

Mireia Recasens[1], Beatriz Almolda[1*], Jeús Pérez-Clausell[2], Iain L. Campbell[3], Berta González[1] and Bernardo Castellano[1]

Abstract

Background: When the homeostasis of the central nervous system (CNS) is altered, microglial cells become activated displaying a wide range of phenotypes that depend on the specific site, the nature of the activator, and particularly the microenvironment generated by the lesion. Cytokines are important signals involved in the modulation of the molecular microenvironment and hence play a pivotal role in orchestrating microglial activation. Among them, interleukin-6 (IL-6) is a pleiotropic cytokine described in a wide range of pathological conditions as a potent inducer and modulator of microglial activation, but with contradictory results regarding its detrimental or beneficial functions. The objective of the present study was to evaluate the effects of chronic IL-6 production on the immune response associated with CNS-axonal anterograde degeneration.

Methods: The perforant pathway transection (PPT) paradigm was used in transgenic mice with astrocyte-targeted IL6-production (GFAP-IL6Tg). At 2, 3, 7, 14, and 21 days post-lesion, the hippocampal areas were processed for immunohistochemistry, flow cytometry, and protein microarray.

Results: An increase in the microglia/macrophage density was observed in GFAP-IL6Tg animals in non-lesion conditions and at later time-points after PPT, associated with higher microglial proliferation and a major monocyte/macrophage cell infiltration. Besides, in homeostasis, GFAP-IL6Tg showed an environment usually linked with an innate immune response, with more perivascular $CD11b^{+}/CD45^{high}/MHCII^{+}/CD86^{+}$ macrophages, higher T cell infiltration, and higher IL-10, IL-13, IL-17, and IL-6 production. After PPT, WT animals show a change in microglia phenotype expressing MHCII and co-stimulatory molecules, whereas transgenic mice lack this shift. This lack of response in the GFAP-IL6Tg was associated with lower axonal sprouting.

Conclusions: Chronic exposure to IL-6 induces a desensitized phenotype of the microglia.

Keywords: Axonal sprouting, Primed microglia, T cell, Monocyte, MHCII

Background

It is well established that perturbation in the central nervous system (CNS) as a consequence of an acute or chronic injury leads to microglial cell activation. This activation is totally dependent on the type, location, and duration of damage as well as the specific environment in which microglial cell activation takes place [45, 61]. Recent progress in cell-specific transcriptome profiling has been contributed in deciphering the role of microglia in both physiological and pathological conditions, revealing microglia acquire different cell activation signatures associated with an acute injury, chronic neurodegenerative diseases, or aging [48]. Among the different factors controlling microglial cell activation, cytokines and especially the balance between pro- and anti-inflammatory molecules play an essential role [46].

* Correspondence: beatriz.almolda@uab.cat
[1]Department of Cell Biology, Physiology and Immunology, Institute of Neuroscience, Universitat Autònoma de Barcelona, 08193, Bellaterra, Barcelona, Spain
Full list of author information is available at the end of the article

Among the plethora of cytokines that can act on microglia, IL-6 is a molecule that plays an important function as a regulator of inflammatory and immunological responses not only in the periphery [54, 55, 89] but also in the CNS. In the healthy CNS, neurons, glial cells, and endothelial cells express low levels of IL-6 and IL-6R [23, 34, 79, 83, 84]. However, an upregulation of these two molecules is observed after acute insults, such as traumatic brain injury and ischemia, as well as in chronic neurodegenerative conditions like Alzheimer's and Parkinson's diseases [11, 13, 30, 71, 86]. Both detrimental and beneficial functions have been described for IL-6 [19, 77]. On the one hand, IL-6 has been classified as a pro-inflammatory cytokine with a noxious role, based on the evidence that, together with other cytokines like TNF-α and IL-1β, acts as a major stimulator of the inflammatory response in the CNS [11, 30, 35], promoting neuronal death [3, 22]. Nevertheless, other studies indicated that IL-6 might have anti-inflammatory and neuroprotective effects after different kind of injuries including spinal cord injury [20], ischemia [64], and sciatic nerve transection [51]. Concerning microglia, in vitro and in vivo studies showed the capacity of IL-6 to induce activation, increasing microglial cell proliferation, as well as the production of microglia-derived pro-inflammatory molecules [15, 17, 21, 57, 91]. Moreover, IL-6 also can drive lymphocyte differentiation as demonstrated by some studies where, in the presence of TGF-b, T cell responses are polarized toward a T-regulatory phenotype, whereas the addition of IL-6 changes the phenotype of T lymphocytes toward a Th17 pathogenic phenotype [12].

The objective of the present study was to investigate the effects of chronic exposure to IL-6 on the phenotype of microglia cells, linked to anterograde axonal degeneration. For this purpose, perforant pathway transection were performed in the GFAP-IL6 transgenic (Tg) mouse model, in which chronic production of IL-6 was selectively targeted to astrocytes in the CNS [16, 17]. This type of lesion produces a dense anterograde and terminal axonal degeneration, glial cell activation, and axonal sprouting within the molecular layer of the fascia dentata, a very specific area of the hippocampus, making it a very useful tool to study modifications in these responses associated to variations in the microenvironment. Hence, the PPT paradigm has been extensively used as a model to study the mechanisms that initiate the innate immune response and the microglial response without blood-brain barrier disruption [6, 32].

Materials and methods

Animals

For the present study, a total of 94 GFAP-IL6Tg animals [17] (6–7 months old) and 79 wild-type (WT) littermates of both sexes were used. Animals were maintained at constant temperature (24 ± 2 °C) and housed on a 12-h light/dark cycle with food and water ad libitum during all the experiment. All experimental animal work was conducted in accordance to Spanish regulations (Ley 32/2007, Real Decreto 1201/2005, Ley 9/2003, and Real Decreto 178/2004) in agreement with European Union directives (86/609/CEE, 91/628/CEE, and 92/65/CEE) and was approved by the Ethical Commission of the Autonomous University of Barcelona. All efforts were made to minimize the number of animals used to produce reliable scientific data, as well as animal suffering.

Perforant pathway transection and experimental groups

GFAP-IL6Tg (n = 76) and WT mice (n = 62) were subjected to wire-knife unilateral perforant pathway transection (PPT). Briefly, animals were anaesthetized with intraperitoneal injection of a solution of ketamine (80 mg/kg) and xylazine (20 mg/kg) at dose of 0.01 mL/g body weight. Anaesthetized mice were placed in a stereotaxic device (Kopf Instruments®) and a small window in the skull was created by drilling in the left side of the skull (4.6 mm dorsal to Bregma and 2.5 mm laterally). A folded wire-knife (McHugh Milleux, m121) was inserted at an angle of 15° anterior and 10° lateral. The knife was unfolded at 3.6 mm ventrally and the perforant pathway (PP) was transected retracting the knife 3.3 mm. Finally, the knife was folded and removed from the brain. After surgery, the skin was sutured with 2-0 silk and the wound cleaned with iodine.

Non-lesioned (NL) and lesioned animals were distributed in different experimental groups for immunohistochemistry (IHC), flow cytometry, and protein analysis, as detailed in Table 1.

5′ Bromodeoxyuridine injections

In order to determine microglia/macrophage proliferation, the labeling of proliferative cells with 5′ bromodeoxyuridine (BrdU) was used. BrdU is a synthetic thymidine analog that incorporates into the DNA of dividing cells during S-phase and can be transferred to daughter cells upon replication. Lesioned WT (n = 5)

Table 1 Experimental groups of animals

		NL	2dpl	3dpl	7dpl	14dpl	21dpl
WT	IHC (n = 45)	6	6	8	10	8	7
	FC (n = 22)	8		7	7		
	Protein (n = 12)	3		3	3	3	
GFAP-IL6Tg	IHC (n = 53)	7	7	9	9	10	11
	FC (n = 24)	8		8	8		
	Protein (n = 17)	3		5	4	5	

and GFAP-IL6Tg animals (n = 6) were intraperitoneally (i.p.) injected with BrdU (50 mg/kg) diluted in TB (0.05 Trizma base, pH 7.4) every 24 h from the day of lesion to 7 days post-lesion (dpl), and subsequently euthanized at 7dpl.

Tissue processing for histological analysis

Animals were anaesthetized as described above, but at 0.015ml/g body weight concentration, and then perfused intracardially for 10 min with 4% paraformaldehyde in 0.1 M phosphate buffer (pH 7.4). Brains were immediately removed and post-fixed for 4 h at 4 °C in the same fixative and, after phosphate buffer rinses, cryopreserved in a 30% sucrose solution in 0.1 M phosphate buffer for 48 h at 4 °C and frozen in ice-cold 2-methylbutane solution (320404, Sigma-Aldrich). A series of horizontal parallel sections (30-μm-thick) were obtained using a Leica CM3050 cryostat and stored free-floating in Olmos anti-freeze solution at -20°C until used.

Toluidine blue staining

Sections were mounted onto gelatinized slides, air dried at RT for 1 h, and then were incubated for 1 min in a solution containing 0.1% toluidine blue diluted in Walpole's buffer (0.05 M, pH 4.5). After washes in distilled water, sections were dehydrated in graded alcohols, *N*-butyl alcohol, and after xylene treatment, coverslipped with DPX mounting media.

Single stain immunohistochemistry

Free-floating sections were processed for the study of microglial morphology, distribution, density, and phenotype using antibodies against Iba1, Pu.1, CD45, MHCII, CD206 (Table 2). For the analysis of microglia proliferation, sections were stained with anti-phospho-histone H3 (pH3) and BrdU, whereas for microglial cell death evaluation, anti-caspase 3 antibody was used. Finally, lymphocyte recruitment was analyzed using antibody against CD3, a pan marker for T lymphocytes. In all cases, sections were washed several times with 0.05 M Tris-buffered saline (TBS) pH 7.4 and with TBS

Table 2 Reagents used for IHC

	Target antigen	Host	Dilution	Cat Number	Manufacturer
Primary antibodies	Iba1	Rabbit	1:3000	019-19741	Wako
	Pu.1	Rabbit	1:400	2258S	Cell Signaling
	CD45	Rat	1:1000	MCA1031G	AbD Serotec
	pH3	Rabbit	1:3000	06-570	Millipore
	BrdU	Rat	1:120	Ab6326	Abcam
	Caspase 3	Rabbit	1:1000	AF835	R&D Systems
	Iba1	Rabbit	1:1000	GTX100042	Genetex
	CD3	Hamster	1:500	MCA2690	AbD Serotec
	MHCII (IA)	Rat hybridoma	1:25	TIB-120	ATCC
	CD206	Rat	1:500	MCA2235GA	AbD Serotec
	CD28	Rabbit	1:50	ab203084	Abcam
	CTLA-4	Rabbit	1:25	ab237712	Abcam
	Laminin	Rabbit	1:500	AMP420	Biorad
	TMEM119	Rabbit	1:1000	ab209064	Abcam
	GFAP	Mouse	1:3000	63893	Sigma
Secondary antibodies	Biotinylated	Rabbit	1:500	BA-1000	Vector Laboratories
	Biotinylated	Hamster	1:500	BA-9100	Vector Laboratories
	Biotinylated	Rat	1:500	BA-4001	Vector Laboratories
	Alexa 555	Rat	1:1000	A11006	Invitrogen
	Alexa 488	Rabbit	1:500	A21206	Invitrogen
	Cy2	Mouse	1:500	PA42003	GE Healthcare Lifescience
Streptavidin Alexa Fluor-555			1:500	S32355	Molecular Probes
Streptavidin Alexa Fluor-488			1:500	S11223	Molecular Probes
Streptavidin-HRP			1:500	SA-5004	Vector Laboratories
DAPI			1:10000	D9542	Sigma Aldrich

containing 1% Triton-X100 (TBST, pH 7.4). In the case of Pu.1 staining, sections were exposed to antigen retrieval by treatment with sodium citrate buffer (pH 8.5) for 40 min at 80 °C. Endogenous peroxidase was blocked by incubating the sections for 10 min with 2% H_2O_2 in 70% methanol. For BrdU detection, DNA was denatured by first incubating in 0.082 N HCl for 10 min at 4 °C and then for 30 min in 0.82 N HCl at 37 °C. Sections were then rinsed with borate buffer (pH 8.5) and 0.5% Triton X-100 in TBS. Afterwards, all sections were incubated for 1 h at room temperature (RT) in blocking buffer solution (BB) containing 10% fetal bovine serum in TBST. After that, sections were incubated overnight at 4 °C followed by 1h at RT with primary antibodies diluted in BB, as specified in Table 2. Sections from spleen and gut were used as positive control whereas sections incubated in BB lacking the primary antibody were used as negative control. After washes with TBST, sections were incubated for 1 h at RT with biotinylated anti-rabbit secondary antibody biotinylated anti-hamster secondary antibody or biotinylated anti-rat secondary antibody (Table 2) diluted in BB. After 1 h at RT in streptavidin-peroxidase, the reaction was visualized by incubating the sections in the 3,3-diaminobenzidine (DAB) kit (SK-4100; Vector Laboratories, USA) following the manufacturer's instructions. Finally, sections were mounted on slides, counterstained with 1% toluidine blue, dehydrated in graded alcohols, and, after xylene treatment, coverslipped with DPX. Sections were analyzed with a Nikon Eclipse 80i brightfield microscope and photographed with a DXM 1200F Nikon digital camera.

Double stain immunohistochemistry

Double immunolabeling for BrdU with either Iba1 or GFAP was carried out to identify proliferating microglia/macrophages and astrocytes. Sections were firstly processed for BrdU as described above, with anti-rat Alexa-Fluor 555-conjugated antibody as secondary antibody (Table 2). After several washes with TBST and 1 h incubation in BB at RT, sections were incubated overnight at 4 °C followed by 1 h at RT with rabbit anti-Iba1 and mouse anti-GFAP antibody diluted in BB (Table 2). After washes in TBST, sections were incubated with either anti-rabbit Alexa-Fluor 488-conjugated or anti-mouse Cy2-conjugated secondary antibodies (Table 2). Finally, sections were washed with TBST, followed by TBS and TB, and the nuclei stained with 4,9,6-diamidino-2-phenylindole (DAPI) for 10 min (Table 2).

To study the expression of co-stimulatory molecules on T cells double immunolabeling combining CD28 or CTLA-4 with CD3 were performed (Table 2). Sections were firstly processed for CD3 as described above, but using Alexa-Fluor 488-conjugated streptavidin instead of horseradish streptavidin-peroxidase (Table 2). Then, sections were incubated overnight at 4 °C and 1 h at RT with anti-CD28 and anti-CTLA-4 followed by anti-rabbit Alexa-Fluor 555-conjugated secondary antibody (Table 2).

To analyze the localization of $MHCII^+$ cells, double immunofluorescence combining MHCII with laminin was performed (Table 2). Sections were firstly processed for MHCII as described above, but using Alexa-Fluor 555-conjugated streptavidin instead of horseradish streptavidin-peroxidase (Table 2). Then, sections were incubated overnight at 4 °C and 1 h at RT with anti-laminin followed by anti-rabbit Alexa-Fluor 488-conjugated secondary antibody (Table 2).

To study the phenotype of $MHCII^+$ cells, double immunofluorescence combining MHCII with Tmem119, a defined microglia-specific marker [10], was performed (Table 2). Sections were firstly processed for Tmem119 as described above, but using Alexa-Fluor 488-conjugated streptavidin instead of horseradish streptavidin-peroxidase (Table 2). After that, sections were incubated overnight at 4 °C and 1 h at RT with anti-MHCII followed by anti-rat Alexa-Fluor 555-conjugated secondary antibody (Table 2).

Sections incubated in BB lacking the primary antibody were used as negative control and sections from spleen and spinal cord from EAE-induced mice were used as positive control for the different immunostains. Finally, all double-immunostained sections were mounted on slides, coverslipped with Fluoromount GTM (0100-01; SouthernBiotech, Birmingham, AL), and analyzed using Nikon Eclipse E600 fluorescence microscope and a Zeiss LSM 700 confocal microscope using a × 40 objective.

Terminal dUTP nick end labeling

In addition to caspase-3 immunohistochemistry, the study of microglial cell death was performed on sections double stained for terminal dUTP nick end labeling (TUNEL) and Iba1. Briefly, sections were mounted on slides and treated for 5 min with 100% methanol for endogenous peroxidase blocking. Then, sections were rinsed in 10 mM Tris buffer (pH 8) and 5 mM EDTA followed by incubation for 15 min at RT in the same buffer plus Proteinase K (20 μg/mL). After several washes with 5 mM EDTA, sections were incubated for 10 min at RT in TdT buffer containing 30 mM Tris, 140 mM sodium cacodilate, and 1 mM cobalt chloride (pH 7.7). After that, sections were incubated for 20 min at 37 °C in TdT buffer plus 0.161 U/μL TdT enzyme (Terminal Transferase, 3333566 Roche, Manheim, Germany) and 0.0161 nmol/μL of biotin-16-dUTP (1093070, Roche, Manheim, Germany). The reaction was stopped by submerging sections twice in citrate buffer (300 mM sodium chloride, 30 mM sodium citrate, 5 mM EDTA) for 5 min. After several washes with TBS, sections were incubated for 1 h at RT with HRP-conjugated streptavidin (Table 2) and the peroxidase

reaction visualized by incubation in a 3,3-DAB kit plus 1% of cobalt (SK-4100; Vector Laboratories, USA), following the manufacturer's instructions. After that, sections were incubated with Iba1 antibody (1:1000) (Table 2) using the same protocol described in the single IHC section. Sections from gut were used as positive control. Finally, sections were dehydrated in graded alcohols and, after xylene treatment, coverslipped in DPX.

Sulfide-silver staining

Collateral sprouting in non-lesioned and lesioned animals was analyzed at 14 and 21 dpl, using a variation of the sulfide-silver staining technique, as described by Danscher [24]. Briefly, animals were injected intraperitoneally with sodium selenite (10 mg/kg) and 1 h later, animals were perfused and postfixed as described above. After that, brains were removed and cryoprotected with 30% sucrose solution in 0.1 M phosphate buffer at 4 °C for 48 h and frozen as described above. Frozen parallel transversal sections (30 μm thick) were obtained using a cryostat (Leica, CM 3050S) and mounted on slides. Sections were incubated to visualize metal precipitates. Briefly, slides were rinsed in 95% EtOH for 15 min, then 2 min in 70% alcohol, 50% alcohol, and rinsed again with dH_2O for 30 min. Following rehydration, sections were incubated with the developer solution that contains 60 mL of arabic gum (0.5 kg/L), 10 mL of sodium citrate buffer 0.2 M, 15 mL hydroquinone (0.85 g diluted in 15 mL of dH_2O), and 15 mL silver lactate (0.12 g diluted in 15 mL of dH_2O) in a water bath at 26 °C protected from light for 60–80 min [24]. After that, sections were rinsed in 5% sodium thiosulfate for 12 min and rinsed again with dH_2O. Sections were postfixated in 70% alcohol for 30 min, dehydrated in alcohol, rinsed in xylene and coverslipped with DPX.

Brightfield microscopy densitometric analysis

Densitometric analysis in NL and lesioned animals was performed on sections immunolabeled for Iba1 to assess microglia state. A minimum of three animals per genotype and experimental time-point were analyzed. A total of 9 photographs from 3 different sections per animal containing the left molecular layer (ML) of the dentate gyrus (DG) were captured using the × 20 objective with a DXM 1200F Nikon digital camera joined to a brightfield Nikon Eclipse 80i microscope, using the software ACT-1 2.20 (Nikon corporation) (Suppl. Fig. 1). By means of analySIS® software, both the percentage of area occupied by the immunolabeling as well as the intensity of the immunostain (Mean Grey Value Mean) was recorded for each photograph. The AI index [2] was calculated as function of the percentage of the immunostained area and the Mean Grey Value Mean.

In order to quantify microglial cell density, sections immunostained for the transcription factor Pu.1 from a minimum of three NL and three lesioned WT and GFAP-IL6Tg at 2, 3, 7, 14, and 21 dpl were analyzed. In this case, a total of 6 photographs from 3 different sections per animal were captured with the × 10 objective, using the same device and software referred above. The number of $Pu.1^+$ cells in the ML of the DG was obtained using the "Automatic Cell Counter" (ITCN) plug-in from NIH Image J® software (Wayne Rasband, National Institutes of Health, USA). Data were expressed in cells/mm^2.

Microglial cell proliferation was quantified on sections immunostained for the mitotic marker pH3 as well as BrdU in NL and PPT-lesioned animals at 2, 3, and 7dpl in the case of pH3 and at 7dpl in the case of BrdU. For pH3, a minimum of three WT and three GFAP-IL6Tg animals per group were analyzed, whereas in the case of BrdU, five WT and six GFAP-IL6Tg animals were used. The number of both $pH3^+$ and $BrdU^+$ cells in the ML of DG was manually counted on 20 (for pH3) and 10 different sections (for BrdU) per animal using a × 20 objective. Data were averaged and represented as $pH3^+$ cells/section or $BrdU^+$ cells/section.

To evaluate T lymphocyte infiltration, sections stained for CD3 were used. At least three WT and three GFAP-IL-6Tg NL animals and at 2, 3, 7, and 14dpl were used. All $CD3^+$ cells in the ML of DG were manually counted on 20 sections per animal using a × 20 objective. Data were averaged and represented as $CD3^+$ cells/section.

To analyze axonal sprouting, sections stained with the sulfide-silver staining were used. At least three WT and five GFAP-IL6Tg NL animals and at 14 and 21 dpl were analyzed. A total of 24 photographs from 8 different hippocampal sections per animal were captured at × 20 magnification using the same device and software referred above. The percentage of area occupied was obtained using the analySIS® software.

Morphometric analysis

Morphometric analysis of microglial cells was done on sections immunolabeled for Iba1. At least three WT and three GFAP-IL6Tg animals were analyzed. For each animal, a total of 30 representative microglial cells were randomly chosen from 9 different photographs from the ML of the DG of the hippocampus and photographed at × 40 magnification. Using the analySIS® software, individual cells were isolated and different parameters including the area occupied, the sphericity (value equal to 1 indicates spherical shape and low values increased elongation), the shape factor (high values indicate round shape and low values ramified morphology), and the elongation (value equal to 1 indicates round morphology and high values increased elongation) were recorded for each cell.

Flow cytometry analysis

The phenotype of the microglia/macrophage populations and the T cell infiltration in NL and lesioned animals (at 3 and 7 dpl) were analyzed using flow cytometry as previously described [1].

Briefly, animals were anaesthetized and intracardially perfused for 1 min with 0.1 M phosphate buffer solution (PBS), brains removed, and the entire ipsilateral hippocampus was quickly dissected out. In order to obtain a cell suspension, samples were dissociated through 140 μm and 70 μm meshes and digested for 30 min at 37 °C using collagenase type IV (17104-019, Life Technologies) and DNAsa I (D5025, Sigma). After that, each cellular suspension was centrifuged at RT for 20 min at 2400 rpm in a discontinuous density Percoll gradient (17-0891-02, Amersham-Pharmacia) between 1.03 and 1.08 g/mL. Myelin in the upper layer was removed. Cells in the interphase and in the clear upper-phase were collected, washed in PBS + 2% serum, and the Fc receptors were blocked by incubation for 10 min in a solution of purified CD16/32 diluted in PBS + 2% serum. Afterwards, cells were labeled for 30 min at 4 °C with the following four combinations of cell surface antibodies: (1) anti-CD11b-APC-Cy7, anti-CD45-PerCPCy5, anti-CD11c-PE, anti-MHCII-FITC, anti-CD86-PE-Cy7, anti-CD80-APC; (2) anti-CD11b-APC-Cy7, anti-CD45-PerCPCy5, anti-Ly6C-FITC, anti-F480-APC, and anti-ICOSL-PE; (3) anti-CD3-FITC, anti-CD4-APC-Cy7, and anti-CD8-PerCPC; and (4) anti-CD3-FITC, anti-CD4-APC-Cy7, anti-Tbet-PerCPCy5.5, anti-RORγt-APC, anti-Foxp3-PE-Cy7, and anti-Gata3-PE (Table 3). In parallel, isotype-matched control antibodies for the different fluorochromes (BD Pharmingen) were used as negative control and a cell suspension of splenocytes as positive control. Data were extrapolated as number of cells using the Cyto Count™ fluorescent beads following the manufacturer's instructions (S2366, Dako Cytomation). Finally, cells were acquired using a FACS Canto flow cytometer (Becton Dickinson, San Jose, CA) and results analyzed using the FlowJo® software. The analysis was performed separately for each animal without any pooling.

Tissue processing for protein analysis

Animals used for protein analysis were i.p anaesthetized (as described above) and perfused for 1 min with cold 0.1 M PBS (pH 7.4). Subsequently, the entire ipsilateral hippocampus was dissected out, snap frozen individually in liquid nitrogen, and stored at − 80 °C. Total protein was extracted by solubilization of samples on lysis buffer, containing 25 mM HEPES, 2% Igepal, 5 mM $MgCl_2$, 1.3 mM EDTA, 1 mM EGTA, 0.1 M PMSF, and protease (1:100, P8340, Sigma Aldrich) and phosphatase inhibitor cocktails (1:100, P0044, Sigma Aldrich), for 2 h at 4 °C. After solubilization, samples were centrifuged at 13,000 rpm for 5 min at 4 °C and the supernatants collected. The hippocampus from each animal was analyzed separately. Total protein concentration was determined with a commercial Pierce® BCA Protein Assay kit (#23225, Thermo Scientific) according to manufacturer's protocol.

Table 3 Antibodies used in flow cytometry

Target antigen		Format	Dilution	Cat Number	Manufacturer
Fc blocker	CD16/32	Purified	1:250	553142	BD Pharmingen
Primary antibodies	CD11b	APC-Cy7	1:400	557657	BD Pharmingen
	CD45	PerCPCy5	1:400	557235	BD Biosciences
	MHCII	FITC	1:400	553623	BD Pharmingen
	CD11c	PE	1:400	557401	BD Pharmingen
	Ly6C	FITC	1:400	553104	BD Pharmingen
	ICOSL	PE	1:400	12-5985-82	BD Bioscience
	CD86	PE-Cy7	1:400	560582	BD Pharmingen
	CD80	APC	1:400	560016	BD Pharmingen
	CD11c	PE	1:400	557401	BD Pharmingen
	F4/80	APC	1:400	17-4801-82	eBioscience
	CD3e	FITC	1:400	553062	BD Pharmingen
	CD4	APC-Cy7	1:400	552051	BD Pharmingen
	CD8	PerCP	1:400	553036	BD Pharmingen
	T-bet	PerCPCy5.5	1:400	45-5825	eBioscience
	RORγt	APC	1:400	17-6988-82	eBioscience
	Foxp3	PECy7	1:400	25-5773-80	eBioscience
	Gata3	PE	1:400	560074	BD Pharmingen

Protein lysates were stored at − 80 °C until used for the protein microarray analysis.

Cytokine analysis

The cytokines IL-2, IL-6, IFN-γ, IL-1β, IL12p70, IL-17, IL-10, IL-13, IL-9, IL-5, and IL-4 and the chemokines CXCL10 and CCL2 were analyzed using a Milliplex® MAP Mouse Cytokine/Chemokine kit (#MCYTOMAG-70K, Merck Millipore) according to the manufacturer's instructions. Briefly, 25 μL of each hippocampus extract with a final total protein concentration of 2.5 μg/μL was added to the plate, along with the standards in separate wells, containing 25 μL of custom fluorescent beads and 25 μL of matrix solution and incubated overnight at 4 °C in a plate-shaker (750 rpm). After two washes with wash buffer (WB), the plate was incubated with 25 μL of detection antibodies for 30 min at RT followed by incubation with 25 μL of Streptavidin-Phycoerythrin for 30 min at RT in a plate-shaker (750 rpm). Finally, the plate was washed two times with WB and 150 μL of Drive fluid was added. Luminex® MAGPIX® device with the xPONENT® 4.2 software was used to read the plate. Data were analyzed using the Milliplex® Analyst 5.1 software and expressed as pg/mL of protein.

Tissue processing for serum samples

Animals used for serum samples were i.p anaesthetized (as described above) and blood extraction were performed by cardiac puncture. After blood extraction, samples were centrifuged at 10,000 rpm for 5 min at 4 °C and the supernatants collected. Finally, samples were stored at − 80 °C until used for the ELISA analysis.

IL-6 ELISA

The IL-6 levels in serum were analyzed using a Mouse IL-6 Uncoated ELISA kit (88-7064, Invitrogen) according to the manufacturer's instructions. Briefly, the plate was coated overnight at 4 °C and after washes; wells were blocked for 1 h at RT. After several washes, 100 μL of each serum extraction and standards, in separated wells, were added and incubated overnight at 4 °C. After reagents incubations, and the addition of TMB solution and Stop solution, results were read at 450 nm in the microplate reader VarioskanTM Lux (ThermoFisher Scientific) and data were expressed as pg/mL of protein.

Statistical analysis

Statistics were performed using the Graph Pad Prism 5.0 ® software. To study the differences between NL WT and NL GFAP-IL6Tg animals unpaired Student's *T* test was used, while two-way ANOVA followed by Tukey's post hoc analysis was used to study the effect of the lesion in both genotypes. All experimental values were expressed as mean values ± SD.

Results

Astrocyte-targeted IL-6 production modifies the number and morphology of microglia/macrophage cell populations

Analysis of microglia/macrophage cell distribution and morphology

To investigate possible changes in the brain cyto-architecture and cell distribution, by astrocyte-targeted IL-6 production in the CNS, a microscopic study was performed on toluidine blue sections (Suppl Fig. 2). In NL conditions, both WT and GFAP-IL6Tg animals showed the same distribution of cells through the ML. However, GFAP-IL6Tg showed an increased number of cells. After PPT, the presence of cells increased in the outer molecular layer (OML) and medial molecular layer (MML) in both WT and GFAP-IL6Tg animals from 3 to 7 dpl. In parallel to changes found in the OML and the MML, both WT and GFAP-IL6Tg animals showed a progressive reduction of cells in the inner molecular layer (IML) along the different time-points (from 3 to 14 dpl) (Suppl Fig. 2).

The possible changes in distribution and morphology of the microglia/macrophage cell population evoked by the transgenic production of IL-6 were analyzed using Iba1 IHC.

In NL WT animals, microglial cells showed the characteristic ramified morphology throughout the ML of the DG (Fig. 1a, f), whereas in the GFAP-IL6Tg mice, microglia had a significant increase of Iba1 immunoreactivity (Fig. 1b) as well as morphological changes mainly characterized by a greater number and thickness of ramifications and an increase in the number of processes (Fig. 1a). These qualitative morphological changes were quantified by a morphometric analysis of different parameters such as the area, shape factor, the elongation, and sphericity of individual Iba1$^+$ microglial cells. Confirming the qualitative findings, GFAP-IL6Tg animals showed a significant increase in the area occupied by individual microglial cells (Suppl Fig. 3A). Moreover, microglial cells in transgenic animals showed a higher ramified morphology, as indicated by less values of shape factor (Suppl Fig. 3D), and a rounded morphology (Suppl Fig. 3B-C).

After PPT, Iba1 immunoreactivity in WT animals increased at 3 dpl and decreased at 21 dpl, whereas in GFAP-IL6Tg animals Iba1 showed a later increase at 7 dpl and remained stable until 21 dpl (Fig. 1a, b). Noticeably, at 2 and 14 dpl (Fig. 1b), GFAP-IL6Tg mice showed higher levels of microglial cell Iba1 compared to WT (1651 ± 376.6 vs. 3145 ± 202.3 AI, WT/2dpl vs. Tg/2dpl, p = 0.014 and 4160 ± 939.0 vs. 2374 ± 63.5 AI, WT/14dpl vs. Tg/14dpl, p = 0.032). To quantify the dynamics of microglial activation following PPT lesion in both WT and GFAP-IL6Tg animals, the fold-changes

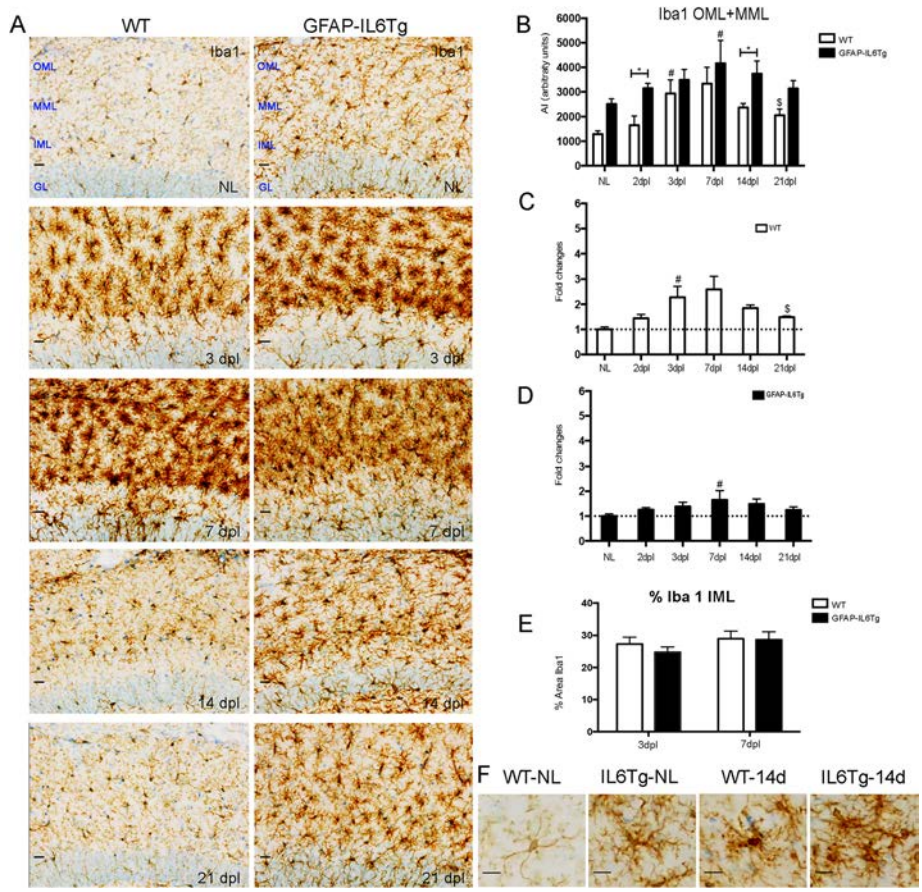

Fig. 1 Microglial cell activation. Representative images from WT and GFAP-IL6Tg mice showing Iba1 staining in the granular (GL) as well as the inner, medial, and outer molecular layer (IML, MML, and OML, respectively) of the dentate gyrus (DG) in non-lesioned (NL) and PPT-lesioned hippocampus from 3 to 21dpl. Scale bar = 20 μm (**a**) and 10 μm (**f**). **b** Graph showing the time course of Iba1 immunostaining, expressed as AI (area x intensity). In comparison with WT, GFAP-IL6Tg animals showed increased levels of Iba1 at 2 and 14dpl. **c**, **d** Graphs showing the fold change increase of Iba1 expression in comparison with the corresponding NL animals in both WT and GFAP-IL6Tg mice. **e** Graph showing the area occupied by Iba1 in the IML in both WT and GFAP-IL6Tg at 3 and 7 dpl. A minimum of 3 animals per genotype and experimental time-point were analyzed. A total of 9 photographs from 3 different hippocampal sections were used. Data are represented as mean ± SD. The significances are represented as #$p \leq 0.05$ vs. NL of respective group; \$$p \leq 0.05$ vs. 7dpl of respective group. Significant differences between genotypes are represented as *$p \leq 0.05$

with respect to the corresponding NL animals were calculated (Fig. 1c, d). This revealed that, although the levels of Iba1 in GFAP-IL6Tg animals were higher than in WT, the upregulation of Iba1 with respect to its basal levels was less pronounced in the transgenic animals than in WT, at specific time-points along the progression of the PPT lesion. Thus, while WT animals showed around a 3-fold increase of Iba1 at 7dpl in comparison with their basal levels (Fig. 1c), in GFAP-IL6Tg mice, this increase remained less than 2-fold at any time-point analyzed (Fig. 1d). Finally, no differences in the area occupied by Iba1 were observed in the IML of both WT and GFAP-IL6Tg animals after PPT (Fig. 1e).

In addition to changes in Iba1 levels, after PPT, both WT and GFAP-IL6Tg mice showed alterations in microglial cell morphology with some differences noted. At early time-points (3 and 7dpl), microglial cells in both genotypes showed the typical "bushy" shapes characterized by short and stubby ramifications (Suppl Fig. 3). At later time-points (14 and 21 dpl), microglial cells in both WT and GFAP-IL6Tg animals returned to ramified morphologies, although comparatively, microglia in the transgenic animals displayed a greater number and thickness of ramifications than WT at these time-points (Fig. 1f).

Analysis of microglia/macrophage cell density

To evaluate possible changes in the number of microglia/macrophages IHC for the transcription factor Pu.1, a specific myeloid marker [40], was used.

In parallel to changes in microglia/macrophage distribution and morphology, our observations revealed

around a 2-fold increase in the number of Pu.1$^+$ cells in the ML of the DG in NL GFAP-IL6Tg animals in comparison with NL WT (Suppl. Fig. 4 and Suppl. Fig. 11B).

After PPT, the number of Pu.1$^+$ cells in WT animals increased progressively from 2 to 3 dpl, whereas in GFAP-IL6Tg animals, this increase was observed only at 3 dpl (Suppl. Fig. 4A). At later time points, in WT animals, Pu.1$^+$ cells exhibited a marked decrease at 14 dpl, whereas in GFAP-IL6Tg mice remained stable until 21 dpl (Suppl. Fig. 4A). Consequently, in transgenic animals, the number of Pu.1$^+$ cells at 14 dpl was significantly higher than WT (759 ± 292.8 vs. 1384 ± 305.2 number of cells, WT/14dpl vs. Tg/14dpl, p = 0.010) (Suppl. Fig. 4B). Notably, when dynamics of Pu.1 upregulation were compared with the corresponding NL, it was found again that WT animals had a nearly 5-fold increase in the number of Pu.1$^+$ cells in the ML of the DG (Suppl. Fig. 4C), whereas GFAP-IL6Tg animals showed only a 2-fold increase in Pu.1$^+$ cells compared with NL GFAP-IL6Tg animals (Suppl. Fig. 4D).

Astrocyte-targeted IL-6 production increases microglial cell proliferation after PPT but has no effects on cell death

In order to study whether changes observed in microglial cell numbers in GFAP-IL6Tg animals were related to changes in either proliferation and/or microglial cell death, pH3 and BrdU detection was used for the analysis of proliferation (Fig. 2) and activated caspase-3 and TUNEL for apoptosis evaluation.

In both NL WT and NL GFAP-IL6Tg animals, few pH3$^+$ cells were observed in the ML of the DG, with no differences between genotypes. After PPT, although the peak of proliferation was at 2 dpl in both genotypes, in WT animals the number of pH3$^+$decreased at 3 dpl, whereas in GFAP-IL6Tg animals the number of pH3$^+$ cells decreased later on, at 7 dpl (Fig. 2a, c). Furthermore, to explore whether, additionally to the dynamics of proliferation, IL-6 overproduction produced modifications in the total amount of proliferating cells, a daily injection of BrdU was performed during 7 days. This study demonstrated that the total number of accumulated BrdU$^+$/Iba1$^+$ cells until 7dpl was significantly higher in GFAP-IL6Tg animals than in WT (23.06 ± 7.39 vs. 36.19 ± 6.16 number of cells, WT/7dpl vs. Tg/7dpl, p = 0.049) (Fig. 2b). Using double stain immunohistochemistry, it was determined that parenchymal BrdU$^+$ cells in both WT and GFAP-IL6Tg animals corresponded mainly to Iba1$^+$ microglia/macrophages, although some scattered proliferating astrocytes (BrdU$^+$/GFAP$^+$) were also found (Fig. 2d, e).

Regarding microglial cell death, no staining for either active caspase-3 or TUNEL was detected in the dennervated ML of the DG in either WT or GFAP-IL6Tg animals from 2 to 21 dpl (data not shown).

Astrocyte-targeted IL-6 production increases the number of monocytes/macrophages

Flow cytometry was used to assess the number of microglia/macrophage populations induced by the transgenic production of IL-6 (Suppl. Fig. 5). The microglia/macrophage population was identified based on the positive CD11b expression in combination with differential expression levels of CD45 (Suppl. Fig. 5A). This helped in

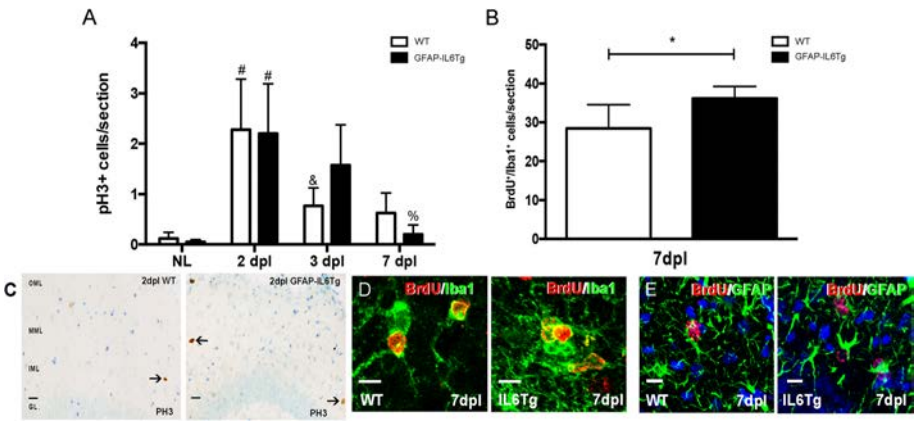

Fig. 2 Microglial proliferation. **a** Graph showing the quantification of pH3$^+$ cells in non-lesioned (NL) and PPT-lesioned animals from 2 to 7 dpl, in WT and GFAP-IL6Tg mice. **b** Graph showing the quantification of BrdU$^+$/Iba1$^+$ cells in PPT-lesioned animals at 7dpl in WT and GFAP-IL6Tg animals. Note that the total number of BrdU$^+$ proliferating cells is significantly higher in transgenic animals. **c** Representative images of pH3$^+$ cells in WT and Tg animals at 2 dpl. Scale bar = 20um. **d** Representative images of double IHC combining BrdU (red) and Iba1 (green). **e** Representative images of double IHC combining BrdU (red) and GFAP (green). Scale bar = 10 μm. For pH3, a minimum of three WT and three GFAP-IL6Tg animals per group were analyzed, whereas in the case of BrdU five WT and six GFAP-IL6Tg animals were used. Data are represented as mean ± SD. The significances are represented as #$p \leq 0.01$ vs. NL of respective group; &$p \leq 0.05$ vs. 2dpl of respective group and %$p \leq 0.01$ vs. 3dpl of respective group. Significant differences between genotypes are represented as *$p \leq 0.05$

differentiating homeostatic from activated microglia as well as macrophages. Thus, ramified or homeostatic microglia were identified as $CD11b^+/CD45^{low}$ and activated microglia as $CD11b^+/CD45^{int}$. In this study, the term $CD11b^+/CD45^{low/int}$ has been used to refer to the population of homeostatic and activated microglia jointly. Moreover, the $CD11b^+/CD45^{high}$ population was identified, which may include highly activated microglia, monocytes, macrophages, and dendritic cells. The percentage of $CD11b^+/CD45^{high}$ population, in the GFAP-IL6Tg, was higher than in WT at all time points analyzed (Suppl. Fig. 7).

Taking in account the total number of cells, in NL animals, our results showed a significant increase of both $CD11b^+/CD45^{low/int}$ (318.3 ± 124.7 vs. 524.3 ± 154.5 number of cells, WT/NL vs. Tg/NL, p = 0.08) and $CD11b^+/CD45^{high}$ populations (7.50 ± 3.06 vs. 45.57 ± 14.06 number of cells, WT/NL vs. Tg/NL, p = 0.001) in GFAP-IL6Tg animals (Suppl. Fig. 11C and D).

After PPT, GFAP-IL6Tg animals exhibited an increase in the number of both $CD11b^+CD45^{low/int}$ and $CD11b^+/CD45^{high}$ cell population at 7dpl when compared to their own NL, while in WT animals no changes were observed. Interestingly, the levels of CD45 (mean fluorescence intensity) were always higher in the $CD11b^+/CD45^{low/int}$ cell population of GFAP-IL6Tg animals than in WT (Suppl. Fig. 5B). However, in $CD11b^+/CD45^{high}$ cell population, no differences between genotypes were observed (Suppl. Fig. 5B).

Using CD45 immunohistochemistry, it was confirmed that GFAP-IL6Tg animals showed a higher activated microglial phenotype (Suppl. Fig. 5C). Also, after PPT, scattered $CD45^+$ cells with round morphology were observed through the ML of the FD in both experimental groups that could correspond to T cells and/or infiltrated monocytes (Suppl. Fig. 5C black arrows).

Taking into account that the population of $CD11b^+/CD45^{high}$ cells includes monocytes, macrophages, dendritic cells, and highly activated microglia, we next addressed whether the changes observed in the number of microglia/macrophages were due specifically to variations in the number of monocytes or rather to the presence of highly activated microglia. For this purpose, the expression of the macrophage marker F4/80 and the monocytic marker Ly6C were evaluated in the $CD11b^+/CD45^{low/int}$ and $CD11b^+/CD45^{high}$ cell populations (Suppl. Fig. 6).

In NL animals, the $CD11b^+/CD45^{low/int}$ cell population in GFAP-IL6Tg animals had a higher number of $F4/80^+$ cells, but not $Ly6C^+$ cells compared to WT (Suppl. Fig. 11E). On the other hand, the $CD11b^+/CD45^{high}$ cell population showed an increased number of cells expressing F4/80 (2.69 ± 2.36 vs. 56.44 ± 32.48 number of cells, WT/NL vs. Tg/NL, p = 0.046) and Ly6C (1.54 ± 0.69 vs. 5.07 ± 2.30 number of cells, WT/NL vs. Tg/NL, p = 0.026) in transgenic animals than WT (Suppl. Fig. 11F and G).

After PPT, in WT animals, no statistically significant differences in the number of $F4/80^+$ and $Ly6C^+$ cells were found after PPT in comparison with the corresponding NL controls. However, in GFAP-IL6Tg animals, the number of $Ly6C^+$ cells increased a 3 dpl within the $CD11b^+/CD45^{high}$ cell population (Suppl. Fig. 6C). Comparisons between genotypes revealed no significant variations in the number of either $F4/80^+$ or $Ly6C^+$ cells within the $CD11b^+/CD45^{low/int}$ cell population (Suppl. Fig. 6A and C). However, a greater number of $F4/80^+$ cells in the $CD11b^+/CD45^{high}$ cell population was found at 3 and 7dpl in GFAP-IL6Tg animals (Suppl. Fig. 6A).

Furthermore, analysis of the levels of F4/80, calculated using the mean fluorescence intensity, demonstrated a higher F4/80 in the $CD11b^+/CD45^{high}$ cell population of GFAP-IL6Tg animals in both NL and at 7 dpl (Suppl. Fig. 6B). However, in the $CD11b^+/CD45^{high}$ cell population, the levels of Ly6C in NL transgenic animals were less than WT (4273 ± 148.1 vs. 2144 ± 523.9 mean fluorescence, WT/NL vs. Tg/NL, p = 0.0001) (Suppl. Fig. 6D).

Astrocyte-targeted IL-6 production modifies the phenotype of $CD11b^+/CD45^{high}$ cell population

In order to investigate the putative changes that transgenic IL-6 production may exert on the phenotype of the microglia and macrophage cell populations, the expression of different cell activation markers mostly related to antigen presentation, including MHCII, CD80, CD86, ICOSL, and CD11c, in both $CD11b^+/CD45^{low/int}$ and $CD11b^+/CD45^{high}$ populations was studied by flow cytometry (Fig. 3 and Suppl. Figs. 9 and 12).

In NL animals, in both WT and GFAP-IL6Tg animals, a small population of $CD11b^+/CD45^{low/int}$ cells expressed MHCII (WT: 1.2 ± 0.6%; Tg: 3.3 ± 0.7%) and ICOSL (WT: 0.22 ± 0.1%; Tg: 0.1 ± 0.08%) (Fig. 3a and Suppl. Fig. 9A), whereas the number increased in the $CD11b^+/CD45^{high}$ population (WT: 53.5 ± 9.4%; Tg: 53.23 ± 6%) (WT: 34.8 ± 5.4%; Tg: 22.4 ± 0.7%) (Fig. 3a and Suppl. Fig. 9B).

The number of cells expressing $MHCII^+$ in both populations was always significantly higher in NL GFAP-IL6Tg animals than in NL WT (Fig. 3a and Suppl. Fig. 11H-I). In the case of the ICOSL population, NL GFAP-IL6Tg animals only showed a significant increase in the $CD11b^+/CD45^{high}$ population compared with WT (Suppl. Fig. 11J).

After PPT, an increase in the number of both $CD11b^+/CD45^{low/int}/MHCII^+$ and $CD11b^+/CD45^{high}/MHCII^+$ population was only observed in GFAP-IL6Tg animals (Fig. 3a). Moreover, in GFAP-IL6Tg animals,

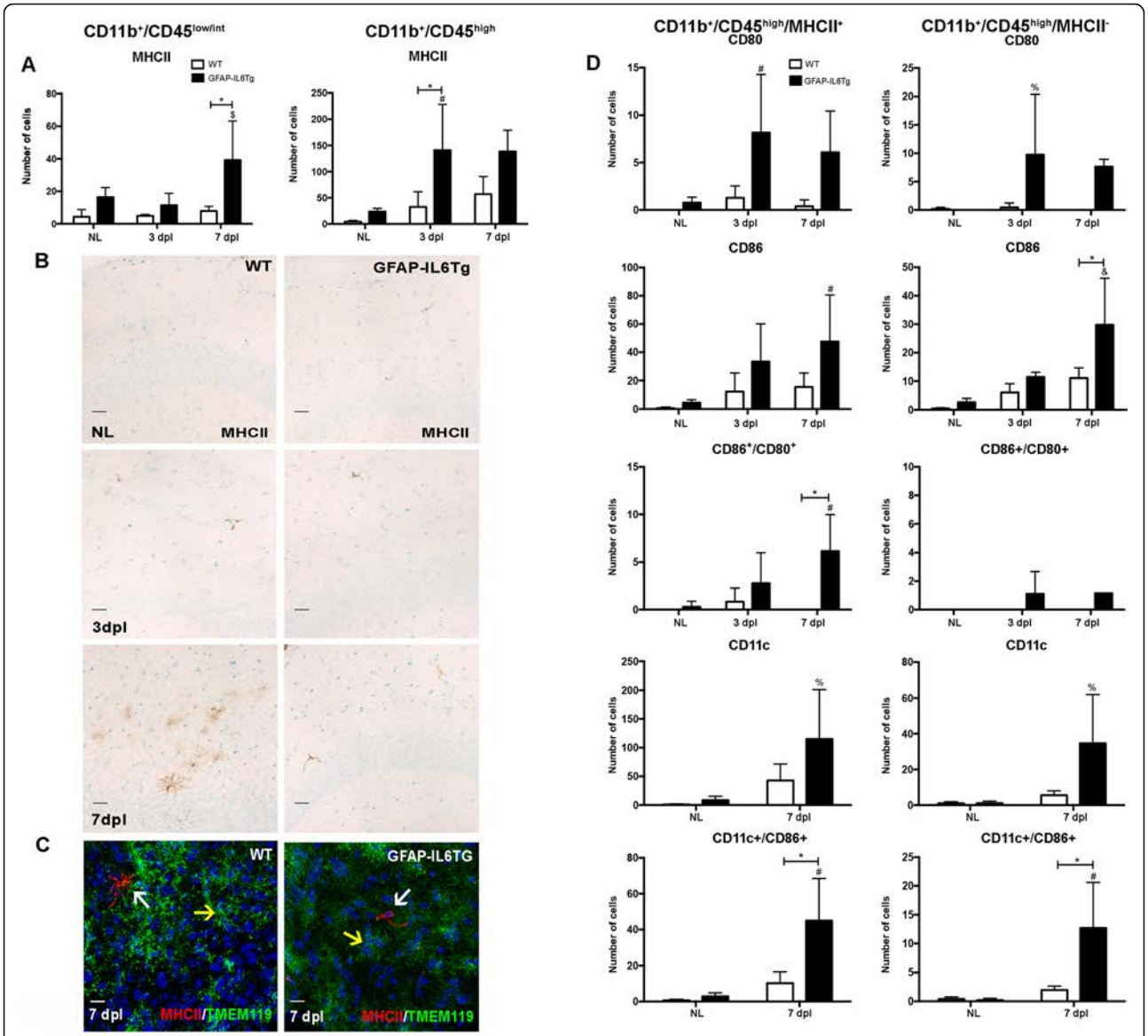

Fig. 3 Phenotypic analysis of microglia and macrophage populations. **a** Graphs showing the number of MHCII$^+$ cells in the CD11b$^+$/CD45$^{low/int}$ and CD11b$^+$/CD45^{high} cell population. **b** Representative images from WT and GFAP-IL6Tg mice showing MHCII staining in the ML of the DG in NL and PPT-lesioned hippocampus from 3 to 7 dpl. Scale bar = 20 μm. **c** Representative images, from WT and GFAP-IL6Tg mice, of double IHC combining MHCII (red) and Tmem119 (green) at 7 dpl. White arrows indicate MHCII$^+$/Tmem119$^-$ cells and yellow arrow indicate microglia Tmem119$^+$ Scale bar = 5 μm. **d** Graphs showing the number of CD80$^+$, CD86$^+$, and CD11c$^+$ cells in the CD11b$^+$/CD45^{high}/MHCII$^+$ and CD11b$^+$/CD45^{high}/MHCII$^-$ cell populations. A minimum of three WT and three GFAP-IL6Tg animals per group were used for this study. Data are represented as mean ± SD. The significances are represented as #$p \leq 0.05$ vs NL of respective group; %$p \leq 0.1$ vs. NL of respective group; &$p \leq 0.001$ vs. NL of respective group and \$$p \leq 0.05$ vs. 3dpl of respective group. Significant differences between genotypes are represented as *$p \leq 0.05$

the number of ICOSL$^+$ cells increased at 7 dpl within the CD11b$^+$/CD45$^{low/int}$ and CD11b$^+$/CD45^{high} population, whereas in WT no changes were observed (Suppl. Fig. 9A-B).

Using MHCII immunostaining, MHCII$^+$ cells in the ML of the DG were morphologically identified as perivascular cells in both WT and transgenic animals in NL and after PPT (Fig. 3b). These cells had an elongated morphology and stained with CD206 a marker commonly used to identify perivascular macrophages (Suppl. Fig. 8A). Furthermore, using double immunofluorescence with laminin, the location of these MHCII$^+$ cells in the perivascular space was established (Suppl. Fig. 8B). Noticeably, at 7 dpl, we observed a subpopulation of MHCII$^+$/Tmem119$^-$

ramified microglia in the parenchyma of WT animals but not in GFAP-IL6Tg mice (Fig. 3c).

Taking into account that the major differences observed in terms of MHCII was in the CD11b/CD45^{high} population, we focused on the study of the co-expression of CD80, CD86, and CD11c with MHCII only in this population (Fig. 3d). In NL conditions, in contrast to WT animals in which these populations were not detected, a small population of CD80$^+$ cells (3 ± 1.1%) and a higher number of CD86$^+$ cells (16.3 ± 4.8%) was observed within the CD11b$^+$/CD45^{high}/MHCII$^+$ population in GFAP-IL6Tg animals. In addition, a population of CD11b$^+$/CD45^{high}/MHCII$^-$/CD86$^+$ was found in NL transgenic animals (Fig. 3d).

In GFAP-IL6Tg animals, it was observed an increase of cells expressing CD80 or CD86 (Fig. 3d), either with or without MHCII. However, the number of cells co-expressing CD80 and CD86 only increased within the CD11b$^+$/CD45^{high}/MHCII$^+$ population. Furthermore, populations of MHCII$^+$/CD11c$^+$ and MHCII$^-$/CD11c$^+$ cells, with or without CD86, were observed at 7 dpl in WT (Fig. 3d). Moreover, the number of CD11c$^+$/CD86$^+$ cells either with or without MHCII was always higher in GFAP-IL6Tg mice than in WT (Fig. 3d).

As mentioned above, no CD80$^+$, CD86$^+$, and cells co-expressing both markers were observed in the CD11b$^+$/CD45$^{low/int}$/MHCII$^+$ population at any time-point analyzed in any genotype (data not shown).

Astrocyte-targeted IL-6 production promotes T cell infiltration after PPT

Another aspect was whether transgenic production of IL-6 was able to modify the infiltration and/or differentiation of T-cells after PPT.

In order to study the dynamics of the lymphocyte populations, the number of CD4$^+$ and CD8$^+$ cells within the gated CD3$^+$ T cell population was analyzed in the entire ipsilateral hippocampus by flow cytometry, in NL and in PPT-lesioned WT and GFAP-IL6Tg mice at 7dpl (Fig. 4a and b).

In comparison with NL WT, NL GFAP-IL6Tg animals showed a higher number of CD4$^+$ T cells (20.44 ± 6.25 vs. 92.27 ± 43.29 number of cells, WT/NL vs. Tg/NL, p = 0.046), CD8$^+$ T cells (29.62 ± 1.63 vs. 294.9 ± 139.9 number of cells, WT/NL vs. Tg/NL, p = 0.031), and CD3$^+$/CD4$^-$/CD8$^-$ cells (8.73 ± 1.59 vs. 15.34 ± 4.27 number of cells, WT/NL vs. Tg/NL, p = 0.07) but similar numbers of CD3$^+$/CD4$^+$/CD8$^+$ cells (Fig. 4b and Suppl. Fig. 11K and L).

After PPT, at 7 dpl, both experimental groups showed an increase in CD3$^+$/CD4$^-$/CD8$^-$ T cells, whereas in the CD3$^+$/CD4$^+$/CD8$^+$ population, only GFAP-IL6Tg animals showed an increase, and in the CD3$^+$/CD4$^+$ population was only observed in WT animals (Fig. 4b). No significant difference was found in any T cell population between WT and GFAP-IL6Tg mice (Fig. 4b).

Finally, the different subtypes of CD4$^+$ T-helper lymphocytes were also determined by flow cytometry using antibodies against lineage-specific transcription factors (Fig. 4d). After gating in the CD3$^+$CD4$^+$ T-helper cell population, the number of Tbet$^+$ (for Th1), Gata 3$^+$ (for Th2), RORγ$^+$ (for Th17) and Foxp3$^+$ (for T-regulatory) cells was analyzed (Fig. 4c). In both NL conditions and after PPT, no significant differences in the number of Th-cell infiltration between the two genotypes were found (Fig. 4d).

The possible changes in the distribution and the pattern of recruitment of T cell population, in the ML of the DG, were analyzed using sections immunostained for CD3 (a pan T cell marker) of NL and in PPT-lesioned WT and GFAP-IL6Tg animals (Fig. 4f). In NL conditions, a higher number of CD3$^+$ cells was detected in GFAP-IL6Tg animals (Suppl. Fig. 11M). After PPT, WT animals showed two waves of T cell infiltration, the first at 2 dpl and the second at 7 dpl. In GFAP-IL6Tg mice, we only detected an increase in lymphocytes at 7 dpl. Moreover, in both genotypes, the CD3$^+$ cells were observed randomly distributed through the ML of the DG and the hilus (Fig. 4f). From 7 to 14dpl, the numbers of these cells did not change in either WT or GFAP-IL6Tg mice (Fig. 4e).

Absence of T cell co-stimulatory molecules after PPT

In order to investigate the putative changes that transgenic IL-6 production may exert on the communication between T cells and microglia/macrophages, we analyzed CTLA-4 and CD28, two identified ligands for CD80 and CD86, in PPT-lesioned WT and transgenic mice at 7dpl. Our results showed no detectable CTLA-4 and CD28 in either WT or GFAP-IL6Tg mice at any time-point studied (data not shown).

Astrocyte-targeted IL-6 production induces alterations in the cytokine/chemokine microenvironment after PPT

We also addressed whether the changes observed in transgenic animals correlated with variations in various cytokines involved in microglial cell activation and T cell differentiation, including pro-inflammatory cytokines such as IL-2, IL-6, IFN-γ, IL-1β, IL-12p70, and IL-17; anti-inflammatory cytokines such as IL-10, IL-13, IL-9, IL-5, and IL-4; and chemokines, related with leukocyte recruitment, like CXCL10 and CCL2 (Suppl. Fig. 10).

In NL conditions, when only animals of the two genotypes are compared, significant differences were observed in the presence of the pro-inflammatory cytokines IL-6 and IL-17 and the anti-inflammatory cytokines IL-10 and IL-13 in the nervous parenchyma (Suppl. Fig. 11N-Q). In contrast, no modifications of IL-

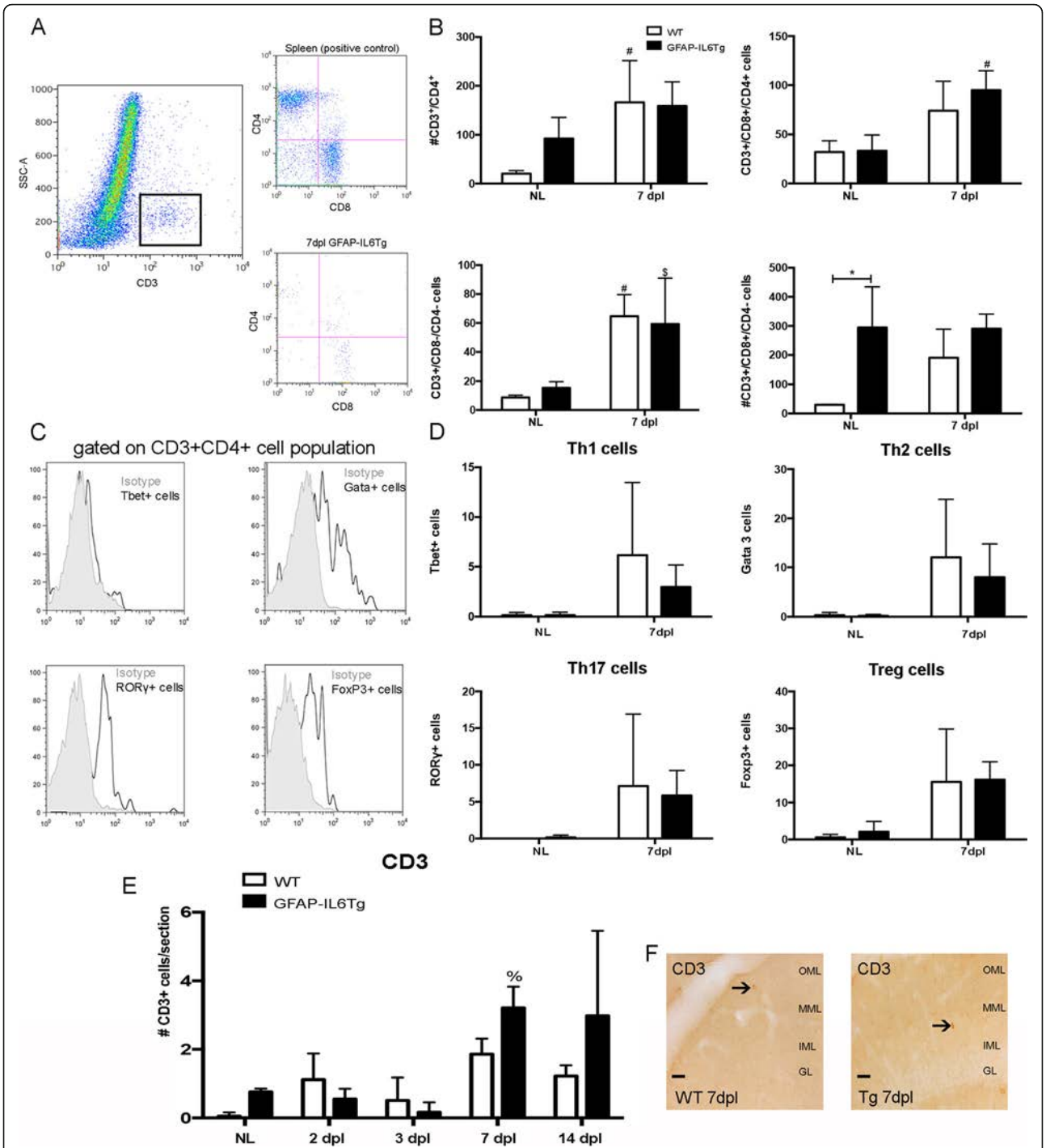

Fig. 4 T cell infiltration after PPT. **a** Representative dot plot of SSC/CD3 expression of cells obtained from the lesioned WT animals. The square delimits the $CD3^+$ cell population used in this study. Representative dot plot of CD3/CD4/CD8 cells obtained from the spleen, positive control (top), and hippocampus (bottom) of lesioned WT. **b** Graphs showing the number of $CD4^+$, $CD3^+/CD4^+/CD8^+$ cells, $CD8^+$ and $CD3^+/CD4^-/CD8^-$ in NL and at 7dpl. **c** Representative histogram-plot showing the expression of Tbet, Gata3, RORgt, and Foxp3 in the population of $CD3^+$Th-cells in comparison to the corresponding isotype control, in which the positive staining was defined. **d** Graphs showing the number of the different subtypes of $CD4^+$ T-helper lymphocytes: $Tbet^+$, Gata 3^+, $RORg^+$, and $Foxp3^+$ in NL and at 7dpl. **e** Graph showing the quantification of $CD3^+$ immunostaining cells in non-lesioned (NL) and PPT-lesioned hippocampus from 2 to 14 dpl, in WT and GFAP-IL6Tg mice. **f** Representative images showing CD3 immunostaining in WT and GFAP-IL6Tg mice at 7 dpl. Scale bar = 20 μm. A minimum of four WT and four GFAP-IL6Tg animals per group were used for this study. Data are represented as mean ± SD. The significances are represented as #$p \leq 0.05$ vs. NL of respective group; \$$p \leq 0.1$ vs. NL of respective group and %$p \leq 0.05$ vs. 3dpl of respective group. Significant differences between genotypes are represented as *$p \leq 0.05$

6 levels in the serum were found in transgenic animals (Suppl. Fig. 10N).

After PPT, WT animals only showed induction of the CXCL10 and CCL2 chemokines, while no induction was detected in any of the cytokines studied at the different time-points analyzed (Suppl. Fig. 10L and M).

PPT-lesioned GFAP-IL6Tg animals showed, in relation to the WT, differences in the levels of pro-inflammatory and anti-inflammatory cytokines as well as in chemokines. In concordance with the transgene expression, the cytokine with the greatest difference was IL-6, which was at significantly higher levels at 3 and 7 dpl. In the case of pro-inflammatory cytokines, transgenic animals had significantly higher IL-1β at 3dpl (Suppl. Fig. 10D), but lower IFN-γ and IL-12p70 at 14dpl (Suppl. Fig. 10C and E). In the case of anti-inflammatory cytokines, GFAP-IL6Tg animals showed higher levels of IL-10 than WT at 7 dpl but had a significant decrease at 14dpl (Suppl. Fig. 10G). Finally, the GFAP-IL6Tg mice had a significant increase in the chemokines CXCL10 and CCL2 at 3dpl that decreased significantly at 7 and 14dpl. Levels of these chemokines were higher in transgenic animals than WT at 3dpl (Suppl. Fig. 10L and M).

Astrocyte-targeted IL-6 production reduces collateral sprouting after PPT

Finally, it was explored whether the modifications detected in the population of microglia/macrophages, as well as in the infiltration of immune cells in GFAP-IL6Tg animals, affects the collateral sprouting after perforant path sectioning. Sprouting evaluation was done at later time points (14 and 21dpl) using the selenium-silver staining technique, which reveals glutamatergic zinc-rich buttons as in the hippocampal mossy fibers (Fig. 5) and other telencephalic pathways.

In NL animals, WT and GFAP-IL6Tg, large labeled buttons were densely packed in the hilus of the dentate gyrus and only few crossed the granular layer and reached the inner third of the molecular layer. After PPT, at 21 dpl, WT animals showed an increase in the area occupied by large, labeled buttons in the ML, indicative of sprouting, whereas in GFAP-IL6Tg animals, the increase was detected

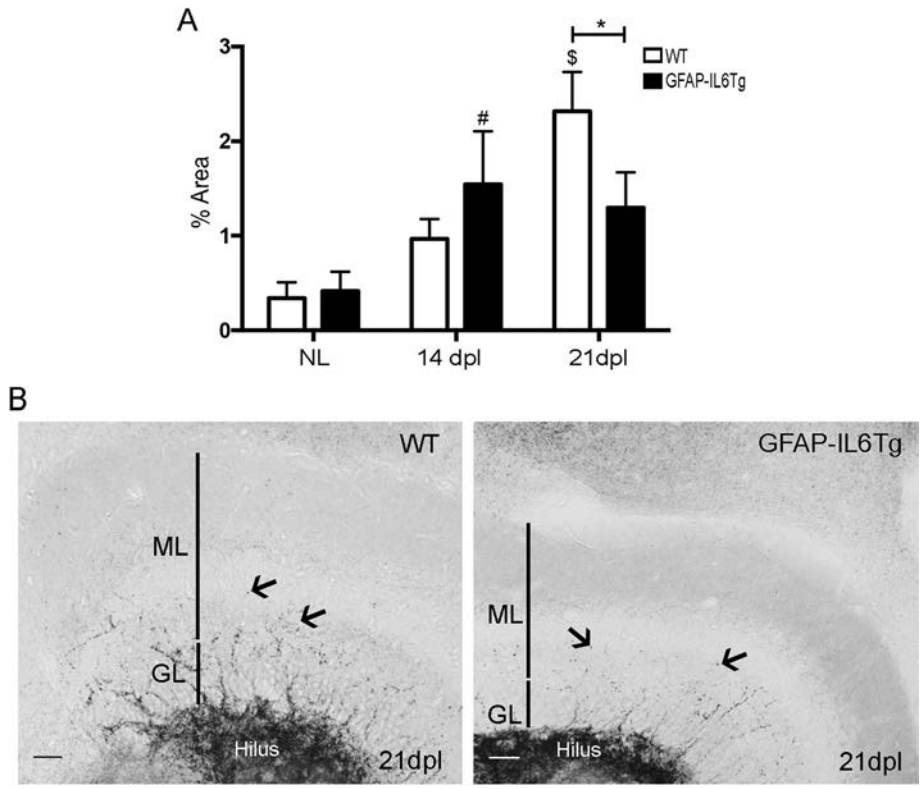

Fig. 5 Collateral sprouting. **a** Graph showing the time course of the selenium-silver staining for zinc (arrows) expressed as proportion of occupied area. Note that GFAP-IL6Tg animals showed a reduction of $Zinc^{+}$ staining at 21dpl. **b** Representative images from WT and GFAP-IL6Tg mice, at 21 dpl, showing staining in the ML of the DG (GL indicates granular layer). Scale bar = 20 μm. At least three WT and five GFAP-IL6Tg animals (NL animals and at 14 and 21dpl) were analyzed. A total of 24 photographs from 8 different hippocampal sections per animal were quantified. Data are represented as mean ± SD. The significances are represented as: #$p \leq 0.05$ vs. NL of respective group and \$$p \leq 0.01$ vs. NL of respective group. Significant differences between genotypes are represented as: *$p \leq 0.05$

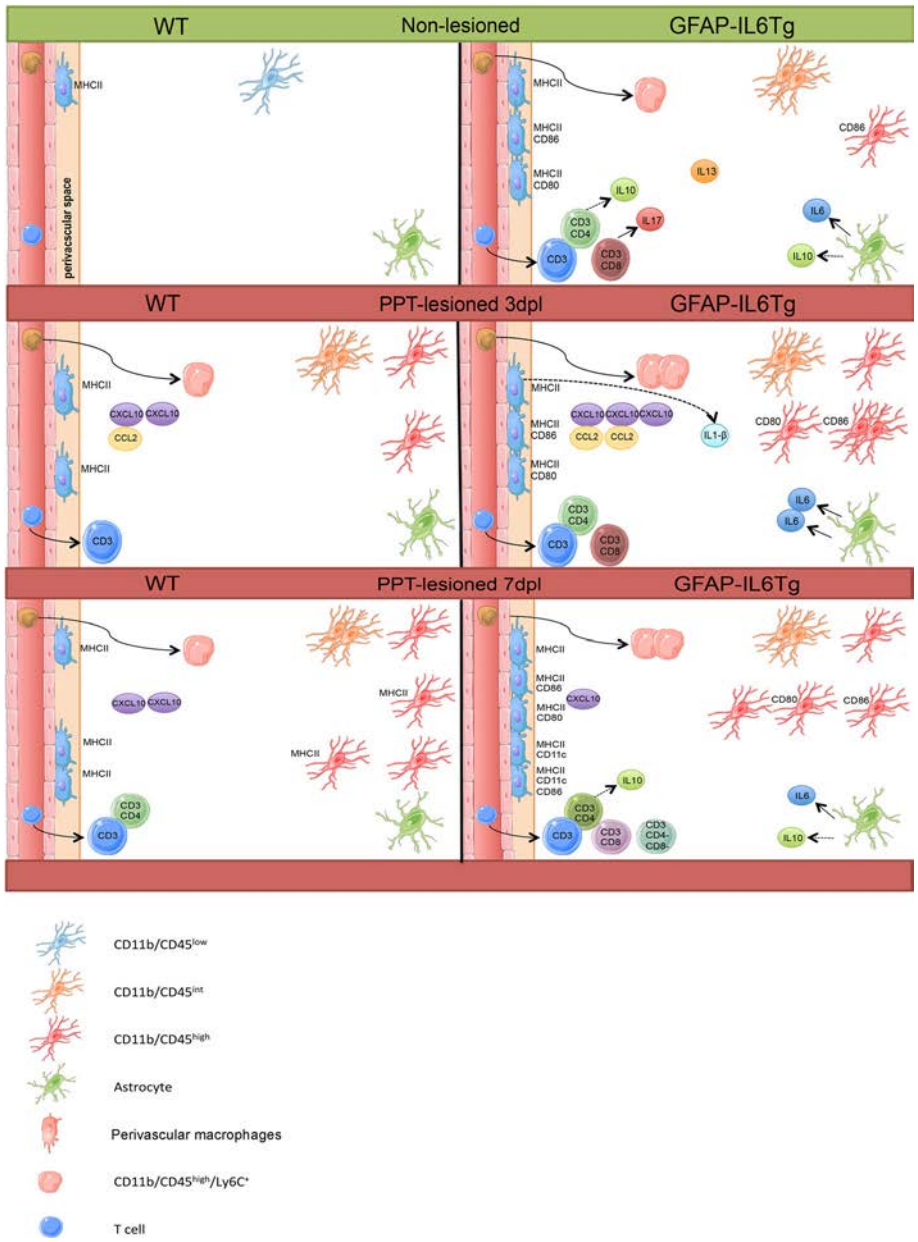

Fig. 6 Summary figure. Schematic representation of the main changes observed in the non-lesioned (NL) (green) and PPT-lesioned hippocampus (red) in both WT and GFAP-IL6Tg animals

at 14 dpl (Fig. 5a). Consequently, at 21 dpl, transgenic animals showed significantly less labeled buttons in the ML compared with WT animals (2.32 ± 0.41 vs. 1.29 ± 0.36% area, WT/21dpl vs. Tg/21dpl, $p = 0.049$) (Fig. 5b and c).

Discussion

The present study demonstrates that astrocyte-targeted IL-6 production causes significant alterations in the phenotype and density of the microglia/macrophage populations in the hippocampus of NL and PPT-lesioned animals. Moreover, an increase in the infiltration of $CD11b^+/CD45^{high}/F4/80^+$ and $CD11b^+/CD45^{high}/Ly6C^+$ monocytes and T lymphocytes were found in GFAP-IL6Tg mice. All these changes are linked to significant modifications in the cytokine/chemokine microenvironment and had a deleterious effect on axonal sprouting.

Astrocyte-targeted production of IL-6 induces alterations in the microglia/macrophage, lymphocyte, and cytokine/chemokine microenvironment

The first interesting result of this study is that the chronic production of IL-6 increased the number of microglia/

macrophages and modified their phenotype in homeostasis. Thus, 2.5 times more $CD11b^+/CD45^{low/int}$ and $CD11b^+/CD45^{high}$ cells were found. Although this increased number might reflect a higher infiltration of monocytes, the number of $CD11b^+/CD45^{high}/F4/80^+$ and $CD11b^+/CD45^{high}/Ly6C^+$ monocytes detected was not enough to explain the increase of microglia/macrophages in transgenic animals. In this regard, unpublished observations from our laboratory, demonstrated a higher number of microglia/macrophages during brain development in GFAP-IL6Tg mice, raising the possibility that the differences found in the number of cells in the adult would be linked to modifications from the post-natal period.

Regarding the phenotype of the microglia/macrophages, our study revealed that IL-6 promotes the activation of the microglial/macrophage cell population towards a more reactive macrophage-like cell, with higher expression of CD45 and F4/80 and a lower Ly6C. This low level of Ly6C could be interpreted as a stabilization of the entrance of these monocytes, whose levels decreased once in the parenchyma [38]. In concordance, IL-6 has been described as a potent activator of microglia/macrophage cells both in vitro and in vivo [15, 17, 21, 57, 91]. Also, astrocyte-targeted production of IL-6 induces an increase in the number of $CD11b^+/CD45^{high}/MHCII^+$ cells and in cells expressing co-stimulatory molecules, including ICOSL, CD80 and CD86, suggesting a putative transformation into competent antigen presenting cells. Importantly, $MHCII^+$ cells corresponded exclusively to perivascular macrophages and not parenchymal microglia, highlighting a necessity to study in more detail the role of these macrophages under homeostatic situations.

In agreement with previous studies describing increased basal lymphocyte infiltration in specific areas of the CNS of GFAP-IL6Tg mice [17, 18], we observed an increase in the number of T cells infiltrating the molecular layer of the DG in transgenic animals. The increase was due to the presence of $CD4^+$ T-helper, $CD8^+$ T-cytotoxic, and $CD3^+CD4^-CD8^-$ γδ T cells. Studies in vitro have demonstrated the ability of IL-6 to induce a unique non-classical effector $CD8^+$T cell subpopulation, called Tc17, characterized by a high production of IL-17 [69], and whose primary function is to contribute to inflammation and the recruitment of lymphocytes and myeloid cells [39]. In concordance, we found elevated IL-17 in NL GFAP-IL6Tg animals.

IL-6-induced modifications in the microglia/macrophage population and T cell infiltration were linked to a specific cytokine/chemokine profile, characterized by higher IL-6, IL-17, IL-13, and IL-10 production. As expected, major differences between WT and GFAP-IL6Tg animals were found for IL-6, which showed around a 5-fold increase in the GFAP-IL6Tg animals. As already commented, the upregulation of the pro-inflammatory cytokine IL-17 could be related with a higher number of $CD8^+$ T cells and γδ T cells, one of the two cell-types that could produce this cytokine in the CNS [69, 93] and could be linked to alterations in the blood-brain barrier (BBB) [50], a well-described feature of these transgenic mice [14, 19] and the higher activation phenotype of microglia observed in basal conditions. Moreover, an effect of IL-17 on the upregulation of microglial activation has been reported, especially in demyelinating and autoimmune diseases [53, 96] coinciding with the higher activation profile observed in our transgenic animals in basal conditions. On the other hand, the higher levels of the classical anti-inflammatory cytokines IL-10 and IL-13 may be related to the increased number of perivascular macrophages and/or $CD8^+$ T cells, two cell-type with the capacity to produce IL-10 [60, 63].

Increased microglia/macrophage in GFAP-IL6Tg mice after PPT might be due to both proliferation and recruitment of bone-marrow derived monocytes

In agreement with previous studies in mice [29, 31, 43, 58, 66, 94], we found a progressive increase in the number of microglia/macrophages as well as an increase in Iba1 expression along with the progression of PPT in the molecular layer of the DG in both genotypes. However, in our study, the density of microglia/macrophages was higher in transgenic animals than in WT. This difference could be related to three changes after PPT: microglial proliferation; infiltration of blood-derived monocytes [5, 7, 59, 95], which transformed into microglial/macrophage cells [52]; and of microglial cells from adjacent non-deafferented areas, such as the CA1, the IML, and the hilus [29, 52, 59, 95].

Our results clearly showed an increase in the number of proliferating $pH3^+$ cells, as well as in the total number of mitotic microglial cells ($BrdU^+$), in GFAP-IL6Tg animals. This result was associated with an increase of IL-6, a potent inducer of microglial proliferation [56, 62, 80, 87]. Beyond proliferation, the recruitment of blood-derived monocytes paralleled this increase of microglia/macrophages in the transgenic mice. Thus, a higher number of $CD11b^+/CD45^{high}$ cells containing a high number of $F4/80^+$ cells and $Ly6C^+$ cells, widely used markers for monocyte/macrophages [49], was observed. As we will comment later, this greater presence of monocytes/macrophages correlated with the increased CCL2 production observed in GFAP-IL6Tg mice, a key chemokine involved in the leukocyte migration in the PPT-model [5], suggesting that not only proliferation but also infiltration is involved in the microglia/macrophages increase.

Another question is why the increased number of microglia/macrophages in PPT-lesioned transgenic animals remained at later time-points. One possibility is that the effects of chronic IL-6 production were related to the prevention of microglial/macrophage cell number

restoration, by affecting either microglial cell death or monocyte exit from the CNS or even both. However, in concordance with previous studies [8, 78], we could not find any conclusive evidence of increased microglia/macrophage death, as we were not able to detect any evidence of apoptosis, monitored by active caspase-3 and TUNEL, at any time-point analyzed in any genotype.

After PPT, astrocyte-targeted production of IL-6 promoted a shift in the phenotype of CD11b$^+$/CD45^{high} cells and avoided the transformation of any parenchymal microglia into putative MHCII$^+$ antigen presenting cells

Phenotypically, we demonstrated that, after PPT, part of the activated microglia/macrophage population in WT animals, expressed CD11c, MHCII, CD86, and ICOSL, molecules commonly associated with an antigen-presenting cell phenotype. These results are in agreement with already published papers reporting the expression of MHCII and CD86, but a lack of CD80 in microglia/macrophages after PPT [9]. The phenotype observed in lesioned GFAP-IL6Tg animals was similar to the reported in lesioned WT animals, and only a slight increase in the number of MHCII$^+$/CD80$^+$ and MHCII$^+$/CD86$^+$ cells at 7dpl and in the number of and MHCII$^-$/CD86$^+$ cells at 3 dpl were found in the CD11b$^+$/CD45^{high} cell population of transgenic mice. Nevertheless, when we investigated the cells responsible for the expression of these molecules using immunohistochemistry, in the molecular layer of the DG, we found major differences between WT and GFAP-IL6Tg mice. In WT animals, in addition to perivascular macrophages, activated ramified microglia in the parenchyma expressed MHCII and CD11c and thus were equipped to engage an adaptive immune response. However, in GFAP-IL6Tg animals, microglia did not express MHCII or CD11c; this property is restricted to perivascular macrophages, suggesting that IL6-induced microglia are inadequate to act as antigen presenting cells and thus to drive an adaptive immune response, despite the higher presence of MHCII$^+$ and CD11c$^+$ cells. This reduction of MHCII observed in microglia might be explained by the higher expression of IL-10 observed at this same time-point in GFAP-IL6Tg mice and the ability of this cytokine to reduce MHCII on macrophages [68, 78].

In the present study, in both genotypes, all MHCII$^+$ cells were TMEM119$^-$, described as a specific marker of microglia that discriminates from blood-derived macrophages in the human brain [81]. However, several studies revealed that in homeostatic conditions, microglia express high levels of TMEM119, while in neurodegeneration disorders microglial cells show a great reduction [82]. In contrast, myeloid cells recruited into the lesions in the course of brain inflammation in rodents and humans do not express TMEM119. However, a recent study has been described that the regulation of microglial TMEM119 in MS is dependent on their inflammatory environment [92]. In this regard, the lack of expression of TMEM119 in MHCII$^+$ cells does not provide evidence if these cells were resident microglia or infiltrated macrophages. Similarly, expression of P2Y12R, another marker commonly used to discriminate between macrophages and microglia, by its stable expression in microglia, was downregulated in our PPT-model [65] making not possible to use it for this purpose.

Another interesting result was the observation of a population of cells within the CD11b$^+$/CD45^{high} population expressing CD86 and CD80 without MHCII in both WT and GFAP-IL6Tg mice. Noticeably, these populations were observed in transgenic animals already in homeostatic situations. This cellular phenotype has been associated with peripheral innate immune responses [74], and makes us hypothesize that transgenic animals presented a "primed microglia" with a desensitized profile in NL conditions, as suggested by other authors [72], and retained microglial activation in an innate immune phenotype after lesion.

Astrocyte-targeted production of IL-6 increased lymphocyte recruitment after PPT without modifying their differentiation

Two different waves of T cell infiltration have been described in the PPT paradigm, the first wave at early time-points (2–3 dpl) and the second, later on, at 7 dpl [5, 6]. Our results showed that, in contrast to WT, GFAP-IL6Tg mice presented an increase in T cell infiltration in the molecular layer only at 7dpl, coinciding with the role attributed to IL-6 as a T cell recruitment molecule in peritoneal inflammation and in CNS-lesion models [3, 67] and a massive decrease in the recruitment of T cells after facial nerve injury in IL-6-deficient mice [36]. In most of these studies, the effects of IL-6 on lymphocyte recruitment have been related to alterations in the production of adhesion molecules and/or chemokines, including CXCL10 and CCL4, among others [67]. In the present study, we observed that after PPT GFAP-IL6Tg animals had elevated levels of CXCL10 and CCL2, two crucial chemoattractant proteins for both lymphocytes and monocytes in this paradigm [5], indicating that IL-6 may be promoting the infiltration of T cells by modifying the chemokine microenvironment.

Taking into consideration the role of IL-6 to drive lymphocyte differentiation, we analyzed the phenotype of infiltrated T cells in the PPT-lesioned hippocampus in more detail, quantifying the number of both CD8$^+$ T-

cytotoxic and $CD4^+$ T-helper lymphocytes, as well as the different subtypes of T-helper cells. Until now, the specific subtypes of T lymphocytes infiltrating the parenchyma of the deafferented hippocampus in the PPT-paradigm were not characterized and to our knowledge, our study is the first to demonstrate the presence of a small population of the four subtypes of T-helper lymphocytes, Th1 ($Tbet^+$), Th2 ($GATA3^+$), Th17 ($RORg^+$), and Treg ($Foxp3^+$), in the PPT-lesioned hippocampus. No differences between WT and GFAP-IL6Tg animals were found in any T-helper populations analyzed or its expression of co-stimulatory molecules, suggesting that the increased number of lymphocytes found in GFAP-IL6Tg animals might be caused by the increased expression of CXCL10 and CCL2 rather than by specific action of IL-6 on T cell differentiation in this paradigm.

Astrocyte-targeted production of IL-6 promoted alterations in the cytokine/chemokine profile associated with PPT

Astrocyte-targeted production of IL-6 markedly altered the cytokine/chemokine profile not only in the unlesioned state, as already discussed (see the first section of this discussion) but also after PPT-lesion. As expected, major differences between WT and GFAP-IL6Tg animals were found for IL-6, which showed around a 5-fold increase in the GFAP-IL6Tg animals in both unlesioned hippocampus and at early time-points after PPT. In addition to modifications in chemokines involved in the recruitment of macrophages and T cells, such as CXCL10 and CCL2, transgenic mice showed disturbances in the cytokine profile that may drive the type of the immune response. In this sense, astrocyte-targeted IL-6 production resulted in increased levels at early time-points (3 dpl) of IL-1β, cytokine more related with innate immune responses [28, 47, 63, 70, 88, 93]. Remarkably, cytokines like IL-17 and IL-13, whose levels we would expect to see increased given their upregulation in basal conditions, remained unaltered in lesioned animals. This fact suggests they are not crucial to the evolution of the PPT lesion and could explain the lack of differences in the shift of T lymphocyte subtypes observed between WT and GFAP-IL6Tg mice.

Astrocyte-targeted production of IL-6 reduced axonal sprouting

Finally, we analyzed whether the modification of the immune response observed in GFAP-IL6Tg mice had any effect on the axonal sprouting of the remaining unlesioned axons of mossy cells, which typically occurs in the deafferented areas after PPT and is used as a marker of lesion outcome at later time-points [4, 25, 27, 33]. Our results indicated that GFAP-IL6Tg animals had lower axonal sprouting at 21 dpl than WT. Although in vitro IL-6 has a beneficial effect on axonal sprouting [44], in vivo our results showed a deleterious effect.

One putative explanation for the decreased axonal sprouting observed in transgenic mice may lie in the distinct cytokine/chemokine microenvironment observed. As we already commented, the molecules observed in WT animals are more related to the acquired immune response [9], whereas in GFAP-IL6Tg, the environment generated was more associated with a pro-inflammatory profile characteristic of the innate immune response.

Also, it is possible that some of the altered cytokines, and especially IL-6, act on the cells directly responsible for this axonal sprouting phenomenon. Astrocytes are the brain cells linked to axonal sprouting, as they secrete proteoglycans, such as neurocan, tenascin-C, brevican, widely demonstrated with an inhibitory role of axonal sprouting after PPT [26, 42, 85, 90]. Moreover, pro-inflammatory environments especially containing cytokines like TNF-α and IL-1β have been linked to the upregulation of these inhibitory proteoglycans, and thus with the inhibition of axonal outgrowth [41, 85]. More studies analyzing the composition of the extracellular matrix associated with PPT in GFAP-IL6Tg animals are needed to confirm this hypothesis.

Taking into consideration all the results observed in NL GFAP-IL6Tg mice, together with the fact that the net change in microglial/macrophage cell activation after PPT was less pronounced in transgenic animals than in WT mice, lead as to speculate that IL-6 induced a "primed" microglia/macrophage phenotype. Accordingly, some of the features observed in the population of microglia/macrophages of transgenic mice are commonly linked to a primed state including higher expression of pro-inflammatory mediators as well as MHCII expression [75]. The first descriptions of primed microglia were done in the context of LPS-administration and after IL-1β treatment and identified primed microglia as an altered state that, among other features, presented an exaggerated response to inflammation. However, nowadays, this primed stated has been also described in physiological aging conditions and stress [37, 73] in relation to the development of chronic neurodegenerative diseases [76]. In fact, the concept of primed microglia has been revised and regarded as having an ongoing state of activation that may respond differently to a secondary stimulation [72]. Furthermore, the concept of microglial "innate immune memory" has been recently demonstrated, with an enhancement or suppression of a secondary insult, depending on the type, duration and intensity of the initial stimulus [72].

Conclusions

Altogether, we propose that chronic exposure to IL6 induced an environment characteristic of an innate immune response, with the presence of "primed" microglia/macrophages with a desensitized profile, infiltrating monocytes and T cells as well as increased in IL-6, IL-17, IL10, and IL-13. After PPT, in WT animals, the immune response is characterized by parenchymal microglia showing MHCII and co-stimulatory molecule phenotype. In contrast, the desensitized microglia in transgenic animals is not able to express molecules linked to antigenic presentation following the PPT. This generates a differential microglial phenotype with increased IL-1β that has a negative effect on the pro-regenerative environment and, maybe through action on astrocytes, reduce the axonal sprouting associated with PPT (see Fig. 6).

Supplementary Information

The online version contains supplementary material available at https://doi.org/10.1186/s12974-020-02063-1.

Additional file 1: Supplementary Fig. 1. Area selected for densitometry study. Representative image from WT mice showing Iba1$^+$ staining after perforant pathway transection. The selected area (black squares) represented the area analyzed for densitometry. Scale bar = 50μm.

Additional file 2: Supplementary Fig. 2. Toluidine blue staining. Representative images, from WT and GFAP-IL6Tg mice, showing toluidine blue staining in the ML of the DG in NL conditions and from 3 to 21 dpl after PPT. Scale bar = 20 μm.

Additional file 3: Supplementary Fig. 3. Morphological characterization of microglia. (A–D) Graphs showing the quantification of the area occupied by Iba1$^+$ labeled cells (A), (B) the elongation values (value equal to 1 indicates round morphology and high values increased elongation), (C) the sphericity values (value equal to 1 indicates index of sphericity) and (D) the shape factor (high values indicate round shape and low values ramified morphology), calculated for individual cells. The significances are represented as #p≤0.001 vs NL of respective group and &p≤0.05 vs 3dpl of respective group. Significant differences between genotypes are represented as *p≤0.05 and **p≤0.01.

Additional file 4: Supplementary Fig. 4. Microglial cell density. (A) Graph showing the quantification of Pu.1$^+$ cells in non-lesioned (NL) and lesioned animals from 2 to 21dpl after PPT, in WT and GFAP-IL6Tg animals. (B) Representative images from WT and GFAP-IL6Tg mice showing Pu.1$^+$ staining in the ML of the DG at 14 dpl. Note that transgenic mice showed an increased number of Pu.1$^+$ cells in NL and at 14 dpl. Scale bar = 20μm. (C and D) Graphs showing the fold changes increase of Pu.1$^+$ cells in WT (C) and GFAP-IL6Tg (D) in comparison to their corresponding NL animals. A minimum of three NL and three lesioned WT and GFAP-IL6Tg at 2, 3, 7, 14 and 21 dpl were analyzed. A total of 6 photographs from 3 different hippocampal sections per animal were used. Data are represented as mean ± SD. The significances are represented as #p≤0.01vs NL of respective group; &p≤0.05 and %p≤0.01 vs 2dpl of respective group and $$p$≤0.001 vs 7dpl of respective group. Significant differences between genotypes are represented as *p≤0.05.

Additional file 5: Supplementary Fig. 5. Microglia/macrophages populations. (A) Representative dot plot of CD11b/CD45 expression of cells obtained from the hippocampus of non-lesioned (NL) WT animals. The square delimits the CD11b$^+$/CD45$^+$ population of cells used in this study. Representative histogram where the populations of CD11b$^+$/CD45$^{low/int}$ (microglia) and CD11b$^+$/CD45^{high} (macrophages) were defined. (B) Graphs showing the number of cells and the mean fluorescence intensity in the CD11b$^+$/CD45$^{low/int}$ and CD11b$^+$/CD45^{high} populations in NL and PPT-lesioned animals. Graphs showing the mean fluorescence intensity of CD45 levels in the CD11b$^+$/CD45$^{low/int}$ and CD11b$^+$/CD45^{high} populations in NL and PPT-lesioned animals. (C) Representative images from WT and GFAP-IL6Tg mice showing CD45 staining in the GL and ML of the DG in NL and PPT-lesioned hippocampus at 3 and 7 dpl. Note that both CD45$^+$ ramified (arrowheads) and CD45$^+$ round cells (arrows) were observed in both genotypes. Scale bar = 20μm. A minimum of five WT and five GFAP-IL6Tg animals per group were used for this study. Scale bar = 50μm. Data are represented as mean ± SD. The significances are represented as &p≤0.01vs NL of respective group; #p≤0.05 vs NL of respective group and $$p$≤0.001vs NL of respective group. Significant differences between genotypes are represented as *p≤0.05 and **p≤0.01.

Additional file 6: Supplementary Fig. 6. Monocyte infiltration. (A-B) Graphs showing the number of cells expressing the F4/80 and the mean fluorescence. (C-D) Graphs showing the number of cells expressing the monocyte-related marker Ly6C and the mean fluorescence. A minimum of five WT and five GFAP-IL6Tg animals per group were used for this study. Data are represented as mean ± SD. The significances are represented as #p≤0.05 vs NL of respective group. Significant differences between genotypes are represented as *p≤0.05, **p≤0.01 and ****p≤0.0001.

Additional file 7: Supplementary Fig. 7. Percentages of microglia/macrophage population in NL and after PPT. Representative graph showing the percentage of CD11b$^+$/CD45$^{low/int}$ (dark grey) and CD11b$^+$/CD45^{high} (light grey) population in both WT and GFAP-IL6Tg animals in NL conditions and after PPT.

Additional file 8: Supplementary Fig. 8. CD206 and Laminin expression after PPT. (A) Representative images from WT and GFAP-IL6Tg mice showing CD206 staining in the ML of the DG at 7 dpl. Black arrows indicate CD206$^+$ cells. Scale bar = 20μm. (B) Representative images, from WT and GFAP-IL6Tg mice, of double IHC combining MHCII (red) and Laminin (green) at 7 dpl. White arrows indicate MHCII$^+$ cells in the perivascular space. Scale bar = 10μm

Additional file 9: Supplementary Fig. 9. ICOSL expression. (A) Graph showing the number of ICOSL$^+$ cells in non-lesioned (NL) and PPT-lesioned hippocampus, from 3 to 7 dpl, within the CD11b$^+$/CD45$^{low/int}$ and CD11b$^+$/CD45^{high} cell populations. A minimum of five WT and five GFAP-IL6Tg animals per group were used for this study. Data are represented as mean ± SD. The significances are represented as #p≤0.05 vs NL of respective group.

Additional file 10: Supplementary Fig. 10. Cytokines and chemokines expression. Graphs showing the time course of expression of IL-2, IL-6, IFNγ, IL1β, IL12p70, IL-17, IL-10, IL-13, IL-9, IL-5, IL-4, CXCL10 and CCL2 in non-lesioned (NL) and PPT-lesioned animals from 3 to 14dpl, in both WT and GFAP-IL6Tg animals. (N) Graph showing the IL-6 levels in serum in both NL WT and NL GFAP-IL6Tg animals. At least four WT and five GFAP-IL6Tg animals for each time point were used. Data are represented as mean ± SD. The significances are represented as #p≤0.05, %p≤0.01 and &p≤0.001 vs NL of respective group; ^p≤0.1, $$p$≤0.05, ´´ p≤0.01 and ∞p≤0.001 vs 3dpl of respective group and αp≤0.05 vs 7dpl of respective group. Significant differences between genotypes are represented as ***p≤0.001, **p≤0.01, *p≤0.05.

Additional file 11: Supplementary Fig. 11. Non-lesioned study in WT and GFAP-IL6Tg animals. Representative graphs showing the differences between WT and GFAP-IL6Tg animals in NL conditions. A minimum of three WT and three GFAP-IL6Tg animals per group were used. Data are represented as mean ± SD. The significances are represented ***p≤0.0001, **p≤0.01, *p≤0.05.

Additional file 12: Supplementary Fig. 12. Gating strategy for flow cytometry. (A – F) Representative dot plot and histogram plot from individual hippocampus from WT and GFAP-IL6Tg animals in NL and after PPT. First, population/live cells were gated based on SSC-A and FSC-A, and then microglia/macrophage cells were gated based on CD45 and CD11b expression. CD11b$^+$/CD45$^{low/int}$ and CD11b$^+$/CD45^{high} population were discriminated according to the levels of CD45. Microglia/macrophages phenotype were studied by MHCII, CD80, CD86, Ly6C and F4/80 expression and gated based on CD11b$^+$/CD45$^+$/Igs isotype control antibodies.

Abbreviations

BB: Blocking buffer; BBB: Blood-brain barrier; BrdU: 5′ Bromodeoxyuridine; CNS: Central nervous system; DAB: 3,3-Diaminobenzidine; DAPI: 4,9,6-Diamidino-2-phenylindole; DG: Dentate gyrus; dpl: Day post lesion; GFAP: Glial fibrillary acidic protein; GFAP-IL6Tg: Transgenic mice with astrocyte-targeted IL6-production; GL: Granular layer; IHC: Immunohistochemistry; IL: Interleukin; IML: Inner molecular layer; i.p.: Intraperitoneally; ML: Molecular layer; MML: Medial molecular layer; NL: Non-lesioned; OML: Outer molecular layer; PBS: Phosphate buffer solution; PP: Perforant pathway; PPT: Perforant pathway transection; RT: Room temperature; TBS: Tris-buffered saline; TBST: TBS containing 1% Triton-X100; Tg: Transgenic; WB: Wash buffer; WT: Wild-type

Acknowledgements

The authors would like to thank Miguel A. Martil and Isabella Appiah for their technical help.
The authors declare that they have no competing interests.

Authors' contributions

MR designed and performed the experiments, including acquiring data and analyzing data; and wrote the manuscript. BA designed experiments, analyzed data, and revised manuscript. JPC contributed to design and perform the sulfide-silver staining. ILC revised the manuscript. BG designed the research and revised the manuscript and BC provided financing, designed the research, and revised the manuscript. The authors read and approved the final manuscript.

Funding

This work was supported by the Spanish Ministry of Science and Innovation grants BFU2014-55459 and BFU2017-87843-R.

Availability of data and materials

All data generated or analyzed during this study are included in this published article [and its supplementary information files].

Ethics approval and consent to participate

All experimental animal work was conducted in accordance to Spanish regulations (Ley 32/2007, Real Decreto 1201/2005, Ley 9/2003 and Real Decreto 178/2004) in agreement with European Union directives (86/609/CEE, 91/628/CEE and 92/65/CEE) and was approved by the Ethical Commission of the Autonomous University of Barcelona. All efforts were made to minimize the number of animals used to produce reliable scientific data, as well as animal suffering.

Consent for publication

Not applicable.

Competing interests

The authors declare that they have no competing interests.

Author details

[1]Department of Cell Biology, Physiology and Immunology, Institute of Neuroscience, Universitat Autònoma de Barcelona, 08193, Bellaterra, Barcelona, Spain. [2]Department of Cell Biology, Physiology and Immunology, Universitat de Barcelona, 08028 Barcelona, Spain. [3]School of Life and Environmental Sciences and Charles Perkins Centre, University of Sydney, Sydney, NSW 2006, Australia.

Received: 15 April 2020 Accepted: 16 December 2020
Published online: 22 January 2021

References

1. Almolda B, Costa M, Montoya M, Gonzalez B, Castellano B. CD4 microglial expression correlates with spontaneous clinical improvement in the acute Lewis rat EAE model. J Neuroimmunol. 2009;209(1-2):65–80. https://doi.org/10.1016/j.jneuroim.2009.01.026.
2. Almolda B, de Labra C, Barrera I, Gruart A, Delgado-Garcia JM, Villacampa N, et al. Alterations in microglial phenotype and hippocampal neuronal function in transgenic mice with astrocyte-targeted production of interleukin-10. Brain Behav Immun. 2015;45:80–97. https://doi.org/10.1016/j.bbi.2014.10.015.
3. Almolda B, Villacampa N, Manders P, Hidalgo J, Campbell IL, Gonzalez B, Castellano B. Effects of astrocyte-targeted production of interleukin-6 in the mouse on the host response to nerve injury. Glia. 2014;62(7):1142–61. https://doi.org/10.1002/glia.22668.
4. Amaral DG, Witter MP. The three-dimensional organization of the hippocampal formation: a review of anatomical data. Neuroscience. 1989;31(3):571–91. https://doi.org/10.1016/0306-4522(89)90424-7.
5. Babcock AA, Kuziel WA, Rivest S, Owens T. Chemokine expression by glial cells directs leukocytes to sites of axonal injury in the CNS. J Neurosci. 2003;23(21):7922–30.
6. Babcock AA, Wirenfeldt M, Holm T, Nielsen HH, Dissing-Olesen L, Toft-Hansen H, et al. Toll-like receptor 2 signaling in response to brain injury: an innate bridge to neuroinflammation. J Neurosci. 2006;26(49):12826–37. https://doi.org/10.1523/JNEUROSCI.4937-05.2006.
7. Bechmann I, Goldmann J, Kovac AD, Kwidzinski E, Simburger E, Naftolin F, et al. Circulating monocytic cells infiltrate layers of anterograde axonal degeneration where they transform into microglia. FASEB J. 2005;19(6):647–9. https://doi.org/10.1096/fj.04-2599fje.
8. Bechmann I, Mor G, Nilsen J, Eliza M, Nitsch R, Naftolin F. FasL (CD95L, Apo1L) is expressed in the normal rat and human brain: evidence for the existence of an immunological brain barrier. Glia. 1999;27(1):62–74.
9. Bechmann I, Peter S, Beyer M, Gimsa U, Nitsch R. Presence of B7--2 (CD86) and lack of B7--1 CD(80) on myelin phagocytosing MHC-II-positive rat microglia is associated with nondestructive immunity in vivo. FASEB J. 2001;15(6):1086–8. https://doi.org/10.1096/fj.00-0563fje.
10. Bennett ML, Bennett FC, Liddelow SA, Ajami B, Zamanian JL, Fernhoff NB, et al. New tools for studying microglia in the mouse and human CNS. Proc Natl Acad Sci U S A. 2016;113(12):E1738–46. https://doi.org/10.1073/pnas.1525528113.
11. Benveniste EN. Cytokine actions in the central nervous system. Cytokine Growth Factor Rev. 1998;9(3-4):259–75.
12. Bettelli E, Carrier Y, Gao W, Korn T, Strom TB, Oukka M, et al. Reciprocal developmental pathways for the generation of pathogenic effector TH17 and regulatory T cells. Nature. 2006;441(7090):235–8. https://doi.org/10.1038/nature04753.
13. Boche D, Nicoll JA. Neuroinflammation in ageing and in neurodegenerative disease. Neuropathol Appl Neurobiol. 2013;39(1):1–2. https://doi.org/10.1111/nan.12009.
14. Brett FM, Mizisin AP, Powell HC, Campbell IL. Evolution of neuropathologic abnormalities associated with blood-brain barrier breakdown in transgenic mice expressing interleukin-6 in astrocytes. J Neuropathol Exp Neurol. 1995;54(6):766–75. https://doi.org/10.1097/00005072-199511000-00003.
15. Brunello AG, Weissenberger J, Kappeler A, Vallan C, Peters M, Rose-John S, Weis J. Astrocytic alterations in interleukin-6/Soluble interleukin-6 receptor alpha double-transgenic mice. Am J Pathol. 2000;157(5):1485–93.
16. Campbell IL. Transgenic mice and cytokine actions in the brain: bridging the gap between structural and functional neuropathology. Brain Res Brain Res Rev. 1998;26(2-3):327–36.
17. Campbell IL, Abraham CR, Masliah E, Kemper P, Inglis JD, Oldstone MB, Mucke L. Neurologic disease induced in transgenic mice by cerebral overexpression of interleukin 6. Proc Natl Acad Sci U S A. 1993;90(21):10061–5.
18. Campbell IL, Hofer MJ, Pagenstecher A. Transgenic models for cytokine-induced neurological disease. Biochim Biophys Acta. 2010;1802(10):903–17. https://doi.org/10.1016/j.bbadis.2009.10.004.
19. Campbell IL, Stalder AK, Akwa Y, Pagenstecher A, Asensio VC. Transgenic models to study the actions of cytokines in the central nervous system. Neuroimmunomodulation. 1998;5(3-4):126–35. https://doi.org/10.1159/000026329.
20. Cao Z, Gao Y, Bryson JB, Hou J, Chaudhry N, Siddiq M, et al. The cytokine interleukin-6 is sufficient but not necessary to mimic the peripheral conditioning lesion effect on axonal growth. J Neurosci. 2006;26(20):5565–73. https://doi.org/10.1523/JNEUROSCI.0815-06.2006.
21. Chiang CS, Stalder A, Samimi A, Campbell IL. Reactive gliosis as a consequence of interleukin-6 expression in the brain: studies in transgenic mice. Dev Neurosci. 1994;16(3-4):212–21. https://doi.org/10.1159/000112109.
22. Conroy SM, Nguyen V, Quina LA, Blakely-Gonzales P, Ur C, Netzeband JG, et al. Interleukin-6 produces neuronal loss in developing cerebellar granule neuron cultures. J Neuroimmunol. 2004;155(1-2):43–54. https://doi.org/10.1016/j.jneuroim.2004.06.014.

23. Cornfield LJ, Sills MA. High affinity interleukin-6 binding sites in bovine hypothalamus. Eur J Pharmacol. 1991;202(1):113–5.
24. Danscher G. Exogenous selenium in the brain. A histochemical technique for light and electron microscopical localization of catalytic selenium bonds. Histochemistry. 1982;76(3):281–93.
25. Deller T, Del Turco D, Rappert A, Bechmann I. Structural reorganization of the dentate gyrus following entorhinal denervation: species differences between rat and mouse. Prog Brain Res. 2007;163:501–28. https://doi.org/10.1016/S0079-6123(07)63027-1.
26. Deller T, Frotscher M. Lesion-induced plasticity of central neurons: sprouting of single fibres in the rat hippocampus after unilateral entorhinal cortex lesion. Prog Neurobiol. 1997;53(6):687–727.
27. Deller T, Nitsch R, Frotscher M. Layer-specific sprouting of commissural fibres to the rat fascia dentata after unilateral entorhinal cortex lesion: a Phaseolus vulgaris leucoagglutinin tracing study. Neuroscience. 1996;71(3):651–60. https://doi.org/10.1016/0306-4522(95)00475-0.
28. Dinarello CA. Overview of the IL-1 family in innate inflammation and acquired immunity. Immunol Rev. 2018;281(1):8–27. https://doi.org/10.1111/imr.12621.
29. Dissing-Olesen L, Ladeby R, Nielsen HH, Toft-Hansen H, Dalmau I, Finsen B. Axonal lesion-induced microglial proliferation and microglial cluster formation in the mouse. Neuroscience. 2007;149(1):112–22. https://doi.org/10.1016/j.neuroscience.2007.06.037.
30. Erta M, Quintana A, Hidalgo J. Interleukin-6, a major cytokine in the central nervous system. Int J Biol Sci. 2012;8(9):1254–66. https://doi.org/10.7150/ijbs.4679.
31. Finsen B, Jensen MB, Lomholt ND, Hegelund IV, Poulsen FR, Owens T. Axotomy-induced glial reactions in normal and cytokine transgenic mice. Adv Exp Med Biol. 1999;468:157–71.
32. Finsen B, Owens T. Innate immune responses in central nervous system inflammation. FEBS Lett. 2011;585(23):3806–12. https://doi.org/10.1016/j.febslet.2011.05.030.
33. Frotscher M, Heimrich B, Deller T. Sprouting in the hippocampus is layer-specific. Trends Neurosci. 1997;20(5):218–23.
34. Gadient RA, Otten U. Expression of interleukin-6 (IL-6) and interleukin-6 receptor (IL-6R) mRNAs in rat brain during postnatal development. Brain Res. 1994;637(1-2):10–4.
35. Gadient RA, Otten UH. Interleukin-6 (IL-6)--a molecule with both beneficial and destructive potentials. Prog Neurobiol. 1997;52(5):379–90.
36. Galiano M, Liu ZQ, Kalla R, Bohatschek M, Koppius A, Gschwendtner A, et al. Interleukin-6 (IL6) and cellular response to facial nerve injury: effects on lymphocyte recruitment, early microglial activation and axonal outgrowth in IL6-deficient mice. Eur J Neurosci. 2001;14(2):327–41.
37. Garner KM, Amin R, Johnson RW, Scarlett EJ, Burton MD. Microglia priming by interleukin-6 signaling is enhanced in aged mice. J Neuroimmunol. 2018;324:90–9. https://doi.org/10.1016/j.jneuroim.2018.09.002.
38. Garre JM, Yang G. Contributions of monocytes to nervous system disorders. J Mol Med. 2018;96(9):873–83. https://doi.org/10.1007/s00109-018-1672-3.
39. Gartlan KH, Markey KA, Varelias A, Bunting MD, Koyama M, Kuns RD, et al. Tc17 cells are a proinflammatory, plastic lineage of pathogenic CD8+ T cells that induce GVHD without antileukemic effects. Blood. 2015;126(13):1609–20. https://doi.org/10.1182/blood-2015-01-622662.
40. Gomez-Nicola D, Fransen NL, Suzzi S, Perry VH. Regulation of microglial proliferation during chronic neurodegeneration. J Neurosci. 2013;33(6):2481–93. https://doi.org/10.1523/JNEUROSCI.4440-12.2013.
41. Gu WL, Fu SL, Wang YX, Li Y, Wang XF, Xu XM, Lu PH. Expression and regulation of versican in neural precursor cells and their lineages. Acta Pharmacol Sin. 2007;28(10):1519–30. https://doi.org/10.1111/j.1745-7254.2007.00659.x.
42. Haas CA, Rauch U, Thon N, Merten T, Deller T. Entorhinal cortex lesion in adult rats induces the expression of the neuronal chondroitin sulfate proteoglycan neurocan in reactive astrocytes. J Neurosci. 1999;19(22):9953–63.
43. Hailer NP, Grampp A, Nitsch R. Proliferation of microglia and astrocytes in the dentate gyrus following entorhinal cortex lesion: a quantitative bromodeoxyuridine-labelling study. Eur J Neurosci. 1999;11(9):3359–64.
44. Hakkoum D, Stoppini L, Muller D. Interleukin-6 promotes sprouting and functional recovery in lesioned organotypic hippocampal slice cultures. J Neurochem. 2007;100(3):747–57. https://doi.org/10.1111/j.1471-4159.2006.04257.x.
45. Hanamsagar R, Bilbo SD. Environment matters: microglia function and dysfunction in a changing world. Curr Opin Neurobiol. 2017;47:146–55. https://doi.org/10.1016/j.conb.2017.10.007.
46. Hanisch UK. Microglia as a source and target of cytokines. Glia. 2002;40(2):140–55. https://doi.org/10.1002/glia.10161.
47. Hewett SJ, Jackman NA, Claycomb RJ. Interleukin-1beta in central nervous system injury and repair. Eur J Neurodegener Dis. 2012;1(2):195–211.
48. Hirbec HE, Noristani HN, Perrin FE. Microglia Responses in Acute and Chronic Neurological Diseases: What Microglia-Specific Transcriptomic Studies Taught (and did Not Teach) Us. Front Aging Neurosci. 2017;9:227. https://doi.org/10.3389/fnagi.2017.00227.
49. Hume DA, Ross IL, Himes SR, Sasmono RT, Wells CA, Ravasi T. The mononuclear phagocyte system revisited. J Leukoc Biol. 2002;72(4):621–7.
50. Huppert J, Closhen D, Croxford A, White R, Kulig P, Pietrowski E, et al. Cellular mechanisms of IL-17-induced blood-brain barrier disruption. FASEB J. 2010;24(4):1023–34. https://doi.org/10.1096/fj.09-141978.
51. Ikeda K, Iwasaki Y, Shiojima T, Kinoshita M. Neuroprotective effect of various cytokines on developing spinal motoneurons following axotomy. J Neurol Sci. 1996;135(2):109–13.
52. Kaminski M, Bechmann I, Pohland M, Kiwit J, Nitsch R, Glumm J. Migration of monocytes after intracerebral injection at entorhinal cortex lesion site. J Leukoc Biol. 2012;92(1):31–9. https://doi.org/10.1189/jlb.0511241.
53. Kawanokuchi J, Shimizu K, Nitta A, Yamada K, Mizuno T, Takeuchi H, Suzumura A. Production and functions of IL-17 in microglia. J Neuroimmunol. 2008;194(1-2):54–61. https://doi.org/10.1016/j.jneuroim.2007.11.006.
54. Kishimoto T. Interleukin-6: discovery of a pleiotropic cytokine. Arthritis Res Ther. 2006;8(Suppl 2):S2. https://doi.org/10.1186/ar1916.
55. Kishimoto T, Akira S, Narazaki M, Taga T. Interleukin-6 family of cytokines and gp130. Blood. 1995;86(4):1243–54.
56. Kloss CU, Kreutzberg GW, Raivich G. Proliferation of ramified microglia on an astrocyte monolayer: characterization of stimulatory and inhibitory cytokines. J Neurosci Res. 1997;49(2):248–54.
57. Krady JK, Lin HW, Liberto CM, Basu A, Kremlev SG, Levison SW. Ciliary neurotrophic factor and interleukin-6 differentially activate microglia. J Neurosci Res. 2008;86(7):1538–47. https://doi.org/10.1002/jnr.21620.
58. Ladeby R, Wirenfeldt M, Dalmau I, Gregersen R, Garcia-Ovejero D, Babcock A, et al. Proliferating resident microglia express the stem cell antigen CD34 in response to acute neural injury. Glia. 2005a;50(2):121–31. https://doi.org/10.1002/glia.20159.
59. Ladeby R, Wirenfeldt M, Garcia-Ovejero D, Fenger C, Dissing-Olesen L, Dalmau I, Finsen B. Microglial cell population dynamics in the injured adult central nervous system. Brain Res Brain Res Rev. 2005b;48(2):196–206. https://doi.org/10.1016/j.brainresrev.2004.12.009.
60. Lapenna A, De Palma M, Lewis CE. Perivascular macrophages in health and disease. Nat Rev Immunol. 2018;18(11):689–702. https://doi.org/10.1038/s41577-018-0056-9.
61. Li Q, Barres BA. Microglia and macrophages in brain homeostasis and disease. Nat Rev Immunol. 2018;18(4):225–42. https://doi.org/10.1038/nri.2017.125.
62. Liva SM, de Vellis J. IL-5 induces proliferation and activation of microglia via an unknown receptor. Neurochem Res. 2001;26(6):629–37.
63. Lobo-Silva D, Carriche GM, Castro AG, Roque S, Saraiva M. Balancing the immune response in the brain: IL-10 and its regulation. J Neuroinflammation. 2016;13(1):297. https://doi.org/10.1186/s12974-016-0763-8.
64. Loddick SA, Turnbull AV, Rothwell NJ. Cerebral interleukin-6 is neuroprotective during permanent focal cerebral ischemia in the rat. J Cereb Blood Flow Metab. 1998;18(2):176–9. https://doi.org/10.1097/00004647-199802000-00008.
65. Manich G, Gomez-Lopez RG, Almolda B, Villacampa N, Shrivastava K, Gonzalez B, Castellano B. Differential roles of TREM2+ microglia in anterograde and retrograde axonal injury models. Front Cell Neurosci. 2020. https://doi.org/10.3389/fncel.2020.567404.
66. Matthews DA, Cotman C, Lynch G. An electron microscopic study of lesion-induced synaptogenesis in the dentate gyrus of the adult rat. II. Reappearance of morphologically normal synaptic contacts. Brain Res. 1976;115(1):23–41.
67. McLoughlin RM, Jenkins BJ, Grail D, Williams AS, Fielding CA, Parker CR, et al. IL-6 trans-signaling via STAT3 directs T cell infiltration in acute inflammation. Proc Natl Acad Sci U S A. 2005;102(27):9589–94. https://doi.org/10.1073/pnas.0501794102.
68. Mittal SK, Cho KJ, Ishido S, Roche PA. Interleukin 10 (IL-10)-mediated Immunosuppression: march-i induction regulates antigen presentation by

macrophages but not dendritic cells. J Biol Chem. 2015;290(45):27158–67. https://doi.org/10.1074/jbc.M115.682708.
69. Mittrucker HW, Visekruna A, Huber M. Heterogeneity in the differentiation and function of CD8(+) T cells. Arch Immunol Ther Exp (Warsz). 2014;62(6):449–58. https://doi.org/10.1007/s00005-014-0293-y.
70. Mori S, Maher P, Conti B. Neuroimmunology of the Interleukins 13 and 4. Brain Sci. 2016;6(2). https://doi.org/10.3390/brainsci6020018.
71. Nakamura M, Okada S, Toyama Y, Okano H. Role of IL-6 in spinal cord injury in a mouse model. Clin Rev Allergy Immunol. 2005;28(3):197–204. https://doi.org/10.1385/CRIAI:28:3:197.
72. Neher JJ, Cunningham C. Priming microglia for innate immune memory in the brain. Trends Immunol. 2019;40(4):358–74. https://doi.org/10.1016/j.it.2019.02.001.
73. Niraula A, Sheridan JF, Godbout JP. Microglia Priming with Aging and Stress. Neuropsychopharmacology. 2017;42(1):318–33. https://doi.org/10.1038/npp.2016.185.
74. Nolan A, Kobayashi H, Naveed B, Kelly A, Hoshino Y, Hoshino S, et al. Differential role for CD80 and CD86 in the regulation of the innate immune response in murine polymicrobial sepsis. PLoS One. 2009;4(8):e6600. https://doi.org/10.1371/journal.pone.0006600.
75. Norden DM, Godbout JP. Review: microglia of the aged brain: primed to be activated and resistant to regulation. Neuropathol Appl Neurobiol. 2013;39(1):19–34. https://doi.org/10.1111/j.1365-2990.2012.01306.x.
76. Perry VH, Holmes C. Microglial priming in neurodegenerative disease. Nat Rev Neurol. 2014;10(4):217–24. https://doi.org/10.1038/nrneurol.2014.38.
77. Raivich G, Jones LL, Werner A, Bluthmann H, Doetschmann T, Kreutzberg GW. Molecular signals for glial activation: pro- and anti-inflammatory cytokines in the injured brain. Acta Neurochir Suppl. 1999;73:21–30.
78. Recasens M, Shrivastava K, Almolda B, Gonzalez B, Castellano B. Astrocyte-targeted IL-10 production decreases proliferation and induces a downregulation of activated microglia/macrophages after PPT. Glia. 2018. https://doi.org/10.1002/glia.23573.
79. Reyes TM, Fabry Z, Coe CL. Brain endothelial cell production of a neuroprotective cytokine, interleukin-6, in response to noxious stimuli. Brain Res. 1999;851(1-2):215–20.
80. Ringheim GE. Mitogenic effects of interleukin-5 on microglia. Neurosci Lett. 1995;201(2):131–4.
81. Satoh J, Kino Y, Asahina N, Takitani M, Miyoshi J, Ishida T, Saito Y. TMEM119 marks a subset of microglia in the human brain. Neuropathology. 2016;36(1):39–49. https://doi.org/10.1111/neup.12235.
82. Satoh JI, Kino Y, Yanaizu M, Ishida T, Saito Y. Microglia express TMEM119 in the brains of Nasu-Hakola disease. Intractable Rare Dis Res. 2019;8(4):260–5. https://doi.org/10.5582/irdr.2019.01123.
83. Schobitz B, de Kloet ER, Sutanto W, Holsboer F. Cellular localization of interleukin 6 mRNA and interleukin 6 receptor mRNA in rat brain. Eur J Neurosci. 1993;5(11):1426–35.
84. Schobitz B, Voorhuis DA, De Kloet ER. Localization of interleukin 6 mRNA and interleukin 6 receptor mRNA in rat brain. Neurosci Lett. 1992;136(2):189–92.
85. Siebert JR, Conta Steencken A, Osterhout DJ. Chondroitin sulfate proteoglycans in the nervous system: inhibitors to repair. Biomed Res Int. 2014;2014:845323. https://doi.org/10.1155/2014/845323.
86. Spooren A, Kolmus K, Laureys G, Clinckers R, De Keyser J, Haegeman G, Gerlo S. Interleukin-6, a mental cytokine. Brain Res Rev. 2011;67(1-2):157–83. https://doi.org/10.1016/j.brainresrev.2011.01.002.
87. Streit WJ. Microglial response to brain injury: a brief synopsis. Toxicol Pathol. 2000;28(1):28–30. https://doi.org/10.1177/019262330002800104.
88. Swardfager W, Winer DA, Herrmann N, Winer S, Lanctot KL. Interleukin-17 in post-stroke neurodegeneration. Neurosci Biobehav Rev. 2013;37(3):436–47. https://doi.org/10.1016/j.neubiorev.2013.01.021.
89. Taga T, Kishimoto T. Gp130 and the interleukin-6 family of cytokines. Annu Rev Immunol. 1997;15:797–819. https://doi.org/10.1146/annurev.immunol.15.1.797.
90. Thon N, Haas CA, Rauch U, Merten T, Fassler R, Frotscher M, Deller T. The chondroitin sulphate proteoglycan brevican is upregulated by astrocytes after entorhinal cortex lesions in adult rats. Eur J Neurosci. 2000;12(7):2547–58.
91. Tilgner J, Volk B, Kaltschmidt C. Continuous interleukin-6 application in vivo via macroencapsulation of interleukin-6-expressing COS-7 cells induces massive gliosis. Glia. 2001;35(3):234–45.
92. van Wageningen TA, Vlaar E, Kooij G, Jongenelen CAM, Geurts JJG, van Dam AM. Regulation of microglial TMEM119 and P2RY12 immunoreactivity in multiple sclerosis white and grey matter lesions is dependent on their inflammatory environment. Acta Neuropathol Commun. 2019;7(1):206. https://doi.org/10.1186/s40478-019-0850-z.
93. Waisman A, Hauptmann J, Regen T. The role of IL-17 in CNS diseases. Acta Neuropathol. 2015;129(5):625–37. https://doi.org/10.1007/s00401-015-1402-7.
94. Wirenfeldt M, Babcock AA, Ladeby R, Lambertsen KL, Dagnaes-Hansen F, Leslie RG, et al. Reactive microgliosis engages distinct responses by microglial subpopulations after minor central nervous system injury. J Neurosci Res. 2005;82(4):507–14. https://doi.org/10.1002/jnr.20659.
95. Wirenfeldt M, Dissing-Olesen L, Anne Babcock A, Nielsen M, Meldgaard M, Zimmer J, et al. Population control of resident and immigrant microglia by mitosis and apoptosis. Am J Pathol. 2007;171(2):617–31. https://doi.org/10.2353/ajpath.2007.061044.
96. Zimmermann J, Emrich M, Krauthausen M, Saxe S, Nitsch L, Heneka MT, et al. IL-17A promotes granulocyte infiltration, myelin loss, microglia activation, and behavioral deficits during cuprizone-induced demyelination. Mol Neurobiol. 2018;55(2):946–57. https://doi.org/10.1007/s12035-016-0368-3.

Publisher's Note